Interference effects in new physics processes at the LHC

vorgelegt von

Elina Fuchs

aus Langenhagen

Hamburg, 2015

Dissertation zur Erlangung des Doktorgrades
an der Fakultät für Mathematik, Informatik und Naturwissenschaften
Fachbereich Physik der Universität Hamburg

Folgende Gutachter empfehlen die Annahme der Dissertation:

Gutachter der Dissertation und Disputation:	Prof. Dr. Georg Weiglein
	Prof. Dr. Géraldine Servant
Gutachter der Disputation:	Jun.- Prof. Dr. Christian Sander
	Dr. Jürgen Reuter
Vorsitzender der Prüfungskommission:	Prof. Dr. Jan Louis
Tag der Disputation:	06. Juli 2015

Erklärung

Hiermit erkläre ich an Eides statt, dass ich die vorliegende Dissertationsschrift selbst verfasst und keine anderen als die angegebenen Quellen und Hilfsmittel benutzt habe.

Elina Fuchs

List of publications

The results presented in this thesis are based on the following publications:

- E. Fuchs, S. Thewes, G. Weiglein: *Interference effects in BSM processes with a generalised narrow-width approximation*, arXiv:1411.4652, accepted for publication by *European Physics Journal C* [1].
- E. Fuchs: *Interference effects of neutral MSSM Higgs bosons with a generalised narrow-width approximation*, arXiv:1411.5239, submitted to *Nuclear Physics B Proceedings Supplement* [2].

Furthermore, two publications are in preparation:

- A. Fowler, E. Fuchs, G. Weiglein: *Breit-Wigner approximation of full Higgs propagator mixing in the MSSM*, in preparation [3].
- E. Fuchs, S. Heinemeyer, O. Stål, G. Weiglein: *Impact of $\mathcal{CP}$-violating phases on searches for MSSM Higgs bosons at the LHC*, in preparation [4].

Declaration of my own contribution

I have worked out all results and produced all figures presented in this thesis unless stated otherwise. Only the implementation of the relative interference contributions obtained in this thesis into the program `HiggsBounds` was carried out by the `HiggsBounds` author Oscar Stål, which lead to the exclusion bounds plotted in Fig. 10.6. Furthermore I compared some numerical results from Chapter 9 with Silja Thewes, who also contributed with conceptual ideas to parts of the project documented in [1].

I have used the program packages `FeynArts`, `FormCalc`, `LoopTools`, `FeynHiggs` and `HiggsBounds`, as well as the latex hepthesis class.

Abstract

Interference effects between nearly mass-degenerate particles are addressed in this thesis, comprising higher-order calculations, a model-independent method to calculate interference terms efficiently and a phenomenological application to current Higgs searches at the LHC.

Predictions of cross sections and decay widths can be severely affected by interference terms between quasi-degenerate states arising in models beyond the Standard Model. We formulate a generalisation of the narrow-width approximation (NWA) which allows for a consistent treatment of such effects by factorising the interference term into on-shell matrix elements of the production and decay parts, optionally further approximated as simple interference weight factors, incorporating one-loop and real corrections in a UV- and IR-finite way. We apply the generalised NWA to interfering MSSM Higgs bosons in the process $\widetilde{\chi}_4^0 \to \widetilde{\chi}_1^0 \Phi \to \widetilde{\chi}_1^0 \tau^+\tau^-,\ \Phi = h, H$ and achieve an agreement of better than 1% with the unfactorised three-body decay of the neutralino $\widetilde{\chi}_4^0$ at NLO. Further, we derive the approximation of the full propagator matrix of the three neutral MSSM Higgs bosons in terms of Breit-Wigner propagators and on-shell wave-function normalisation factors $\hat{\mathbf{Z}}$. This is found to accurately reproduce the full mixing properties also in the case of complex MSSM parameters. Moreover, it enables the implementation of the total width at the highest available order. Using the Breit-Wigner and $\hat{\mathbf{Z}}$-factor formalism, we calculate $\mathcal{CP}$-violating interference effects of the neutral MSSM Higgs bosons in the process $b\bar{b} \to h_{1,2,3} \to \tau^+\tau^-$, induced by the phase ϕ_{A_t}. We find a very significant, destructive interference between h_2 and h_3, particularly for large μ. As a consequence, a considerable parameter region in the complex $M_h^{\text{mod+}}$ scenario, which would appear to be ruled out if this interference were neglected, actually escapes the current exclusion bounds from the LHC.

Zusammenfassung

Interferenzeffekte in Prozessen neuer Physik am LHC
Interferenzeffekte zwischen quasi-massenentarteten Teilchen stehen im Fokus dieser Arbeit, in der wir uns mit Strahlungskorrekturen, einer modellunabhängigen Methode für die effiziente Berechnung von Interferenztermen und einer phänomenologischen Anwendung auf aktuelle Higgs-Suchen am LHC beschäftigen.

Interferenzterme zwischen nahezu massenentarteten Zuständen, die häufig in Modellen jenseits des Standardmodells auftreten, können Vorhersagen von Wirkungsquerschnitten und Zerfallsbreiten maßgeblich beeinflussen. Wir verallgemeinern die bisherige Näherung schmaler Breiten (narrow-width approximation, NWA) so, dass Interferenzeffekte konsistent berücksichtigt werden. Der Interferenzterm wird in Matrixelemente des Produktions- und des Zerfallsanteils, jeweils ausgewertet auf der Massenschale des zerfallenden Teilchens, faktorisiert und lässt sich weiter durch Interferenz-Gewichtungsfaktoren nähern. In beiden Optionen können virtuelle und reelle Strahlungskorrekturen auf UV- und IR-endliche Weise hinzugefügt werden. Mit der verallgemeinerten NWA berechnen wir den Prozess $\widetilde{\chi}_4^0 \to \widetilde{\chi}_1^0 \Phi \to \widetilde{\chi}_1^0 \tau^+\tau^-$, $\Phi = h, H$ inklusive der Interferenz von h und H. Die genäherte Zerfallsbreite weicht in nächstführender Ordnung um weniger als 1% vom entsprechenden unfaktorisierten Drei-Körper-Zerfall des Neutralinos $\widetilde{\chi}_4^0$ ab. Außerdem leiten wir her, wie sich die volle Propagatormatrix der neutralen Higgs-Bosonen durch Breit-Wigner-Propagatoren und Wellenfunktions-Normierungsfaktoren ($\hat{\mathbf{Z}}$) nähern lässt. Dadurch werden die vollen Mischungseigenschaften auch im Fall von komplexen MSSM -Parametern sehr präzise wiedergegeben. Zusätzlich ermöglicht diese Formulierung die Berücksichtigung der totalen Breite in der höchstmöglichen Ordnung. Unter Verwendung der Breit-Wigner-Propagatoren und $\hat{\mathbf{Z}}$-Faktoren berechnen wir die durch die Phase ϕ_{A_t} hervorgerufenen $\mathcal{CP}$-verletzenden Interferenzeffekte neutraler MSSM Higgs-Bosonen im Prozess $b\bar{b} \to h_{1,2,3} \to \tau^+\tau^-$. Dabei stellen wir insbesondere für große μ eine erhebliche destruktive Interferenz zwischen h_2 und h_3 fest. Diese führt dazu, dass eine beträchtliche Parameterregion im komplexen $M_h^{\text{mod}+}$-Szenario, die unter Vernachlässigung des Interferenzterms ausgeschlossen schiene, durch aktuelle experimentelle Ergebnisse bisher nicht ausgeschlossen werden kann.

Contents

Chapter 1.

Introduction

Run II of the LHC is just starting operation at an unprecedented energy and luminosity with the purpose to look for signs of physics beyond the Standard Model. Such signs may show up directly as new particles or indirectly as deviations from Standard Model (SM) properties. New physics might not only become visible as an excess of measured data over the expected background. Another interesting case could be a deficit of events due to reduced couplings or a destructive interference of a new physics signal with the SM background continuum. A different kind of interference could also occur between two nearby resonances of particles from a model beyond the SM spectrum. Such an effect would modify the expectation for detecting those particles of the particular model.

The first run of the LHC has been highly successful with the discovery of a Higgs boson [5, 6], which had been predicted [7] almost half a century before the discovery as a consequence of a mechanism that was proposed to explain electroweak symmetry breaking [7–11].

The Higgs boson is the last particle that can be accomodated within the SM. Any discovery of a new particle would be a clear sign for physics beyond the Standard Model (BSM). However, the discovered state itself might already carry footprints of a BSM model with one or several Higgs bosons. More data is needed to learn more about the observed boson whose properties are so far compatible with those predicted by the SM.

Many BSM models such as supersymmetry, a symmetry relating bosons and fermions, introduce new particles. Their production and decay may lead to long processes that are challenging to calculate without further approximations if higher-order corrections are required. Therefore the narrow-width approximation (NWA), which splits a complicated process into the on-shell production and decay of an unstable particle with a narrow width, is a helpful simplification that is often employed. However, this treatment does not take interference effects into account. In this thesis, we develop a generalisation of the standard NWA in order to include also interference terms from nearly mass-degenerate particles in the prediction of a cross section or decay width while maintaining the convenient factorisation of the complete process into smaller pieces.

So far, neither additional Higgs bosons beyond the SM-like observed state nor other new particles have been detected. Confronting the predictions for the production and decay of neutral Higgs bosons in the Minimal Supersymmetric Standard Model (MSSM) with observed limits from LHC searches allows to constrain the experimentally viable parameter space of the model. However, these conclusions are based on the standard NWA where any interference term is neglected. Among the Higgs bosons in the MSSM with real parameters, only the neutral $\mathcal{CP}$-even states h and H can interfere. This effect can play a role in a small parameter region. The situation is different for complex parameters, where also h_2 and h_3 can interfere and their interference is relevant in a large area of parameters. We investigate the implications of this interference for the interpretation of search results from the LHC.

Thesis outline

This thesis is structured as follows. Chapter 2 gives a short overview of the interactions of the SM with a focus on the electroweak symmetry breaking by a minimal Higgs sector. After mentioning shortcomings of the SM, we turn to the MSSM in Chapter 3, introducing our notation for the MSSM at lowest order with complex parameters, describing the particle content and particularly the two Higgs doublets. In Chapter 4 we specify the renormalisation schemes used in our calculations, and we compare the stability of different schemes for the neutralino-chargino sector. Chapter 5 begins with an analysis of the pole structure of the propagator matrix of the neutral Higgs bosons. We then discuss wave function normalisation factors, $\hat{\mathbf{Z}}$, which are needed for the correct on-shell properties of Higgs bosons in the $\overline{\text{DR}}$ renormalisation scheme. The key result of Chapter 6 is the approximation of the full propagators in terms of Breit-Wigner propagators and $\hat{\mathbf{Z}}$-factors obtained by expanding the full propagators around all of their complex poles. In Chapter 7 we first review the principles and limitations of the NWA. In the main part of the chapter, we develop an extension of the standard NWA for the consistent on-shell approximation of the interference term including higher order corrections. Chapter 8 presents the NLO calculation of the three-body decay $\tilde{\chi}_4^0 \to \tilde{\chi}_1^0 \tau^+\tau^-$ via resonant Higgs bosons in a scenario with real parameters where h and H interfere. This interference effect is approximated in Chapter 9 by applying the generalised NWA to the two subprocesses $\tilde{\chi}_4^0 \to \tilde{\chi}_1^0\,\Phi$ and $\Phi \to \tilde{\chi}_1^0 \tau^+\tau^-$, $\Phi = h, H$ including vertex corrections, soft photon radiation and $\hat{\mathbf{Z}}$-factors. In Chapter 10, for a scenario with a non-vanishing complex phase ϕ_{A_t}, we examine $\mathcal{CP}$-violating Higgs interference effects in the process $b\bar{b} \to \tau^+\tau^-$ and their impact on LHC exclusion bounds. Finally, we conclude in Chapter 11.

Chapter 2.

Standard Model

The Standard Model of particle physics (SM) successfully describes all known elementary particles and – apart from gravity – all fundamental forces, namely the electroweak [12–15] and strong [16–19] interactions. The last missing piece of the SM was the Higgs boson predicted to generate masses of the matter particles and force carriers. The long awaited discovery of a new scalar at the LHC in 2012 and its confirmation over the last years as a SM-like Higgs boson therefore represents a breakthrough of particle physics.

In this chapter, we provide a brief introduction of the underlying symmetries and the particle content of the SM. In particular, we focus on the breaking of the electroweak symmetry by a Higgs field before pointing out some shortcomings of the SM that require new physics beyond the SM, mainly following Refs. [20–24].

2.1. Symmetries and interactions

The SM is a relativistic quantum field theory characterised by its global and local symmetries. Its Lagrangian is invariant under the global symmetries defined by the Poincaré group, i.e. the (homogeneous) Lorentz transformations and (inhomogeneous) translations in Minkowski space-time. Besides, the SM is gauge invariant under local transformation of the non-abelian, semi-simple Lie-group $SU(3)_C \otimes SU(2)_L \otimes U(1)_Y$, where the C denotes colour, L left-handed fields charged under the weak isospin and Y the weak hypercharge.

The SM contains fermions ψ (spin 1/2) as matter fields in the fundamental representation of the gauge groups, vector bosons A^a_μ (spin 1) as mediators of the interactions in the adjoint representation and one scalar field Φ (spin 0). Poincaré invariance determines their kinetic terms in the Lagrangian $\mathcal{L}_{\text{kin}}$, which contains derivatives of the fields. However, demanding also invariance under the gauge transformations requires to substitute the derivatives by covariant derivatives (where summation over the gauge index a is implied)

$$\partial_\mu \to D_\mu := \partial_\mu - igT^a A^a_\mu, \tag{2.1}$$

with the coupling g, $N^2 - 1$ generators T_a and generic gauge fields A^a_μ of a general $SU(N)$ gauge group. The symmetry group of quantum chromodynamics (QCD), the theory of the strong interaction, is $SU(3)_C$ with a conserved charge called colour. The generators of $SU(3)$ are $\frac{\lambda^a}{2}$ where λ^a, $a = 1...8$ are the Gell-Mann matrices. The eight gauge fields

g^a_μ are called gluons, and the strong coupling is denoted by g_s. Electroweak interactions are characterised by the $SU(2)_L \otimes U(1)_Y$ symmetry. For the $SU(2)_L$ group, which is generated by the three Pauli matrices σ^a, there are three fields W^a_μ, $a = 1, 2, 3$, the coupling g_2 and the weak isospin $I^a = \frac{\sigma^a}{2}$. The abelian $U(1)_Y$ has the coupling g_1, the hypercharge Y and one gauge field B_μ. Hence, the covariant derivative involving all generators of the SM symmetry groups reads

$$D_\mu = \partial_\mu \, - \, ig_1 \frac{Y}{2} B_\mu \, \pm \, ig_2 \frac{\sigma^a}{2} W^a_\mu - ig_s \frac{\lambda^a}{2} g^a_\mu. \tag{2.2}$$

The sign convention is $-$ in the SM and $+$ in the MSSM (see Chapter 3). Applying the covariant derivative, the kinetic term of the fermions reads (with $\not{D} = \gamma^\mu D_\mu$)

$$\mathcal{L}_{\text{kin,f}} = \overline{\psi} i \not{D} \psi. \tag{2.3}$$

The field strength tensors $F^a_{\mu\nu} = \partial_\mu A_\nu - \partial_\mu A_\nu + g f^{abc} A^b_\mu A^c_\nu$ of all gauge groups, where g are the specific gauge couplings and f^{abc} the structure constants defining the respective algebra (they vanish for the abelian $U(1)$), appear in the kinetic term of the vector bosons:

$$\mathcal{L}_{\text{gauge}} = -\frac{1}{4} F^a_{\mu\nu} F^{a\mu\nu} \equiv -\frac{1}{4} g^a_{\mu\nu} g^{a\mu\nu} - \frac{1}{4} W^a_{\mu\nu} W^{a\mu\nu} - \frac{1}{4} B_{\mu\nu} B^{\mu\nu} \tag{2.4}$$

The electric charge operator Q is given by the Gell-Mann-Nishijima relation:

$$Q = I^3 + \frac{Y}{2}. \tag{2.5}$$

2.2. Electroweak symmetry breaking

Higgs field and spontaneous symmetry breaking The SM in its form described above predicts massless fermions and gauge bosons – in contradiction to experimental results of non–zero fermion masses and three massive gauge bosons. Explicit mass terms in the Lagrangian would violate gauge invariance and thereby spoil unitarity and renormalisability. The only known mechanism of introducing massive gauge bosons of the electroweak interactions in a renormalisable [25, 26] way is by spontaneous breaking of the electroweak symmetry. In this case, only the symmetry of the vacuum is broken while keeping the Lagrangian invariant. This is the so-called Brout-Englert-Higgs (BEH) mechanism [7–11]. The breaking is achieved by a complex scalar $SU(2)_L$ doublet Φ with hypercharge $Y = 1$,

$$\Phi(x) = \begin{pmatrix} \phi^+(x) \\ \phi^0(x) \end{pmatrix}, \tag{2.6}$$

giving rise to a scalar term in the Lagrangian

$$\mathcal{L}_H = (D_\mu \Phi)^\dagger (D_\mu \Phi) - V(\Phi). \tag{2.7}$$

In order to guarantee renormalisability, no higher powers than $(\Phi^\dagger\Phi)^2$ are allowed in the potential $V(\Phi)$. Moreover, the potential needs to be bounded from below so that odd powers of Φ are forbidden. Thus, the potential only depends on $|\Phi|^2 = \Phi^\dagger\Phi$:

$$V(\phi) = -\mu^2\Phi^\dagger\Phi + \frac{\lambda}{4}(\Phi^\dagger\Phi)^2. \tag{2.8}$$

Further, for a stable potential (bounded from below), $\lambda > 0$ is required. If $\mu^2 < 0$, then the minimum of the potential at $\Phi = 0$ respects the full $SU(2)_L \otimes U(1)_Y$ symmetry and no breaking emerges. Contrarily, $\mu^2 > 0$ induces the so-called "Mexican hat" potential which exhibits an infinite set of degenerate minima on a circle of radius $|\Phi| = \sqrt{\frac{2\mu^2}{\lambda}} = \frac{v}{\sqrt{2}} \neq 0$, where v is the non-vanishing vacuum expectation value (vev). The degenerate ground states transform into each other under gauge transformations. However, selecting a specific ground state spontaneously breaks the full $SU(2)_L \otimes U(1)_Y$ symmetry. Up to a phase convention, the choice of the ground state is determined by the requirement that the non-zero vev must reside in the neutral component of the Higgs doublet so that the remnant symmetry is the unbroken $U(1)_{em}$ of electromagnetic gauge transformations:

$$\langle\Phi\rangle = \begin{pmatrix} 0 \\ \frac{v}{\sqrt{2}} \end{pmatrix}. \tag{2.9}$$

The complex scalar doublet $\Phi(x)$ with four real degrees of freedom (dof) is then expanded around the ground state,

$$\Phi(x) = \begin{pmatrix} \phi^+(x) \\ \frac{1}{\sqrt{2}}(v + H(x) + i\chi^0(x)) \end{pmatrix}, \tag{2.10}$$

where ϕ^+, $\phi^- = \phi^{+\dagger}$ and χ^0 are three would-be Goldstone bosons [27, 28] with vanishing vev. As unphysical degrees of freedom, they are absent in the unitary gauge and give rise to the longitudinal modes of three gauge bosons. In contrast, the fourth dof is the physical Higgs field $H(x)$ that has led to the prediction of a massive Higgs boson [7]. Expanding the potential in terms of the physical fields, one identifies the Higgs mass, which arises from the Higgs self-coupling λ, in the quadratic term:

$$m_H^2 = \frac{\partial V(H)}{\partial H^2} = 2\mu^2 = \lambda\frac{v^2}{2}. \tag{2.11}$$

The Higgs mass is a free parameter of the SM and must be fixed by experimental measurements.

Masses of the gauge bosons One further expands the kinetic term around the ground state

$$(D_\mu\Phi)^\dagger(D_\mu\Phi) = \frac{1}{2}(\partial_\mu H)(\partial_\mu H) + \frac{1}{8}g_2^2(v+H)^2(W_\mu^1 - iW_\mu^2)(W^{1\mu} + iW^{2\mu}) \\ + \frac{1}{8}(v+H)^2(g_2 W_\mu^3 + g_1 B_\mu)(g_2 W^{3\mu} + g_1 B^\mu). \qquad (2.12)$$

The first term is the kinetic term of the physical Higgs field. The second term allows the definition of two electrically charged bosons $W_\mu^\pm$ as mass eigenstates with the mass M_W (extracted from the part proportional to v^2):

$$W_\mu^\pm = \frac{1}{\sqrt{2}}\left(W_\mu^1 \mp iW_\mu^2\right), \qquad M_W = \frac{v}{2}\,g_2. \qquad (2.13)$$

The v^2-part of the last term is equal to $\frac{1}{2}(W_\mu^3, B_\mu)\mathbf{M}_0^2(W_\mu^3, B_\mu)^T$, where the mass matrix of the neutral vector bosons

$$\mathbf{M}_0^2 = \frac{v^2}{4}\begin{pmatrix} g_1^2 & g_1 g_2 \\ g_1 g_2 & g_2^2 \end{pmatrix} \qquad (2.14)$$

needs to be diagonalised in order to obtain the neutral mass eigenstates. Owing to $\det\left[\mathbf{M}_0^2\right] = 0$, one eigenvalue is zero. As the gauge boson of the unbroken $U(1)_{em}$, the photon γ has to remain massless also after electroweak symmetry breaking. The other eigenvalue $M_Z^2 = \mathrm{Tr}\left[\mathbf{M}_0^2\right]$ belongs to the massive, neutral Z-boson. The mass eigenstates result from the following rotation:

$$\begin{pmatrix} Z_\mu \\ A_\mu \end{pmatrix} = \begin{pmatrix} c_W & s_W \\ -s_W & c_W \end{pmatrix}\begin{pmatrix} W_\mu^3 \\ B_\mu \end{pmatrix}, \qquad \begin{array}{l} M_Z = \frac{v}{2}\sqrt{g_1^2 + g_2^2}, \\ M_\gamma = 0, \end{array} \qquad (2.15)$$

where the weak mixing angle θ_W is given by

$$s_W \equiv \sin\theta_W = \frac{g_1}{\sqrt{g_1^2 + g_2^2}}, \qquad c_W \equiv \cos\theta_W = \frac{g_2}{\sqrt{g_1^2 + g_2^2}} = \frac{M_W}{M_Z}. \qquad (2.16)$$

The electric unit charge can be expressed as $e = g_2 s_W = g_1 c_W$. All non-vanishing gauge boson masses are proportional to v because they are generated by the spontaneus breaking of $SU(3)_C \otimes SU(2)_L \otimes U(1)_Y \longrightarrow SU(3)_C \otimes U(1)_{em}$ by the ground state of the Higgs doublet. The $SU(3)_C$ is unaffected so that the gluons remain massless. They carry colour and couple to colour-charged fermions. The photon interacts with all electrically charged fields. The mediators of the weak interaction are the neutral Z-boson, to which all fermions couple, and the charged $W^\pm$-bosons, whose couplings to fermions are purely left-handed. Apart from the photon, the gauge bosons have self-interactions. The interactions of $V = W^\pm, Z$ with the Higgs boson are introduced by the trilinear (VVH) and quadrilinear $(VVHH)$ terms in Eq. (2.12). As a result, the physical Higgs field restores unitarity of vector boson scattering, which would otherwise grow with energy.

Fermions and Yukawa couplings Fermions are categorised as colour-charged quarks q, which are $SU(3)_C$-triplets, and colour-neutral leptons l, i.e. singlets under $SU(3)_C$. They come in three generations with the same quantum numbers. As a chiral theory, left- and right-handed fermions transform in different representations. Left-handed fermions f_L are $SU(2)_L$ doublets, right-handed fermions are weak singlets. A quark doublet $q_{i,L}$ of generation $i = 1, 2, 3$ contains an up-type (u_i) and a down-type (d_i) quark. Inside a lepton doublet $l_{i,L}$, the up-type lepton is a neutral neutrino ν_i, and the down-type lepton is charged. The SM does not contain any right-handed neutrinos. The right-handed quarks and leptons are denoted by $u_{i,R}, d_{i,R}$ and $e_{i,R}$.

An explicit mass term for the fermions would not respect the gauge symmetries of the SM. Instead, they acquire their masses through Yukawa interactions between the fermions and the Higgs fields,

$$\mathcal{L}_{\mathrm{Y}} = -\overline{q}_L \mathbf{y}_d \, \Phi \, d_R - \overline{q}_L \mathbf{y}_u \, \overline{\Phi} \, u_R - \overline{l}_L \mathbf{y}_l \, \Phi \, e_R + h.c., \tag{2.17}$$

where $\overline{\Phi} = i\sigma_2 \Phi^* = (\phi^{0*}, -\phi^-)^T$, and $\mathbf{y}_{d,u,l}$ are the 3×3 Yukawa matrices (in family space) of the down-type quarks, up-type quarks and charged leptons, respectively. This interaction is renormalisable and preserves the symmetries of the SM before electroweak symmetry breaking. When the Higgs field obtains its vev, the fermions become massive. The Yukawa matrices can be diagonalised by unitary transformations V in order to obtain the diagonal mass matrices for $f = u, d, l$:

$$\mathbf{M}_f = V_L^f \mathbf{y}_f V_R^{f\dagger} \frac{v}{\sqrt{2}}. \tag{2.18}$$

The unitary CKM (Cabibbo, Kobayashi, Maskawa [29, 30]) matrix

$$V_{\mathrm{CKM}} = V_L^u V_L^{d\dagger} \tag{2.19}$$

provides a change from the weak eigenstate basis into the physical mass eigenbasis of the quarks in the interaction terms of the Lagrangian. As a unitary 3×3 matrix, V_{CKM} contains one complex phase, which is the only source of $\mathcal{CP}$-violation in the SM. Neutrinos are assumed to be massless (although neutrino oscillations indicate small, but non-zero neutrino masses, which hints at physics beyond the SM). Remarkably, as a direct consequence of the BEH mechanism, the coupling strength y_f of a massive fermion f to the Higgs field is proportional to its mass: $y_f = \frac{\sqrt{2} m_f}{v}$ (and analogously for the $W^\pm$- and Z-bosons).

As an interesting fact, one Higgs doublet suffices in the SM to render both the up- and the down-type fermions massive. The reason is that in $\overline{\Phi}$, the neutral ϕ^{0*}, which develops a vev, stands in the upper component. Thus, electroweak symmetry breaking is possible in the SM with a minimal Higgs sector consisting of only one complex scalar doublet (the case is different in supersymmetry, see Chapter 3).

SM Lagrangian The full Lagrangian of the SM is composed of the following terms:

$$\mathcal{L}_{\text{SM}} = \mathcal{L}_{\text{gauge}} + \mathcal{L}_H + \mathcal{L}_f + \mathcal{L}_{\text{fix}} + \mathcal{L}_{\text{FP}}. \tag{2.20}$$

The fermionic contributions are summarised in $\mathcal{L}_f = \mathcal{L}_{\text{kin,f}} + \mathcal{L}_Y$. Each of the terms $\mathcal{L}_{\text{gauge}}$, $\mathcal{L}_H$ and $\mathcal{L}_f$ is separately gauge invariant. However, quantisation and higher order corrections require to fix a gauge by a new term in $\mathcal{L}_{\text{fix}}$ involving the unphysical degrees of freedom of the gauge bosons. These need to be compensated for by introducing so-called Faddeev-Popov ghost fields, giving rise to $\mathcal{L}_{\text{FP}}$.

2.3. Shortcomings of the Standard Model

Despite its tremendous success in describing very precisely almost all measurements of particle physics experiments performed in the last decades, the SM cannot be the complete theory of nature. It rather serves as an effective theory up to a cut-off scale Λ. However, there are several experimental and theoretical indications for new physics at higher energies than Λ.

The first issue concerns gravity, which cannot be accomplished as a quantum field theory within the SM. Around the energy scale currently probed by particle colliders, gravitational effects are expected to be negligible, but they become relevant at the Planck scale of $M_P \sim \mathcal{O}(10^{19})$ GeV. Hence the validity of the SM is at the latest limited by M_P. The deficit of the SM to describe all four fundamental forces in a consistent framework valid at all energies directly necessitates the embedding of the SM into a more universal theory.

The SM is renormalisable so that it can in principle be run all the way up to the maximal cut-off scale $\Lambda \sim M_P$ if no new physics exists between the electroweak scale M_W and the Planck scale M_P. In the absence of any physics beyond the Standard Model (BSM) the enormous difference between these two scales by 17 orders of magnitude could not be explained. On the other hand, the hierarchy of scales does not per se pose a problem, but the question remains how this huge hierarchy can be stable in the presence of quantum corrections. In fact, the mass of the Higgs boson is affected by quantum effects of new physics. Fermion masses are protected by the approximate chiral symmetry. Their quantum corrections are proportional to the mass and depend only logarithmically on the cut-off scale, $\Delta m_f \sim m_f \ln \Lambda$ so that $\Delta m_f \to 0$ in the chiral limit of $m_f \to 0$. In contrast, masses of scalars are not protected by any symmetry of the SM. Radiative corrections to squared scalar masses are independent of the bare mass itself and quadratically sensitive to the cut-off scale. If no new physics enters below M_P, the Higgs mass $M_H^2 = M_{H,0}^2 + \Delta M_H^2$ receives a huge correction,

$$\Delta M_H^2 \sim \Lambda^2 \sim M_P^2. \tag{2.21}$$

In view of the discovered Higgs boson with $M_H \simeq 125\,\text{GeV}$, an enormous cancellation between the bare mass $M_{H,0}^2$ and the correction term ΔM_H^2 is necessary in order to yield the observed value at the electroweak scale. Since the Higgs mass is a free parameter of the SM, this cancellation is technically possible, but it is perceived as an extreme, accidental fine-tuning and referred to as the "hierarchy problem".

Moreover, if one demands the unification of all gauge couplings at a high scale, new particles need to contribute to the coefficients of the running couplings, otherwise the couplings g_1, g_2, g_3 do not coincide [31]. It would be appealing to embed the semi-simple SM group into a larger simple group of a Grand Unified Theory (GUT) with $M_W \ll M_{\mathrm{GUT}} < M_P$. In addition, the SM does not explain the hierarchy of fermion masses.

Besides the theoretical motivations to extend the SM, there is also experimental evidence that new physics must exist. As mentioned above, the measurement of neutrino oscillations, e.g. in Refs. [32, 33], are indicative of non-vanishing neutrino masses. Furthermore, astrophysical observations imply that only 5% of the energy content of the universe is made of ordinary matter, whereas Dark Matter (DM) and Dark Energy (DE) constitute 27% and 68% [34], respectively. However, the SM does not offer any viable candidate for DM, which ought to be stable on cosmological time scales and to interact only weakly with SM particles. In addition, the observed matter-antimatter asymmetry in the universe calls for additional sources of $\mathcal{CP}$-violation beyond the single complex phase in the CKM matrix in order to meet the Sakharov conditions [35].

Various extensions of the SM have been proposed in order to tackle its shortcomings. For example additional dimensions of space-time, new strong dynamics in composite Higgs models, further symmetries (such as supersymmetry or larger gauge groups of a GUT) and string theory –or combinations of those approaches – offer interesting concepts (see e.g. Refs. [36–39]) whereas no particles beyond the SM have been observed yet.

Among the BSM options, a strikingly elegant and widely studied solution to several of the aforementioned problems of the SM is supersymmetry (SUSY) - a new symmetry relating fermions to bosons. In this thesis we focus on SUSY, but mention also few characteristics of other models beyond the SM when developing a model-independent method in Chap. 7 for interference effects between new particles.

Chapter 3.

Minimal Supersymmetric Standard Model with complex parameters

Based on Refs. [22,40–45], this chapter introduces some basic concepts of supersymmetry and outlines properties of the MSSM relevant for this thesis, with a focus on the Higgs sector and the role of complex phases of MSSM parameters.

3.1. Supersymmetry

3.1.1. Features of supersymmetry

Supersymmetry relates bosons to fermions by a symmetry. It is mathematically well motivated and has profound phenomenological implications, which are probed at the LHC. For each SM fermion f, SUSY predicts a scalar superpartner, a sfermion denoted by $\tilde{f}$. Vice versa, each SM gauge boson receives a fermionic superpartner, a gaugino. SUSY requires at least two Higgs doublets (see Sect. 3.2.1) and their fermionic partners are called higgsinos. Each SM particle has the same quantum numbers as its superpartner except the spin.

SUSY may offer a solution to the hierarchy problem. SM fermion loops in the Higgs self-energy contribute proportional to $-y_f^2\Lambda^2$, where y_f is the Yukawa coupling and Λ the cut-off of the integral. The sfermion contributions are proportional to $y_{\tilde{f}}\Lambda^2$ and therefore also quadratically sensitive to the cut-off, where $y_{\tilde{f}}$ is the quartic scalar coupling involving two Higgs bosons and two sfermions. Thus, the quadratic corrections to the Higgs mass vanish if each fermion chirality state $f_{L/R}$ has a superpartner $\tilde{f}_{L/R}$[1] and if the dimensionless couplings are related by

$$y_{\tilde{f}} = y_f^2. \tag{3.1}$$

The cancellation of the Λ^2-term holds independently of the masses of the superpartners. In addition, ΔM_H^2 contains terms proportional to $\ln\Lambda$. If furthermore the masses were exactly degenerate, $m_f = m_{\tilde{f}}$, also the logarithmic contributions would vanish so that $\Delta M_H^2 = 0$ in the case of exact SUSY (see Sect. 3.1.2). However, the non-observation of SUSY partners so far indicates that SUSY – if existing in nature – must be broken (see

[1] The sfermions as scalars do not have a chirality. The subscript L/R of $\tilde{f}$ just denotes the superpartner of the chiral fermion $f_{L/R}$.

Sect. 3.2.3). SUSY breaking induces a mass splitting in $m_{\tilde{f}}^2 = m_f^2 + \Delta^2$. The cancellation of the problematic quadratic correction is not spoiled by Δ^2, but the logarithmic terms combine to $\Delta M_H^2 \sim \ln\left(\frac{m_{\tilde{f}}}{m_f}\right)$, which stays acceptably small if the splitting is of the order or slightly above the weak scale. So in order not to re-introduce the fine-tuning of the Higgs mass, SUSY is best motivated for superpartner masses around the TeV scale.

Another feature of SUSY is that it improves the unification of the running gauge couplings because group theoretical factors of the superpartners influence the renormalisation group equation. Furthermore, the SUSY particle spectrum provides new neutral and weakly interacting fields which constitute suitable candidates for cold dark matter. Moreover, several parameters introduced by SUSY and SUSY breaking can in principle be complex, offering contributions to the amount of $\mathcal{CP}$-violation necessary to explain the observed baryon asymmetry of the universe (see Sect. 3.4).

It is compelling that the phenomenological consequences of SUSY address many of the shortcomings of the SM although the initial mathematical motivation for SUSY was independent of them.

3.1.2. SUSY algebra and superpotential

Symmetry is a driving principle of constructing physical theories and has led to accurate predictions in the case of the SM. However, the SM gauge groups might not exhaust all symmetries of nature which are compatible with Lorentz invariance. In their famous no-go theorem, Coleman and Mandula proved [46] that the only Lie group containing the Poincaré group for a relativistic quantum field theory in $3+1$ dimensions is the direct product of the Poincaré space-time symmetries and inner symmetries. Since in a direct product of groups all generators of one group commute with all generators of the other group, this is only a trivial extension.

However, Haag, Łopuszanski and Sohnius [36] proposed to replace the ordinary Lie algebra by a graded (or super-)Lie algebra. This bypasses the no-go theorem with supersymmetry as the unique non-trivial extension of the spacetime symmetries of the Poincaré algebra.

The supersymmetry generator Q alters the spin of a particle by $1/2$ and thus relates fermions to bosons. With Lorentz index μ, spinor indices $\alpha, \beta, \dot{\alpha}, \dot{\beta}$ and four-momentum P^μ, the SUSY algebra combines commutators and anticommutators:

$$\left\{Q_\alpha, Q_{\dot{\alpha}}^\dagger\right\} = -2\sigma^\mu_{\alpha\dot{\alpha}} P_\mu, \quad \{Q_\alpha, Q_\beta\} = \left\{Q_{\dot{\alpha}}^\dagger, Q_{\dot{\beta}}^\dagger\right\} = 0, \quad [P^\mu, Q_\alpha] = \left[P^\mu, Q_{\dot{\alpha}}^\dagger\right] = 0. \tag{3.2}$$

Irreducible representations of the SUSY algebra are so-called supermultiplets, which comprise SM particles and their superpartners and contain an equal number of fermionic and bosonic degrees of freedom. Eq. (3.2) even implies

$$\left[Q_\alpha, P^2\right] = [Q_\alpha, P_\mu] P^\mu + P_\mu [Q_\alpha, P^\mu] = 0, \tag{3.3}$$

which predicts that all fields in one supermultiplet are mass degenerate if SUSY is unbroken. Further, the SUSY generators $Q, Q^\dagger$ commute with all generators of the gauge group so that all fields within one multiplet share the same quantum numbers except the spin. For the embedding of the SM into SUSY, there are on the one hand chiral multiplets containing a left-handed SM Weyl spinor ψ, a scalar superpartner ϕ and a bosonic auxiliary field F. On the other hand, a vector supermultiplet consists of a SM gauge boson A^a_μ, a gaugino λ^a and a real, bosonic auxiliary field D^a, where the index a refers to the adjoint representation of each gauge group. The auxiliary fields need to be introduced in order to close the SUSY algebra[2] also off-shell, i.e. without imposing the equations of motion of the propagating fields, by balancing the fermionic and bosonic degrees of freedom within one supermultiplet. F and D^a vanish on-shell, have no kinetic term, do not propagate, but can be involved in interaction terms. The most general set of renormalisable, SUSY preserving non-gauge interactions is collected in the superpotential

$$W = L^i \phi_i + \frac{1}{2} M^{ij} \phi_i \phi_j + \frac{1}{6} y^{ijk} \phi_i \phi_j \phi_k, \tag{3.4}$$

which is a holomorphic function of the complex scalar fields ϕ_i. The linear term is only allowed if ϕ_i is a gauge singlet. The SUSY Lagrangian $\mathcal{L}_{\text{SUSY}} = \mathcal{L}_{\text{chiral}} + \mathcal{L}_{\text{gauge}} + \mathcal{L}_{\text{SUSYgauge}}$ consists of terms with the free and interacting chiral supermultiplets, the gauge supermultiplets and the supersymmetric gauge interactions, respectively,

$$\mathcal{L}_{\text{chiral}} = -D^\mu \phi^{*i} D_\mu \phi_i + i \psi^{\dagger i} \overline{\sigma}^\mu D_\mu \psi_i + F^{*i} F_i + \left[\left(-\frac{1}{2} W^{ij} \psi_i \psi_j + W^i F_i \right) + c.c. \right], \tag{3.5}$$

$$\mathcal{L}_{\text{gauge}} = -\frac{1}{4} F^a_{\mu\nu} F^{\mu\nu a} + i \lambda^{a\dagger} \overline{\sigma}^\mu D_\mu \lambda^a + \frac{1}{2} D^a D^a, \tag{3.6}$$

$$\mathcal{L}_{\text{SUSYgauge}} = -\sqrt{2} g \left((\phi^* T^a \psi) \lambda^a + \lambda^{\dagger a} (\psi^\dagger T^a \phi) \right) + g (\phi^* T^a \phi) D^a, \tag{3.7}$$

where $F^a_{\mu\nu}$ are the field strength tensors, g the gauge couplings, T^a the gauge group generators and $W_i = \frac{\partial W}{\partial \phi_i}$, $W_{ij} = \frac{\partial^2 W}{\partial \phi_i \partial \phi_j}$. In the extraction of the scalar potential V, one substitutes the auxiliary fields by their equations of motion, which reveal that F_i and D^a are algebraic in the scalar fields (i.e., no derivatives involved): $F_i = -W_i^*$, $F^{i*} = -W^i$ and $D^a = -g(\phi^* T^a \phi)$. Therefore, the scalar potential consisting of an "F-term" V_F and a "D-term" V_D,

$$V(\phi, \phi^*) = V_F + V_D = F^{i*} F_i + \frac{1}{2} D^a D^a = W_i^* W^i + \frac{1}{2} g_a^2 (\phi^* T^a \phi)^2, \tag{3.8}$$

is bounded from below (on account of the sum of squares). Remarkably, it is determined by those parameters of the theory that are already present in the SM, such as fermion masses, Yukawa couplings in V_F and gauge couplings in V_D.

[2]The closure of the SUSY algebra means that the action is invariant under SUSY transformations. Hence, the variation of the Lagrangian must be at most a total derivative.

3.2. Definition of the MSSM

The minimal supersymmetric extension of the Standard Model (MSSM) [47–49] is the minimal extension of the SM that introduces SUSY. Any supersymmetric model calls for at least two Higgs doublets in order to render both the up-type and the down-type fermions massive. In the SM (see Sect. 2.2), this is achieved by one scalar doublet Φ with the vev in the lower component and $\overline{\Phi}$ with the vev in the upper component. This characteristic of the SM contrasts with the demand for a holomorphic superpotential W where the complex conjugate of the Higgs doublet would break SUSY. Furthermore, two Higgs doublets $\mathcal{H}_1 \equiv \mathcal{H}_d = (h_d^0, h_d^-)^T$ and $\mathcal{H}_2 \equiv \mathcal{H}_u = (h_u^+, h_u^0)^T$ with opposite hypercharges $Y_{\mathcal{H}_{1,2}} = \pm 1$ are required for the cancellation of a gauge anomaly.

The MSSM is a two-Higgs doublet model constrained by supersymmetry. Three out of the eight real degrees of freedom originating from the two complex scalar doublets turn into longitudinal modes of the massive gauge bosons upon electroweak symmetry breaking. Thus, five degrees of freedom remain that give rise to five physical Higgs bosons (see Sect. 3.3.4). Their partners are the Higgsinos $\tilde{h}_d^0, \tilde{h}_d^-, \tilde{h}_u^+, \tilde{h}_u^0$.

Apart from the additional Higgs doublet, the particle content is doubled with respect to the SM. There is one scalar superpartner per left- or right-handed fermion. The left-handed quark doublets are denoted as $q_i = (u_{i,L}, d_{i,L})$, and their superpartners are $\tilde{q}_i = (\tilde{u}_{i,L}, \tilde{d}_{i,L})$, where $i = 1, 2, 3$ is the family index. Both q_i and $\tilde{q}_i$ are contained in the chiral supermultiplet Q_i. As mentioned before, all members of a supermultiplet transform in the same representation under the SM gauge groups; their representation is listed in Tab. 3.1. As for the right-handed quarks, they are expressed as the conjugates of the left-handed ones in order to define all chiral supermultiplets in terms of left-handed Weyl spinors. In this convention, $\overline{u}_i$[3] stands for the supermultiplet made of a right-handed up-type quark singlet $u_{i,R}^\dagger \sim \overline{u}_{i,L}$ and its superpartner $\tilde{\overline{u}}_{i,R}^* \sim \tilde{\overline{u}}_{i,L}$. Likewise for the down-type quark singlets, $\overline{d}_i$ denotes the supermultiplet made up of $\overline{d}_{i,L}$ and $\tilde{\overline{d}}_{i,L}$.

The left-handed lepton doublets $e_i = (\nu_i, e_{i,L})$ appear with the sleptons $\tilde{e}_i = (\tilde{\nu}_i, \tilde{e}_{i,L})$ in the supermultiplet L_i. Since there are no right-handed neutrinos in the SM and MSSM, the supermultiplet $\overline{e}_i$ simply contains the charged lepton singlets $e_R^\dagger$ and $\tilde{e}_R^*$.

Concerning the gauge supermultiplets, the partner of the B is called bino $\tilde{B}$, the $W^\pm$, W^3-fields are grouped with the winos $\widetilde{W}^\pm, \widetilde{W}^3$ and gluons g^a with gluinos $\tilde{g}^a$, $a = 1...8$. All chiral and gauge supermultiplets of the MSSM with their representations are assembled in Tab. 3.1.

3.2.1. The MSSM superpotential

The non-gauge interactions of the MSSM are specified by the following superpotential:

$$W^{\mathrm{MSSM}} = \overline{u}\, \mathbf{y_u}\, Q \cdot \mathcal{H}_2 - \overline{d}\, \mathbf{y_d}\, Q \cdot \mathcal{H}_1 - \overline{e}\, \mathbf{y_e}\, L \cdot \mathcal{H}_1 + \mu\, \mathcal{H}_1 \cdot \mathcal{H}_2, \tag{3.9}$$

[3]The bar over the fermion name should be understood as a part of the symbol representing the antiparticle instead of an operation like Dirac conjugation in the notation of Ref. [41].

Chiral		**spin-0** ($R=-1$)	**spin-1/2** ($R=+1$)	$SU(3)_C$	$SU(2)_L$	$U(1)_Y$
(s)quarks	Q	$(\widetilde{u}_L, \widetilde{d}_L)$	(u_L, d_L)	**3**	**2**	1/3
	$\bar{u}$	$\widetilde{u}_R^*$	$u_R^\dagger$	$\bar{\mathbf{3}}$	**1**	-4/3
	$\bar{d}$	$\widetilde{d}_R^*$	$d_R^\dagger$	$\bar{\mathbf{3}}$	**1**	2/3
(s)leptons	L	$(\widetilde{\nu}, \widetilde{e}_L)$	(ν, e_L)	**1**	**2**	-1
	$\bar{e}$	$\widetilde{e}_R^*$	$e_R^\dagger$	**1**	**1**	2
		$(R=+1)$	$(R=-1)$			
Higgs, Higgsinos	$\mathcal{H}_1$	(h_d^0, h_d^-)	$(\widetilde{h}_d^0, \widetilde{h}_d^-)$	**1**	**2**	-1
	$\mathcal{H}_2$	(h_u^+, h_u^0)	$(\widetilde{h}_u^+, \widetilde{h}_u^0)$	**1**	**2**	1
Gauge		**spin-1** ($R=+1$)	**spin-1/2** ($R=-1$)			
B-boson, bino		B	$\widetilde{B}$	**1**	**1**	0
W-boson, wino		$W^\pm, W^3$	$\widetilde{W}^\pm, \widetilde{W}^3$	**1**	**3**	0
gluon, gluino		g^a	$\widetilde{g}^a$	**8**	**1**	0

Table 3.1.: Chiral and gauge supermultiplets of the MSSM (with $SU(3)_C$ gauge index $a = 1, ..., 8$, but family indices suppressed) [40, 41]. Some of them mix into mass eigenstates, see Tab. 3.2.

where the dot denotes the $SU(2)$-invariant product contracted by the total antisymmetric tensor $\epsilon_{\alpha\beta}$ with the convention $\epsilon_{12} = 1$. For instance, the last term can be expresses as $\epsilon^{\alpha\beta}\mu\,\mathcal{H}_{1\alpha}\mathcal{H}_{2\beta}$. The Yukawa matrices $\mathbf{y_{u,d,e}}$ in family space (the sum over family indices is implied) are the same as in the SM. They give rise to masses of the chiral supermultiplets. A conventional mass term involving a scalar and its conjugate would violate SUSY. In Eq. 3.4, however, the superpotential W of a general SUSY theory contains a bilinear combination of scalar fields. In the MSSM, only one such combination is possible, namely the μ-term with each of the Higgs doublets. The dimensionful parameter μ may be understood a supersymmetric version of a Higgs and Higgsino mass term.

3.2.2. R-parity

In the SM Lagrangian, no renormalisable terms are possible that violate the lepton number L or baryon number B so that they are rather accidentally conserved. On the contrary, in the MSSM gauge invariance and renormalisability do not exclude B and L violating terms (in addition to the B, L conserving superpotential given in Eq. (3.9)), which may lead to a rapid proton decay. Although B- and L- violating processes have not been observed experimentally, baryon and lepton number conservation cannot be assumed to be a fundamental symmetry. So a new symmetry, called R-parity [50] as the discrete subgroup $\mathbb{Z}_2$ of a continuous $U(1)$, is introduced. It forbids the baryon and lepton number violating terms, but allows all interactions in Eq. (3.9). The R-parity $R := (-1)^{3B+L+2s}$, where s denotes the spin, assigns $+1$ to SM particles and -1 to their SUSY partners. The conservation of the R-parity implies that SUSY particles can only be pair-produced and that the lightest supersymmetric particle (LSP) is absolutely stable. As a consequence, the final state in a decay of any sparticle must contain an odd number of LSPs. If the LSP is neutral under charge and colour, it interacts only weakly and it is suited as a candidate for non-baryonic cold dark matter [51, 52]. In the MSSM this role might be played for instance by the lightest neutralino $\widetilde{\chi}^0_1$.

3.2.3. Soft SUSY breaking

If SUSY were an exact symmetry, particles and their superpartners would have exactly the same mass. The non-observation of SUSY particles at energies reached up to now implies that SUSY can only be realised as a broken symmetry. Breaking can be triggered by non-vanishing F- or D-terms. Yet it remains an open question how this breaking of supersymmetry is accomplished. Approaches of spontaneous SUSY breaking are not viable in the MSSM. Instead, the breaking is assumed to happen in a hidden sector which has no direct renormalisable couplings to the visible sector of the SM fields together with their superpartners. While the phenomenology is largely insensitive to the exact dynamics of the SUSY breaking in the hidden sector, it does depend on the so far unknown way of mediation from the hidden to the visible sector. A crucial point is that SUSY breaking terms in the Lagrangian must not reintroduce the quadratic divergences in the Higgs mass correction whose cancellation were one feature of exact SUSY. The terms proportional to Λ^2 in ΔM_H^2 are avoided by allowing only so-called *soft* terms that, by having a positive mass dimension, are super-renormalisable and maintain the relations between dimensionless couplings, namely all gauge and Lorentz invariant terms of dimension two and three.

In order to describe the SUSY breaking irrespective of the actual SUSY breaking mechanism, the ignorance of the precise mediation of the breaking is parametrised in the soft Lagrangian, $\mathcal{L}_{\text{soft}}$. The most general Lagrangian for soft SUSY breaking terms that is allowed by gauge invariance and conserves R-parity is [40, 41]

$$\begin{aligned}
\mathcal{L}_{\text{soft}} = &-\frac{1}{2}\Big(M_3\,\tilde{g}^a\tilde{g}^a + M_2\,\tilde{W}^a\tilde{W}^a + M_1\,\tilde{B}\tilde{B} + c.c.\Big)\\
&-\tilde{Q}^\dagger\mathbf{m}^{\mathbf{2}}_{\tilde{\mathbf{Q}}}\,\tilde{Q} - \widetilde{L}^\dagger\mathbf{m}^{\mathbf{2}}_{\tilde{\mathbf{L}}}\,\widetilde{L} - \tilde{\bar{u}}\,\mathbf{m}^{\mathbf{2}}_{\tilde{\bar{\mathbf{u}}}}\,\tilde{\bar{u}}^\dagger - \tilde{\bar{d}}\,\mathbf{m}^{\mathbf{2}}_{\tilde{\bar{\mathbf{d}}}}\,\tilde{\bar{d}}^\dagger - \tilde{\bar{e}}\,\mathbf{m}^{\mathbf{2}}_{\tilde{\bar{\mathbf{e}}}}\,\tilde{\bar{e}}^\dagger\\
&-\Big(\tilde{\bar{u}}\,\mathbf{a_u}\,\widetilde{Q}\cdot\mathcal{H}_2 - \tilde{\bar{d}}\,\mathbf{a_d}\,\widetilde{Q}\cdot\mathcal{H}_1 - \tilde{\bar{e}}\,\mathbf{a_e}\,\widetilde{Q}\cdot\mathcal{H}_1 + c.c.\Big)\\
&-m^2_{\mathcal{H}_1}\mathcal{H}_1^*\cdot\mathcal{H}_1 - m^2_{\mathcal{H}_2}\mathcal{H}_2^*\cdot\mathcal{H}_2 - (m^2_{12}\,\mathcal{H}_1\cdot\mathcal{H}_2 + c.c.).
\end{aligned}\tag{3.10}$$

In the first line of Eq. (3.10), a denotes the gauge index and M_1, M_2, M_3 are the soft gaugino masses of the bino, winos and gluinos, respectively. Explicit mass terms of gauginos do not damage gauge invariance because gauginos are in a real representation of the gauge groups [41]. The second line provides the soft sfermion squared masses $\mathbf{m}^{\mathbf{2}}_{\tilde{\mathbf{f}}}$ for $\tilde{f} = \tilde{Q}, \tilde{L}, \tilde{u}, \tilde{d}, \tilde{e}$. As a result of those mass terms, SM particles and their superpartners are no longer mass degenerate. The third line introduces dimensionful trilinear couplings $\mathbf{a_u}$, $\mathbf{a_d}$, $\mathbf{a_e}$, which appear as the interaction between a Higgs boson and two sfermions. Finally, the last line contains squared masses for the Higgs supermultiplets as well as a bilinear term in the Higgs fields. The $\mathbf{a_{u,d,e}}$ and the m^2_{12} terms are analogous to the SUSY-conserving Yukawa interactions and the μ-term in Eq. (3.9), but here only the

Higgses and not the Higgsinos are involved so that each line in Eq. (3.10) breaks SUSY. Non-vanishing soft Higgs masses are required for electroweak symmetry breaking in the MSSM, as we will see in Sect. 3.3.4.

While the SUSY preserving superpotential introduced only one additional parameter (μ) with respect to the SM, the soft breaking gives rise to numerous masses, mixing angles and couplings with possibly complex phases. Effectively, the MSSM contains 105 independent new parameters, which reduce the predictivity of the model. Therefore simplifying assumptions, such as presuming universal masses and couplings at a high scale or reducing the number of free parameters at a low scale, are often employed to facilitate experimental analyses and phenomenological studies in a lower dimensional parameter space. In fact, experimental constraints point to universal structures.

Since most MSSM parameters stem from the flavour sector, regarding SUSY breaking as “flavour-blind”, i.e. universal with respect to flavour, reduces the set of free parameters and simultaneously avoids severely constrained flavour changing neutral currents. This reduces the sfermion mass matrices, which are generally 3×3 matrices in family space, to their diagonal entries. Supposing in addition minimal flavour violation (MFV) [53–55], namely that SUSY does not introduce any flavour violation beyond that already present in the SM, the structure of the trilinear couplings is given by the Yukawa matrices:

$$\mathbf{a}_u = A_u\,\mathbf{y_u}, \qquad \mathbf{a}_d = A_d\,\mathbf{y_d}, \qquad \mathbf{a}_e = A_e\,\mathbf{y_e}. \tag{3.11}$$

If one further neglects quark mixing between generations (as we do in fact in this thesis), the $\mathbf{a}$-matrices become diagonal:

$$a_{u_i} = A_{u_i}\,y_{u_i}, \qquad a_{d_i} = A_{d_i}\,y_{d_i}, \qquad a_{e_i} = A_{e_i}\,y_{e_i}. \tag{3.12}$$

Another simplifying assumption is the unification of gaugino masses M_1 and M_2 at the GUT scale:

$$M_1 = \frac{5}{3}\frac{s_W^2}{c_W^2} M_2. \tag{3.13}$$

3.3. Physical fields of the MSSM

The field content of the MSSM allows for mixing of the particles introduced so far into physical states, see Tab. 3.2. The mass eigenstates and mixing properties of the different sectors will be described in more detail in the next sections.

Names	Physical states	Gauge eigenstates
neutral Higgs bosons	h, H, A	h_u^0, h_d^0
charged Higgs bosons	$H^\pm$	h_u^+, h_d^-
neutral gauge bosons	A, Z	B, W^3, h_u^0, h_d^0
charged gauge bosons	$W^\pm$	$W^\pm, h_u^+, h_d^-$
sfermions	$\tilde{f}_1, \tilde{f}_2$	$\tilde{f}_L, \tilde{f}_R^*$
neutralinos	$\widetilde{\chi}_1^0, \widetilde{\chi}_2^0, \widetilde{\chi}_3^0, \widetilde{\chi}_4^0$	$\widetilde{B}, \widetilde{W}^3, \tilde{h}_u^0, \tilde{h}_d^0$
charginos	$\widetilde{\chi}_1^\pm, \widetilde{\chi}_2^\pm$	$\widetilde{W}^\pm, \tilde{h}_u^+, \tilde{h}_d^-$

Table 3.2.: Physical mass eigenstates of the MSSM (apart from SM fermions, gluons and gluinos) arising from mixtures of gauge eigenstates in Tab. 3.1.

3.3.1. Sfermion sector

The mixing of sfermions $\tilde{f}_L, \tilde{f}_R$ within one generation into mass eigenstates $\tilde{f}_1, \tilde{f}_2$ is parametrised by the matrix

$$M_{\tilde{f}}^2 = \begin{pmatrix} M_{\tilde{f}_L}^2 + m_f^2 + M_Z^2 \cos 2\beta (I_f^3 - Q_f s_W^2) & m_f X_f^* \\ m_f X_f & M_{\tilde{f}_R}^2 + m_f^2 + M_Z^2 \cos 2\beta Q_f s_W^2 \end{pmatrix}, \tag{3.14}$$

$$X_f := A_f - \mu^* \cdot \begin{cases} \cot\beta, & f = \text{up-type} \\ \tan\beta, & f = \text{down-type.} \end{cases} \tag{3.15}$$

The trilinear couplings $A_f = |A_f| e^{i\phi_{A_f}}$, as well as $\mu = |\mu| e^{i\phi_\mu}$, can be complex. These phases enter the Higgs sector via sfermion loops starting at one-loop order. Diagonalising $M_{\tilde{f}}^2$ for all $\tilde{f}$ separately, one obtains the sfermion masses $m_{\tilde{f}_1} \leq m_{\tilde{f}_2}$:

$$\begin{pmatrix} \tilde{f}_1 \\ \tilde{f}_2 \end{pmatrix} = U_{\tilde{f}} \begin{pmatrix} \tilde{f}_L \\ \tilde{f}_R \end{pmatrix}, \tag{3.16}$$

where $U_{\tilde{f}}$ is a unitary matrix that leads to $U_{\tilde{f}} M_{\tilde{f}} U_{\tilde{f}}^\dagger = \mathrm{diag}(m_{\tilde{f}_1}, m_{\tilde{f}_2})$. The Langrangian can then be expressed in terms of the mass eigenstates,

$$\mathcal{L}_{\tilde{f}} = -\left(\tilde{f}_1^\dagger, \tilde{f}_2^\dagger\right) U_{\tilde{f}} M_{\tilde{f}} U_{\tilde{f}}^\dagger \left(\tilde{f}_1^\dagger, \tilde{f}_2^\dagger\right)^T. \tag{3.17}$$

For the first two generations, the sfermion masses exceed the masses of their SM partners so that the hierarchy of the matrix elements in Eq. (3.14) is approximately diagonal. However, in the case of the stop and, for sufficiently high $\tan\beta$, also sbottom, the mixing can be rather large.

3.3.2. Gluino sector

The gluino $\tilde{g}^a,\ a = 1, 2, 3$ with spin $s = \frac{1}{2}$ has a mass of

$$m_{\tilde{g}} = |M_3|, \tag{3.18}$$

where $M_3 = |M_3|\, e^{i\phi_{M_3}}$ is the possibly complex gluino mass parameter. The gluino cannot mix with any other fields and its mass term in the tree-level Lagrangian is given by

$$\mathcal{L}_{\tilde{g}} = -\frac{1}{2}\bar{\tilde{g}}|M_3|\tilde{g}. \tag{3.19}$$

Since the gluino does not directly couple to the Higgs, the phase ϕ_{M_3} enters the Higgs sector at the two-loop level, but has an impact for example on the bottom Yukawa coupling already at one-loop order.

3.3.3. Neutralino and chargino sector

At tree-level, mixing in the chargino sector is governed by the higgsino and wino mass parameters μ and M_2, respectively. In the neutralino sector it additionally depends on the bino mass parameter M_1. The charginos $\widetilde{\chi}_i^\pm,\ i = 1, 2$, as mass eigenstates are superpositions of the charged winos $\widetilde{W}^\pm$ and higgsinos $\widetilde{H}^\pm$, with mass matrix X,

$$\begin{pmatrix} \widetilde{\chi}_1^+ \\ \widetilde{\chi}_2^+ \end{pmatrix} = V \begin{pmatrix} \tilde{W}^+ \\ \widetilde{\chi}_i^+ \end{pmatrix}, \qquad \begin{pmatrix} \widetilde{\chi}_1^- \\ \widetilde{\chi}_2^- \end{pmatrix} = U \begin{pmatrix} \tilde{W}^- \\ \widetilde{\chi}_i^- \end{pmatrix}, \qquad X = \begin{pmatrix} M_2 & \sqrt{2}M_W s_\beta \\ \sqrt{2}M_W c_\beta & \mu \end{pmatrix}. \tag{3.20}$$

In order to obtain the Dirac chargino masses, X is diagonalised by the biunitary transformation

$$\mathrm{diag}(m_{\widetilde{\chi}_1^\pm}, m_{\widetilde{\chi}_2^\pm}) = U^* X V^\dagger. \tag{3.21}$$

At lowest order, the chargino Lagrangian reads [45]

$$\mathcal{L}_{\widetilde{\chi}^\pm} = \overline{\widetilde{\chi}_i^-}[\not{p}\delta_{ij} - \omega_L(U^* X V^\dagger)_{ij} - \omega_R(V X^\dagger U^T)_{ij}]\widetilde{\chi}_j^-, \tag{3.22}$$

where $\overline{\widetilde{\chi}_i^-} = \widetilde{\chi}_j^{-\dagger}\gamma^0$. Likewise in the neutralino sector, the neutral electroweak gauginos $\widetilde{B}$, $\widetilde{W}^3$ and the neutral Higgsinos $\tilde{h}_d^0$, $\tilde{h}_u^0$ mix into the mass eigenstates $\widetilde{\chi}_i^0$, $i = 1, ..., 4$. The mixing is encoded in the gaugino mass matrix Y,

$$\begin{pmatrix} \widetilde{\chi}_1^0 \\ \widetilde{\chi}_2^0 \\ \widetilde{\chi}_3^0 \\ \widetilde{\chi}_4^0 \end{pmatrix} = N \begin{pmatrix} \widetilde{B} \\ \widetilde{W}^3 \\ \tilde{h}_d^0 \\ \tilde{h}_u^0 \end{pmatrix}, \qquad Y = \begin{pmatrix} M_1 & 0 & -M_Z c_\beta s_W & M_Z s_\beta s_W \\ 0 & M_2 & M_Z c_\beta c_W & -M_Z s_\beta c_W \\ -M_Z c_\beta s_W & M_Z c_\beta c_W & 0 & -\mu \\ M_Z s_\beta s_W & -M_Z s_\beta c_W & -\mu & 0 \end{pmatrix}. \tag{3.23}$$

Since neutralinos are Majorana particles, one unitary matrix $\tilde{N}$ suffices to diagonalise the symmetric mass matrix Y, which has real, but not necessarily positive eigenvalues,

$$\tilde{N}^* Y \tilde{N}^{-1} =: D' = \mathrm{diag}(m'_{\tilde{\chi}_1^0}, m'_{\tilde{\chi}_2^0}, m'_{\tilde{\chi}_3^0}, m'_{\tilde{\chi}_4^0}). \tag{3.24}$$

In order to obtain non-negative mass eigenvalues, the Takagi factorisation [56, 57] can be applied. If $m'_{\tilde{\chi}_j^0}$ is negative, one can rotate this eigenvalue by a unitary transformation T which can be chosen as a 4×4 unit matrix with an i on the jth position instead of the 1. Then, with $N := T \cdot \tilde{N}$, the diagonalisation

$$\begin{aligned} N^* D' N^{-1} &= T^*(\tilde{N}^* Y \tilde{N}^{-1}) T^{-1} = N^* Y N^{-1} \\ &=: D = \mathrm{diag}(m_{\tilde{\chi}_1^0}, m_{\tilde{\chi}_2^0}, m_{\tilde{\chi}_3^0}, m_{\tilde{\chi}_4^0}) \end{aligned} \tag{3.25}$$

yields $m_{\tilde{\chi}_i^0} \geq 0 \ \forall i = 1, .., 4$. Using $\tilde{\chi}_i^0 = N_{ij} \psi_j^0$ with $\psi^0 = (\tilde{B}, \tilde{W}^3, \tilde{h}_d^0, \tilde{h}_u^0)$, the neutralino part in the Lagrangian can be expressed in the mass eigenbasis:

$$\mathcal{L}_{\tilde{\chi}^0} = \frac{1}{2} \overline{\tilde{\chi}_i^0} [\not{p} \delta_{ij} - \omega_L (N^* Y N^\dagger)_{ij} - \omega_R (N Y^\dagger N^T)_{ij}] \tilde{\chi}_j^0. \tag{3.26}$$

The gaugino mass parameters M_1 and M_2 as well as the higgsino mass parameter can in principle be complex. However, only two of them are independent and one conventionally sets $\phi_{M_2} = 0$.

3.3.4. Higgs sector

3.3.4.1. Scalar potential

As mentioned before, the MSSM incorporates two complex scalar Higgs doublets with opposite hypercharge $Y_{\mathcal{H}_{1,2}} = \pm 1$,

$$\mathcal{H}_1 = \begin{pmatrix} h_d^0 \\ h_d^- \end{pmatrix} = \begin{pmatrix} v_d + \frac{1}{\sqrt{2}}(\phi_1^0 - i\chi_1^0) \\ -\phi_1^- \end{pmatrix} \tag{3.27}$$

$$\mathcal{H}_2 = \begin{pmatrix} h_u^+ \\ h_u^0 \end{pmatrix} = e^{i\xi} \begin{pmatrix} \phi_2^+ \\ v_u + \frac{1}{\sqrt{2}}(\phi_2^0 + i\chi_2^0) \end{pmatrix}. \tag{3.28}$$

The Higgs potential is composed of the Higgs parts of the F- and D-terms,

$$V_F = \left| \frac{\partial W}{\partial \mathcal{H}_1} \right|^2 + \left| \frac{\partial W}{\partial \mathcal{H}_2} \right|^2 \tag{3.29}$$

$$V_D = \frac{g_2^2}{2} \sum_{a=1}^{3} \left(\mathcal{H}_1^\dagger \frac{\sigma^a}{2} \mathcal{H}_1 + \mathcal{H}_2^\dagger \frac{\sigma^a}{2} \mathcal{H}_2 \right)^2 + \frac{g_1^2}{2} \left(\mathcal{H}_2^\dagger \frac{1}{2} \mathcal{H}_2 - \mathcal{H}_1^\dagger \frac{1}{2} \mathcal{H}_1 \right)^2, \tag{3.30}$$

and the soft breaking terms from the last line of Eq. (3.10):

$$\begin{aligned} V_H =&\ (V_F + V_D - \mathcal{L}_{\text{soft}})\big|_H \\ =&\ (|\mu|^2 + m^2_{\mathcal{H}_2})(|h^0_u|^2 + |h^+_u|^2) + (|\mu|^2 + m^2_{\mathcal{H}_1})(|h^0_d|^2 + |h^-_u|^2) \\ &+ [m^2_{12}(h^+_u h^-_d - h^0_u h^0_d) + h.c.] + \frac{g_1^2 + g_2^2}{8}\left[|h^0_u|^2 + |h^+_u|^2 - |h^0_d|^2 - |h^-_d|^2\right]^2. \end{aligned} \tag{3.31}$$

Hence the quadratic terms of V_H contain on the one hand the SUSY parameter $|\mu|^2$ and on the other hand the soft terms $m_{\mathcal{H}_1}, m_{\mathcal{H}_2}$. The bilinear terms come with the soft coefficient m^2_{12} whose phase can be absorbed in a redefinition of μ and m^2_{12} by means of a Peccei-Quinn symmetry [58, 59]. As a special feature of SUSY, the quartic term is determined by the gauge couplings g_1, g_2.

3.3.4.2. Conditions for electroweak symmetry breaking

Realising spontaneous electroweak symmetry breaking in the MSSM is more intricate than in the SM due to the second doublet. With a $SU(2)_L$ transformation, one component of each Higgs doublet can be rotated to have a vanishing vacuum expectation value, $\langle h^+_u \rangle = \langle h^-_d \rangle = 0$ so that $U(1)_{em}$ is conserved in the vacuum state. Therefore we discuss from now on the terms of neutral Higgs states in V_H,

$$V^0_H = (|\mu|^2 + m^2_{\mathcal{H}_2})|h^0_u|^2 + (|\mu|^2 + m^2_{\mathcal{H}_1})|h^0_d|^2 - [m^2_{12} h^0_u h^0_d + h.c.] + \frac{g_1^2 + g_2^2}{8}\left[|h^0_u|^2 - |h^0_d|^2\right]^2. \tag{3.32}$$

Breaking of the $SU(2)_L \otimes U(1)_Y$ gauge symmetry by this scalar potential can only be realised by a stable minimum of V^0_H different from the origin in field space. First of all, a stable theory requires the potential to be bounded from below, but the quartic D-term contribution vanishes identically for $|h_d| = |h_d|$ ("D-flat direction"). Hence for stability in the critical $|h_d| = |h_d|$ direction, the following relation between μ and the soft parameters must be fulfilled:

$$2|\mu|^2 + m^2_{\mathcal{H}_2} + m^2_{\mathcal{H}_1} > 2m^2_{12} > 0. \tag{3.33}$$

On the other hand, electroweak symmetry breaking requires an unstable origin $(h^0_u, h^0_d) = (0, 0)$, hence a saddle point at $|h^0_u| = |h^0_u| = 0$,

$$(\mu|^2 + m^2_{\mathcal{H}_2})\,(\mu|^2 + m^2_{\mathcal{H}_1}) < m^2_{12}. \tag{3.34}$$

Eqs. (3.33) and (3.34) cannot be simultaneously satisfied for $m^2_{\mathcal{H}_2} = m^2_{\mathcal{H}_1}$ – in particular not for $m^2_{\mathcal{H}_1} = m^2_{\mathcal{H}_2} = 0$. Thus, the breaking of $SU(2)_L \otimes U(1)_Y$ to $U(1)_{em}$ requires non-zero soft Higgs mass terms. Consequently, there is no EWSB in exact SUSY[4].

[4] If $m^2_{\mathcal{H}_1} = m^2_{\mathcal{H}_2}$ at the GUT scale, radiative corrections involving the large top Yukawa coupling can drive $m^2_{\mathcal{H}_2}$ to small values (unequal to $m^2_{\mathcal{H}_1}$) at the electroweak scale ("radiative EWSB").

If, however, $m^2_{\mathcal{H}_1}, m^2_{\mathcal{H}_2}$ are non-degenerate and at least one of them non-zero, the neutral Higgs components acquire non-vanishing, real vacuum expectation values

$$v_d \equiv \langle h_d^0 \rangle, \qquad v_u \equiv \langle h_u^0 \rangle, \tag{3.35}$$

which follow from the conditions $\partial_{h_u^0} V = \partial_{h_u^0} V = 0$ for a stationary point of V_H^0 at $(|h_u^0| = v_u, |h_d^0| = v_d)$. The vevs v_u and v_d are related to the vev of the SM Higgs by

$$v_u^2 + v_d^2 = v_{\text{SM}}^2, \tag{3.36}$$

and their ratio represents the up- and the down-type contribution to EWSB:

$$\tan\beta := \frac{v_u}{v_d}. \tag{3.37}$$

The minimisation conditions yield the following relation:

$$\frac{M_Z^2}{2} = -\mu^2 + \frac{m^2_{\mathcal{H}_1} - m^2_{\mathcal{H}_2}\tan^2\beta}{\tan^2\beta - 1}. \tag{3.38}$$

The three involved scales have a different origin. While μ is a SUSY parameter, $m^2_{\mathcal{H}_1}, m^2_{\mathcal{H}_2}$ come from the soft breaking scale m_{soft}, which is expected somewhat above the weak scale. However, these a priori unrelated parameters need to combine to the left-hand side of Eq. (3.38). This so-called μ-problem or little hierarchy problem might be solved in the next-to minimal supersymmetric SM (NMSSM) [60] where μ arises naturally at the electroweak scale as the vev of an additional Higgs singlet. Nevertheless, this thesis deals with the MSSM.

3.3.4.3. Masses and mixings

Analogously to the SM, the Higgs doublets can be expanded around the vevs as shown in the second equality of Eqs. (3.27,3.28), where ϕ_i denote the $\mathcal{CP}$-even states and χ_j the $\mathcal{CP}$-odd ones. This expansion is inserted into the scalar potential, which contains (apart from trilinear and quartic terms) the following linear tadpole and bilinear mass terms with $\Phi^0 := (\phi_1^0, \phi_2^0, \chi_1^0, \chi_2^0)$ and $\Phi^\pm := (\phi_1^\pm, \phi_2^\pm)$:

$$V_H \supset -\sum_i T_i \Phi_i^0 + \frac{1}{2}\Phi^0 \mathbf{M}_{\phi\phi\chi\chi}\Phi^{0T} + \frac{1}{2}\Phi^- \mathbf{M}_{\phi^\pm\phi^\pm}\Phi^{+T}, \tag{3.39}$$

where T_i are the tadpole coefficients, $\mathbf{M}_{\phi\phi\chi\chi}$ the 4×4 real, symmetric mass matrix of the neutral degrees of freedom and $\mathbf{M}_{\phi^\pm\phi^\pm}$ the 2×2 Hermitian mass matrix of the charged Higgs components. The minimum conditions for V_H require the tadpole coefficients and the relative phase ξ between $\mathcal{H}_1$ and $\mathcal{H}_2$ to vanish at tree level[5]. Since no phase is left, the Higgs sector conserves $\mathcal{CP}$ at lowest order. Hence, $\mathbf{M}_{\phi\phi\chi\chi}$ becomes block-diagonal because entries of the type $M_{\phi_i\chi_j}$ would involve $\mathcal{CP}$-violating mixing. The mass eigenstates are

[5] The tadpole coefficients T_i and the phase ξ drop out at the tree-level, but they need to be considered for the renormalisation. So the minimisation of the potential is necessary order-by-order.

obtained by a diagonalisation of $\mathbf{M}_{\phi\phi\chi\chi}$ and $\mathbf{M}_{\phi^\pm\phi^\pm}$ (by unitary matrices $\mathbf{U}_n(\alpha,\beta_n)$ and $\mathbf{U}_c(\beta_c)$, respectively):

$$\begin{pmatrix} h \\ H \\ A \\ G \end{pmatrix} = \begin{pmatrix} -s_\alpha & c_\alpha & 0 & 0 \\ c_\alpha & s_\alpha & 0 & 0 \\ 0 & 0 & -s_{\beta_n} & c_{\beta_n} \\ 0 & 0 & c_{\beta_n} & s_{\beta_n} \end{pmatrix} \begin{pmatrix} \phi_1^0 \\ \phi_2^0 \\ \chi_1^0 \\ \chi_2^0 \end{pmatrix}, \qquad \begin{pmatrix} H^\pm \\ G^\pm \end{pmatrix} = \begin{pmatrix} -s_{\beta_c} & c_{\beta_c} \\ c_{\beta_c} & s_{\beta_c} \end{pmatrix} \begin{pmatrix} \phi_1^\pm \\ \phi_2^\pm \end{pmatrix}, \tag{3.40}$$

where we introduced the short-hand notation $s_x \equiv \sin x,\ c_x \equiv \cos x$. For later use we define $t_\beta \equiv \tan\beta$. The mixing angle α acts for the $\mathcal{CP}$-even Higgs bosons h, H; β_n for the neutral $\mathcal{CP}$-odd Higgs A and Goldstone boson G and β_c for the charged Higgs $H^\pm$ and the charged Goldsone boson $G^\pm$. The minimum conditions for V_H lead to $\beta = \beta_n = \beta_c$ at tree level. At higher orders, however, $\tan\beta$ must be renormalised whereas the mixing angles α, β_n and β_c are not renormalised, see Sect. 4.4. The angles α and β are related by

$$\tan(2\alpha) = \frac{m_A^2 + M_Z^2}{m_A^2 - M_Z^2}\tan(2\beta). \tag{3.41}$$

At tree-level, the relation

$$m_{h/H}^2 = \frac{1}{2}\left(m_A^2 + M_Z^2 \mp \sqrt{\left(m_A + M_Z^2\right)^2 - 4m_A^2 M_Z^2\cos^2(2\beta)}\right) \tag{3.42}$$

leads to the upper limit $m_h \leq M_Z$, which was excluded by LEP for a $\mathcal{CP}$-even Higgs boson [61]. Nevertheless, sizable 1-loop corrections (especially from the third generation quarks and their superpartners due to the largest coupling) shift this upper bound to roughly 140 GeV or higher [62–66]. Many diagrams contribute to M_h at one-loop order; the leading one-loop correction is

$$M_h^2 \lesssim M_Z^2 + \frac{3g^2 m_t^4}{8\pi^2 M_W^2}\left[\ln\left(\frac{M_S^2}{m_t^2}\right) + \frac{X_t^2}{M_S^2}\left(1 - \frac{X_t^2}{12M_S^2}\right)\right] \tag{3.43}$$

$$\text{with } X_t \equiv A_t - \mu\cot\beta, \quad M_S^2 = \frac{1}{2}(m_{\tilde{t}_1}^2 + m_{\tilde{t}_2}^2), \tag{3.44}$$

where A_t is the trilinear top coupling and M_S^2 the average squared stop mass, see Sect. 3.3.1. However, the leading 2-loop corrections [67] lead to a considerable reduction of the upper bound on M_h to about 130 GeV.

The masses of the $\mathcal{CP}$-odd and the charged Higgs bosons are at tree level related by

$$m_{H^\pm}^2 = m_A^2 + M_W^2, \tag{3.45}$$

$$m_A^2 = \frac{2m_{12}^2}{\sin(2\beta)}. \tag{3.46}$$

Three of the initially five independent parameter combinations in Eq. (3.32) are eliminated by Eq. (3.36) via the measured gauge boson masses and by the two minimisation conditions.

Thus, the Higgs sector is at lowest order fully determined by the two SUSY input parameters (in addition to SM masses and gauge couplings) $\tan\beta$ and $m_{H^\pm}$ (or, for conserved $\mathcal{CP}$, equivalently m_A). Particles from other sectors can enter in loops so that the Higgs boson masses also depend in particular on parameters from the sfermion sector, such as the trilinear coupling A_f, the stop and sbottom masses and in the sub-leading terms on the higgsino mass parameter μ.

3.3.4.4. Higgs couplings and the decoupling limit

Models with a non-minimal Higgs sector consisting of doublets and singlets feature a sum rule for the couplings of Higgs bosons ϕ to gauge bosons $V = Z, W^\pm$:

$$\sum_\phi g^2_{\phi VV} = g^2_{H_{\mathrm{SM}}VV}, \tag{3.47}$$

so that the SM coupling is "shared" among the BSM Higgs bosons due to unitarity [68,69], and, for example, the MSSM Higgs couplings to the gauge bosons are limited by those of the SM, $g^{\mathrm{MSSM}}_{\phi_i VV} \leq g_{H_{\mathrm{SM}}VV}$. However, if $M_A \gg M_Z$, the mixing angle α approaches

$$\sin(\alpha) \to -\cos(\beta), \quad \cos(\alpha) \to \sin(\beta), \quad \sin(\beta-\alpha) \to 1, \quad \cos(\beta-\alpha) \to 0, \tag{3.48}$$

so that H and A decouple from VV, and the hAZ-coupling $g_{hAZ} = \cos(\beta-\alpha)\frac{g}{2c_W}$ vanishes, while h couples like the SM Higgs boson. Hence, in this *decoupling limit* [70] the MSSM Higgs sector appears SM-like, and the heavy Higgs bosons are difficult to find in production and decay channels with gauge bosons. On the other hand, the couplings to fermions can be either suppressed or enhanced, depending on the angles α and β. The couplings of the neutral MSSM Higgs bosons to SM fields are shown in Tab. 3.3, expressed in terms of the corresponding SM couplings, where u, d denote the up- and down-type quarks and charged leptons. In the considered processes later in this thesis, the couplings of Higgs bosons to τ-leptons and b-quarks are involved [42],

$$g^{\mathrm{tree}}_{h\tau\tau,bb} = +\frac{igm_{\tau,b}s_\alpha}{2M_W c_\beta}, \qquad\qquad g^{\mathrm{tree}}_{H\tau\tau,bb} = -\frac{igm_{\tau,b}c_\alpha}{2M_W c_\beta}. \tag{3.49}$$

XY	$g_{hXY}/g^{(SM)}_{hXY}$	$g_{HXY}/g^{(SM)}_{HXY}$	$g_{AXY}/g^{(SM)}_{AXY}$
VV	$\sin(\beta-\alpha)$	$\cos(\beta-\alpha)$	0
uu	c_α/s_β	s_α/s_β	$i\gamma_5\cot\beta$
dd	$-s_\alpha/c_\beta$	c_α/c_β	$i\gamma_5\tan\beta$

Table 3.3.: The couplings of the MSSM Higgs bosons to SM particles. V denotes the massive vector bosons and u, d the massive fermions.

3.4. Complex parameters in the MSSM

While the SM contains 19 free parameters (most of them from the flavour sector), the MSSM with complex parameters comes with additional 105 parameters, most of which model our lack of knowledge by which mechanism SUSY is broken. Assuming minimal flavour violation, 41 parameters on top of the SM ones are left. There are the gaugino mass parameters $|M_1|, |M_2|, |M_3|, |\mu|$, the masses $m_{\tilde{e}_i}, m_{\tilde{u}_i}, m_{\tilde{d}_i}, m_{\tilde{L}_i}, m_{\tilde{Q}_i}$ for the generations $i = 1, 2, 3$, trilinear couplings $|A_f|$ of the sfermions with $f = u, d, c, s, b, t, e, \mu, \tau$, and $\tan\beta$ and a mass in the Higgs sector. For the general MSSM including complex parameters it is convenient to choose $M_{H^\pm}$ as the input mass because even with $\mathcal{CP}$-violation the charged Higgs bosons remain mass eigenstates. In the $\mathcal{CP}$-conserving case, m_A can be chosen equally well.

In addition to these 29 real parameters, there can be 14 $\mathcal{CP}$-violating phases from the complex parameters, but only 12 of them are physically independent. As mentioned above, ϕ_{M_2}, the phase of the wino parameter M_2, and $\phi_{m_{12}^2}$, the phase of the soft breaking parameter m_{12}^2, can be rotated away a redefinition of the fields. Hence 12 independent phases remain:

$$\phi_{M_1}, \phi_{M_3}, \phi_\mu, \phi_{A_f}. \tag{3.50}$$

However, the phases are constrained by existing experimental bounds. Electric dipole moments (EDMs) are via loop contributions sensitive to the particle spectrum of the underlying model and therefore provide an opportunity to restrict the viable range of the 12 phases listed in Eq. (3.50). Experimental bounds on EDMs of the neutron [71], Thallium [72] and mercury [73] constrain the MSSM phases most severely. Furthermore, bounds on EDMs of heavy fermions [74, 75], the electron [76, 77] and deuteron [78] are also useful in restricting $\mathcal{CP}$-violating phases of the MSSM. For example, Ref. [79] addresses the possibility of measuring $\mathcal{CP}$-asymmetries at the LHC, which are induced by $\mathcal{CP}$-violating phases. Despite the smallness of the measured EDMs, several sizeable phases are allowed [80]. However, in scenarios where large $\mathcal{CP}$-violating SUSY contributions to the EDMs should cancel to result in values below the experimental bounds, some fine-tuning would be needed. Nevertheless, even without cancellations, not all phases are tightly constrained so that there is still open parameter space for complex MSSM parameters. Refs. [81–83] review the interpretation of those bounds within the MSSM. The Higgsino phase ϕ_μ is strongly constrained in the convention where ϕ_{M_2} is rotated away. The limits on ϕ_{M_1} are less restrictive. The phases of the trilinear couplings ϕ_{A_f} contribute only at two-loop order to the EDMs and are therefore less constrained. In general, larger values of $\phi_{A_{t,b}}$ are allowed than for those of the first and second generation squarks. The gluino phase ϕ_{M_3} is only strictly constrained if the first and second generation sfermions are light. The phase of the trilinear selectron coupling ϕ_{A_e} is weakly constrained, but $\phi_{A_{\mu,\tau}}$ and $\phi_{A_{c,s}}$ are hardly constrained at all. One has to keep in mind that the limits are parameter dependent; especially $\tan\beta$ has a significant impact on the translation of EDM bounds into limits of phases of MSSM parameters.

In Chapter 10 we will investigate the impact of complex phases on the phenomenology of MSSM Higgs bosons, applied to processes that are relevant at the LHC. Masses, couplings and mixings in the Higgs sector are significantly affected by loop contributions from the whole MSSM spectrum. Because of the large top Yukawa coupling, stop loops have a leading effect at the one-loop level. Therefore we take ϕ_{A_t} into account, but an extension to other phases such as ϕ_{A_b} and ϕ_{M_3} is also possible. In our study, we set the $A_{f_{1,2}}$-phases of the sfermions from the first and second generation to zero.

Non-vanishing phases in the MSSM also have important consequences for cosmology and might contribute to the explanation of the observed matter-antimatter asymmetry in the universe.

Chapter 4.

Higher-order corrections in the MSSM

In this chapter, we give a short overview of the basic concepts of regularisation and renormalisation in different schemes, following Refs. [20, 21, 84]. Some parts of the text are strongly based on [85]. After the introductory section, we will describe in Sect. 4.3 the on-shell renormalisation of the neutralino-chargino sector of the MSSM and discuss the stability of different versions of the scheme. The topic of Sect. 4.4 will be the renormalisation of the MSSM Higgs sector in an hybrid on-shell and $\overline{\mathrm{DR}}$-scheme.

4.1. Concept of regularisation and renormalisation

A thorough comparison between theoretical predictions and experimental results demands high precision calculations of the physical quantities. From the theoretical side, observables such as cross sections or decay widths can be (for small enough couplings) perturbatively expanded as a power series in the couplings. Achieving an appropriate precision requires calculations beyond tree level in many processes because the contributions from higher orders in perturbation theory can be very important. Higher-order effects exist as real corrections by external particles or as virtual corrections in a loop.

However, technical problems arise because the momentum in a loop is not constrained so that it has to be integrated over all possible values, potentially leading to divergent integrals. At one-loop order, the arising tensor integrals can be fully decomposed into scalar integrals, known as Passarino-Veltman reduction [86]. The type of divergence caused by infinite momenta is known as ultraviolet (UV) divergence. In contrast, infrared (IR) divergences can emerge in real and in virtual corrections with massless objects approaching zero momentum.

The two-step procedure of regularisation and renormalisation consistently treats the infinities to render all physical observables finite. In the general approach, regularisation is an intermediate step to make divergent integrals mathematically well-defined. The divergences are cancelled by so-called counterterms which are fixed by renormalisation conditions so that the remaining physical parameters and fields become finite. This may be performed in various schemes some of which are presented in the following sections.

4.1.1. Regularisation

Dimensional regularisation (DREG) The procedure starts with regularistation. Broadly applied in the SM is Dimensional Regularisation (DREG) [26] in which momenta and Lorentz covariants are changed from 4 to $D = 4 - 2\epsilon$ dimensions. Yet, there is no well-defined generalisation of γ_5 in arbitrary D dimensions. The concept of DREG is that divergent integrals in $D = 4$ become finite in $D < 4$ with the replacement

$$\int \frac{\mathrm{d}^4 q}{(2\pi)^4} \to \mu^{4-D} \int \frac{\mathrm{d}^D q}{(2\pi)^D}, \tag{4.1}$$

where the arbitrary mass scale μ, the renormalisation scale, is introduced to preserve the correct mass dimension of the expression. The UV and IR singularities manifest themselves as $\frac{1}{\epsilon}$-poles. DREG has the benefit of regularising UV and IR divergences simultaneously and preserving both Lorentz and gauge invariance.

Cut-off regularisation An alternative regularisation is, for example, a cut-off at a scale Λ for the absolute value of the momentum, $|p| \leq \Lambda$, in a divergent integral. In this scheme, which is neither Lorentz nor gauge invariant, the UV divergences will appear as logarithms or powers of Λ.

Dimensional reduction (DRED) Despite the appealing benefits of DREG described above, this regularisation leads to a mismatch of bosonic and fermionic degrees of freedom and breaks supersymmetry explicitly [87] so that SUSY restoring counterterms need to be introduced. In the MSSM, it is replaced by the scheme of *dimensional reduction* (*DRED*) [88–90]. Here, space-time, momenta and momentum integrals are dealt with in $D = 4 - 2\epsilon$ dimensions, whereas fields and γ-matrices remain in 4 dimensions. It has been confirmed to be mathematically well-defined and SUSY preserving [91].

4.1.2. Renormalisation

Renormalisation removes divergences by a redefinition of the physical meaning of parameters and fields in the Lagrangian order by order in perturbation theory. First of all, a set of independent parameters must be chosen. A counterterm is assigned to each divergent ("bare") parameter a_0 and field ϕ_0 by an additive or multiplicative prescription with a renormalisation constant Z_a or Z_ϕ, where a hat denotes a renormalised, i.e., finite quantity

$$a_0 = Z_a \hat{a} = \hat{a} + \delta a \tag{4.2}$$

$$\phi_0 = \sqrt{Z_\phi}\hat{\phi} = \left(1 + \frac{1}{2}\delta Z_\phi\right)\hat{\phi}. \tag{4.3}$$

Then the Lagrangian can be split into two parts,

$$\mathcal{L}_0(a_0, \phi_0) = \mathcal{L}(\hat{a}, \hat{\phi}) + \delta\mathcal{L}(\hat{a}, \delta a, \hat{\phi}, \delta Z_\phi), \tag{4.4}$$

where $\mathcal{L}_0(a_0, \phi_0)$ has the same functional form as $\mathcal{L}$, but it depends on the bare fields and parameters, and $\delta\mathcal{L}$ contains the counterterms. The set of Feynman rules is extended to the existing rules with renormalised parameters plus new rules for counterterm vertices.

The divergent parts of the bare parameters or fields and their counterterms have to cancel exactly to render the renormalised quantities and physical observables finite. After the renormalisation has been carried out, the limit of removing the regularisation is taken (e.g. $\epsilon \to 0$ in DREG or $\Lambda \to \infty$ in the cut-off regularisation scheme). This procedure results in finite Green's functions.

While the coefficients in front of the divergences are unambiguous, the definition of the finite parts of the counterterms is not unique. It depends on the chosen renormalisation scheme. Physical results are independent of the scheme and the renormalisation scale only if all orders of perturbation theory are included. Yet, in a truncated series the remnant dependence on the renormalisation prescription is of the order of the higher uncalculated orders [92]. Thus, a different physical meaning and a different numerical value is attributed for example to the mass in different schemes. When comparing experiment to theory, one has to keep in mind which renormalisation scheme has been used.

Modified minimal subtraction ($\overline{\mathbf{MS}}$) scheme Among the most commonly used schemes, there are the *(modified) minimal subtraction* (MS/$\overline{\text{MS}}$) and the *on-shell scheme*. While the MS scheme, used in connection with DREG, only absorbs the term proportional to the divergence $\frac{1}{\epsilon}$ into the counterterm, the $\overline{\text{MS}}$ scheme subtracts also finite constants for convenience because $\frac{1}{\epsilon} - \gamma_E + \ln(4\pi)$ always appears as a combination, where γ_E is the Euler constant.

Minimal subtraction scheme for SUSY: $\overline{\mathbf{DR}}$ Similar to the $\overline{\text{MS}}$ scheme, the $\overline{\text{DR}}$ scheme is also a renormalisation scheme employing minimal subtraction in the definition of the counterterms. In order to apply it to supersymmetric theories, it is used in conjunction with regularisation by dimensional reduction.

Instead of introducing counterterms, the scheme of *constrained differential renormalisation (CDR)* [93] makes Green functions already finite. Divergent expressions are written as derivatives of finite functions in coordinate space. Finally, they are transformed back to momentum space. This enables a direct identification with the scalar and tensor one-loop integrals. At one loop-level, CDR has been shown to be equivalent to DRED [94].

On-shell renormalisation scheme The on-shell scheme, on the other hand, fixes the mass and field renormalisation constants through a condition that identifies the renormalised ("physical") mass with the pole of the propagator. The field renormalisation constant is fixed by requiring a unit residue of the full propagator. As an example, we mention the self-energy $\Sigma(p^2)$ of a scalar field ϕ with bare mass m_0 (dropping the hat on the renormalised mass $m^2 \equiv \widehat{m}^2$). Requiring at the one-loop level a pole of the propagator at the physical (renormalised) mass $p^2 = m^2$ yields

$$p^2 - m^2 - \delta m^2 + \Sigma(p^2) \stackrel{!}{=} 0 \text{ for } p^2 = \widehat{m}^2 \qquad \Rightarrow \qquad \delta m^2 = \Sigma(m^2). \tag{4.5}$$

Furthermore, the field renormalisation constant is determined from the unit residue:

$$\delta Z_\phi = -\frac{\partial \Sigma(p^2)}{\partial p^2}\bigg|_{p^2=\widehat{m}^2} \equiv -\Sigma^{'}(\widehat{m}^2). \tag{4.6}$$

Using Eqs. (4.5) and (4.6), the renormalised one-loop self-energy can be expressed as

$$\hat{\Sigma}(p^2) = \Sigma(p^2) - \delta m^2 + (p^2 - m^2)\delta Z_\phi = \Sigma(p^2) - \Sigma(m^2) - (p^2 - m^2)\Sigma^{'}(m^2), \tag{4.7}$$

which is a finite quantity. We will often encounter renormalised self-energies in Chaps. 5 and 6. If the self-energy develops an imaginary part, the pole of the propagator is located off the real momentum axis and the complex pole has to be taken into account in the on-shell condition, see Chapter 5.

4.1.3. Infrared divergences

Mass singularities appear for small or collinear momenta of massless particles such as gluons and photons. Particles with a small momentum are called "soft". Massless soft particles lead to a divergence if the momentum approaches zero, therefore this kind of divergence is termed "infrared" (IR). These mass singularities can be regularised by introducing a ficticious mass $\lambda = m_\gamma, m_g$ in the propagator of the particle. They are not renormalised by a counterterm. Instead, one considers mass singularities arising in virtual loops together with real amplitudes where photons (or gluons) are radiated off electrically (or colour-)charged particles, and sums over all degenerate initial and final states[1]. The real and virtual contributions have the same IR-structure so that they cancel each other. This is an important result of the Kinoshita-Lee-Nauenberg (KLN) theorem [95, 96], which holds at all orders of perturbation theory in the SM. For the cancellation of IR-divergences in pure quantum electrodynamics (QED), it is sufficient to sum over all final states with any number of soft emitted photons according to the Bloch-Nordsieck theorem [97]. Furthermore, the real contribution of soft photons is proportional to the lowest-order result,

$$\mathrm{d}\sigma^{\text{real,soft}} = \delta_{\text{SB}}\, \mathrm{d}\sigma^{\text{tree}}, \tag{4.8}$$

where δ_{SB} is the factor for soft bremsstrahlung. It depends on the energy cut-off $\Delta E^{\text{max}}_{\text{soft}}$ according to which photons are regarded "soft" ($E_\gamma < \Delta E^{\text{max}}_{\text{soft}}$) or "hard" ($E_\gamma > \Delta E^{\text{max}}_{\text{soft}}$). Eq. (4.8) holds at the level of cross sections or squared amplitudes. In Chap. 7.4 we will derive how to transfer it to the product of on-shell amplitudes and apply it to an example process with soft photon bremsstrahlung in Chap. 8.

[1] States with additional soft or collinear radiation are indistinguishable in a detector with limited energy or angular resolution, respectively.

4.2. Renormalisation of the Standard Model

In renormalisable theories, a finite number of counterterms is sufficient to cancel all divergences. Gauge theories containing spontaneous symmetry breaking - such as the SM - are renormalisable to all orders of perturbation theory [25, 26]. We summarise in this section the renormalisation of the SM at the one-loop level in the on-shell scheme.

4.2.1. Renormalisation of masses and fields

The renormalisation constants for the following SM masses, the electric charge and the CKM-matrix,

$$\begin{aligned} M_Z^2 &\to M_Z^2 + \delta M_Z^2, & M_W^2 &\to M_W^2 + \delta M_W^2, \\ M_H^2 &\to M_H^2 + \delta M_H^2, & m_{f_i}^2 &\to m_{f_i}^2 + \delta m_{f_i}^2, \\ e &\to (1+\delta Z_e)e, & V_{ij} &\to V_{ij} + \delta V_{ij}, \end{aligned} \tag{4.9}$$

are sufficient for finite S-matrix elements, but for finite Green's functions the field renormalisation constants are also needed,

$$W^\pm \to \left(1 + \frac{1}{2}\delta Z_{WW}\right) W^\pm, \quad V_i^0 \to \left(\delta_{ij} + \frac{1}{2}\delta Z_{ij}\right) V_j^0,\ V_1^0 \equiv Z,\ V_2^0 \equiv \gamma, \tag{4.10}$$

$$H \to \left(1 + \frac{1}{2}\delta Z_H\right) H, \quad f_i^{L/R} \to \left(\delta_{ij} + \frac{1}{2}\delta Z_{ij}^{L/R}\right). \tag{4.11}$$

Counterterms of parameters that depend on those listed in Eq. (4.9) can be expressed in terms of the above renormalisation constants, such as the weak mixing angle $c_W = \frac{M_W}{M_Z}$ (at 1-loop order),

$$\delta c_W = \frac{c_W}{2}\left(\frac{\delta M_W^2}{M_W^2} - \frac{\delta M_Z^2}{M_Z^2}\right) \qquad \delta s_W = \frac{c_W^2}{2 s_W}\left(\frac{\delta M_Z^2}{M_Z^2} - \frac{\delta M_W^2}{M_W^2}\right). \tag{4.12}$$

The renormalisation conditions are determined by the on-shell conditions that diagonal propagators ought to have unit residues, fields (in the SM, it concerns γ, Z and quarks) should not mix on-shell and the propagator has a pole at the physical mass. As an example, this yields for the gauge bosons $V = W, Z$ with the transverse part of the self-energy Σ_T^V and for $\gamma - Z$ mixing:

$$\delta M_V^2 = \mathrm{Re}\Sigma_T^V(M_V^2), \quad \delta Z_V = -\Sigma_T^{\prime V}(M_V^2), \quad \delta Z_{\gamma Z} = -\frac{2\Sigma_T^{\gamma Z}(M_Z^2)}{M_Z^2}, \quad \delta Z_{\gamma Z} = \frac{2\Sigma_T^{Z\gamma}(0)}{M_Z^2}. \tag{4.13}$$

4.2.2. Charge renormalistion

In the on-shell scheme following Ref. [45, 98], which avoids the introduction of effective quark masses, the electric charge e is renormalised in the Thomson limit. The renormalisation constant δZ_e is fixed by the requirement that it coincides with the $ee\gamma$ coupling in the case of on-shell external particles and for vanishing photon momentum in the transverse self-energy $\Sigma_T^{\gamma Z}$ and in the photon vacuum polarisation $\Pi_\gamma(0) = \frac{\partial \Sigma^{\gamma\gamma}(k^2)}{\partial k^2}|_{k^2=0}$:

$$\delta Z_e = \frac{1}{2}\Pi_\gamma(0) + \frac{s_W}{c_W}\frac{\mathrm{Re}\Sigma_T^{\gamma Z}(0)}{M_Z^2}. \tag{4.14}$$

From the very precise experimental input of the measured electromagnetic coupling constant $\alpha_{\mathrm{em}}(0) = \frac{e(0)^2}{4\pi}$ it can be extrapolated to M_Z by $\alpha(M_Z^2) = \frac{\alpha(0)}{1-\Delta\alpha}$. The shift

$$\Delta\alpha = \Delta\alpha_{\mathrm{lep}} + \Delta\alpha_{\mathrm{had}}^{(5)} = -\left(\mathrm{Re}\hat{\Pi}_\gamma^{\mathrm{lep}}(M_Z^2) + \mathrm{Re}\hat{\Pi}_\gamma^{\mathrm{had},5}(M_Z^2)\right) \tag{4.15}$$

has a leptonic and a hadronic contribution (considering only the five lightest quarks) to the photon vacuum polarisation Π_γ. The renormalised vacuum polarisation evaluated at M_Z^2 is related to $\Pi_\gamma(0)$ by the photon self-energy,

$$\mathrm{Re}\hat{\Pi}_\gamma(M_Z^2) = \frac{\mathrm{Re}\Sigma^{\gamma\gamma}(M_Z^2)}{M_Z^2} - \Pi_\gamma(0). \tag{4.16}$$

While $\Delta\alpha_{\mathrm{lep}}$ has been calculated in Ref. [99], $\Delta\alpha_{\mathrm{had}}^{(5)}$ has to be determined from measurements [100]. The renormalisation constant δZ_e can then be expressed in terms of $\Delta\alpha$ by defining $\Pi_\gamma^{\mathrm{heavy}}(0)$ as the photon vacuum polarisation restricted to exclusively heavy particles (no leptons and the five light quarks) in the loops. Large logarithms from $\alpha(M_Z^2)$ at 1-loop order are absorbed into the tree-level expression. The final result is

$$\delta Z_e^{(M_Z^2)} = \delta Z_e - \frac{\Delta\alpha_{\mathrm{lep}} + \Delta\alpha_{\mathrm{had}}^{(5)}}{2} = \frac{1}{2}\Pi_\gamma^{\mathrm{heavy}}(0) + \frac{s_W}{c_W}\frac{\mathrm{Re}\Sigma_T^{\gamma Z}(0)}{M_Z^2} + \frac{1}{2}\mathrm{Re}\Pi_\gamma^{\mathrm{light}}(M_Z^2). \tag{4.17}$$

4.3. Renormalisation of the neutralino-chargino sector

On-shell renormalisation schemes of the neutralino-chargino sector have been developed at the one-loop level in Refs. [101–108] for the MSSM with real parameters and extended to the general case of complex parameters in Refs. [45, 109–111]. We have re-derived (also in Ref. [85]) the renormalisation constants and mass corrections and implemented our results into a `FeynArts` model file. We found agreement with the analytical results and the model file from Ref. [45].

4.3.1. Renormalisation transformations for parameters and fields

As seen in Sect. 3.3.3, the bino mass parameter M_1, wino mass parameter M_2 and Higgsino mass parameter μ are, besides $\tan\beta$ and SM quantities, the three independent parameters in the neutralino and chargino sector. Hence, the counterterms of their mass matrices $X,\ Y$,

$$Y \to Y + \delta Y, \qquad\qquad X \to X + \delta X, \tag{4.18}$$

depend on the renormalisation constants $\delta M_1,\ \delta M_2,\ \delta\mu$,

$$M_1 \to M_1 + \delta M_1, \qquad M_2 \to M_2 + \delta M_2, \qquad \mu \to \mu + \delta\mu. \tag{4.19}$$

The expressions for all elements can be found in the Appendix B.1. The field renormalisation constants are introduced such that left- and right-handed components are distinguished and the renormalisation constants of incoming (unbarred) and outgoing (barred) fields are treated independently in order to allow for the most general case of $\mathcal{CP}$-violation. The renormalisation transformations for the neutralinos read:

$$\begin{aligned}
\omega_L \widetilde{\chi}_i^0 &\to (1 + \frac{1}{2}\delta Z_0^L)_{ij}\omega_L \widetilde{\chi}_j^0, \quad \overline{\widetilde{\chi}_i^0}\omega_R \to \overline{\widetilde{\chi}_i^0}(1 + \frac{1}{2}\delta \bar{Z}_0^L)_{ij}\omega_R \\
\omega_R \widetilde{\chi}_i^0 &\to (1 + \frac{1}{2}\delta Z_0^R)_{ij}\omega_R \widetilde{\chi}_j^0, \quad \overline{\widetilde{\chi}_i^0}\omega_L \to \overline{\widetilde{\chi}_i^0}(1 + \frac{1}{2}\delta \bar{Z}_0^R)_{ij}\omega_L.
\end{aligned} \tag{4.20}$$

The transformations are analogous for charginos. However, targeted at a later application to a process with external neutralinos, we focus on neutralinos in the following.

4.3.2. On-shell renormalisation conditions and field renormalisation

The two-point vertex function $\hat{\Gamma}_{ij}$ and the propagator $\hat{S}_{ij}^{-1}$ are expressed with $\hat{\Sigma}_{ij}$ as follows:

$$\hat{S}_{ij}(p) = -[\hat{\Gamma}_{ij}(p)]^{-1} = -i[(\not{p} - m_{\widetilde{\chi}_i^0})\delta_{ij} + \hat{\Sigma}_{ij}(p)]^{-1}. \tag{4.21}$$

Imposing on-shell conditions, we require that external on-shell particles do not mix,

$$\hat{\Gamma}_{ij}\widetilde{\chi}_j^0(p)|_{p^2 = m^2_{\widetilde{\chi}_j^0}} = 0, \qquad\qquad \overline{\widetilde{\chi}_i^0}(p)\hat{\Gamma}_{ij}|_{p^2 = m^2_{\widetilde{\chi}_i^0}} = 0, \tag{4.22}$$

and that the residues of the diagonal propagators are normalised to unity,

$$\lim_{p^2 \to m^2_{\widetilde{\chi}_i^0}} \frac{1}{\not{p} - m_{\widetilde{\chi}_i^0}}\hat{\Gamma}_{ii}\widetilde{\chi}_i^0(p) = i\widetilde{\chi}_i^0, \qquad \lim_{p^2 \to m^2_{\widetilde{\chi}_i^0}} \overline{\widetilde{\chi}_i^0}(p)\hat{\Gamma}_{ii}\frac{1}{\not{p} - m_{\widetilde{\chi}_i^0}} = i\overline{\widetilde{\chi}_i^0}. \tag{4.23}$$

The fermion self-energies $\Sigma_{ij}(p^2)$ of the neutralinos and charginos are decomposed into left- and right-handed contributions as well as vector and scalar parts,

$$\Sigma_{ij}(p^2) = \not{p}\left(\omega_L \Sigma_{ij}^L(p^2) + \omega_R \Sigma_{ij}^R(p^2)\right) + \omega_L \Sigma_{ij}^{SL}(p^2) + \omega_R \Sigma_{ij}^{SR}(p^2). \tag{4.24}$$

The renormalised self-energies of the neutralinos have the form

$$\hat{\Sigma}_{ij}^{(S)R/L}(p^2) = \Sigma_{ij}^{(S)R/L}(p^2) + \Delta\Sigma_{ij}^{(S)R/L}, \tag{4.25}$$

where the counterterms of the scalar and vector self-energies $\Delta\Sigma_{ij}^{(S)R/L}$ are determined from the counterterm part of the neutralino Lagrangian, see Eq. (B.10) in the Appendix B.1,

$$\Delta\Sigma_{ij}^{R/L} = \frac{1}{2}(\delta\bar{Z}_0^{R/L} + \delta Z_0^{R/L}), \tag{4.26}$$

$$\Delta\Sigma_{ij}^{SR} = [-N\delta Y^\dagger N^T - \frac{1}{2}(NY^\dagger N^T\delta Z_0^R + \delta\bar{Z}_0^L NY^\dagger N^T)]_{ij}, \tag{4.27}$$

$$\Delta\Sigma_{ij}^{SL} = [-N^*\delta Y N^\dagger - \frac{1}{2}(N^*YN^\dagger\delta Z_0^L + \delta\bar{Z}_0^R N^*YN^\dagger)]_{ij}. \tag{4.28}$$

The neutralino field renormalisation constants occuring in Eqs.(4.26)-(4.28) are found by solving the renormalisation conditions in Eqs. (4.22) and (4.23):

$$\begin{aligned}
\delta Z_{0,ij}^{L/R} &= \frac{2}{m_{\tilde{\chi}_i^0}^2 - m_{\tilde{\chi}_j^0}^2} \cdot [m_{\tilde{\chi}_j^0}^2 \Sigma_{ij}^{L/R}(m_{\tilde{\chi}_j^0}^2) + m_{\tilde{\chi}_i^0} m_{\tilde{\chi}_j^0} \Sigma_{ij}^{R/L}(m_{\tilde{\chi}_j^0}^2) + m_{\tilde{\chi}_i^0}\Sigma_{ij}^{SL/SR}(m_{\tilde{\chi}_j^0}^2) \\
&\quad + m_{\tilde{\chi}_j^0}\Sigma_{ij}^{SR/SL}(m_{\tilde{\chi}_j^0}^2) - m_{\tilde{\chi}_{i/j}}(N^*\delta Y N^\dagger)_{ij} - m_{\tilde{\chi}_{j/i}}(N\delta Y^\dagger N^T)_{ij}], &(4.29)\\
\delta \bar{Z}_{0,ij}^{L/R} &= \frac{2}{m_{\tilde{\chi}_j^0}^2 - m_{\tilde{\chi}_i^0}^2} \cdot [m_{\tilde{\chi}_i^0}^2 \Sigma_{ij}^{L/R}(m_{\tilde{\chi}_i^0}^2) + m_{\tilde{\chi}_i^0} m_{\tilde{\chi}_j^0} \Sigma_{ij}^{R/L}(m_{\tilde{\chi}_i^0}^2) + m_{\tilde{\chi}_i^0}\Sigma_{ij}^{SL/SR}(m_{\tilde{\chi}_i^0}^2) \\
&\quad + m_{\tilde{\chi}_j^0}\Sigma_{ij}^{SR/SL}(m_{\tilde{\chi}_i^0}^2) - m_{\tilde{\chi}_{i/j}}(N^*\delta Y N^\dagger)_{ij} - m_{\tilde{\chi}_{j/i}}(N\delta Y^\dagger N^T)_{ij}], &(4.30)\\
\delta Z_{0,ii}^{L/R} &= -\Sigma_{ii}^{L/R}(m_{\tilde{\chi}_i^0}^2) - m_{\tilde{\chi}_i^0}^2\left[\hat{\Sigma}_{ii}^{\prime L}(m_{\tilde{\chi}_i^0}^2) + \hat{\Sigma}_{ii}^{\prime R}(m_{\tilde{\chi}_i^0}^2)\right] - m_{\tilde{\chi}_i^0}\left[\hat{\Sigma}_{ii}^{\prime SL}(m_{\tilde{\chi}_i^0}^2) + \hat{\Sigma}_{ii}^{\prime SR}(m_{\tilde{\chi}_i^0}^2)\right] \\
&\quad \mp \frac{1}{2m_{\tilde{\chi}_i^0}}\left[\Sigma_{ii}^{SR}(m_{\tilde{\chi}_i^0}^2) - \Sigma_{ii}^{SL}(m_{\tilde{\chi}_i^0}^2) + (N^*\delta Y N^\dagger)_{ii} - (N\delta Y^\dagger N^T)_{ii}\right], &(4.31)\\
\delta \bar{Z}_{0,ii}^{L/R} &= -\Sigma_{ii}^{L/R}(m_{\tilde{\chi}_i^0}^2) - m_{\tilde{\chi}_i^0}^2\left[\hat{\Sigma}_{ii}^{\prime L}(m_{\tilde{\chi}_i^0}^2) + \hat{\Sigma}_{ii}^{\prime R}(m_{\tilde{\chi}_i^0}^2)\right] - m_{\tilde{\chi}_i^0}\left[\hat{\Sigma}_{ii}^{\prime SL}(m_{\tilde{\chi}_i^0}^2) + \hat{\Sigma}_{ii}^{\prime SR}(m_{\tilde{\chi}_i^0}^2)\right] \\
&\quad \pm \frac{1}{2m_{\tilde{\chi}_i^0}}\left[\Sigma_{ii}^{SR}(m_{\tilde{\chi}_i^0}^2) - \Sigma_{ii}^{SL}(m_{\tilde{\chi}_i^0}^2) + (N^*\delta Y N^\dagger)_{ii} - (N\delta Y^\dagger N^T)_{ii}\right]. &(4.32)
\end{aligned}$$

Owing to the Majorana nature of neutralinos, the renormalisation constants of incoming and outgoing fields are related by $\delta Z_{0,ij}^{L/R} = \delta\bar{Z}_{0,ij}^{R/L}$.

4.3.3. Parameter renormalisation and mass corrections

Independent parameters While the phase ϕ_{M_2} can be rotated away, the other phases, in principle, have to be renormalised in addition to the absolute values of the parameters.

$$\begin{aligned}
|\mu| &\to |\mu| + \delta|\mu|, & \phi_\mu &\to \phi_\mu + \delta\phi_\mu & (4.33)\\
|M_1| &\to |M_1| + \delta|M_1|, & \phi_{M_1} &\to \phi_{M_1} + \delta\phi_{M_1} & (4.34)\\
|M_2| &\to |M_2| + \delta|M_2| & & & (4.35)
\end{aligned}$$

However, the phase counterterms, $\delta\phi_\mu$ and $\delta\phi_{M_1}$ turn out to be UV-finite [45, 110] so that the phases ϕ_μ and ϕ_{M_1} can be kept unrenormalised.

Loop-corrected masses The neutralino-chargino sector contains in total six masses, the neutralino masses $m_{\tilde{\chi}_i^0}, i = 1,2,3,4$ as well as the chargino masses $m_{\tilde{\chi}_i^\pm}, i = 1,2$. On the other hand, the number of independent parameters limits the number of renormalisation conditions. In this case, the independent parameters are $|\mu|, |M_1|$ and $|M_2|$, so that on-shell conditions can be imposed for no more than three out of the six states. The masses of the three chosen states remain on-shell, while the remaining three masses receive a non-zero loop-correction $\Delta m_{\tilde{\chi}_i}$ to the one-loop-corrected mass $M_{\tilde{\chi}_i^0} = m_{\tilde{\chi}_i^0} + \Delta m_{\tilde{\chi}_i}$. Here and in the following, we denote tree-level masses by lower-case m and a loop-corrected, physical mass by an upper-case M.

The renormalisation conditions for the fields ensure correct on-shell properties, i.e. fields do not mix on the mass shell, so that no mixing needs to be taken into account. The physical masses are determined from the complex poles of the diagonal propagators $\hat{S}_{ii}$,

$$\mathcal{M}_i^2 = M_{\tilde{\chi}_i}^2 - iM_{\tilde{\chi}_i}\Gamma_{\tilde{\chi}_i}, \tag{4.36}$$

which solve

$$\mathcal{M}_i^2 \left[1 + \hat{\Sigma}_{ii}^L(\mathcal{M}_i^2)\right] \left[1 + \hat{\Sigma}_{ii}^R(\mathcal{M}_i^2)\right] - \left[m_{\tilde{\chi}_i} - \hat{\Sigma}_{ii}^{SL}(\mathcal{M}_i^2)\right] \left[m_{\tilde{\chi}_i} - \hat{\Sigma}_{ii}^{SR}(\mathcal{M}_i^2)\right] = 0. \tag{4.37}$$

The corrections to the masses which do not belong to the input states amount to

$$\begin{aligned}\Delta m_{\tilde{\chi}_i} &= -\frac{m_{\tilde{\chi}_i}}{2}\mathrm{Re}\{\hat{\Sigma}_{ii}^L(m_{\tilde{\chi}_i}^2) + \hat{\Sigma}_{ii}^R(m_{\tilde{\chi}_i^2})\} - \frac{1}{2}\mathrm{Re}\{\hat{\Sigma}_{ii}^{SL}(m_{\tilde{\chi}_i}^2) + \hat{\Sigma}_{ii}^{SR}(m_{\tilde{\chi}_i^2})\} \\ &= -m_{\tilde{\chi}_i}\mathrm{Re}\hat{\Sigma}_{ii}^L(m_{\tilde{\chi}_i}^2) - \mathrm{Re}\hat{\Sigma}_{ii}^{SL}(m_{\tilde{\chi}_i}^2).\end{aligned} \tag{4.38}$$

Explicit expressions for the self-energies can be found, for instance, in Refs. [104, 112].

The counterterms of the renormalised parameters are fixed by the on-shell conditions, but the exact structure depends on the chosen renormalisation scheme, i.e., which three among the six neutralino (denoted by N) and chargino (denoted by C) masses are on-shell. In total, there are 20 distinct combinations. The following renormalisation schemes are labelled by the choice of on-shell masses of the fixed input states:

- **NCC:** 4 possibilities to choose one neutralino and two charginos,
- **NNC:** 12 possibilities to choose two neutralinos and one chargino,
- **NNN:** 4 possibilities to choose three neutralinos. In particular, NNNi refers to the scheme in which the mass of the ith neutralino (in addition to both chargino masses) is shifted by $\Delta_{m_{\tilde{\chi}_i^0}}$ while the other three neutralinos stay on-shell.

In any case, the three input states must be chosen carefully [45, 108, 110, 113]. If all three on-shell masses depend only weakly on one of the bino-, wino- or higgsino mass parameters (M_1, M_2 or μ, respectively), the imposed renormalisation conditions are not sufficiently sensitive to the underlying parameters. This insufficient fixing can give rise to unphysically large loop contributions which are problematic for perturbativity and numerical stability. Hence it is of utmost importance to choose a bino-, a wino- and a higgsino-like state for the three on-shell renormalisation conditions, instead of three fixed states. Having defined a particular scheme, the on-shell conditions $\Delta m_{\tilde{\chi}_i^0} = 0$ for the three selected input states $\widetilde{\chi}_i$ (a combination of one to three neutralinos and zero to two charginos) are translated into the parameter counterterms. For the class of NNN schemes, the resulting expressions of $\delta|M_1|, \delta|M_1|, \delta|\mu|$ can be found in the Appendix B.2.

4.3.4. Comparison of NNN renormalisation schemes

Refs. [45,108] provide a comprehensive overview of stable renormalisation schemes across the NCC, NNC and NNN classes with some examples from each class. In this section, we present a detailed comparison of parameter counterterms and mass corrections in all four NNN schemes. Our application to an example process in Chaps. 8 and 9 does not involve any external charginos, but only external neutralinos, in particular $\widetilde{\chi}_1^0$ and $\widetilde{\chi}_4^0$. Consequently, we choose a scheme which sets three neutralino masses on-shell. In order to determine which NNN scheme is most appropriate in the considered modified $M_h^{\max}$-scenario (see Sect. 8.2.3 and Tab. A.1), we investigate the stability of the four possible choices numerically in this section. The mixing matrix N, which diagonalises Y as in Eq. (3.25), has the following values in the example scenario:

$$N = \begin{pmatrix} 0.928 & -0.119 & 0.318 & -0.152 \\ -0.327 & -0.692 & 0.509 & -0.394 \\ -i\,0.097 & i\,0.137 & i\,0.678 & i\,0.716 \\ -0.147 & 0.699 & 0.425 & -0.556 \end{pmatrix}. \tag{4.39}$$

Consequently, $\widetilde{\chi}_1^0$ is mostly bino ($\tilde{B}$)-like, $\widetilde{\chi}_2^0$ is an admixture of mostly wino ($\tilde{W}^3$) and higgsino ($\tilde{h}_d^0$), $\widetilde{\chi}_3^0$ consists of both higgsinos ($\tilde{h}_d^0, \tilde{h}_u^0$), and $\widetilde{\chi}_4^0$ is predominantly composed of even three states, $\tilde{W}^0, \tilde{h}_d^0$ and $\tilde{h}_u^0$. This highly mixed neutralino composition instead of a clear gaugino hierarchy leads to an ambiguous choice of the numerically most stable renormalisation scheme.

Following the prescription of Ref. [108], the bino-like state is identified with the neutralino $\widetilde{\chi}_i^0$ that has the largest bino-content, i.e. $|N_{i1}| \geq |N_{i'1}|\ \forall i' \neq i$. According to Eq. (4.39), this is $\widetilde{\chi}_1^0$ in our case. Among the remaining three neutralinos, the wino-like state $\widetilde{\chi}_j^0$ is determined by $|N_{j2}| \geq |N_{j'2}|\ \forall j' \neq j$. Here we encounter $|N_{22}| \simeq |N_{42}|$, so there is an ambiguity whether to denote $\widetilde{\chi}_2^0$ or $\widetilde{\chi}_4^0$ as the wino-like state. These two options are pursued in Tab. 4.1. Independent of this wino-choice, the most higgsino-like state $\widetilde{\chi}_k^0$ with the largest $|N_{k3}|^2 + |N_{k4}|^2$ among the remaining two is in both cases $\widetilde{\chi}_3^0$. The emerging schemes are referred to as NNN4 or NNN2 since the mass of $\widetilde{\chi}_4^0$ or $\widetilde{\chi}_2^0$, respectively, receives a loop correction. In contrast, the NNN1 scheme contains only wino ($\widetilde{\chi}_2^0, \widetilde{\chi}_4^0$)- and higgsino ($\widetilde{\chi}_3^0$)-like input states so that M_1 would be only weakly fixed. Similarly, the NNN3 input states $\widetilde{\chi}_1^0$ (bino) and $\widetilde{\chi}_2^0, \widetilde{\chi}_4^0$ (wino) miss a proper μ-fixing.

According to Ref. [108], after the identification of the most bino- and wino-like states, the residual choice of a higgsino-like state is not crucial for stability - unless $M_2 \simeq |\mu|$ or $-M_1 \simeq \mu$. The modified $M_h^{\max}$-scenario under consideration features $M_2 = \mu$. Therefore we pay special attention to possible instabilities of the renormalisation constants in our numerical evaluation with $M_2 = 200\,\text{GeV}$ fixed, but with a variation of $\mu \in$

state	choice 1	choice 2
bino-like	1	1
wino-like	2	4
higgsino-like	3	3
scheme	NNN4	NNN2

Table 4.1.: Definition of the most bino-, wino- and higgsino-like states according to the largest $|N_{i1}|^2$, $|N_{j2}|^2$ and $|N_{k3}|^2+|N_{k4}|^2$ in Eq. (4.39). The choice of the most wino-like $\tilde{\chi}_j^0$ is ambiguous, resulting in the two comparably stable schemes NNN4 and NNN2.

[195 GeV, 250 GeV], thus including the case of $\mu = M_2$. Fig. 4.1 shows the finite parts of the parameter counterterms $\delta|M_1|, \delta|M_2|$ and $\delta|\mu|$. While all of them are well-behaved in the schemes NNN2 and NNN4 defined in Tab. 4.1, the three counterterms have indeed an instability in the NNN3 scheme around $\mu = M_2$. Additionally, the scheme NNN1 is not robust in the region of $\mu \simeq 240\,\text{GeV}$.
The instabilities observed in the counterterms are also reflected by the shifts of the physical masses. In scheme NNNi, the masses $m_{\tilde{\chi}_i^0}$ and $m_{\tilde{\chi}1,2^\pm}$ are shifted from their tree-level value to the loop-corrected mass by a correction $\Delta m_{\tilde{\chi}}$. Fig. 4.2(a) shows $\Delta m_{\tilde{\chi}}$ of neutralino $\tilde{\chi}_i^0$ in the corresponding scheme NNNi while the other $\tilde{\chi}_j^0$, $j \neq i$ remain on-shell in the same scheme. Therefore their vanishing mass shifts are omitted in the plot. $\Delta m_{\tilde{\chi}_2^0}$ and $\Delta m_{\tilde{\chi}_4^0}$ do not exceed 3.5 GeV in the NNN2 and NNN4 scheme, while the correction to $m_{\tilde{\chi}_1^0}$ in the NNN1 scheme and $m_{\tilde{\chi}_3^0}$ in the NNN3 scheme become unphysically large. Turning to Figs. 4.2(b) and 4.2(c), we see that also the chargino masses are badly behaved on account of very large shifts $\Delta M^{\pm}_{\tilde{\chi}_{1,2}}$ whereas they remain stable in the suitably chosen schemes NNN2 and NNN4 even in the critical regions of $\mu \simeq 200\,\text{GeV}$ and $\mu \simeq 240\,\text{GeV}$.

As a consequence, also physical observables like decay widths involving neutralinos or charginos suffer from instabilities if the renormalisation scheme is inappropriate. Fig. 4.3(a) displays the decay width of the process $\tilde{\chi}_4^0 \to \tilde{\chi}_1^0 h$ at the improved Born level (lowest order supplemented by finite $\hat{\mathbf{Z}}$-factors to account for the mixing of Higgs bosons, see Sect. 5.3.2) and at the one-loop level, comparing all NNN schemes. The relative loop contribution $r = \Gamma^{\text{loop}}/\Gamma^{\text{Imp.Born}}$ can be found in Fig. 4.3(b). While the NNN1 and NNN3 schemes result in very large loop corrections due to the choice of unstable schemes particularly for $\mu \simeq 200\,\text{GeV}$ and $\mu \simeq 240\,\text{GeV}$, the schemes NNN2 and NNN4 both are well-behaved.

In conclusion, we have identified stable and unstable on-shell renormalisation conditions within the class of NNN schemes. We observed instabilities in particular for $\mu = M_2$ in accordance with Ref. [108] if the scheme is not appropriately chosen. Consequently, the choice of a suitable renormalisation scheme depends on the parameter values and the resulting bino, wino and higgsino admixture of neutralinos and charginos. In our modified $M_h^{\max}$ scenario, both the NNN2 and the NNN4 scheme provide a stable fixing of M_1, M_2 and μ, whereas NNN1 and NNN3 proved to be badly behaved for the underlying

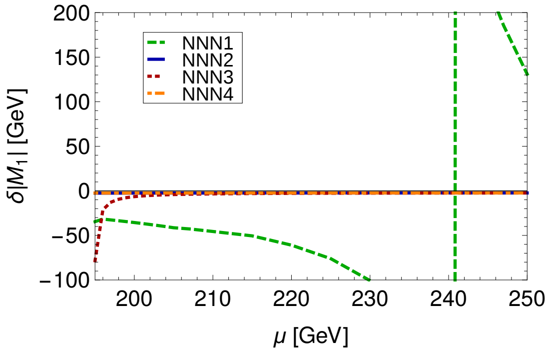

(a)

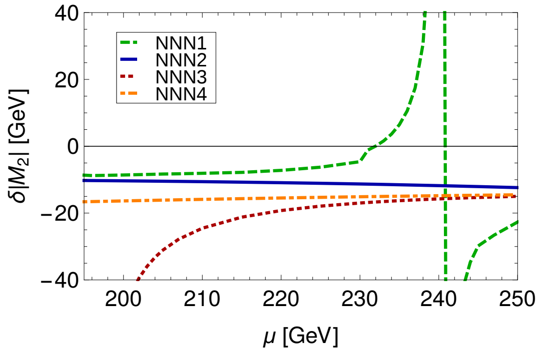

(b)

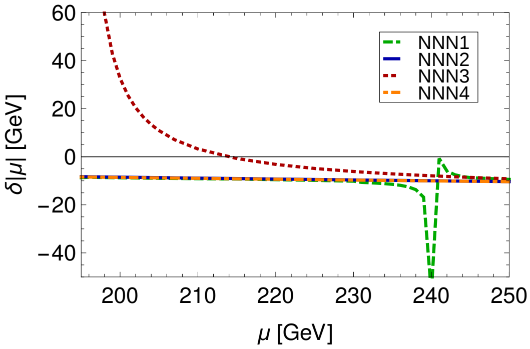

(c)

Figure 4.1.: On-shell parameter renormalisation: **(a)** $\delta|M_1|$, **(b)** $\delta|M_2|$, **(c)** $\delta|\mu|$ in the NNN1 (green), NNN2 (blue), NNN3 (red) and NNN4 (orange) schemes as functions of μ in the modified $M_h^{\max}$ scenario. NNNi denotes the scheme where $\tilde{\chi}_i^0$ and $\tilde{\chi}_{1,2}^\pm$ receive loop corrections to the masses, whereas $\tilde{\chi}_j^0$ with $i \neq j$ are the on-shell input states.

neutralino mixing structure[2]. For a later application to a process with external $\tilde{\chi}_1^0$ and $\tilde{\chi}_4^0$ in this scenario, we prefer to set $m_{\tilde{\chi}_1^0}$ and $m_{\tilde{\chi}_4^0}$ on-shell so that we choose NNN2 as a suitable and stable scheme.

[2]In the meantime, the selection of a stable renormalisation scheme has been automatised in `FeynArts` [114–118] and `FormCalc` [94, 119–122] in a model file with MSSM counterterms [123, 124]. When we investigated this issue, we selected a stable scheme manually according to our study performed here.

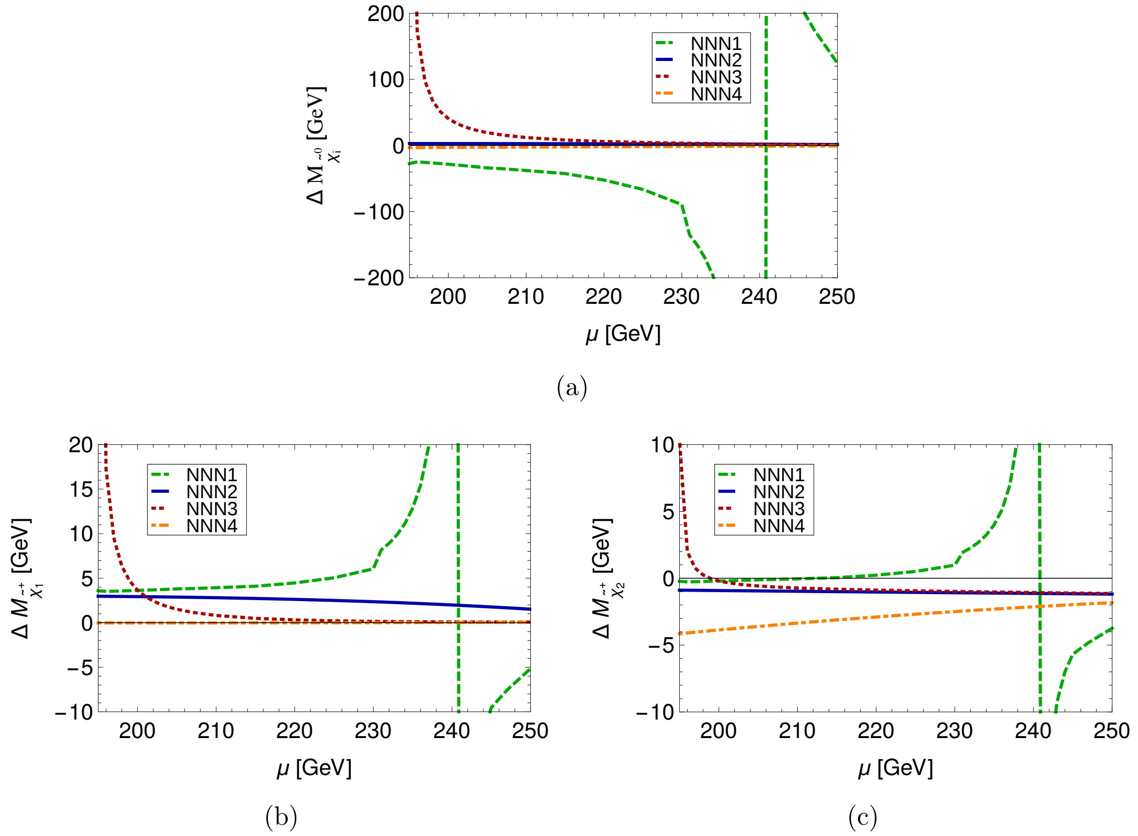

Figure 4.2.: Mass shifts of neutralinos and charginos. **(a)** The mass correction $\Delta M_{\widetilde{\chi}^0_i}$ of neutralino $\widetilde{\chi}^0_i$ in scheme NNNi, while $\Delta M_{\widetilde{\chi}^0_j} = 0$ for $i \neq j$ in scheme NNNi; **(b)** $\Delta M^{\pm}_{\widetilde{\chi}_1}$, **(c)** $\Delta M^{\pm}_{\widetilde{\chi}_2}$ in all NNN schemes depending on μ. Scenario and colour coding identical to those in Fig. 4.1.

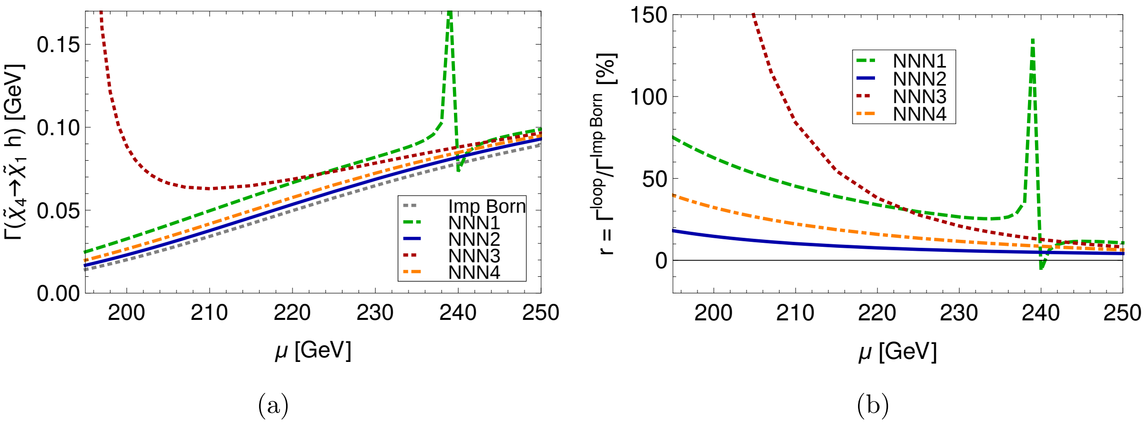

Figure 4.3.: Stability of NNN renormalisation schemes: **(a)** 2-body decay width $\Gamma(\widetilde{\chi}^0_4 \to \widetilde{\chi}^0_1 h)$ at the improved Born level (tree level with $\hat{\mathbf{Z}}$-factors, grey dotted) and at one-loop order in the NNNi schemes; **(b)** Relative one-loop contribution $r = \Gamma^{\text{loop}}/\Gamma^{\text{Imp.Born}}$ under variation of μ. Scenario and colour coding identical to those in Fig. 4.1.

4.4. Renormalisation of the MSSM Higgs sector

Higher-order corrections in the MSSM Higgs sector are very relevant and they have a big impact on the phenomenology and thus the interpretation of searches for additional Higgs bosons. Particles from other sectors contribute via loop diagrams to Higgs observables. Hence beyond the lowest order, the Higgs sector is influenced by more parameters than only $M_{H^\pm}$ (or M_A) and $\tan\beta$. Much effort has been devoted to the precise calculation of the masses and mixing properties of Higgs bosons in the MSSM with real [67, 125–142] and with complex parameters [84, 143–148]. We adopt the hybrid on-shell and $\overline{\text{DR}}$-renormalisation scheme defined in Ref. [84].

4.4.1. Renormalisation of the Higgs potential

For a one-loop renormalisation of the MSSM Higgs sector, one renormalises the linear and bilinear terms in the Higgs potential from Eq. (3.31) by the following transformations:

$$\mathbf{M}_{\phi\phi\chi\chi} \to \mathbf{M}_{\phi\phi\chi\chi} + \delta\mathbf{M}_{\phi\phi\chi\chi} \qquad \mathbf{M}_{\phi^\pm\phi^\pm} \to \mathbf{M}_{\phi^\pm\phi^\pm} + \delta\mathbf{M}_{\phi^\pm\phi^\pm} \tag{4.40}$$
$$T_i \to T_i + \delta T_i, \quad i = h, H, A \tag{4.41}$$
$$\tan\beta \to \tan\beta(1 + \delta\tan\beta), \tag{4.42}$$

where the elements of the mass counterterm matrices in the mass eigenbasis are denoted by

$$(\delta\mathbf{M}_{hHAG})_{ij} = \left(\mathbf{U}_n \delta\mathbf{M}_{\phi\phi\chi\chi}\mathbf{U}_n^\dagger\right)_{ij} = \delta m_{ij}^2, \quad i,j = h, H, A, G, \quad \delta m_{ii}^2 \equiv \delta m_i^2, \tag{4.43}$$
$$(\delta\mathbf{M}_{H^\pm G^\pm})_{kl} = \left(\mathbf{U}_c \delta\mathbf{M}_{\phi^+\phi^+}\mathbf{U}_c^\dagger\right)_{kl} = \delta m_{kl}^2, \quad k,l = H^\pm, G^\pm, \qquad \delta m_{kk}^2 \equiv \delta m_k^2. \tag{4.44}$$

The rotation matrices $\mathbf{U}_n(\alpha, \beta_n)$ and $\mathbf{U}_c(\beta_c)$ stay unrenormalised. Finite Higgs self-energies with the full momentum dependence require one field renormalisation constant per Higgs doublet:

$$\mathcal{H}_i \to (1 + \frac{1}{2}\delta Z_{\mathcal{H}_i})\mathcal{H}_i, \quad i = 1, 2. \tag{4.45}$$

The field renormalisation constants $\delta Z_{ij}, \delta Z_{kl}$ of the physical fields are then obtained as combinations of $\delta Z_{\mathcal{H}_1}, \delta Z_{\mathcal{H}_1}$ and α, β:

$$\delta Z_{hh} = s_\alpha^2 \delta Z_{\mathcal{H}_1} + c_\alpha^2 \delta Z_{\mathcal{H}_2}, \qquad \delta Z_{AA} = \delta Z_{H^-H^+} = s_\beta^2 \delta Z_{\mathcal{H}_1} + c_\beta^2 \delta Z_{\mathcal{H}_2} \tag{4.46}$$
$$\delta Z_{hH} = s_\alpha c_\alpha(\delta Z_{\mathcal{H}_2} - \delta Z_{\mathcal{H}_1}), \qquad \delta Z_{AG} = \delta Z_{H^\pm G^\mp} = s_\beta c_\beta(\delta Z_{\mathcal{H}_2} - \delta Z_{\mathcal{H}_1}) \tag{4.47}$$
$$\delta Z_{HH} = c_\alpha^2 \delta Z_{\mathcal{H}_1} + s_\alpha^2 \delta Z_{\mathcal{H}_2}, \qquad \delta Z_{GG} = \delta Z_{G^-G^+} = c_\beta^2 \delta Z_{\mathcal{H}_1} + s_\beta^2 \delta Z_{\mathcal{H}_2}, \tag{4.48}$$

whereas the $\mathcal{CP}$-violating terms vanish: $\delta Z_{hA} = \delta Z_{hG} = \delta Z_{HA} = \delta Z_{HG} = 0$.

4.4.2. Field and parameter renormalisation conditions

The gauge bosons (as in the SM, but with a different sign convention) and the charged Higgs mass are renormalised on-shell resulting at one-loop order in

$$\delta m^2_{H^\pm} = \mathrm{Re}\Sigma_{H^\pm H^\pm}(M_{H^\pm}). \tag{4.49}$$

In order to minimise the potential, the one-loop tadpole coefficients have to vanish:

$$T_i^{(1)} + \delta T_i = 0 \qquad \Rightarrow \qquad \delta T_i = -T_i; \quad i = h, H, A. \tag{4.50}$$

The parameter $\tan\beta$ is not directly related to a (pseudo-)observable like a mass which could be defined on-shell. Therefore, the $\overline{\mathrm{DR}}$-scheme is employed both for field renormalisation constants of the Higgs doublets and, constructed from them, for $\tan\beta$ such that only purely divergent parts contribute,

$$\delta Z_{\mathcal{H}_1}^{\overline{\mathrm{DR}}} = -\mathrm{Re}\left[\Sigma'^{(\mathrm{div})}_{HH}(m_H^2)\right]_{\alpha=0}, \tag{4.51}$$

$$\delta Z_{\mathcal{H}_2}^{\overline{\mathrm{DR}}} = -\mathrm{Re}\left[\Sigma'^{(\mathrm{div})}_{hh}(m_h^2)\right]_{\alpha=0}, \tag{4.52}$$

$$\delta \tan\beta^{\overline{\mathrm{DR}}} = \frac{1}{2}(\delta Z_{\mathcal{H}_2}^{\overline{\mathrm{DR}}} - \delta Z_{\mathcal{H}_1}^{\overline{\mathrm{DR}}}). \tag{4.53}$$

4.4.3. Renormalised Higgs self-energies

Because the MSSM Higgs sector has only seven independent counterterms for the parameters, $\delta m_{H^\pm}, \delta M_Z^2, \delta M_W^2$, δT_h, δT_H, δT_A and $\delta\tan\beta$, the renormalised self-energies can be expressed in terms of the previously defined quantities. For example in the neutral Higgs sector,

$$\hat{\Sigma}_{ij}(p^2) = \Sigma_{ij}(p^2) + \delta Z_{ij}\left(p^2 - \frac{1}{2}(m_i^2 + m_j^2)\right) - \delta m^2_{ij}, \tag{4.54}$$

$$\hat{\Sigma}_{ik}(p^2) = \Sigma_{ik}(p^2) - \delta m^2_{ik}, \tag{4.55}$$

where $i, j = h, H$ denote the $\mathcal{CP}$-even states and $k = A$ the $\mathcal{CP}$-odd state, the mass counterterms $\delta m^2_{ij}, \delta m^2_{ik}$ and the field renormalisation constants δZ_{ij} do not need to be fixed by imposing another on-shell condition, but they are already given by Eqs. (4.43), (4.44) and (4.46)-(4.48), respectively. In the MSSM with complex parameters, the $\mathcal{CP}$-violating self-energies in Eq. (4.55) contribute, and their impact on masses and mixings will be analysed in detail in Chapters 5 and 6.

Use of programme packages for loop calculations in the MSSM We frequently make use of the programme packages `FeynArts` [114–118] to generate the considered processes, `FormCalc` [94, 119–122] to perform the computation and `FeynHiggs` [67, 146, 149–151] to incorporate precise, state-of-the-art quantities from the Higgs sector into our calculations. In particular, we obtain the renormalised self-energies, loop-corrected Higgs masses and wave function normalisation factors (see Sect. 5.3.2) from `FeynHiggs`. Loop integrals are evaluated with `LoopTools` [94].

In Sections 4.3.4, 6.4, 6.5, 8 and 9, we use `FeynArts-3.7`, `FormCalc-7.4`, `LoopTools-2.8` and `FeynHiggs-2.9.3`, whereas in the remaining chapters we use the updated versions `FeynArts-3.9`, `FormCalc-8.4`, `LoopTools-2.12` and `FeynHiggs-2.10.2`.

Chapter 5.

Mixing properties of Higgs bosons in the complex MSSM

5.1. Higgs propagators

5.1.1. Propagator matrix and the effective self-energy

Radiative corrections give rise to a mixing between the neutral bosons. In general, the Higgs bosons $i, j = h, H, A$ do not only mix among themselves, but also with the Goldstone and electroweak gauge bosons. For the propagators of the neutral Higgs bosons, this implies in principle a 6×6 mixing of $\{h, H, A, G, Z, \gamma\}$. However, the Goldstone and Z-boson contribute only from the order of $(\hat{\Sigma}_{i,G/Z})^2$ on (and the photon even only from four-loop order on) to the Higgs propagators [84]. We neglect these terms because they arise at the same sub-leading two-loop order as the G/Z contributions to the two-loop self-energies $\hat{\Sigma}_{ij}$ that are also not contained in `FeynHiggs` [67, 146, 149, 150]. In contrast, Higgs-G/Z mixings appear already at the one-loop level in processes with external Higgs bosons, such as decay processes, so that they need to be included for a full one-loop result. This is taken into account for an example process in Sect. 9.3. Apart from there, we consider the 3×3 mixing of $\{h, H, A\}$ as an approximation of the originally 6×6 mixing.

Furthermore, if $\mathcal{CP}$ is conserved, the $\mathcal{CP}$-violating self-energies vanish, $\hat{\Sigma}_{hA} = \hat{\Sigma}_{HA} = 0$, so that only the two $\mathcal{CP}$-even states h and H mix. However, in general we will allow for non-zero phases from complex parameters. Hence all renormalised self-energies $\hat{\Sigma}_{ij}(p^2)$ of the Higgs bosons $i, j = h, H, A$ are important ingredients in the description of the mixing between the different interaction eigenstates. Thus, the matrix $\mathbf{M}$ of mass squares does not only contain the tree-level masses m_i^2 on the diagonal, but also the renormalised diagonal and off-diagonal self-energies,

$$\mathbf{M}(p^2) = \begin{pmatrix} m_h^2 - \hat{\Sigma}_{hh}(p^2) & -\hat{\Sigma}_{hH}(p^2) & -\hat{\Sigma}_{hA}(p^2) \\ -\hat{\Sigma}_{Hh}(p^2) & m_H^2 - \hat{\Sigma}_{HH}(p^2) & -\hat{\Sigma}_{HA}(p^2) \\ -\hat{\Sigma}_{Ah}(p^2) & -\hat{\Sigma}_{AH}(p^2) & m_A^2 - \hat{\Sigma}_{AA}(p^2) \end{pmatrix}. \tag{5.1}$$

The renormalised irreducible 2-point vertex functions

$$\hat{\Gamma}_{ij}(p^2) = i\left[(p^2 - m_i^2)\delta_{ij} + \hat{\Sigma}_{ij}(p^2)\right] \tag{5.2}$$

can be collected in the 3×3 matrix $\hat{\mathbf{\Gamma}}_{hHA}$ in terms of $\mathbf{M}$ as

$$\hat{\mathbf{\Gamma}}_{hHA}(p^2) = i\left[p^2\mathbf{1} - \mathbf{M}(p^2)\right]. \tag{5.3}$$

Finally, the propagator matrix $\mathbf{\Delta}_{hHA}$ equals, up to the sign, the inverse of $\hat{\mathbf{\Gamma}}_{hHA}$,

$$\mathbf{\Delta}_{hHA}(p^2) = -\left[\hat{\mathbf{\Gamma}}_{hHA}(p^2)\right]^{-1}. \tag{5.4}$$

Accordingly, the matrix inversion yields the individual propagators $\Delta_{ij}(p^2)$ as the the (ij) elements of the 3×3 matrix $\mathbf{\Delta}_{hHA}(p^2)$,

$$\mathbf{\Delta}_{hHA} = \begin{pmatrix} \Delta_{hh} & \Delta_{hH} & \Delta_{hA} \\ \Delta_{Hh} & \Delta_{HH} & \Delta_{HA} \\ \Delta_{Ah} & \Delta_{AH} & \Delta_{AA} \end{pmatrix}. \tag{5.5}$$

The off-diagonal entries (for $i \neq j$) result in:

$$\Delta_{ij}(p^2) = \frac{\hat{\Gamma}_{ij}\hat{\Gamma}_{kk} - \hat{\Gamma}_{jk}\hat{\Gamma}_{ki}}{\hat{\Gamma}_{ii}\hat{\Gamma}_{jj}\hat{\Gamma}_{kk} + 2\hat{\Gamma}_{ij}\hat{\Gamma}_{jk}\hat{\Gamma}_{ki} - \hat{\Gamma}_{ii}\hat{\Gamma}_{jk}^2 - \hat{\Gamma}_{jj}\hat{\Gamma}_{ki}^2 - \hat{\Gamma}_{kk}\hat{\Gamma}_{ij}^2}. \tag{5.6}$$

All 2-point vertex functions $\hat{\Gamma}(p^2)$ depend on p^2 via Eq. (5.2). Here we do not write the p^2-dependence explicitly for the purpose of an simpler notation, but the full p^2-dependence is implied also below. The solutions of the diagonal propagators, Δ_{ii}, can be compactified in the following way:

$$\begin{aligned}
\Delta_{ii}(p^2) &= \frac{\hat{\Gamma}_{jj}\hat{\Gamma}_{kk} - \hat{\Gamma}_{jk}^2}{-\hat{\Gamma}_{ii}\hat{\Gamma}_{jj}\hat{\Gamma}_{kk} + \hat{\Gamma}_{ii}\hat{\Gamma}_{jk}^2 - 2\hat{\Gamma}_{ij}\hat{\Gamma}_{jk}\hat{\Gamma}_{ki} + \hat{\Gamma}_{jj}\hat{\Gamma}_{ki}^2 + \hat{\Gamma}_{kk}\hat{\Gamma}_{ij}^2} && (5.7)\\
&= \frac{i\left[\hat{\Gamma}_{jj}\hat{\Gamma}_{kk} - \hat{\Gamma}_{jk}^2\right]}{-i\left(\hat{\Gamma}_{ii}\left[\hat{\Gamma}_{jj}\hat{\Gamma}_{kk} - \hat{\Gamma}_{jk}^2\right] + \left[2\hat{\Gamma}_{ij}\hat{\Gamma}_{jk}\hat{\Gamma}_{ki} - \hat{\Gamma}_{jj}\hat{\Gamma}_{ki}^2 - \hat{\Gamma}_{kk}\hat{\Gamma}_{ij}^2\right]\right)} && (5.8)\\
&= \frac{i}{p^2 - m_i^2 + \hat{\Sigma}_{ii} - i\frac{2\hat{\Gamma}_{ij}\hat{\Gamma}_{jk}\hat{\Gamma}_{ki} - \hat{\Gamma}_{jj}\hat{\Gamma}_{ki}^2 - \hat{\Gamma}_{kk}\hat{\Gamma}_{ij}^2}{\hat{\Gamma}_{jj}\hat{\Gamma}_{kk} - \hat{\Gamma}_{jk}^2}} && (5.9)\\
&= \frac{i}{p^2 - m_i^2 + \hat{\Sigma}_{ii}^{\text{eff}}(p^2)}. && (5.10)
\end{aligned}$$

In Eq. (5.10), the effective self-energy is introduced,

$$\hat{\Sigma}_{ii}^{\text{eff}}(p^2) = \hat{\Sigma}_{ii}(p^2) - i\frac{2\hat{\Gamma}_{ij}(p^2)\hat{\Gamma}_{jk}(p^2)\hat{\Gamma}_{ki}(p^2) - \hat{\Gamma}_{ki}^2(p^2)\hat{\Gamma}_{jj}(p^2) - \hat{\Gamma}_{ij}^2(p^2)\hat{\Gamma}_{kk}(p^2)}{\hat{\Gamma}_{jj}(p^2)\hat{\Gamma}_{kk}(p^2) - \hat{\Gamma}_{jk}^2(p^2)}. \tag{5.11}$$

It separates the diagonal self-energy, $\hat{\Sigma}_{ii}$ (which exists already at 1-loop order) from the mixing 2-point functions (whose products only contribute to $\hat{\Sigma}_{ii}^{\text{eff}}$ from 2-loop order on). Hence, replacing the pure self-energy $\hat{\Sigma}_{ii}$ by the effective one, $\hat{\Sigma}_{ii}^{\text{eff}}$, includes also the 3×3 mixing contributions to the diagonal propagator in Eq. (5.10) while preserving formally the structure of the propagator as in the unmixed case. In the limit of no mixing, the second term in Eq. (5.11) vanishes.

5.1.2. Treatment of imaginary parts

In order to account for complex momenta (see below) and imaginary parts of self-energies, we expand the self-energies around the real part of the complex momentum:

$$p^2 \equiv p_r^2 + ip_i^2, \tag{5.12}$$

$$\hat{\Sigma}_{ij}(p^2) \simeq \hat{\Sigma}_{ij}(p_r^2) + ip_i^2\hat{\Sigma}_{ij}'(p_r^2), \tag{5.13}$$

where $\hat{\Sigma}_{ij}'(p^2) \equiv \frac{d\hat{\Sigma}_{ij}(p^2)}{dp^2}$. The reason for this expansion is that `FeynHiggs` evaluates the self-energies at real momenta. For the inclusion of all products of real and imaginary parts, we do not expand the effective self-energy from Eq. (5.11) directly according to Eq. (5.12). Instead, in the same way as in Refs. [45,98], we expand all $\hat{\Gamma}_{ij}(p^2)$ individually before combining them into $\hat{\Sigma}_{ii}^{\text{eff}}$.

5.2. Higgs masses

5.2.1. Pole structure of the propagators depending on the mixing

Due to imaginary parts of the self-energies, the propagator poles are not real, but they lie in the complex mometum plane. The Higgs masses are determined as the complex poles $\mathcal{M}^2$ of the diagonal propagators, or equivalently as the zeros of the inverse diagonal propagators. For this purpose, we need to find the roots of the determinant of the matrix $\hat{\mathbf{\Gamma}}(p^2)$,

$$\det\left[\hat{\mathbf{\Gamma}}_{hHA}\right] = -\frac{1}{\det\left[\mathbf{\Delta}_{hHA}\right]} \stackrel{!}{=} 0. \tag{5.14}$$

Then the loop-corrected masses M are obtained from the real parts of the complex poles and the total widths Γ from the imaginary parts via

$$\mathcal{M}^2 = M^2 - iM\Gamma. \tag{5.15}$$

In the following, we will discuss the impact of higher-order and mixing contributions on the pole structure of the propagators.

5.2.1.1. Lowest order

At lowest order, the self-energy contributions in Eq. (5.2) are absent and the matrix $\hat{\mathbf{\Gamma}}$ simply reads

$$\hat{\mathbf{\Gamma}}^{(0)}_{hHA}(p^2) = i\,\mathrm{diag}\left\{D_h(p^2), D_H(p^2), D_A(p^2)\right\}, \tag{5.16}$$

$$D_i(p^2) = p^2 - m_i^2, \tag{5.17}$$

and the solutions of Eq. (5.14) are the three tree-level masses m_i^2.

5.2.1.2. Higher order without mixing

Beyond tree-level, the self-energies are added at the available order. Restricting them to the unmixed case, $\hat{\Sigma}_{ij} = 0$ for $i \neq j$, leads to

$$\hat{\mathbf{\Gamma}}^{(\text{no mix})}_{hHA}(p^2) = i\,\mathrm{diag}\left\{D_h(p^2) + \hat{\Sigma}_{hh}(p^2), D_H(p^2) + \hat{\Sigma}_{HH}(p^2), D_A(p^2) + \hat{\Sigma}_{AA}(p^2)\right\}, \tag{5.18}$$

so that

$$\det\left[\hat{\mathbf{\Gamma}}^{(\text{no mix})}_{hHA}(p^2)\right] = \prod_{i=h,H,A} D_i(p^2) + \hat{\Sigma}_{ii}(p^2) = 0 \tag{5.19}$$

is achieved if p^2 fulfils the following on-shell relation

$$p^2 - m_i^2 + \hat{\Sigma}_{ii}(p^2) = 0 \tag{5.20}$$

for any $i = h, H, A$. Thus, the full propagator matrix $\mathbf{\Delta}$ has three poles and each propagator $\Delta_{ii}(p^2)$ has exactly one pole $p^2 = \mathcal{M}_i^2$ that solves Eq. (5.20).

5.2.1.3. Higher order with 2 × 2 mixing

If we now turn on the mixing between h and H, the matrix $\hat{\mathbf{\Gamma}}$ becomes block-diagonal with the 2×2 matrix $\hat{\mathbf{\Gamma}}_{hH}$ and the 2-point vertex function of A, which does not mix with any other state:

$$\hat{\mathbf{\Gamma}}_{hHA}(p^2) = \begin{pmatrix} \hat{\mathbf{\Gamma}}_{hH}(p^2) & 0 \\ 0 & \hat{\Gamma}_A(p^2) \end{pmatrix}, \tag{5.21}$$

$$\det\left[\hat{\mathbf{\Gamma}}_{hHA}(p^2)\right] = \det\left[\hat{\mathbf{\Gamma}}_{hH}(p^2)\right] \cdot \det\left[\Gamma_A(p^2)\right]. \tag{5.22}$$

For a closer look at the relation between the roots of the determinant and the roots of the inverse propagator, we write down the propagators and the effective self-energy of the $\{h, H\}$ system explicitly. They follow from Eqs.(5.6), (5.7) and (5.11) by setting $\hat{\Sigma}_{hA} = \hat{\Sigma}_{HA} = 0$ or equivalently from the inversion of the 2×2 submatrix $\hat{\mathbf{\Gamma}}_{hH}$:

$$\Delta_{ii}(p^2) = \frac{i\left[D_j(p^2) + \hat{\Sigma}_{jj}(p^2)\right]}{\left[D_i(p^2) + \hat{\Sigma}_{ii}(p^2)\right]\left[D_j(p^2) + \hat{\Sigma}_{jj}(p^2)\right] - \hat{\Sigma}^2_{ij}(p^2)} = \frac{i}{p^2 - m_i^2 + \hat{\Sigma}^{\text{eff}}_{ii}(p^2)}, \tag{5.23}$$

$$\Delta_{ij}(p^2) = \frac{-i\hat{\Sigma}_{ij}(p^2)}{\left[D_i(p^2) + \hat{\Sigma}_{ii}(p^2)\right]\left[D_j(p^2) + \hat{\Sigma}_{jj}(p^2)\right] - \hat{\Sigma}^2_{ij}(p^2)}, \tag{5.24}$$

$$\hat{\Sigma}^{\text{eff}}_{ii}(p^2) = \hat{\Sigma}_{ii}(p^2) - \frac{\hat{\Sigma}^2_{ij}(p^2)}{D_j(p^2) + \hat{\Sigma}_{jj}(p^2)}. \tag{5.25}$$

Comparing the inverse diagonal propagators with the determinant of the submatrix $\hat{\mathbf{\Gamma}}_{hH}$, we find for $i, j \in \{h, H\}\,,\ i \neq j$,

$$\frac{1}{\Delta_{ii}(p^2)} = \frac{i}{D_j(p^2) + \hat{\Sigma}_{jj}(p^2)}\ \det\left[\hat{\mathbf{\Gamma}}_{hH}(p^2)\right]. \tag{5.26}$$

Eq. (5.26) reveals that both inverse diagonal propagators, $1/\Delta_{hh}$ and $1/\Delta_{HH}$, are proportional to the determinant of $\hat{\mathbf{\Gamma}}_{hH}$, which has two zeros. As opposed to the unmixed case, both zeros of $\det\left[\hat{\mathbf{\Gamma}}_{hH}(p^2)\right]$ are poles of *each* of the diagonal propagators Δ_{hh}, Δ_{HH}. Consequently, it is not clear a priori how to label the poles and the masses. The interaction eigenstates h and H are mixed into the mass eigenstates h_1 and h_2 with the loop-corrected masses M_{h_1}, M_{h_2}. The corresponding poles $\mathcal{M}^2_{h_1}, \mathcal{M}^2_{h_2}$ solve

$$p^2 - m_i^2 + \hat{\Sigma}^{\text{eff}}_{ii}(p^2) = 0. \tag{5.27}$$

for $p^2 = \mathcal{M}^2_{h_a}$ in any combination of $i = h, H$ and $a = 1, 2$, where the effective self-energy is defined in Eq. (5.25). In the 2×2 mixing system, it is convenient to choose $M_{h_1} \leq M_{h_2}$. As for the nomenclature in the 2×2 case, the lighter mass eigenstate h_1 is often denoted as h and the heavier one as H because both are $\mathcal{CP}$-even states. Remarkably, both roots of $\hat{\mathbf{\Gamma}}_{hH}$, $\mathcal{M}^2_{h_1}$ and $\mathcal{M}^2_{h_2}$, are also complex poles of the off-diagonal propagators $\Delta_{hH}(p^2) \equiv \Delta_{Hh}(p^2)$ due to

$$\frac{1}{\Delta_{ij}(p^2)} = \frac{-i}{\hat{\Sigma}_{ij}(p^2)}\ \det\left[\hat{\mathbf{\Gamma}}_{hH}(p^2)\right]. \tag{5.28}$$

Since in this case A does not mix with h and H, the third pole $\mathcal{M}^2_A$ solely solves

$$\mathcal{M}^2_A - m_A^2 + \hat{\Sigma}_{AA}(\mathcal{M}^2_A) = 0, \tag{5.29}$$

but no other combination of A and h_a satisfies the on-shell condition. M_A is the loop-corrected mass of the mass and interaction eigenstate A. In conclusion, solving

$\det\left[\hat{\mathbf{\Gamma}}_{hHA}(p^2)\right] = 0$ is equivalent to solving $\frac{1}{\Delta_{ii}(p^2)} = 0$, where two of the three zeros stem from each of the Δ_{ij}, $i, j = h, H$, and the third solution from Δ_{AA}.

5.2.1.4. Higher order with 3 × 3 mixing

Now we turn to the most general case where complex MSSM parameters lead to $\mathcal{CP}$-violating self-energies $\hat{\Sigma}_{hA}, \hat{\Sigma}_{HA}$. Thus, all three neutral Higgs interaction and $\mathcal{CP}$ eigenstates h, H, A mix into the loop-corrected mass eigenstates h_1, h_2, h_3, which have no longer well-defined $\mathcal{CP}$ quantum numbers, but are admixtures of $\mathcal{CP}$-even and $\mathcal{CP}$-odd components. In this framework, $\hat{\mathbf{\Gamma}}_{hHA}$ is a full 3×3 matrix with the determinant

$$\begin{aligned}\det[\hat{\mathbf{\Gamma}}_{hHA}] = -i \Big[&(D_h + \hat{\Sigma}_{hh})(D_H + \hat{\Sigma}_{HH})(D_A + \hat{\Sigma}_{AA}) + 2\hat{\Sigma}_{hH}\hat{\Sigma}_{HA}\hat{\Sigma}hA \\ &- (D_h + \hat{\Sigma}_{hh})\hat{\Sigma}_{HA} - (D_H + \hat{\Sigma}_{HH})\hat{\Sigma}_{hA} - (D_A + \hat{\Sigma}_{AA})\hat{\Sigma}_{hH}\Big], \end{aligned} \tag{5.30}$$

where we dropped the explicite p^2-dependence of each term for an ease of notation. Comparing Eq. (5.30) with the diagonal and off-diagonal propagators from Eqs. (5.7) and (5.6), respectively, we see that their inverse is proportional to the determinant of $\hat{\mathbf{\Gamma}}_{hHA}$:

$$\frac{1}{\Delta_{ii}} = \frac{\det\left[\hat{\mathbf{\Gamma}}_{hHA}\right]}{(D_j + \hat{\Sigma}_{jj})(D_j + \hat{\Sigma}_{jj}) - \hat{\Sigma}^2_{jk}}, \tag{5.31}$$

$$\frac{1}{\Delta_{ij}} = \frac{\det\left[\hat{\mathbf{\Gamma}}_{hHA}\right]}{\hat{\Sigma}_{jk}\hat{\Sigma}_{ki} - \hat{\Sigma}_{ij}(D_k + \hat{\Sigma}_{kk})}. \tag{5.32}$$

From Eq. (5.31) we conclude that all three roots $p^2 = \mathcal{M}^2_{h_a}$, $a = 1, 2, 3$ of $\det\left[\hat{\mathbf{\Gamma}}_{hHA}(p^2)\right]$ are complex poles of *each* of the three diagonal propagators Δ_{ii}, $i = h, H, A$. This means that

$$\mathcal{M}^2_{h_a} - m_i^2 + \hat{\Sigma}^{\text{eff}}_{ii}(\mathcal{M}^2_{h_a}) = 0 \tag{5.33}$$

holds for any combination of i and a in the presence of 3×3 mixing. Moreover, Eq. (5.32) implies that also the off-diagonal propagators have as many poles as the determinant has zeros, namely three in the case of $\mathcal{CP}$-violating mixing. In the unmixed case, $\hat{\Sigma}^{\text{eff}}_{ii} = \hat{\Sigma}_{ii}$ and each propagator has exactly one pole so that there is a unique mapping between i and a, see Eq. (5.20). But for the general mixing case, it is not unique how to relate the mass eigenstates to the interaction eigenstates. An assignment will be needed for the definition of on-shell wave-function normalisation factors in Sect. 5.3.

5.3. On-shell wave function normalisation factors

5.3.1. Ratios of propagators

As we have seen in the previous sections and as it is also explained in Refs. [45, 98], the effective self-energy $\hat{\Sigma}^{\text{eff}}_{ii}$ can be split into the unmixed part $\hat{\Sigma}_{ii}$ and the mixing terms. One can further simplify Eq. (5.11) by writing

$$\hat{\Sigma}^{\text{eff}}_{ii}(p^2) = \hat{\Sigma}_{ii}(p^2) + \frac{\Delta_{ij}(p^2)}{\Delta_{ii}(p^2)}\hat{\Sigma}_{ij}(p^2) + \frac{\Delta_{ik}(p^2)}{\Delta_{ii}(p^2)}\hat{\Sigma}_{ik}(p^2) \tag{5.34}$$

for $i \neq j \neq k \neq i$. Eq. (5.34) represents the sum of the diagonal and off-diagonal self-energies involving a Higgs boson i where the off-diagonal contributions are weighted by the ratio between the respective off-diagonal and the diagonal propagator. For the 2×2 mixing, this relation between Eqs. (5.23-5.25) can be directly seen. In the 3×3 case, Eq. (5.34) follows from Eq. (5.11) due to

$$\frac{\Delta_{ij}}{\Delta_{ii}} = -\frac{\hat{\Gamma}_{ij}\hat{\Gamma}_{kk} - \hat{\Gamma}_{jk}\hat{\Gamma}_{ki}}{\hat{\Gamma}_{jj}\hat{\Gamma}_{kk} - \hat{\Gamma}^2_{jk}} = -\frac{\hat{\Sigma}_{ij}\,(D_k + \hat{\Sigma}_{kk}) - \hat{\Sigma}_{jk}\hat{\Sigma}_{ki}}{(D_j + \hat{\Sigma}_{jj})\,(D_k + \hat{\Sigma}_{kk}) - \hat{\Sigma}^2_{jk}}, \tag{5.35}$$

analogously for $j \leftrightarrow k$, and $\hat{\Sigma}_{ij} = -i\hat{\Gamma}_{ij}$ from Eq. (5.2) with $i \neq j$. The structure of the ratio of propagators in Eq. (5.35) is illustrated by the comparison to the simple expansion of the diagonal and off-diagonal propagators in powers of the self-energies, here up to two-loop order,

$$\Delta_{ii}(p^2) = i\left(\frac{1}{D_i} - \frac{\hat{\Sigma}_{ii}}{D_i^2} + \frac{\hat{\Sigma}^2_{ii}}{D_i^3} + \frac{\hat{\Sigma}^2_{ij}}{D_i^2 D_j} + \frac{\hat{\Sigma}^2_{ik}}{D_i^2 D_k} + \mathcal{O}(\hat{\Sigma}^3)\right), \tag{5.36}$$

$$\Delta_{ij}(p^2) = i\left(-\frac{\hat{\Sigma}_{ij}}{D_i D_j} + \frac{\hat{\Sigma}_{ii}\hat{\Sigma}_{ij}}{D_i^2 D_j} + \frac{\hat{\Sigma}_{ij}\hat{\Sigma}_{jj}}{D_i D_j^2} + \frac{\hat{\Sigma}_{ik}\hat{\Sigma}_{kj}}{D_i D_k D_j} + \mathcal{O}(\hat{\Sigma}^3)\right), \tag{5.37}$$

where we dropped again the explicit p^2-dependence on the right-hand side. The first term in Eq. (5.36) simply represents the tree-level propagator of particle i. The second term contributes at one-loop order with a diagonal self-energy between two lowest order i-propagators. At the 2-loop level, there are several combinations that have a lowest order i-propagator at each side. The propagator between the two self-energies can then be of the Higgs boson i (between $\hat{\Sigma}^2_{ii}$) or j (between $\hat{\Sigma}^2_{ij}$) or k (between $\hat{\Sigma}^2_{ik}$). The off-diagonal propagator in Eq. (5.37) starts from the one-loop level. At the two-loop level, there are three contributions. These terms are illustrated by the diagrams in Fig. 5.1. If the mixing is restricted to the 2×2 case involving the states i and j, then the expressions containing $\hat{\Sigma}_{ik}$ and $\hat{\Sigma}_{jk}$ vanish.

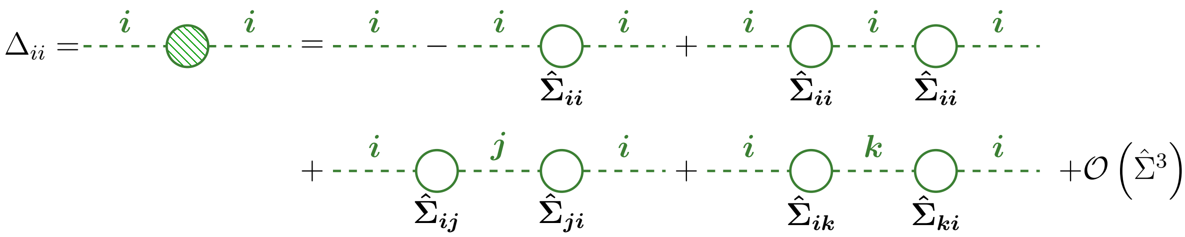

(a) Diagonal Δ_{ii}.

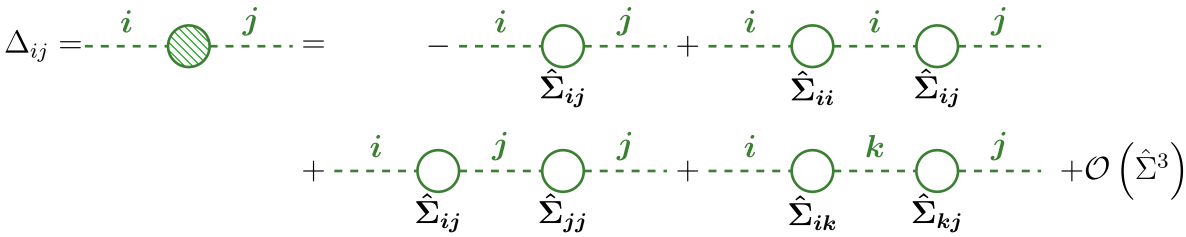

(b) Off-diagonal Δ_{ij}.

Figure 5.1.: Diagrammatic representation of the 3×3 propagators up to 2-loop order. **(a):** diagonal Δ_{ii}, contributing from lowest order on; **(b):** off-diagonal Δ_{ij}, starting at 1-loop order, where i, j, k is a permutation of h, H, A.

Now, we expand the ratio of the propagators Δ_{ij} and Δ_{ii} from Eq. (5.35) up to 2-loop order,

$$\frac{\Delta_{ij}}{\Delta_{ii}} = -\frac{\hat{\Sigma}_{ij}}{D_j} + \frac{\hat{\Sigma}_{ij}\hat{\Sigma}_{jj}}{D_j^2} + \frac{\hat{\Sigma}_{ik}\hat{\Sigma}_{kj}}{D_j D_k} + \mathcal{O}(\hat{\Sigma}^3). \tag{5.38}$$

These terms are visualised in Fig. 5.2. All of them begin with a self-energy starting on i and end on a tree-level propagator of j.

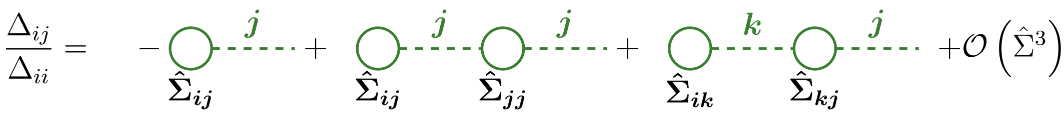

Figure 5.2.: Diagrammatic representation of the ratio of the propagators Δ_{ij} and Δ_{ii} from Eq. (5.38) expanded up to 2-loop order, where $i, j = h, H, A$. Each diagram begins with a self-energy starting on i.

If we multiply Eq. (5.38) by $\hat{\Sigma}_{ji}$, each term begins and ends on a off-diagonal self-energy with index i and contains neither a lowest-order i-propagator nor $\hat{\Sigma}_{ii}$. This also holds for the omitted higher orders. Likewise, Δ_{ik}/Δ_{ii} ends on $1/D_k$, and multiplied by $\hat{\Sigma}_{ki}$ it starts and ends on the index i. Hence, the second and third term in Eq. (5.34) are composed of a combination of self-energies excluding $\hat{\Sigma}_{ii}$ so that they indeed constitute the mixing part of the effective self-energy.

Furthermore, the ratios of off-diagonal and diagonal propagators

$$R_{ij}^{(a)} := \left.\frac{\Delta_{ij}(p^2)}{\Delta_{ii}(p^2)}\right|_{p^2=\mathcal{M}_a^2}, \tag{5.39}$$

stay finite at the complex poles $\mathcal{M}_a^2,\ a = 1, 2, 3$, in contrast to the propagators themselves.

5.3.2. Ẑ-matrix for on-shell properties of external Higgs bosons

Higgs bosons appearing as *external* particles in a process need the right on-shell properties for a correct normalisation of the S-matrix. This is automatically the case in renormalisation schemes with on-shell renormalisation conditions for the fields such that their residues equal unity and that different fields do not mix on their mass shells at the loop level. In the Higgs sector, however, we apply the $\overline{\text{DR}}$ scheme for the parameter $\tan\beta$ and for the field renormalisation, see Sect. 4.4.2 and Ref. [84]. The $\overline{\text{DR}}$ field renormalisation conditions in Eqs. (4.51,4.52) do not ensure proper on-shell properties of the Higgs bosons. In fact, the loop-corrected mass eigenstates h_1, h_2, h_3, which occur as external, on-shell particles e.g. in decay processes, are a mixture of the lowest order states h, H, A. Thus, due to the mixing of on-shell states, finite wave function normalisation factors need to be introduced.

They are calculated according to the LSZ reduction formula (Lehmann, Symanzik, Zimmermann [152]) which shows that the S-matrix element with n external particles is determined by the amputated n-point Green's function $G_{(n)}$ taken on-shell, multiplied by a wave function normalisation factor $Z^{-1/2}$ per external particle. Following Ref. [20], for a propagator $G_{(2)}$ with mass M, thus a 2-point Green's function, the corresponding 2-point vertex function $\Gamma_{(2)} = -G_{(2)}^{-1}$ recscaled by Z is required to have a unit residue at M^2,

$$\text{Res}_{M^2}(Z\Gamma_{(2)}) = \lim_{p^2\to M^2}\left(\frac{-i}{p^2 - M^2} Z\Gamma_{(2)}\right) \overset{!}{=} 1. \tag{5.40}$$

Hence we can calculate the normalisation factor Z as

$$Z = \text{Res}_{M^2}\left\{G_{(2)}\right\}. \tag{5.41}$$

The Green's function is given in terms of the interaction eigenstates. In the case with mixing, where the propagators have several poles, it is not clear how to relate the wave-function normalisation factors of the interaction eigenstates to the poles corresponding to the mass eigenstates. Applying this formalism to the MSSM Higgs sector, we obtain the Z-factors for a neutral Higgs boson $i = h, H, A$ on an external line from the residue of the propagators at the complex pole $\mathcal{M}_a^2, a = 1, 2, 3$ [153, 154]

$$\hat{Z}_i^a := \text{Res}_{\mathcal{M}_a^2}\left\{\Delta_{ii}(p^2)\right\}. \tag{5.42}$$

In order to perform the limit, we expand the diagonal propagator around the complex pole $\mathcal{M}_a^2$. Close to $\mathcal{M}_a^2$, the momentum-dependence of the effective self-energy $\hat{\Sigma}_{ii}^{\text{eff}}(p^2)$

can be approximated by

$$\hat{\Sigma}^{\text{eff}}_{ii}(p^2) = \hat{\Sigma}^{\text{eff}}_{ii}(\mathcal{M}_a^2) + (p^2 - \mathcal{M}_a^2) \cdot \hat{\Sigma}^{\text{eff}\prime}_{ii}(\mathcal{M}_a^2) + \mathcal{O}\left((p^2 - \mathcal{M}_a^2)^2\right). \tag{5.43}$$

Using Eq. (5.43) and the on-shell condition at the complex pole from Eq. (5.33), we obtain [45], up to higher powers of $(p^2 - \mathcal{M}_a^2)$ in the denominator,

$$\begin{aligned}
\Delta_{ii}(p^2) &= \frac{i}{p^2 - m_i^2 + \hat{\Sigma}^{\text{eff}}_{ii}(p^2)} \\
&= \frac{i}{p^2 - m_i^2 + \hat{\Sigma}^{\text{eff}}_{ii}(\mathcal{M}_a^2) + (p^2 - \mathcal{M}_a^2) \cdot \hat{\Sigma}^{\text{eff}\prime}_{ii}(\mathcal{M}_a^2) + \mathcal{O}\left((p^2 - \mathcal{M}_a^2)^2\right)} \\
&= \frac{i}{(p^2 - \mathcal{M}_a^2) \cdot \left[1 + \hat{\Sigma}^{\text{eff}\prime}_{ii}(\mathcal{M}_a^2) + \mathcal{O}(p^2 - \mathcal{M}_a^2)\right]}.
\end{aligned} \tag{5.44}$$

Thus, the residue of the propagator Δ_{ii} yields

$$\hat{Z}_i^a = \lim_{p^2 \to \mathcal{M}_a^2} \left\{ -i(p^2 - \mathcal{M}_a^2) \frac{i}{(p^2 - \mathcal{M}_a^2)\left[1 + \hat{\Sigma}^{\text{eff}\prime}_{ii}(\mathcal{M}_a^2) + \mathcal{O}(p^2 - \mathcal{M}_a^2)\right]} \right\} \tag{5.45}$$

$$= \left. \frac{1}{\frac{\partial}{\partial p^2} \frac{i}{\Delta_{ii}(p^2)}} \right|_{p^2 = \mathcal{M}_a^2} \tag{5.46}$$

$$= \frac{1}{1 + \hat{\Sigma}^{\text{eff}\prime}_{ii}(\mathcal{M}_a^2)}. \tag{5.47}$$

Considering a diagram with the Higgs boson i on an external line, whose propagator has three poles, there are three possibilities which residue to compute. If the amputated Green's function is evaluated at $\mathcal{M}_a^2$, the external i-line has to be multiplied by $\sqrt{\hat{Z}_i^a}$ for the correct S-matrix normalisation. So the resulting mass eigenstate as an outgoing particle is h_a. Alternatively, if the Green's function is amputated at $\mathcal{M}_b^2$, it has to be normalised by

$$\sqrt{\hat{Z}_i^b} = \frac{1}{\sqrt{1 + \hat{\Sigma}^{\text{eff}\prime}_{ii}(\mathcal{M}_b^2)}} \tag{5.48}$$

to achieve the correct S-matrix element. For this choice, the external mass eigenstate is h_b. Moreover, mixing of the particles i and j can occur where the external particle is denoted as i, and j is connected to the rest of the diagram. Then the complete normalisation factor (see Refs. [154, 155]) is given by

$$(\hat{Z}_i^a)^{-1/2} \cdot \text{Res}_{\mathcal{M}_a^2}\left\{\Delta_{ij}(p^2)\right\} = \sqrt{\hat{Z}_i^a} \left. \frac{\Delta_{ij}(p^2)}{\Delta_{jj}(p^2)} \right|_{p^2 = \mathcal{M}_a^2}, \tag{5.49}$$

where the ratio $\frac{\Delta_{ij}(p^2)}{\Delta_{jj}(p^2)}$ does not have a pole at $p^2 = \mathcal{M}_a^2$, see Eq. (5.35). Thus, the wave function normalisation factor for $i - j$ mixing on an external on-shell line at $\mathcal{M}_a^2$ is composed of the overall normalisation factor $\sqrt{\hat{Z}_i^a}$ times the on-shell transition ratio

$$\hat{Z}_{ij}^a \equiv R_{ij}^a = \left.\frac{\Delta_{ij}(p^2)}{\Delta_{ii}(p^2)}\right|_{p^2=\mathcal{M}_a^2}. \tag{5.50}$$

Since Δ_{ii} and Δ_{ij} have – in the case of 3×3 mixing – 3 complex poles, any of them can be chosen for the evaluation of $\hat{Z}_i$, $\hat{Z}_{ij}$ and $\hat{Z}_{ik}$, for example $\mathcal{M}_a^2$. Correspondingly, $\hat{Z}_j, \hat{Z}_{ji}$ and $\hat{Z}_{jk}$ will be evaluated at $\mathcal{M}_b^2$ and $\hat{Z}_k, \hat{Z}_{ki}$ and $\hat{Z}_{kj}$ at $\mathcal{M}_c^2$ where a, b, c are a permutation of 1,2,3, and i, j, k a permutation of h, H, A [156]. For 2×2 mixing, only the two indices involved in the mixing can be permuted.

All choices allowed by the mixing structure are generally possible owing to the several poles of each propagator. However, they might not be equally numerically stable. If the mass eigenstate h_a contains only a small admixture of the interaction eigenstate i, the propagator still has a pole at $\mathcal{M}_a^2$, but the contribution of i to h_a is suppressed at $p^2 \neq \mathcal{M}_a^2$.

In order to be definite, it is in any case necessary to define at which pole to evaluate which normalisation and mixing $\hat{Z}$-factor. This choice corresponds to fixing an assignment between the indices i, j, k of the lowest-order states and the indices a, b, c of the higher-order mixed states and then using it consistently. The assignment $(i, a), (j, b), (k, c)$, which we label as scheme I, prescribes to evaluate $\hat{Z}_i$, $\hat{Z}_{ij}$ and $\hat{Z}_{ik}$ at $\mathcal{M}_a^2$. Once the indices have been assigned we can clear up the notation by writing

$$\hat{Z}_a\big|_I := \hat{Z}_i^a, \quad \hat{Z}_{aj}\big|_I := \hat{Z}_{ij}^a, \quad \hat{Z}_{bi}\big|_I := \hat{Z}_{ji}^b, \tag{5.51}$$

accordingly for the other indices such that the first index always refers to a mass eigenstate $(a, b, c \in \{1, 2, 3\})$[1] and the second index to an interaction eigenstate $(i, j, k \in \{h, H, A\})$. Note that $\hat{Z}_{ai} = \hat{Z}_{bj} = \hat{Z}_{ck} \equiv 1$ in the index scheme I defined above. Once the index scheme has been specified, one can leave out the subscript I.

Furthermore, it is convenient [84] to arrange the products of the normalisation factors $\sqrt{\hat{Z}_a}$ and transition ratios $\hat{Z}_{aj}$

$$\hat{\mathbf{Z}}_{aj} = \sqrt{\hat{Z}_a}\hat{Z}_{aj} \tag{5.52}$$

(note the difference between $\hat{Z}_{aj}$ and $\hat{\mathbf{Z}}_{aj}$) into a non-unitary matrix:

$$\hat{\mathbf{Z}} = \begin{pmatrix} \sqrt{\hat{Z}_1}\hat{Z}_{1h} & \sqrt{\hat{Z}_1}\hat{Z}_{1H} & \sqrt{\hat{Z}_1}\hat{Z}_{1A} \\ \sqrt{\hat{Z}_2}\hat{Z}_{2h} & \sqrt{\hat{Z}_2}\hat{Z}_{2H} & \sqrt{\hat{Z}_2}\hat{Z}_{2A} \\ \sqrt{\hat{Z}_3}\hat{Z}_{3h} & \sqrt{\hat{Z}_3}\hat{Z}_{3H} & \sqrt{\hat{Z}_3}\hat{Z}_{3A} \end{pmatrix}. \tag{5.53}$$

[1] This index notation differs from Refs. [45, 84, 147, 156, 157], but it is only a matter of convention. We regard our notation more intuitive in view of the use of $\hat{\mathbf{Z}}$-factors e.g. in Eq. (5.74)

The $\hat{\mathbf{Z}}$-matrix defined above in Eq. (5.53) fulfils the unit residue condition for the mixing case, written in the following compact form [45, 98, 147, 156]:

$$\lim_{p^2 \to \mathcal{M}_a^2} -\frac{i}{p^2 - \mathcal{M}_a^2} \left(\hat{\mathbf{Z}} \cdot \hat{\Gamma}_{hHA} \cdot \hat{\mathbf{Z}}^T\right)_{hh} = 1, \tag{5.54}$$

$$\lim_{p^2 \to \mathcal{M}_b^2} -\frac{i}{p^2 - \mathcal{M}_b^2} \left(\hat{\mathbf{Z}} \cdot \hat{\Gamma}_{hHA} \cdot \hat{\mathbf{Z}}^T\right)_{HH} = 1, \tag{5.55}$$

$$\lim_{p^2 \to \mathcal{M}_c^2} -\frac{i}{p^2 - \mathcal{M}_c^2} \left(\hat{\mathbf{Z}} \cdot \hat{\Gamma}_{hHA} \cdot \hat{\mathbf{Z}}^T\right)_{AA} = 1. \tag{5.56}$$

It is equally possible to begin with these equations (5.54-5.56) requiring unit residues to derive the elements of the $\hat{\mathbf{Z}}$-matrix whose solutions are given in Eqs. (5.47) and (5.50).

In the literature, different conventions for the $\hat{\mathbf{Z}}$-factors have been employed. While Refs. [153, 154, 158, 159] introduce the normalisation factors for $h-H$ mixing in the MSSM with real parameters, the full 3×3 mixing in the presence of complex parameters is considered in Refs. [45, 84, 98, 147, 156, 157]. In Ref. [157] and earlier publications, the $\hat{Z}$-factors were evaluated at the real parts of the complex poles, i.e. the loop corrected masses and only the real parts of $\hat{Z}_a$ were included. In Ref. [156] the evaluation at the full complex poles and the inclusion of imaginary parts according to Eq. 5.13 were introduced which leads to more stable results as well as to the physically equivalent choices of index assignments. The calculation of the $\hat{\mathbf{Z}}$-factors of MSSM Higgs bosons can be performed with the program `FeynHiggs`. Within `FeynHiggs`, their ordering, described in Refs. [84, 160], proceeds through an algorithm that minimizes the sum over the differences between the masses obtained from the diagonalisation and the associated masses of the $\hat{\mathbf{Z}}$-factor ordering, comparing all possible permutations of the Higgs states involved in the mixing. With this prescription, discontinuities of $\hat{\mathbf{Z}}$-factors can occur at level crossings if two masses are nearly degenerate. Such a behaviour corresponds to a swap of the composition of the mass eigenstates in terms of interaction eigenstates. Those "jumps" of the $\hat{\mathbf{Z}}$-factors can be avoided by the method for the assignment discussed in Sect. 5.4.2.

5.3.2.1. Index scheme independence of the $\hat{\mathbf{Z}}$-matrix

As discussed above, the pole structure of the full propagators allows for the freedom at which pole to evaluate which $\hat{Z}$-factor. This initial ambiguity, however, results in physically equivalent results, as we will proof in this section. For example, the residue of Δ_{ii} at $\mathcal{M}_a^2$ differs from the residue of Δ_{ii} at $\mathcal{M}_b^2$ and from the residue of Δ_{jj} at $\mathcal{M}_a^2$ such that

$$\hat{Z}_a\big|_I = \frac{1}{1+\hat{\Sigma}_{ii}^{\text{eff}\prime}(\mathcal{M}_a^2)} \neq \frac{1}{1+\hat{\Sigma}_{ii}^{\text{eff}\prime}(\mathcal{M}_b^2)} = \hat{Z}_b\big|_I, \tag{5.57}$$

$$\hat{Z}_a\big|_I \neq \hat{Z}_a\big|_{II} = \frac{1}{1+\hat{\Sigma}_{jj}^{\text{eff}\prime}(\mathcal{M}_a^2)} \tag{5.58}$$

where the schemes denoted by I and II represent the following assignments

$$I \leftrightarrow (i,a),(j,b),(k,c), \tag{5.59}$$
$$II \leftrightarrow (j,a),(i,b),(k,c). \tag{5.60}$$

Furthermore, for the choice $(h,1),(H,2),(A,3)$, the diagonal elements of the $\hat{\mathbf{Z}}$-matrix are equal to $\sqrt{\hat{Z}_a},\ a=1,2,3$ in scheme I. For other choices of the index assignment, these simpler expressions (where the ratio of propagators equals 1) appear on 3 off-diagonal positions in the $\hat{\mathbf{Z}}$-matrix. While the values $\hat{Z}_a$ and $\hat{Z}_{aj},\ a=1,2,3; j=h,H,A$ do depend on the assignment of (a,b,c) and $(1,2,3)$, the values of the physical combinations $\hat{\mathbf{Z}}_{aj}=\sqrt{\hat{Z}_a}\hat{Z}_{aj}$ appearing as elements of the matrix in Eq. (5.53) are scheme independent. We derive this property from the general ratios of propagators (for simplicity, we only consider the 2×2 mixing in this derivation, but the arguments can be directly transferred to the 3×3 case),

$$\frac{\Delta_{ji}(p^2)}{\Delta_{jj}(p^2)} = \frac{-\hat{\Sigma}_{ij}(p^2)}{D_i(p^2)+\hat{\Sigma}_{ii}(p^2)}, \tag{5.61}$$
$$\frac{\Delta_{ii}(p^2)}{\Delta_{jj}(p^2)} = \frac{D_j(p^2)+\hat{\Sigma}_{jj}(p^2)}{D_i(p^2)+\hat{\Sigma}_{ii}(p^2)}. \tag{5.62}$$

Furthermore we exploit two relations that only hold at a complex pole, using the effective self-energy from Eq. (5.25),

$$\left.\frac{\hat{\Sigma}^2_{ij}(p^2)}{D_i(p^2)+\hat{\Sigma}_{ii}(p^2)}\right|_{p^2=\mathcal{M}_a^2} = \hat{\Sigma}_{jj}(\mathcal{M}_a^2) - \hat{\Sigma}^{\text{eff}}_{jj}(\mathcal{M}_a^2) = \left.\left(\hat{\Sigma}_{jj}(p^2)+D_j(p^2)\right)\right|_{p^2=\mathcal{M}_a^2}, \tag{5.63}$$

and applying the on-shell condition from Eq. (5.33) on the ratio of diagonal propagators,

$$\left.\frac{\Delta_{ii}(p^2)}{\Delta_{jj}(p^2)}\right|_{p^2=\mathcal{M}_a^2} = \frac{1+\hat{\Sigma}^{\text{eff}\prime}_{jj}(\mathcal{M}_a^2)}{1+\hat{\Sigma}^{\text{eff}\prime}_{ii}(\mathcal{M}_a^2)}. \tag{5.64}$$

Now we are able to show that

$$\frac{1+\hat{\Sigma}^{\text{eff}\prime}_{jj}(\mathcal{M}_a^2)}{1+\hat{\Sigma}^{\text{eff}\prime}_{ii}(\mathcal{M}_a^2)} \overset{5.64}{=} \left.\frac{\Delta_{ii}(p^2)}{\Delta_{jj}(p^2)}\right|_{p^2=\mathcal{M}_a^2} \overset{5.62}{=} \left.\frac{D_j(p^2)+\hat{\Sigma}_{jj}(p^2)}{D_i(p^2)+\hat{\Sigma}_{ii}(p^2)}\right|_{p^2=\mathcal{M}_a^2} \overset{5.63}{=} \left(\frac{\hat{\Sigma}_{ij}}{D_i+\hat{\Sigma}_{ii}}\right)^2_{p^2=\mathcal{M}_a^2} \tag{5.65}$$

$$\overset{5.61}{=} \left(\frac{\Delta_{ji}(p^2)}{\Delta_{jj}(p^2)}\right)^2_{p^2=\mathcal{M}_a^2}. \tag{5.66}$$

This equality provides a transformation between scheme I (where i and a are associated, hence $\hat{Z}_{ai} \equiv 1$) and scheme II (where j and a are matched):

$$\begin{aligned}\hat{\mathbf{Z}}_{ai}|_I = \left(\sqrt{\hat{Z}_a}\hat{Z}_{ai}\right)_I &= \frac{1}{\sqrt{1+\hat{\Sigma}^{\text{eff}\prime}_{ii}(\mathcal{M}_a^2)}} \\ &= \frac{1}{\sqrt{1+\hat{\Sigma}^{\text{eff}\prime}_{jj}(\mathcal{M}_a^2)}}\frac{\Delta_{ji}}{\Delta_{jj}}\bigg|_{p^2=\mathcal{M}_a^2} = \left(\sqrt{\hat{Z}_a}\hat{Z}_{ai}\right)_{II} = \hat{\mathbf{Z}}_{ai}\bigg|_{II}. \end{aligned} \tag{5.67}$$

While the values of $\hat{Z}_a$ and $\hat{Z}_{ai}$ depend on the choice of the index mapping, Eq. (5.67) ensures that the elements of the $\hat{\mathbf{Z}}$-matrix are invariant under the choice of a, b, c as a permutation of $1, 2, 3$. We also tested this relation numerically for various parameter points and always found agreement within the numerical precision.

5.4. Relation between interaction and mass eigenstates

The complex poles are strictly ordered according to their real parts such that $M_{h_1} \leq M_{h_2} \leq M_{h_3}$. If two masses $M_a \simeq M_b$ are close to each other, the composition of the two states h_a, h_b in terms of the original states $i, j \in h, H, A$ might be interchanged at a crossover. However, this might not always proceed smoothly as a function of the input parameters, but a sudden exchange of the "characters" of h_a and h_b is possible. In such a case, the effective self-energies and ratios of propagators needed for the $\hat{\mathbf{Z}}$-factors are evaluated at a different complex pole than before the crossing, corresponding to an interchange of two rows of the $\hat{\mathbf{Z}}$-matrix. We will analyse how the loop corrected masses of the interaction eigenstates in the case without mixing evolve into the masses M_{h_a}, $a = 1, 2, 3$, by continuously switching on the mixing contributions.

5.4.1. Numerical determination of the Higgs boson masses

There are several ways of how to compute the Higgs masses numerically. On the one hand, `FeynHiggs` [67, 146, 149, 150] is based on the Feynman-diagrammatic approach where the Higgs boson self-energies are calculated in the on-shell scheme. The masses are determined from the complex poles of the propagators. `FeynHiggs` numerically diagonalizes the mass matrix $\mathbf{M}$ applying a Jacobi-type algorithm [161]. With $\mu_a(p^2)$ being the ath eigenvalue of $\mathbf{M}(p^2)$, the real parts of the zeros of the function $\mu_a^2(p^2) - p^2$ yield the mass eigenvalues $M_{h_a}^2$ [157]. On the other hand, as argued in Sect. 5.2 and e.g. in Refs. [84, 98, 157], finding the roots of $\hat{\mathbf{\Gamma}}_{hHA}(p^2)$ is equivalent to solving

$$\frac{1}{\Delta_{ii}(p^2)} = 0 \tag{5.68}$$

for any $i = h, H, A$. This feature suggests an iterative procedure to solve Eq. (5.33) because the momentum p^2 appears both explicitly and as the argument of the effective self-energy. We use the self-energies from `FeynHiggs`, evaluate them at complex momenta according to Eq. (5.13) and calculate the effective self-energies. Starting at a tree-level mass $p^2 = m_i^2$, we insert this initial momentum into the effective self-energy and obtain the subsequent iteration of the momentum from Eq. (5.33) until the inverse diagonal propagator approaches zero. In this iterative method, all poles of one propagator can be found by starting at different initial momenta. In the special case of no mixing or 2×2 mixing, the convergence is faster than for the 3×3 mixing. The mass values that we obtain by our iteration are in agreement with those obtained from `FeynHiggs`.

5.4.2. Dependence on the mixing term in the effective self-energy

Regarding the mixing contribution to the diagonal propagators, Eq. (5.11) demonstrates that the effective self-energy consists of an unmixed part, $\hat{\Sigma}_{ii}$, and the second term with the mixing. In order to study the impact of the mixing on the mass determination and the connection between the two Higgs bases, we multiply the mixing term by an artificially introduced coefficient $\lambda \in [0, 1]$:

$$\hat{\Sigma}_{ii}^{\text{eff}}(p^2, \lambda) := \hat{\Sigma}_{ii}(p^2) - \lambda \cdot i \frac{2\hat{\Gamma}_{ij}(p^2)\hat{\Gamma}_{jk}(p^2)\hat{\Gamma}_{ki}(p^2) - \hat{\Gamma}_{ki}^2(p^2)\hat{\Gamma}_{jj}(p^2) - \hat{\Gamma}_{ij}^2(p^2)\hat{\Gamma}_{kk}(p^2)}{\hat{\Gamma}_{jj}(p^2)\hat{\Gamma}_{kk}(p^2) - \hat{\Gamma}_{jk}^2(p^2)}, \tag{5.69}$$

such that the limit $\lambda = 1$ recovers Eq. (5.11) and $\lambda = 0$ switches the mixing off. In the next step, we investigate how the masses depend on the mixing coefficient in Eq. (5.69). Varying λ in steps of $\Delta\lambda = 0.05$, we run the iteration of finding the masses for each value of $\lambda \in [0, 1]$. This means that every mass point shown in Fig. 5.3 represents the square root of the real part of a complex pole, which has been determined by the value of the final momentum of the iteration. Fig. 5.3 shows the iteratively determined, loop corrected Higgs boson masses in the $\mathcal{CP}$-violating $M_h^{\text{mod+}}$ scenario (see Tab. A.1) with

$$M_{H^\pm} = 300\,\text{GeV}, \quad \tan\beta = 25, \quad \phi_{A_t} = \pi/4, \quad \mu = 1000\,\text{GeV}. \tag{5.70}$$

The mass solutions from the roots of the inverse propagator $1/\Delta_{hh}(p^2)$ are shown in Fig. 5.3(a) for the initial momenta m_h^2 (red circles), m_H^2 (blue triangles) and m_A^3 (green diamonds). Analogously, Fig. 5.3(b) displays the masses found from $1/\Delta_{HH}(p^2)$ and Fig. 5.3(c) those from $1/\Delta_{AA}(p^2)$ - all depending on λ.

As expected, for $\lambda = 0$ each propagator $\Delta_{ii}(p^2)$ has only a single pole $\mathcal{M}_i^2$ so that there is a unique assignment between each lowest order mass m_i^2 and the loop-corrected mass $M_i^2 = \text{Re}\mathcal{M}_i^2$. In this case, all iterations for the determination of poles of $\Delta_{ii}(p^2)$ result in the same (unique) pole and therefore yield the same loop-corrected mass value regardless of the start momentum.

On the contrary, for the physical mixing ($\lambda = 1$), each propagator has three poles so that there is no unique assignment between the tree-level mass of an interaction eigenstate and a higher-order mass of a mixed state. However, with our mixing-dependent analysis we can identify the mapping that provides the "smoothest" transition when λ is varied from 0 to 1. Imposing the criterion that there should be no jumps and requiring the smallest difference $|M(\lambda = 1) - M(\lambda = 0)|$, we obtain in this case the assignment

$$M_{h_1} \leftrightarrow h, \quad M_{h_3} \leftrightarrow H, \quad M_{h_2} \leftrightarrow A, \tag{5.71}$$

where $M_{h_1} < M_{h_2} < M_{h_3}$. Fig. 5.3(b) shows that the value of M_{h_2} at $\lambda = 1$ can also be reached from $M_H(\lambda = 0)$, but the difference is larger. This prescription helps in avoiding jumps of the $\hat{\mathbf{Z}}$-factors.

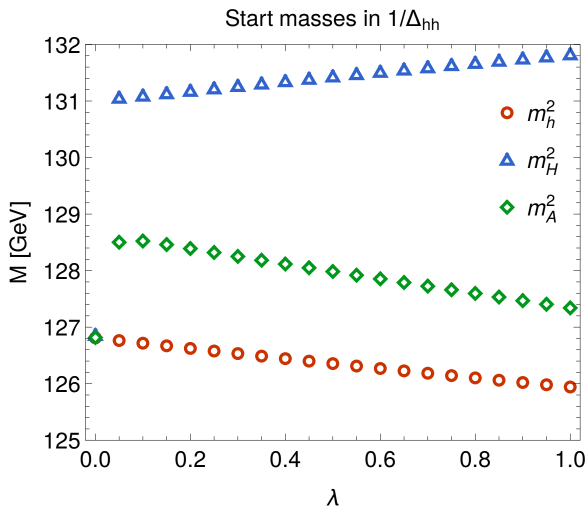

(a)

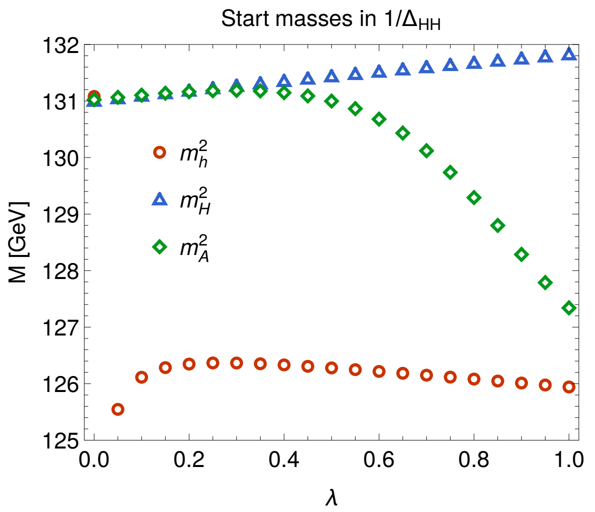

(b)

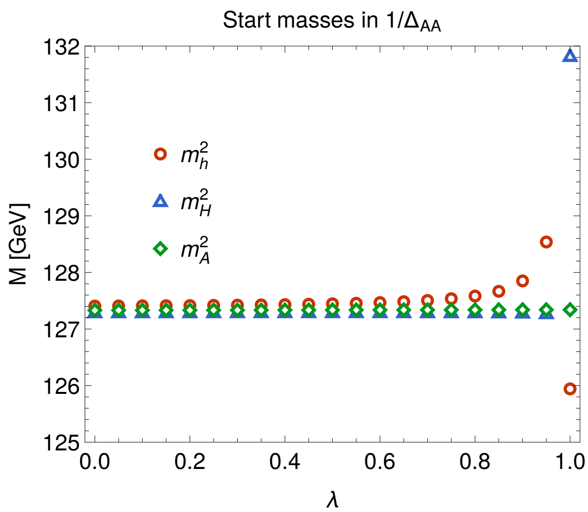

(c)

Figure 5.3.: Higgs boson masses determined iteratively, with variable mixing coefficient λ, in the $\mathcal{CP}$-violating $M_h^{\text{mod}+}$ scenario with $M_{H^\pm} = 300\,\text{GeV}, \tan\beta = 25$, $\phi_{A_t} = \pi/4$ and $\mu = 1000\,\text{GeV}$. The iterations starting at the tree-level masses m_h^2 (red circles), m_H^2 (blue triangles) and m_h^3 (green diamonds) result in the roots of **(a)** $1/\Delta_{hh}(p^2)$, **(b)** $1/\Delta_{HH}(p^2)$ and **(c)** $1/\Delta_{AA}(p^2)$.

5.5. Use of $\hat{\mathbf{Z}}$-factors for external Higgs bosons

The $\hat{\mathbf{Z}}$-factors have been introduced for the correct normalisation of matrix elements with external, on-shell Higgs bosons h_a, $p^2 = \mathcal{M}_a^2$. It should be noted that $\hat{\mathbf{Z}}$ as a non-unitary matrix does not provide a unitary transformation between the interaction basis and the mass basis. The fact that $\hat{\mathbf{Z}}$ is a non-unitary matrix is related to the imaginary parts appearing in the poles of unstable particles. Using the $\hat{\mathbf{Z}}$-matrix, one can express the one-particle irreducible (1PI) vertex functions $\hat{\Gamma}_{h_a}$ involving a mass eigenstate h_1, h_2, h_3 as an external particle as a linear combination of the well defined 1PI vertex functions of the interaction eigenstates, $\hat{\Gamma}_i$:

$$\hat{\Gamma}_{h_a} = \hat{\mathbf{Z}}_{ah}\hat{\Gamma}_h + \hat{\mathbf{Z}}_{aH}\hat{\Gamma}_H + \hat{\mathbf{Z}}_{aA}\hat{\Gamma}_A + \ldots \tag{5.72}$$

$$= \sqrt{\hat{Z}_a}\,\left(\hat{Z}_{ah}\hat{\Gamma}_h + \hat{Z}_{aH}\hat{\Gamma}_H + \hat{Z}_{aA}\hat{\Gamma}_A\right) + \ldots, \tag{5.73}$$

where the ellipsis refers to additional terms arising from the mixing with Goldstone and vector bosons, which are not described by the $\hat{\mathbf{Z}}$-matrix. Thus, the overall normalisation factor $\sqrt{\hat{Z}_a}$ accounts for the unstable particle h_a appearing as an external line. In addition, the factors $\hat{Z}_{ai}$ from Eqs. (5.50) and (5.51) as ratios of propagators at $p^2 = \mathcal{M}_a^2$ describe the transition between the states h_a and i. The transition factor $\hat{Z}_{ai}$ occurs in a diagram where h_a is the external particle, but i directly couples to the vertex. All possibilities for $i = h, H, A$ need to be included for each h_a, hence the sum arises. This is depicted in Fig. 5.4 (cf. also Refs. [98, 160]). Conveniently, Eq. (5.73) can be written

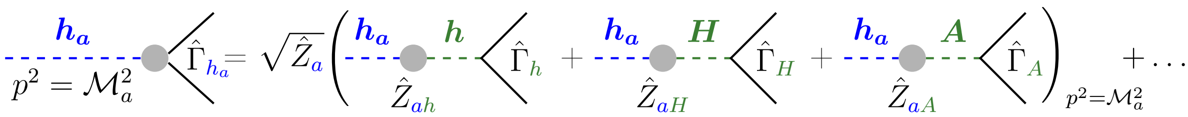

Figure 5.4.: $\hat{\mathbf{Z}}$-factors for external Higgs bosons: The vertex function $\hat{\Gamma}_{h_a}$ is constructed from vertex functions $\hat{\Gamma}_i$, $i = h, H, A$, the transition factors $\hat{Z}_{ai}$ and the overall normalisation factor $\sqrt{\hat{Z}_a}$. Mixing with Goldstone and gauge bosons is omitted.

in matrix form for all h_1, h_2, h_3 as

$$\begin{pmatrix} \hat{\Gamma}_{h_1} \\ \hat{\Gamma}_{h_2} \\ \hat{\Gamma}_{h_3} \end{pmatrix} = \hat{\mathbf{Z}} \cdot \begin{pmatrix} \hat{\Gamma}_h \\ \hat{\Gamma}_H \\ \hat{\Gamma}_A \end{pmatrix} + \ldots\,. \tag{5.74}$$

In this way, propagator corrections at external legs are effectively absorbed into the vertices of neutral Higgs bosons. In Sects. 8-10 we will apply the $\hat{\mathbf{Z}}$-factors to supplement the Born result such that only other propagator type corrections (such as mixing with the Goldstone and Z-bosons) as well as vertex, box and real corrections will have to be calculated individually. On the other hand, we will numerically compare the $\hat{\mathbf{Z}}$-factor approximation with the full propagator mixing in Sect. 6.

5.6. Effective couplings

Since the $\hat{\mathbf{Z}}$-matrix is not unitary, it does not represent a unitary transformation between the $\{h, H, A\}$ and the $\{h_1, h_2, h_3\}$ basis. However, it is not necessary to diagonalise the mass matrix for the determination of the poles of the propagators. Hence there is a priori no need to introduce a unitary transformation. Though, if a unitary matrix $\mathbf{U}$ is desired for the definition of effective couplings, an approximation of the momentum dependence of $\hat{\mathbf{Z}}$ is required. There is no unique prescription of how to achieve a unitary mixing matrix, but a possible choice is the $p^2 = 0$ approximation [84, 160]. As in the effective potential approach, the external momentum p^2 is set to zero in the renormalised self-energies $\hat{\Sigma}_{ij}(p^2) \to \hat{\Sigma}_{ij}(0)$ so that they become real. Then $\mathbf{U}$ diagonalises the real matrix $\mathbf{M}(0)$ and the propagators have real poles. $\mathbf{U}$ can be chosen real and it transform the $\mathcal{CP}$-eigenstates into the mass eigenstates,

$$\begin{pmatrix} h_1 \\ h_2 \\ h_3 \end{pmatrix} = \mathbf{U} \begin{pmatrix} h \\ H \\ A \end{pmatrix}, \qquad \mathbf{U} = \begin{pmatrix} \mathbf{U}_{1h} & \mathbf{U}_{1H} & \mathbf{U}_{1A} \\ \mathbf{U}_{2h} & \mathbf{U}_{2H} & \mathbf{U}_{2A} \\ \mathbf{U}_{3h} & \mathbf{U}_{3H} & \mathbf{U}_{3A} \end{pmatrix}, \tag{5.75}$$

so that U_{aA}^2 quantifies the admixture of an $\mathcal{CP}$-odd component inside h_a [84]. The elements of $\mathbf{U}$ can then be used to introduce effective couplings of the loop-corrected states h_a to any other particles X in terms of the couplings of the unmixed states i by the relation

$$C^U_{h_a X} = \sum_{i=h,H,A} \mathbf{U}_{ai} C_{iX}. \tag{5.76}$$

absorbing some higher-order corrections, but neglecting imaginary parts and the full momentum dependence of the self-energies. Hence, the application of $\mathbf{U}$ resembles the use of $\hat{\mathbf{Z}}$-factors in Eq. (5.72). Yet, the rotation matrix $\mathbf{U}$ introduced for effective couplings as a unitary approximation is conceptually quite different from the $\hat{\mathbf{Z}}$-matrix arising from propagator corrections and introduced for the correct normalisation of the S-matrix. They coincide only in the limit of $p^2 = 0$. However, both capture effects of higher orders that can conveniently be incorporated into an improved Born result. We shall compare both approaches numerically in Sect. 6.3.2.3 while using $\hat{\mathbf{Z}}$-factors everywhere else in this thesis.

Chapter 6.

Breit-Wigner approximation of the full Higgs propagators

In the previous chapter, $\hat{\mathbf{Z}}$-factors were introduced that account for propagator corrections in the presence of mixing of the lowest-order Higgs bosons h, H, A into the loop-corrected mass eigenstates h_1, h_2, h_3. These $\hat{\mathbf{Z}}$-factors arise from the on-shell values of different combinations of the full mixing propagators, which depend on the momentum p^2 in a twofold way. On the one hand, the constituents $D_i(p^2) = p^2 - m_i^2$ give rise to an explicit p^2-dependence. On the other hand, the self-energies $\hat{\Sigma}_{ij}(p^2)$ depend on the momentum as well, but away from thresholds, their p^2 dependence is not particularly pronounced.

In this chapter, we will develop an approximation of the full mixing propagators with the aim to maintain the leading momentum dependence, but to simplify the mixing contributions by making use of the on-shell $\hat{\mathbf{Z}}$-factors. The real parts of the complex poles are interpreted as the physical masses whereas the imaginary parts of the poles give rise to decay widths of the Higgs bosons. Thereby, the physical meaning of the complex poles is connected to the question of how to treat unstable particles in quantum field theory.

6.1. Unstable particles and the total decay width

In the context of determining complex poles of propagators, we now briefly discuss resonances and unstable particles, see e.g. Refs. [162–166]. While stable particles are associated with a real pole of the S-matrix, for unstable particles the associated self-energy develops an imaginary part, so that the pole of the propagator is located off the real axis within the complex plane. As in the previous chapter, we denote the complex pole of a Higgs boson h_a by $\mathcal{M}_a^2$, whereas $\mathcal{M}$ (without an index or square) stands for the scattering matrix. For a single pole, the scattering matrix $\mathcal{M}$ as a function of the squared centre-of-mass energy s can be schematically written in the vicinity of the complex pole in a gauge-invariant way as

$$\mathcal{M}(s) = \frac{R}{s - \mathcal{M}_a^2} + F(s), \tag{6.1}$$

where R denotes the residue and F represents non-resonant contributions. Writing the complex pole as $\mathcal{M}_a^2 = M_{h_a}^2 - iM_{h_a}\Gamma_{h_a}$, the mass M_{h_a} of the unstable particle h_a is obtained from the real part of the complex pole, while the total width is obtained from the imaginary part. Accordingly, the expansion around the complex pole $\mathcal{M}_a^2$ leads to a Breit–Wigner propagator with a constant width,

$$\Delta_a^{\mathrm{BW}}(p^2) := \frac{i}{p^2 - \mathcal{M}_a^2} = \frac{i}{p^2 - M_{h_a}^2 + iM_{h_a}\Gamma_{h_a}}. \tag{6.2}$$

In the following, we will use a Breit–Wigner propagator of this form, i.e. with a constant width, to express the contribution of the unstable scalar h_a with mass M_{h_a} and total width Γ_{h_a} in the resonance region (a Breit–Wigner propagator with a running width can be obtained from a reparametrisation of the mass and width appearing in Eq. (6.2)).

The transition from the Higgs propagators in the case of mixing to the Breit-Wigner propagators corresponds to a change of basis from h, H, A to h_1, h_2, h_3. The Breit-Wigner propagators are obtained from poles of the S-matrix and therefore correspond to the mass eigenstates.

6.2. Expansion of the full propagators around the complex poles

Eqs. (5.31) and (5.32) imply for 3×3 mixing that each propagator Δ_{ii}, Δ_{ij} has a pole at $\mathcal{M}_1^2, \mathcal{M}_2^2$ and $\mathcal{M}_3^2$. Because of this structure, an expansion of the full propagators near one single pole is not expected to yield a sufficient approximation. Instead, we will expand the full propagators around all three poles.

6.2.1. Expansion of the diagonal propagators

Beginning with an expansion of $\Delta_{ii}(p^2)$ in the vicinity of $\mathcal{M}_a^2$ and making use of the expansion of the effective self-energy performed in Eq. (5.43), we obtain as in (5.44) for $p^2 \simeq \mathcal{M}_a^2$

$$\Delta_{ii}(p^2) = \frac{i}{p^2 - m_i^2 + \hat{\Sigma}_{ii}^{\mathrm{eff}}(p^2)} \simeq \frac{i}{p^2 - \mathcal{M}_a^2} \cdot \frac{1}{1 + \hat{\Sigma}_{ii}^{\mathrm{eff}\prime}(\mathcal{M}_a^2)}, \tag{6.3}$$

where the first factor equals the definition of the Breit-Wigner propagator of the state h_a and the second factor is the $\hat{Z}_a$ in scheme I where i and a are associated indices. On top of that, $\hat{Z}_a\big|_I = \hat{\mathbf{Z}}_{ai}^2$ as defined in in Eq.(5.52), and the elements of the $\hat{\mathbf{Z}}$-matrix are independent of the index scheme (see Eq. (5.67)). Thus, the following scheme-independent approximation holds for $p^2 \simeq \mathcal{M}_a^2$:

$$\Delta_{ii}(p^2) \simeq \Delta_a^{\mathrm{BW}}(p^2)\,\hat{Z}_a\big|_I = \Delta_a^{\mathrm{BW}}(p^2)\,\hat{\mathbf{Z}}_{ai}^2 \tag{6.4}$$

In this approach, the mixing contributions are summarised in the on-shell Z-factor evaluated at $\mathcal{M}_a^2$. In contrast, the leading momentum dependence is contained in the Breit-Wigner propagator parametrised by the loop-corrected mass M_{h_a} and the total width Γ_{h_a} from the complex pole. In addition, $\Delta_{ii}(p^2)$ has a second pole at $\mathcal{M}_b^2$ because $p^2 - m_i^2 + \hat{\Sigma}_{ii}^{\text{eff}}(p^2) = 0$ holds also at $p^2 = \mathcal{M}_b^2$. Analogously to Eq. (5.43), we can expand $\hat{\Sigma}_{ii}^{\text{eff}}$ around $\mathcal{M}_b^2$ and obtain for the diagonal propagator

$$\begin{aligned}
\Delta_{ii}(p^2) &= \frac{i}{p^2 - m_i^2 + \hat{\Sigma}_{ii}^{\text{eff}}(p^2)} \\
&\simeq \frac{i}{p^2 - m_i^2 + \hat{\Sigma}_{ii}^{\text{eff}}(\mathcal{M}_b^2) + (p^2 - \mathcal{M}_b^2)\cdot \hat{\Sigma}_{ii}^{\text{eff}\prime}(\mathcal{M}_b^2)} \\
&= \frac{i}{(p^2 - \mathcal{M}_b^2)\cdot \left[1 + \hat{\Sigma}_{ii}^{\text{eff}\prime}(\mathcal{M}_b^2)\right]}. \qquad (6.5)
\end{aligned}$$

Formally, $\frac{1}{1+\hat{\Sigma}_{ii}^{\text{eff}\prime}(\mathcal{M}_b^2)}$ has the structure of the definition of a $\hat{Z}$-factor from Eq. (5.47), but in the index scheme II where b is assigned to i, whereas Eq. (6.4) has been obtained in scheme I with the (i, a) assignment. Using the relation (5.67), we can rewrite Eq. (6.5) as

$$\begin{aligned}
\Delta_{ii}(p^2) &\simeq \Delta_b^{\text{BW}}(p^2)\cdot \frac{1}{1 + \hat{\Sigma}_{ii}^{\text{eff}\prime}(\mathcal{M}_b^2)} \\
&= \Delta_b^{\text{BW}}(p^2)\cdot \frac{1}{1 + \hat{\Sigma}_{jj}^{\text{eff}\prime}(\mathcal{M}_b^2)} \left(\frac{\Delta_{ji}}{\Delta_{jj}}\right)^2_{p^2=\mathcal{M}_b^2} \qquad (6.6) \\
&= \Delta_b^{\text{BW}}(p^2)\cdot \left(\hat{Z}_b\, \hat{Z}_{bi}^2\right)\Big|_I \qquad (6.7) \\
&= \Delta_b^{\text{BW}}(p^2)\cdot \hat{\mathbf{Z}}_{bi}^2, \qquad (6.8)
\end{aligned}$$

where the $\hat{Z}$-factors in Eq. (6.7) are expressed in the same scheme as in Eq. (6.4). Hence, in the vicinity of $p^2 \simeq \mathcal{M}_b^2$, the diagonal propagator Δ_{ii} can be approximated by the Breit-Wigner propagator of h_b weighted by the square of $\hat{\mathbf{Z}}_{bi}$ that ensures the coupling to the incoming fields as Higgs boson i, propagation as the mass eigenstate h_b and the coupling to the outgoing fields again as Higgs boson i. In the same manner, Δ_{ii} can be expanded around the third complex pole, $\mathcal{M}_c^2$, yielding

$$\begin{aligned}
\Delta_{ii}(p^2) &\simeq \frac{i}{(p^2 - \mathcal{M}_c^2)\cdot \left[1 + \hat{\Sigma}_{ii}^{\text{eff}\prime}(\mathcal{M}_c^2)\right]} \qquad (6.9) \\
&\simeq \Delta_c^{\text{BW}}(p^2)\cdot \frac{1}{1 + \hat{\Sigma}_{kk}^{\text{eff}\prime}(\mathcal{M}_c^2)} \left(\frac{\Delta_{ki}}{\Delta_{kk}}\right)^2\Bigg|_{p^2=\mathcal{M}_c^2} \qquad (6.10) \\
&= \Delta_c^{\text{BW}}(p^2)\cdot \hat{\mathbf{Z}}_{ci}^2. \qquad (6.11)
\end{aligned}$$

Thus, close to one of the complex poles (e.g. $\mathcal{M}_a^2$), the dominant contribution to the full propagator Δ_{ii} can be approximated by the corresponding Breit-Wigner propagator (Δ_a^{BW}) multiplied by the square of the respective $\hat{\mathbf{Z}}$-factor ($\hat{\mathbf{Z}}_{ai}^2$). However, close-by poles may cause overlapping resonances. In order to include this possibility and to extend the range of validity of the Breit-Wigner approximation to a more general case, we take the sum of all three Breit-Wigner contributions into account:

$$\Delta_{ii}(p^2) \simeq \Delta_a^{\mathrm{BW}}(p^2)\,\hat{\mathbf{Z}}_{ai}^2 + \Delta_b^{\mathrm{BW}}(p^2)\,\hat{\mathbf{Z}}_{bi}^2 + \Delta_c^{\mathrm{BW}}(p^2)\,\hat{\mathbf{Z}}_{ci}^2 = \sum_{a=1}^{3} \Delta_a^{\mathrm{BW}}(p^2)\,\hat{\mathbf{Z}}_{ai}^2. \tag{6.12}$$

6.2.2. Expansion of the off-diagonal propagators

We proceed similarly for the off-diagonal propagators, which also have three complex poles so that we can expand the propagators around them. Note that $\hat{\mathbf{Z}}_{ai} = \sqrt{\hat{Z}_a}$ and $\hat{\mathbf{Z}}_{aj} = \sqrt{\hat{Z}_a}\hat{Z}_{aj}$ as defined in Eq. (5.52). Starting at $p^2 \simeq \mathcal{M}_a^2$, we express the $\hat{Z}$-factors in scheme I,

$$\Delta_{ij}(p^2) = \frac{\Delta_{ij}(p^2)}{\Delta_{ii}(p^2)}\Delta_{ii}(p^2) \simeq \hat{Z}_{aj}\hat{\mathbf{Z}}_{ai}^2\,\Delta_a^{\mathrm{BW}}(p^2) = \hat{\mathbf{Z}}_{aj}\hat{\mathbf{Z}}_{ai}\,\Delta_a^{\mathrm{BW}}(p^2), \tag{6.13}$$

Next, we approximate Δ_{ij} near $p^2 = \mathcal{M}_b^2$:

$$\Delta_{ij}(p^2) = \frac{\Delta_{ji}(p^2)}{\Delta_{jj}(p^2)}\Delta_{jj}(p^2) \simeq \hat{Z}_{bi}\hat{\mathbf{Z}}_{bj}^2\,\Delta_b^{\mathrm{BW}}(p^2) = \hat{\mathbf{Z}}_{bi}\hat{\mathbf{Z}}_{bj}\,\Delta_b^{\mathrm{BW}}(p^2). \tag{6.14}$$

For $p^2 \simeq \mathcal{M}_c^2$, we switch to a scheme where the indices i and c belong together. Thereby we can write

$$\Delta_{ij}(p^2) = \frac{\Delta_{ij}(p^2)}{\Delta_{ii}(p^2)}\Delta_{ii}(p^2) \simeq \hat{Z}_{cj}\hat{\mathbf{Z}}_{ci}^2\,\Delta_c^{\mathrm{BW}}(p^2) = \hat{\mathbf{Z}}_{cj}\hat{\mathbf{Z}}_{ci}\,\Delta_c^{\mathrm{BW}}(p^2), \tag{6.15}$$

which is expressed in scheme-invariant $\hat{\mathbf{Z}}$-factors. Finally, we take the sum of Eqs. (6.13)-(6.15) to obtain

$$\Delta_{ij}(p^2) \simeq \sum_{a=1}^{3} \hat{\mathbf{Z}}_{ai}\,\Delta_a^{\mathrm{BW}}(p^2)\,\hat{\mathbf{Z}}_{aj}. \tag{6.16}$$

This sum is illustrated diagrammatically in Fig. 6.1.

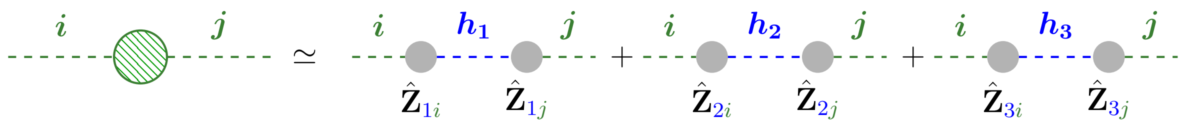

Figure 6.1.: Diagrammatic illustration of the full mixing Higgs propagators compared to the Breit-Wigner propagators where the $\hat{\mathbf{Z}}$-factors encode the transition between the interaction and the mass eigenstates.

Eq. (6.16) represents the central result of this chapter, covering also the diagonal propagators in the special case of $i = j$. It shows how the full propagator can be approximated by the contributions of the three resonance regions, expressed by the

Breit-Wigner propagators $\Delta_a(p^2)$, $a = 1, 2, 3$, reflecting the main momentum dependence. The mixing among the Higgs bosons is comprised in the $\hat{\mathbf{Z}}$-factors which are evaluated on-shell. Nonetheless, even a part of the momentum dependence of the self-energies is accounted for because the derivation of Eq. (6.12) is based on a first-order expansion of the momentum-dependent effective self-energies. Furthermore, the $\hat{\mathbf{Z}}$-factors serve as transition factors between the mass eigenstates h_a and the interaction eigenstates i (altough $\hat{\mathbf{Z}}$ is not a unitary matrix tranforming the states into each other). Pictorially, Δ_{ij} is a propagator that begins on the state i and ends on j while mixing occurs in between, cf. Fig. 5.1. As Eq. (6.16) implies, the same picture emerges in the h_1, h_2, h_2 basis. Also here, the propagator begins with i and ends on j. Thus, the coupling to the rest of the diagram connected to the propagator is well-defined. In between, each of the h_a can propagate, and the correct transition is ensured by $\hat{\mathbf{Z}}_{ai}$ and $\hat{\mathbf{Z}}_{aj}$. All three combinations are visualised in Fig. 6.1.

If $\mathcal{CP}$ is conserved and only h and H mix or if the two heavy states are nearly degenerate and their resonances widely separated from the first complex pole, the full 3×3 mixing is (exactly or approximately) reduced to the 2×2 mixing. Then the mixing $\hat{\mathbf{Z}}$-factors involving the unmixed state vanish or become negligible so that some terms in Eq. (6.16) become zero.

Beyond that, if no mixing occurs among the neutral Higgs bosons, all off-diagonal full propagators as well as the off-diagonal $\hat{\mathbf{Z}}$-factors vanish and each diagonal full propagator consists of only a single Breit-Wigner term where the $\hat{\mathbf{Z}}$-factor is based on the diagonal self-energy instead of the effective self-energy. Thus, Eq. (6.16) covers all special cases.

6.2.3. Amplitude with Higgs mixing based on full or Breit-Wigner propagators

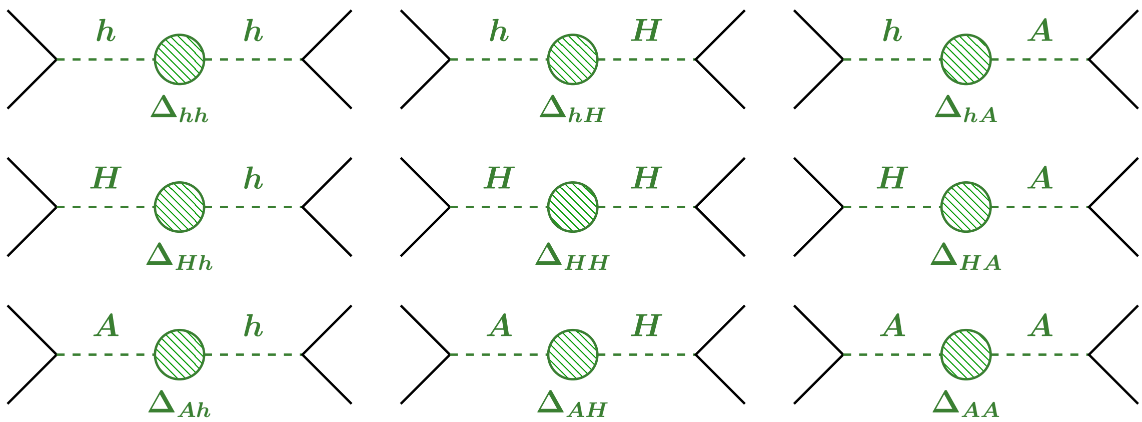

Figure 6.2.: Contributions from all full mixing propagators $\Delta_{ij}(p^2)$ for $, i, j = h, H, A$ to a generic amplitude (cf. Ref. [45]). If the $\hat{\mathbf{Z}}$-factor approach is applied, each of the 9 full propagators needs to be approximated by the sum of the three corresponding Breit-Wigner diagrams as shown in Fig. 6.1.

In a physical process where neutral Higgs bosons can appear as intermediate particles, all of them need to be included in the prediction, see Fig. 6.2 and Ref. [45]. The Higgs part of the amplitude then contains a sum over the irreducible vertex functions $\hat{\Gamma}_i^X$ (for a coupling of Higgs i at the first vertex X) and $\hat{\Gamma}_j^Y$ (for a coupling of Higgs j at the second vertex Y) times the fully momentum-dependent mixing propagators,

$$\mathcal{A} = \sum_{i,j=h,H,A} \hat{\Gamma}_i^X \, \Delta_{ij}(p^2) \, \hat{\Gamma}_j^Y. \tag{6.17}$$

Applying Eq. (6.16), the amplitude in Eq. (6.17) can be approximated by the sum over Breit-Wigner propagators multiplied by on-shell Z-factors, in agreement with Ref. [45],

$$\begin{aligned}
\mathcal{A} &\simeq \sum_{i,j=h,H,A} \hat{\Gamma}_i^X \left[\sum_{a=1}^{3} \hat{\mathbf{Z}}_{ai} \, \Delta_a^{\mathrm{BW}}(p^2) \, \hat{\mathbf{Z}}_{aj}\right] \hat{\Gamma}_j^Y & (6.18)\\
&= \sum_{a=1}^{3} \left(\sum_{i=h,H,A} \hat{\mathbf{Z}}_{ai} \hat{\Gamma}_i^X\right) \Delta_a^{\mathrm{BW}}(p^2) \left(\sum_{j=h,H,A} \hat{\mathbf{Z}}_{aj} \hat{\Gamma}_j^Y\right) & (6.19)\\
&= \sum_{a=1}^{3} \left(\hat{\mathbf{Z}}_{ah}\hat{\Gamma}_h^X + \hat{\mathbf{Z}}_{aH}\hat{\Gamma}_H^X + \hat{\mathbf{Z}}_{aA}\hat{\Gamma}_A^X\right) \Delta_a^{\mathrm{BW}}(p^2) \left(\hat{\mathbf{Z}}_{ah}\hat{\Gamma}_h^Y + \hat{\mathbf{Z}}_{aH}\hat{\Gamma}_H^Y + \hat{\mathbf{Z}}_{aA}\hat{\Gamma}_A^Y\right) & (6.20)\\
&= \sum_{a=1}^{3} \hat{\Gamma}_{h_a}^X \, \Delta_a^{\mathrm{BW}}(p^2) \, \hat{\Gamma}_{h_a}^Y. & (6.21)
\end{aligned}$$

The first bracket in Eq. (6.20) represents $\hat{\Gamma}_{h_a}^X$, i.e., the vertex X connected to the mass eigenstate h_a as for an external Higgs boson in Eq. (5.73). Subsequently, the second bracket is equal to the coupling of h_a at vertex Y, $\hat{\Gamma}_{h_a}^Y$. As opposed to Sect. 5.5, the h_a is not on-shell here, but a propagator with momentum p^2 between the vertices X and Y, represented by the Breit-Wigner propagator $\Delta_a^{\mathrm{BW}}(p^2)$. So the $\hat{\mathbf{Z}}$-factors are not only useful for the on-shell properties of external Higgs bosons, but they can also be used as an on-shell approximation of the mixing between Higgs propagators. This will be investigated numerically in Sect. 6.3.

6.2.4. Calculation of the interference term in the Breit-Wigner formulation

In Eq. (6.16), the Breit-Wigner propagators are combined such that they approximate a given full propagator. Conversely, we will now separate the h_a part from the contribution of the other mass eigenstates in the amplitude with Higgs exchange between the vertices X and Y:

$$\mathcal{A}_{h_a} = \hat{\Gamma}_{h_a}^X \, \Delta_a^{\mathrm{BW}}(p^2) \, \hat{\Gamma}_{h_a}^Y \equiv \sum_{i,j=h,H,A} \hat{\Gamma}_i^X \, \hat{\mathbf{Z}}_{ai} \, \Delta_a^{\mathrm{BW}}(p^2) \, \hat{\mathbf{Z}}_{aj} \, \hat{\Gamma}_j^Y, \tag{6.22}$$

i.e. the exchange of the state h_a coupling with the mixed vertices $\hat{\Gamma}_{h_a}$ from Eq. (5.73) as for an external Higgs.

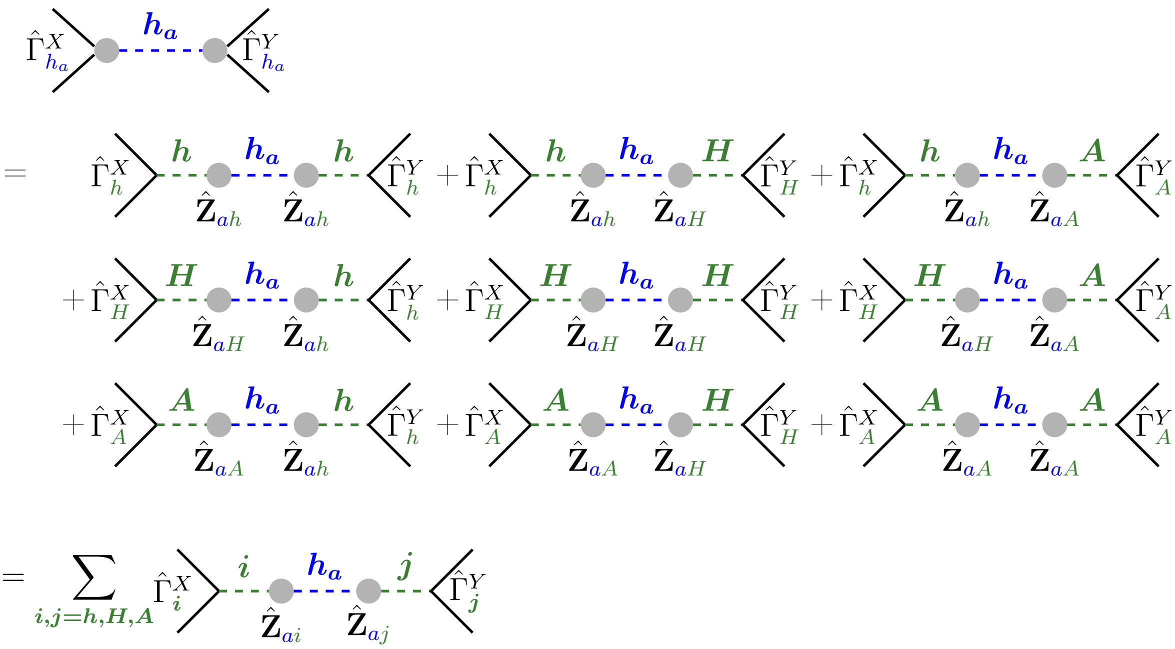

Figure 6.3.: Diagrammatic representation of the contribution $\mathcal{A}_{h_a}$ from Eq. 6.22 of h_a ($a = 1, 2, 3$) to the amplitude $\mathcal{A}$. The blue lines labelled by h_a denote the Breit-Wigner propagator $\Delta_a^{\mathrm{BW}}(p^2)$ and the green lines labelled by $i, j = h, H, A$ denote lowest order propagators of h, H, A.

In order to calculate the squared amplitude as a *coherent* sum, all contributions of h_1, h_2, h_3 are summed up first before taking the absolute square,

$$|\mathcal{A}|^2_{\mathrm{coh}} = \left| \sum_{a=1}^{3} \mathcal{A}_{h_a} \right|^2 . \tag{6.23}$$

On the contrary, the *incoherent* sum is the sum of the squared individual amplitudes, which misses the interference contribution,

$$|\mathcal{A}|^2_{\mathrm{incoh}} = \sum_{a=1}^{3} \left| \mathcal{A}_{h_a} \right|^2 , \tag{6.24}$$

Thus, an advantage of the Breit-Wigner propagators is also the possibility to discern the interference of several resonances from their individual contributions in a squared amplitude

$$|\mathcal{A}|^2_{\mathrm{int}} = |\mathcal{A}|^2_{\mathrm{coh}} - |\mathcal{A}|^2_{\mathrm{inccoh}} = \sum_{a<b} 2\,\mathrm{Re}\left[\mathcal{A}_{h_a} \mathcal{A}^*_{h_b}\right] , \tag{6.25}$$

which will be helpful in distinguishing genuine interference effects from general non-zero phase effects on the cross section in Sect. 10.2.2. In contrast, the squared amplitude based on the full propagators

$$|\mathcal{A}_{\text{full}}|^2 = \Big| \sum_{i,j=h,H,A} \hat{\Gamma}_i^X \, \Delta_{ij}(p^2) \, \hat{\Gamma}_j^Y \Big|^2 \tag{6.26}$$

is sensitive to the overall effect of complex phases on the masses, couplings and mixing propagators, but this formulation does not allow for the straightforward determination of the pure interference term.

6.3. Numerical comparison of full and Breit-Wigner propagators

After the analytical considerations so far, in this section we will numerically compare the full propagators with their approximation as a combination of Breit-Wigner propagators and $\hat{\mathbf{Z}}$-factors. In order to investigate the applicability of the expansion of the full propagators in one or all three resonance regions, we will first use a complex input momentum around the three complex poles. For the later application to physical processes where the squared momentum equals the centre-of-mass energy s, we will also evaluate the propagators at $p^2 = s$ near the real parts of the complex poles. In Sect. 6.3.1 we choose a scenario where all three Higgs bosons are relatively light so that we can study their mutual overlap. As a test of the $\hat{\mathbf{Z}}$-factor approximation, we work in a scenario with large mixing between H and A in Sect. 6.3.2

6.3.1. Scenario with 3 light Higgs bosons

For the numerical evaluation of the propagators, we work in the $M_h^{\text{mod}+}$ scenario [167] (see Tab. A.1). In this example, we fix the variable parameters

$$\begin{aligned} \mu &= 200\,\text{GeV}, \\ M_{H^\pm} &= 160\,\text{GeV}, \\ \tan\beta &= 50, \end{aligned} \tag{6.27}$$

and introduce the complex phase $\phi_{A_t} = \pi/4$ to allow for $\mathcal{CP}$-violating mixing. These parameter values result in the following complex poles:

$$\mathcal{M}_1^2 = (15791 - 70i)\,\text{GeV}^2, \quad \mathcal{M}_2^2 = (16202 - 525i)\,\text{GeV}^2, \quad \mathcal{M}_3^2 = (17388 - 385i)\,\text{GeV}^2. \tag{6.28}$$

All of the loop-corrected masses obtained from the real parts of the complex poles listed above are relatively light:

$$M_{h_1} = 125.7\,\text{GeV}, \quad M_{h_2} = 127.3\,\text{GeV}, \quad M_{h_3} = 131.9\,\text{GeV} \tag{6.29}$$

so that the mass differences are of the order of – but not smaller than – the total widths from the imaginary parts of the complex poles, $\Gamma_{h_1} = 0.6\,\text{GeV}$, $\Gamma_{h_2} = 4.1\,\text{GeV}$, $\Gamma_{h_3} = 2.9\,\text{GeV}$. This parameter choice is not meant to be the experimentally viable. The purpose is just to provide a setting with nearby, but resolvable resonances so that the test of the Breit-Wigner approximation is not limited to well separated poles. The phase of A_t induces $\mathcal{CP}$-violating mixing, and the on-shell mixing properties are reflected by the $\hat{\mathbf{Z}}$-matrix obtained with `FeynHiggs`,

$$\hat{\mathbf{Z}} = \begin{pmatrix} 0.95 - 0.04i & 0.34 + 0.09i & -0.05 - 0.05i \\ 0.05 - 0.05i & 0.02 + 0.03i & 0.99 - 0.02i \\ -0.35 - 0.09i & 0.94 - 0.05i & -0.006 - 0.003i \end{pmatrix}, \tag{6.30}$$

which indicates that h_1 couples mostly h-like, h_2 mostly A-like and h_3 mostly H-like. Thus, the contribution of h_a to Δ_{ij}, i.e.

$$\Delta_{ij}\Big|_{h_a}(p^2) = \hat{\mathbf{Z}}_{ai}\,\Delta_a^{\text{BW}}(p^2)\,\hat{\mathbf{Z}}_{aj}, \tag{6.31}$$

is only significant if the product $\hat{\mathbf{Z}}_{ai}\hat{\mathbf{Z}}_{aj}$ is not suppressed. In this case, we can already estimate that, for example, h_3 hardly contributes to Δ_{AA}.

We have analysed all propagators Δ_{ij} around $\mathcal{M}_1^2$, $\mathcal{M}_2^2$ and $\mathcal{M}_3^2$ as well as for real momenta. In the following, we show and discuss a selection of these cases.

6.3.1.1. Propagators depending on complex momenta

The analytical derivation of Eq. (6.16) builds on the expansion of the full propagators around the complex poles, and the on-shell condition in Eq. (5.33) holds exactly only at complex momentum. Therefore, we want to evaluate the self-energies and propagators around the complex poles. Fig. 6.4 displays $\Delta_{hh}(p^2)$ for $p^2 = 0.5\,\mathcal{M}_1^2 \ldots 1.5\,\mathcal{M}_1^2$. In particular, Fig. 6.4(a) shows $\text{Re}\,[\Delta_{hh}]$, and Fig. 6.4(b) shows $\text{Im}\,[\Delta_{hh}]$ versus the ratio $x_1 = p^2/\mathcal{M}_1^2$ such that $x_1 = 1$ corresponds to the complex pole $p^2 = \mathcal{M}_a^2$. The black line (labelled by Δ full) represents the fully momentum dependent mixing propagator from Eq. (5.10). Since the three poles do not have the same ratio between the real and imaginary parts, scaling x_1 does not run into $\mathcal{M}_2^2$ and $\mathcal{M}_3^2$. Δ_{hh} has a pole $x = 1$ and a second peak at $x \simeq 1.1$ which is close to the real part of $\mathcal{M}_3^2$. This structure is very precisely reproduced by the sum $\sum_{a=1}^{3} \hat{\mathbf{Z}}_{ah}^2\,\Delta_a^{\text{BW}}(p^2)$ according to Eq. (6.12) – as can be seen from the red dotted line (labelled as $\sum \text{BW} \cdot Z$), which lies directly on top of the black solid line.

In order to understand which of the Breit-Wigner propagators and $\hat{\mathbf{Z}}$-factors dominate at which momentum, we have a closer look at the dashed curves. The blue line (labelled by h_1) represents the contribution of h_1 to Δ_{hh}, i.e., $\hat{\mathbf{Z}}_{1h}^2\,\Delta_1^{\text{BW}}(p^2)$. It clearly reveals the pole at $x = 1$, but strongly deviates from the full propagator at different momenta. The orange line (labelled by h_2) represents $\hat{\mathbf{Z}}_{2h}^2\,\Delta_1^{\text{BW}}(p^2)$. Since $\hat{\mathbf{Z}}_{2h}$ is small in this scenario, the contribution of h_2 to Δ_{hh} is numerically suppressed, but a tiny share is visible near $\mathcal{M}_2^2$.

The green line (labelled by h_3) stands for $\hat{\mathbf{Z}}^2_{3h}\,\Delta_3^{\rm BW}(p^2)$ and it contributes significantly to Δ_{hh} near $\mathcal{M}_3^2$ because $\hat{\mathbf{Z}}_{3h} = -0.35 - 0.09i$ is sizeable in this scenario. So we notice that none of the individual Breit-Wigner propagators multiplied by the appropriate $\hat{\mathbf{Z}}$-factors suffices to approximate the full propagator, which has three complex poles. As a result, only the sum of all three Breit-Wigner propagators times $\hat{\mathbf{Z}}$-factors yields an accurate approach to the full mixing. This holds for the real and the imaginary part.

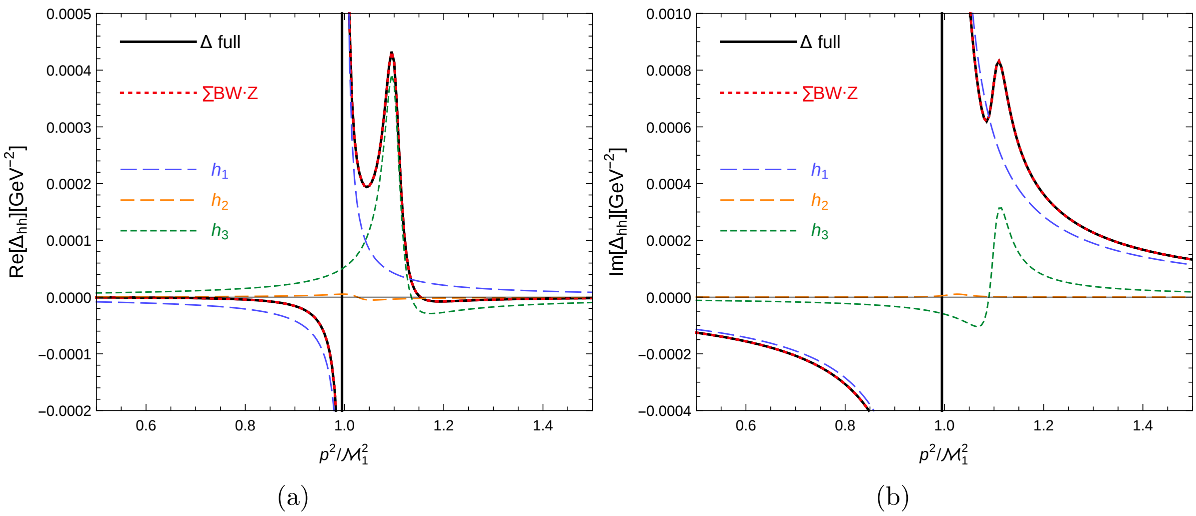

Figure 6.4.: Diagonal propagator $\Delta_{hh}(p^2)$ depending on the complex momentum p^2 around $\mathcal{M}_1^2$ with $p^2/\mathcal{M}_1^2 = 0.5...1.5$. **(a)** real part, **(b)** imaginary part. The full mixing propagator Δ_{ii}, $i = h, H, A$ (black, labelled by Δ full) is compared to the *sum* of Breit-Wigner propagators weighted by $\hat{\mathbf{Z}}$-factors according to Eq. (6.12) (red dotted, labelled by $\sum$BW·Z). The individual contribution of h_a, i.e. $\hat{\mathbf{Z}}^2_{ah}\Delta_a^{\rm BW}$, is shown for h_1 (blue, long-dashed), h_2 (orange, dashed) and h_3 (green, short-dashed).

Having discussed the example of a diagonal propagator, we will now assess whether the $\hat{\mathbf{Z}}$-factor approximation succeeds also for off-diagonal propagators. For instance, Fig. 6.5 depicts Δ_{HA} versus $x_2 = p^2/\mathcal{M}_2^2$ such that $x = 1$ matches $p^2 = \mathcal{M}_2^2$ where the propagator diverges. Owing to the different ratio between the real and imaginary part of each complex pole, scaling x_2 does not run into $\mathcal{M}_1^2$ and $\mathcal{M}_3^2$, but Δ_{HA} peaks close to their real parts. As in Fig. 6.4, the black line representing the full propagator and the red, dotted line representing the sum of Breit-Wigner propagators according to Eq. (6.16) agree very well. Additionally, we can tell apart the individual Breit-Wigner shapes. Because the products of the relevant $\hat{\mathbf{Z}}$-factors, here $\hat{\mathbf{Z}}_{aH}\hat{\mathbf{Z}}_{aA}$, are non-negligible for all $a = 1, 2, 3$, each Breit-Wigner propagator is important in the complete approximation of both the real part (Fig. 6.5(a)) and the imaginary part (Fig. 6.5(b)) of Δ_{HA}. The other diagonal and off-diagonal propagators which are not displayed here have an equally good agreement between the full calculation and the approximation.

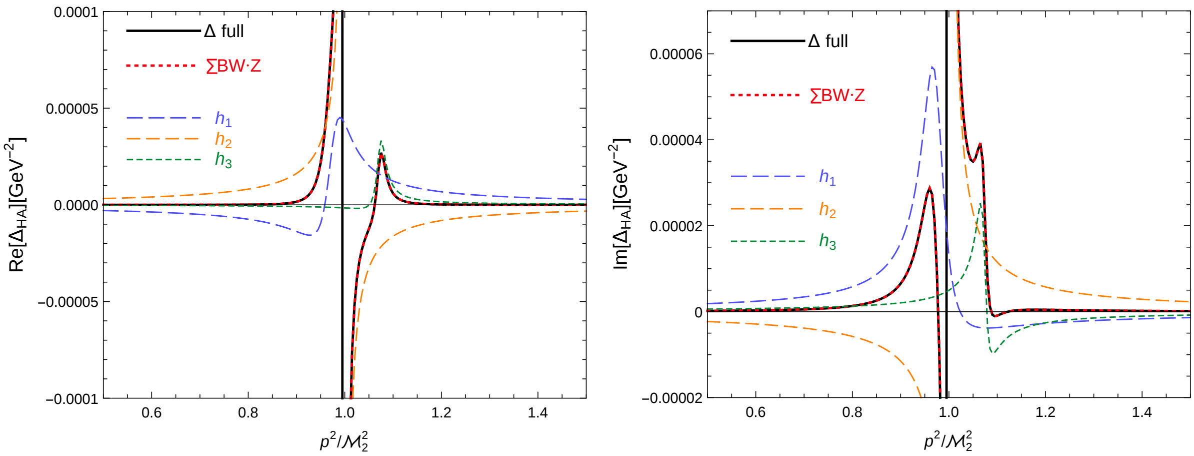

(a) (b)

Figure 6.5.: Off-diagonal propagator $\Delta_{HA}(p^2)$ depending on the complex momentum p^2 around $\mathcal{M}_2^2$ with $p^2/\mathcal{M}_2^2 = 0.5...1.5$. **(a)** real part, **(b)** imaginary part. Labelling as in Fig. 6.4.

6.3.1.2. Propagators depending on real momentum $p^2 = s$

The calculation of the propagators at and around the complex poles together with the evaluation of the self-energies at complex momenta according to Eq. (5.13) was needed to fulfil the assumptions of the approximation. However, in collider processes, the Higgs propagator might appear for example in the s-channel of a $2 \to 2$ scattering process where the squared momentum equals the square of the centre-of-mass energy s. So here we will check the Breit-Wigner approximation around the real parts of the complex poles.

Fig. 6.6(a) shows $\mathrm{Re}\,[\Delta_{hh}]$ in the range $\sqrt{p^2} \simeq M_{h_1}, M_{h_2}, M_{h_3}$ of the three loop-corrected masses given in Eq. (6.29). The propagator has a pronounced peak around M_{h_1} and a smaller and broader one at M_{h_3}. Again, the approximation (red, dotted) defined in Eq. (6.12) meets the full propagator (black) very precisely. The contribution of h_1 multiplied by $\hat{\mathbf{Z}}_{1h}$ of $\mathcal{O}(1)$ dominates near M_{h_1}. At M_{h_3} the Breit-Wigner shape of h_3 is dominant although multiplied only by $\hat{\mathbf{Z}}_{3h} = -0.35 - 0.09i$, but also the tail of Δ_1^{BW} is relevant. The resonance of h_2 is strongly suppressed by the small $\hat{\mathbf{Z}}_{2h}$.

Fig. 6.6(b) visualises $\mathrm{Re}\,[\Delta_{AA}]$ with a broad peak at M_{h_2}. The black curve of the full propagator is again directly beneath the red, dotted curve of the Breit-Wigner approximation, which in this case stems nearly entirely from h_2 because $\hat{\mathbf{Z}}_{2A} \simeq 1$. Within Δ_{AA}, the contribution of h_1 only has a minor impact, which can be seen as a small kink in Fig. 6.6(b). Although $\Delta_1^{\mathrm{BW}}(p^2)$ gets close to its pole, the resonance of h_1 is strongly suppressed by the small $\hat{\mathbf{Z}}$-factor $\hat{\mathbf{Z}}_{1A} = 0.05(1+i)$. As we anticipated above from the structure of $\hat{\mathbf{Z}}$ in Eq. (6.30), Δ_3^{BW} is a negligible component of Δ_{AA} for this parameter point.

So far we have seen that the Breit-Wigner formulation combined with on-shell $\hat{\mathbf{Z}}$-factors reproduces accurately the main momentum dependence of the full diagonal

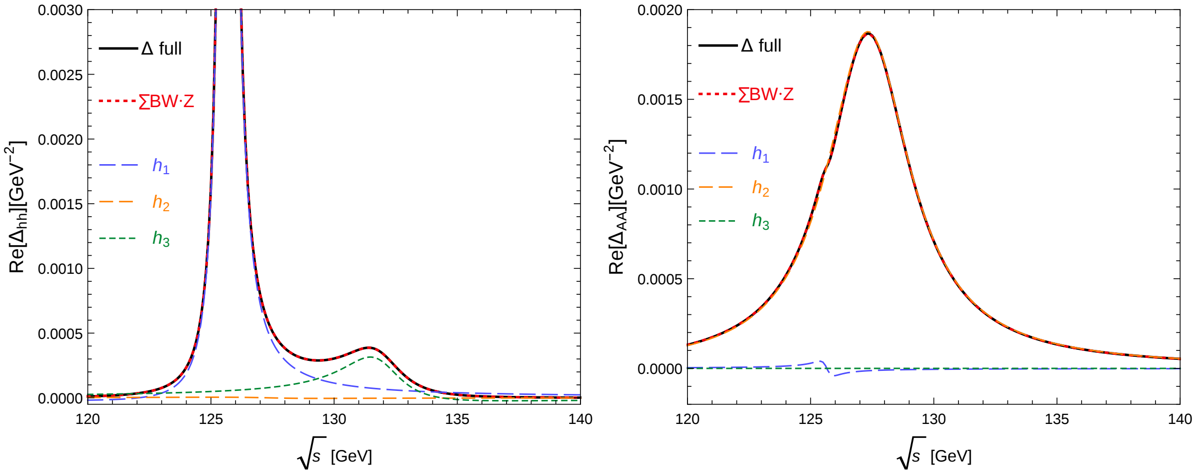

(a) (b)

Figure 6.6.: Diagonal propagators $\Delta_{hh}(p^2)$ ((**a**)) and $\Delta_{AA}(p^2)$ ((**b**)) depending on the real momentum $p^2 = s$ around $\sqrt{s} \simeq M_{h_1}, M_{h_2}, M_{h_3}$. Labelling as in Fig. 6.4.

and off-diagonal propagators by adding the contributions from all resonance regions. If all resonances are sufficiently separated (not shown in this example) or if all but one contributing products of $\hat{\mathbf{Z}}$-factors are negligible, a single Breit-Wigner term is enough to approximate the full propagator in one of the resonance regions. In the general case, however, all Breit-Wigner terms need to be included. Even if the peaks are not located very close to each other compared to their widths, the tail of one resonance supported by a substantial product of $\hat{\mathbf{Z}}$-factors can leak into another resonance region.

6.3.2. Scenario with large mixing

While the scenario in the previous section is characterised by three relatively similar masses, we now choose a setting with quasi degenerate heavy states h_2 and h_3. In Sect. 6.3.1 we considered the $M_h^{\text{mod+}}$-scenario with the standard value of $\mu = 200\,\text{GeV}$ in combination with the complex phase $\phi_{A_t} = \pi/4$, leading to a moderate mixing predominantly between h and A. In Ref. [167] it was suggested to choose also different values, $\mu = \pm 200, \pm 500, \pm 1000\,\text{GeV}$. So in addition to the choice above, we now apply the following modification of the parameters in Eq. (6.27):

$$\begin{aligned} \mu &= 1000\,\text{GeV}, \\ M_{H^\pm} &= 650\,\text{GeV}, \\ \tan\beta &= 20. \end{aligned} \tag{6.32}$$

This results in the complex poles

$$\mathcal{M}_1^2 = (15797 - 0.2i)\,\text{GeV}^2, \quad \mathcal{M}_2^2 = (415336 - 1673i)\,\text{GeV}^2, \quad \mathcal{M}_3^2 = (415554 - 1857i)\,\text{GeV}^2, \tag{6.33}$$

therefore in similar masses of the heavy Higgs bosons,

$$M_{h_1} = 125.33 \text{ GeV}, \quad M_{h_2} = 644.47\,\text{GeV}, \quad M_{h_3} = 644.63\,\text{GeV}, \tag{6.34}$$

and in a large mixing between H and A, visible in the $\hat{\mathbf{Z}}$-factors evaluated with `FeynHiggs`.

$$\hat{\mathbf{Z}} \simeq \begin{pmatrix} 1.01 & 0 & 0 \\ 0 & 1.15 - 0.27i & -0.47 - 0.66i \\ 0 & 0.49 + 0.65i & 1.13 - 0.28i. \end{pmatrix} \tag{6.35}$$

The quantity $\hat{\mathbf{Z}}$ is defined in Eq. (5.53) as a non-unitary matrix for the correct normalisation of vertices with on-shell Higgs bosons. Here, we apply the $\hat{\mathbf{Z}}$-factors in a slightly different context, namely on Higgs bosons appearing as momentum-dependent propagators connecting the incoming and outgoing state. In the scenario in Sect. 6.3.1, $\hat{\mathbf{Z}}$ is approximately unitary,

$$\hat{\mathbf{Z}} \cdot \hat{\mathbf{Z}}^{\dagger}(\mu = 200\,\text{GeV}) \simeq \begin{pmatrix} 1 & -0.1i & 0.2i \\ 0.1i & 1 & 0 \\ -0.2i & 0 & 1 \end{pmatrix} \simeq \mathbb{1}. \tag{6.36}$$

On the contrary, in this scenario with $\mu = 1000\,\text{GeV}$, the product $\hat{\mathbf{Z}} \cdot \hat{\mathbf{Z}}^{\dagger}$ deviates strongly from $\mathbb{1}$:

$$\hat{\mathbf{Z}} \cdot \hat{\mathbf{Z}}^{\dagger}(\mu = 1000\,\text{GeV}) \simeq \begin{pmatrix} 1 & 0 & 0 \\ 0 & 2 & -1.7i \\ 0 & 1.7i & 2 \end{pmatrix}. \tag{6.37}$$

Hence we want to examine whether the Breit-Wigner propagators with $\hat{\mathbf{Z}}$-factors still yield a viable approximation of the full mixing in this scenario with large mixing.

6.3.2.1. Propagators depending on complex momenta

Due to the large difference between M_{h_1} and $M_{h_2} \simeq M_{h_3}$, the propagators Δ_{hh}, Δ_{hH} and Δ_{hA} are strongly suppressed around $\mathcal{M}_2^2$. Fig. 6.7(a) shows $\text{Re}\,[\Delta_{HH}]$ for complex momentum around $\mathcal{M}_2^2$. The full calculation (black) and the Breit-Wigner approximation (red, dotted) are in good agreement although the curves do not lie directly on top of one another as in the scenario of Sect. 6.3.1. The two heavy states h_2 and h_3 with a mass difference of less than $0.2\,\text{GeV}$ and total widths of $\Gamma_{h_2} = 2.6\,\text{GeV}$ and $\Gamma_{h_3} = 2.9\,\text{GeV}$ are too close to be resolved. $\hat{\mathbf{Z}}^2_{2H}\Delta_{h_2}$ (orange) and $\hat{\mathbf{Z}}^2_{3H}\Delta_{h_3}$ contribute with similar magnitude, but opposite signs so that the result differs strongly from the single terms. A comparable situation is shown in Fig. 6.7(b) for $\text{Re}\,[\Delta_{HA}]$.

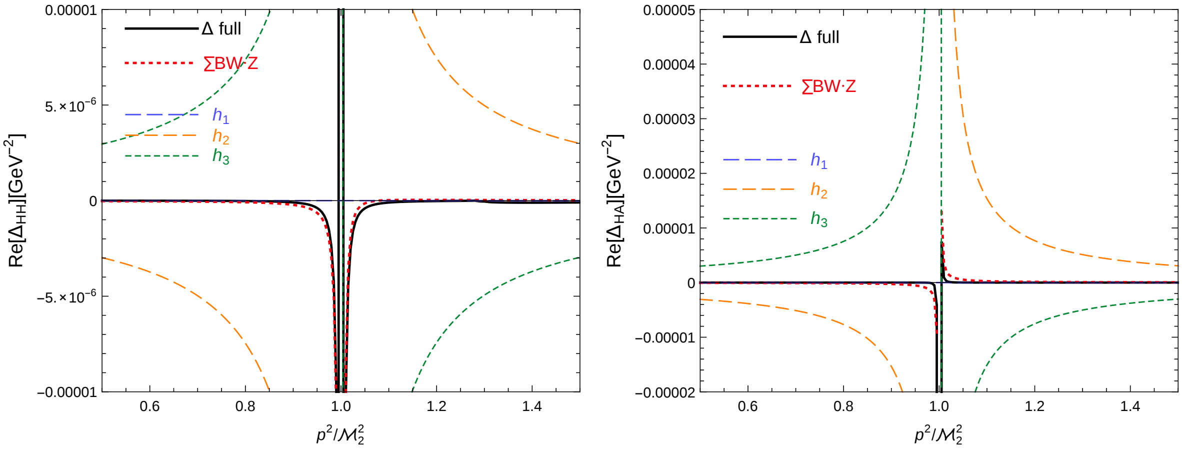

(a) (b)

Figure 6.7.: Real parts of **(a)** the diagonal propagator $\Delta_{HH}(p^2)$ and **(b)** the off-diagonal $\Delta_{HA}(p^2)$ depending on the complex momentum p^2 around $\mathcal{M}_2^2$ with $p^2/\mathcal{M}_2^2 = 0.5 \ldots 1.5$. Labelling as in Fig. 6.4.

6.3.2.2. Propagators depending on real momentum $p^2 = s$

Fig. 6.8 shows the same selection of propagators as in Fig. 6.7, but in this version evaluated at real momentum. The approximation from Eq. (6.16) leads to a good agreement between the propagators in the full mixing calculation (black) and the Breit-Wigner formulation (red, dotted), displayed for $\mathrm{Re}[\Delta_{HH}]$ in Fig. 6.8(a) and for $\mathrm{Re}[\Delta_{HA}]$ in Fig. 6.8(b). While the h_1-part (blue) is negligible due to the much lower mass M_{h_1}, h_2 (orange) and h_3 (green) both contribute substantially because their complex poles are very close to each other. These comparisons show that the Breit-Wigner approximation is also applicable in scenarios of quasi-degenerate states and a strong resonance-enhanced mixing. However, we note that the agreement between the full propagators and those with on-shell mixing factors is slightly less accurate here than in the scenario with moderate, nearly unitary mixing.

6.3.2.3. Comparison of the $\hat{\mathbf{Z}}$-factor approach with effective couplings

The effective coupling approach mentioned in Sect. 5.6 makes use of the unitary, real $\mathbf{U}$-matrix instead of the $\hat{\mathbf{Z}}$-matrix. However, $\mathbf{U}$ is not evaluated at the complex pole, but at $p^2 = 0$ (see Sect. 5.6) and it does not comprise the imaginary parts of the self-energies. As $\mathbf{U}$ is applied in the effective coupling approach, we compare it to the $\hat{\mathbf{Z}}$-factor approach which does take the imaginary parts into account, but cannot be directly interpreted as a unitary transformation between the states of the different bases.

Based on $\hat{\mathbf{Z}}$- and $\mathbf{U}$-factors from `FeynHiggs`, Fig. 6.9 displays the real parts of Δ_{HH} and Δ_{HA} at real momentum around $M_{h_2} \simeq M_{h_3}$, calculated as a fully momentum dependent mixing propoagator (black), using the $\hat{\mathbf{Z}}$-matrix approach (red, dotted) defined in Eq. (6.16), i.e. $\Delta^Z_{ij} \simeq \sum_{a=1}^{3} \hat{\mathbf{Z}}_{ai}\, \Delta^{\mathrm{BW}}_a\, \hat{\mathbf{Z}}_{aj}$, and the $\mathbf{U}$-matrix variant (grey, dashed) in

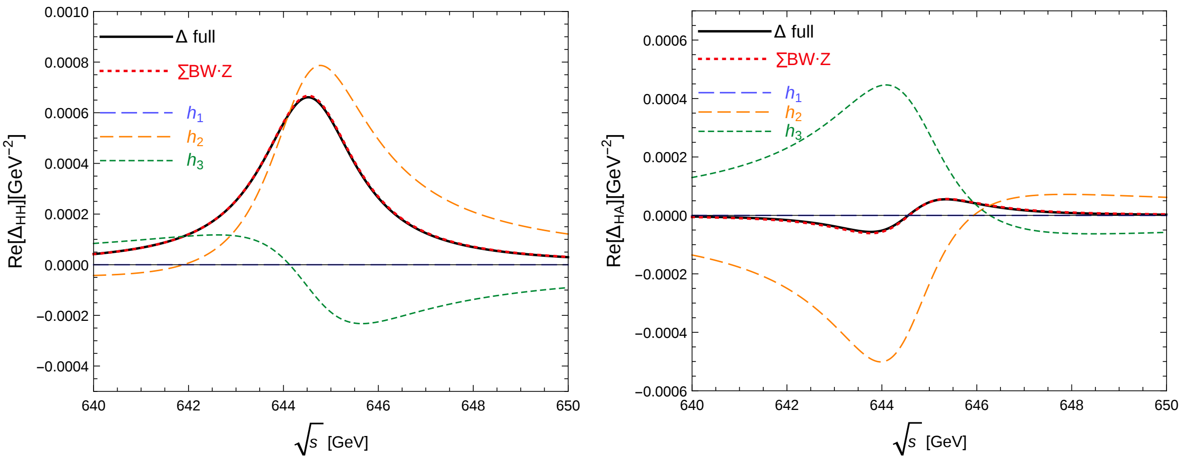

(a) (b)

Figure 6.8.: Real parts of **(a)** the diagonal propagator $\Delta_{HH}(p^2)$ and **(b)** the off-diagonal $\Delta_{HA}(p^2)$ depending on the real momentum $p^2 = s$ around $\sqrt{s} \simeq M_{h_2}, M_{h_3}$. Labelling as in Fig. 6.4.

the $p^2 = 0$ approximation as

$$\Delta_{ij}^{U} \simeq \sum_{a=1}^{3} \mathbf{U}_{ai}\, \Delta_a^{\mathrm{BW}}\, \mathbf{U}_{aj}. \tag{6.38}$$

While in Fig. 6.9(a) the curve representing the $\hat{\mathbf{Z}}$-factor method is almost identical to the curve of the full Δ_{HH} (with a relative deviation at the peak of 0.8%), the $\mathbf{U}$-method differs from the full result by up to 14%. In Fig. 6.9(b), not even the shape of Δ_{HA} is correctly approximated by the $\mathbf{U}$-approach whereas the $\hat{\mathbf{Z}}$-approach comes close to the full Δ_{HA} (albeit visible deviations).

From this analysis we conclude that the $\hat{\mathbf{Z}}$-factors combined with Breit-Wigner propagators are well-suited to describe the Higgs propagators including their mixing as mass eigenstates also in scenarios with close-by resonances and strong mixing. This approach captures the leading momentum dependence and adequately accounts for the imaginary parts. In contrast, the combination of $\mathbf{U}$-factors and Breit-Wigner propagators is – despite its unitary nature – incomplete with respect to the mixing effects in the resonance region and regarding the significance of imaginary parts.

6.4. Breit-Wigner and full propagators in cross sections

As an application of the derivations above, we calculate a cross section with Higgs exchange. We study the example process $b\bar{b} \to h, H, A \to \tau^+\tau^-$, where the intermediate Higgs bosons are once represented by the full mixing propagators Δ_{ij} and once by Breit-

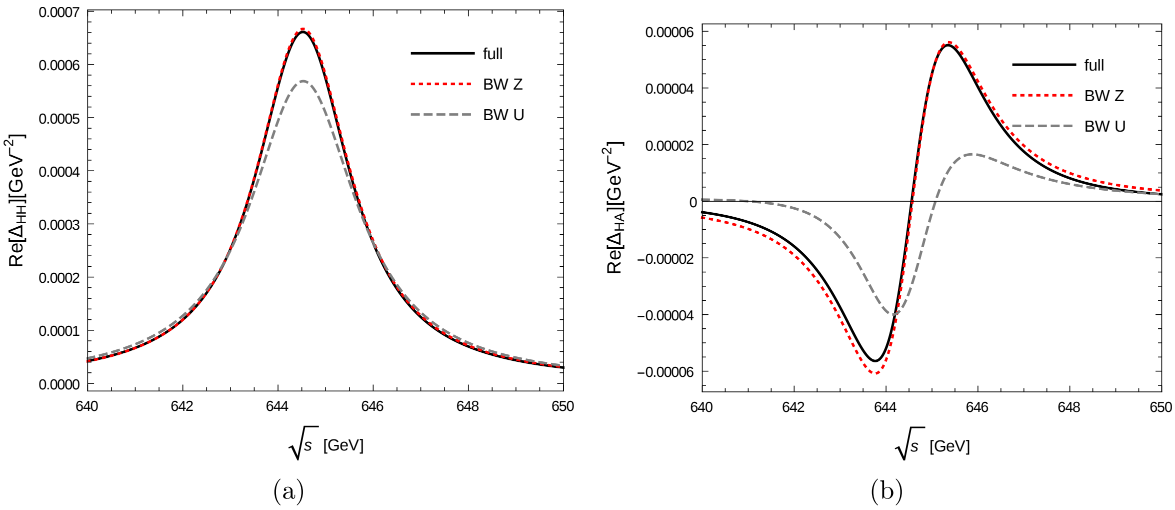

Figure 6.9.: Comparison of the $\mathbf{U}$ (grey, dashed) and $\hat{\mathbf{Z}}$ (red, dotted) approximation with the full propagators (black, solid) for real parts of the diagonal propagator $\Delta_{HH}(p^2)$ and the off-diagonal $\Delta_{HA}(p^2)$ depending on the real momentum $p^2 = s$ around $\sqrt{s} \simeq M_{h_2}, M_{h_3}$. **(a)** $\Delta_{HH}(p^2)$ and **(b)** Δ_{HA}.

Wigner propagators multiplied by $\hat{\mathbf{Z}}$-factors. In order to disentangle this investigation from other higher-order effects, we restrict the Higgs-fermion-fermion vertices to the tree-level and do not include the emission of real particles in the initial or final state, but focus on the propagator corrections.

For the implementation of the full propagator method, we adapted, checked and extended a model file obtained [45]. New scalars ij are introduced that correspond to the full propagator $\Delta_{ij}(p^2)$ and couple to the first vertex as the interaction eigenstate i and to the second vertex as j. Those propagators are used in the `FormCalc` calculation supplemented by two-loop self-energies from `FeynHiggs` with the full momentum dependence.

Considering only mixing between h and H at this point, we choose a $\mathcal{CP}$-conserving scenario, the so-called $M_h^{\max}$-scenario [168, 169] with $\tan\beta = 50$, $M_{H^\pm} = 153\,\text{GeV}$, but we modify it by setting $A_{f_3} = 2504\,\text{GeV}$. The outcome are large off-diagonal Z-factors $\hat{\mathbf{Z}}_{12} \simeq 0.65 + 0.29i$, $\hat{\mathbf{Z}}_{21} \simeq -0.64 - 0.29i$ and $\hat{\mathbf{Z}}_{11} \simeq 0.85 - 0.22i$, $\hat{\mathbf{Z}}_{22} \simeq 0.84 - 0.23i$. The masses of the $\mathcal{CP}$-even Higgs bosons are very close, $M_{h_1} = 126.20\,\text{GeV}$ and $M_{h_2} = 127.55\,\text{GeV}$, while the widths obtained from the imaginary part of the complex poles are $\Gamma_{h_1} = 0.94\,\text{GeV}$ and $\Gamma_{h_2} = 1.21\,\text{GeV}$. Despite its large width of $\Gamma_A = 3.58\,\text{GeV}$, the third neutral Higgs boson does not overlap significantly with the other two resonances due to the mass of $M_{h_3} = 119.91\,\text{GeV}$, and no mixing with the other two states occurs due to the real parameters implying $\mathcal{CP}$-conservation.

Fig. 6.10 shows the partonic cross section $\hat{\sigma}(b\bar{b} \to h, H, A \to \tau^+\tau^-)$ as a function of the centre-of-mass energy $\sqrt{\hat{s}}$, where $\hat{s} = (p_b + p_{\bar{b}})^2$ is the squared sum of the momenta of the b- and $\bar{b}$-quarks in the initial state. The calculation based on the full propagators (represented by the blue, solid line) is in very good agreement with the cross section based on the coherent sum of the h_1, h_2, h_3 contributions (red, dashed) according to

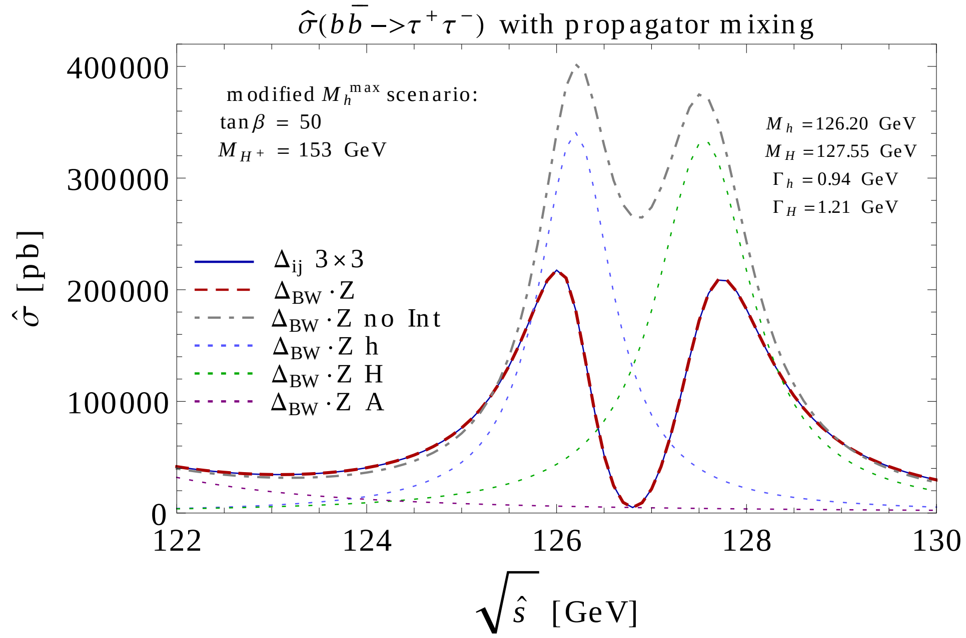

Figure 6.10.: The partonic cross section $\sigma(b\bar{b} \to \tau^+\tau^-)$ in a modified $M_h^{\max}$-scenario with $\tan\beta = 50$ and $M_{H^\pm} = 153\,\text{GeV}$. The cross section is calculated with the full mixing propagators (blue, solid), approximated by the coherent sum of Breit-Wigner propagators times $\hat{\mathbf{Z}}$-factors with the interference term (red, dashed) and the incoherent sum without the interference term (grey, dot-dashed). The individual contributions mediated by h_1 (light blue), h_2 (green) and h_3 (purple) are shown as dotted lines.

Eq. (6.23). Both curves lie on top of each other and contain two peaks originating from h_1 (light blue, dotted) and h_2 (green, dotted). The resonances of h_1 and h_2 partly overlap due to the mass difference of the order of the total widths, but the two peaks can still be distinguished. The term of h_3 peaks at a lower mass in this scenario, but for completeness it is also shown (purple, dotted). The incoherent sum $|h_1|^2 + |h_2|^2 + |h_3|^2$ (grey, dash-dotted) from Eq. (6.24) clearly overestimates the full cross section on account of the missing interference term that turns out to be destructive in this case. It is accurately taken into account in the full calculation and in the coherent sum of Breit-Wigner propagators with $\hat{\mathbf{Z}}$-factors. Chapters 7-10 of this thesis will further deal with interference phenomena of this kind in more detail and how to efficiently compute them.

6.5. Impact of the total width

This section addresses the impact of the precise value of the total width. So far, we have obtained the Higgs widths from the imaginary part of the complex pole as in Eq. (5.15) in order to consistently compare with the full propagator mixing. If the self-energies in $\hat{\Sigma}^{\text{eff}}_{ii}$ are calculated at the one-loop level, the total width extracted from a complex pole of Δ_{ii} is then a tree-level width. Correspondingly, partial two-loop contributions to the imaginary parts of the self-energies give rise to partial one-loop corrections of the decay width. However, two-loop self-energies evaluated at $p^2 = 0$, as they are approximated in `FeynHiggs`, do not contribute to the imaginary part of the pole so that the width determined from the imaginary part of the complex pole remains at its tree-level value. Corrections to Higgs boson decays in the MSSM at and beyond the one-loop level are known and turn out to be important, see e.g. Ref. [147]. Thus, the sum of the partial decay widths into any final state X of a Higgs boson h_a,

$$\Gamma^{\text{tot}}_{h_a} = \sum_X \Gamma(h_a \to X), \tag{6.39}$$

leads to a more accurate result for its total width than from the imaginary part of the corresponding complex pole,

$$\Gamma^{\text{Im}}_{h_a} = -\text{Im}[\mathcal{M}_a^2]/M_{h_a}, \tag{6.40}$$

at the same order. `FeynHiggs` contains the partial Higgs decay widths and their sum at the leading two-loop order. Having checked the excellent agreement between the full propagators and the Breit-Wigner propagators with the width from the imaginary part of the complex pole in the previous sections, now we implement the total width from `FeynHiggs` into the Breit-Wigner propagators for the most precise phenomenological prediction.

In the modified M_h^{max} scenario, the higher-order corrections have a significant impact on the Higgs decay widths so that $\Gamma^{\text{tot}}_{h_1} = 2.55\,\text{GeV}$ and $\Gamma^{\text{tot}}_{h_2} = 3.24\,\text{GeV}$ are much larger than the widths obtained from the imaginary part of the complex pole. This affects the order of magitude of the cross-section $\hat{\sigma}\left(b\bar{b} \to \tau^+\tau^-\right)$ and the structure of the resonances as can be seen in Fig. 6.11. The coherent sum of Breit-Wigner propagators including the interference term (red, dashed) and the incoherent sum without the interference term (grey, dash-dotted) using Γ^{Im} from the imaginary parts of the complex poles are the same as in Fig. 6.10. In contrast, total widths $\Gamma^{\text{tot}}_{\text{FH}}$ obtained from `FeynHiggs` as the sum of higher-order partial width are implemented into the Breit-Wigner propagators in the cross section based on the coherent sum of all h_a-contributions (black, solid) and the incoherent sum (black, dotted).

The larger widths have a drastic effect. Not only do they suppress the cross section, but the separate resonances are also less pronounced. Here, the incoherent sum without the interference term again overestimates the cross-sections. In addition, it lacks the two-peak structure. This observation emphasizes the importance of including the total width at the highest available precision and to take the interference term into account. One can also see that two resonances might be too close to be resolved if they are smeared by large widths.

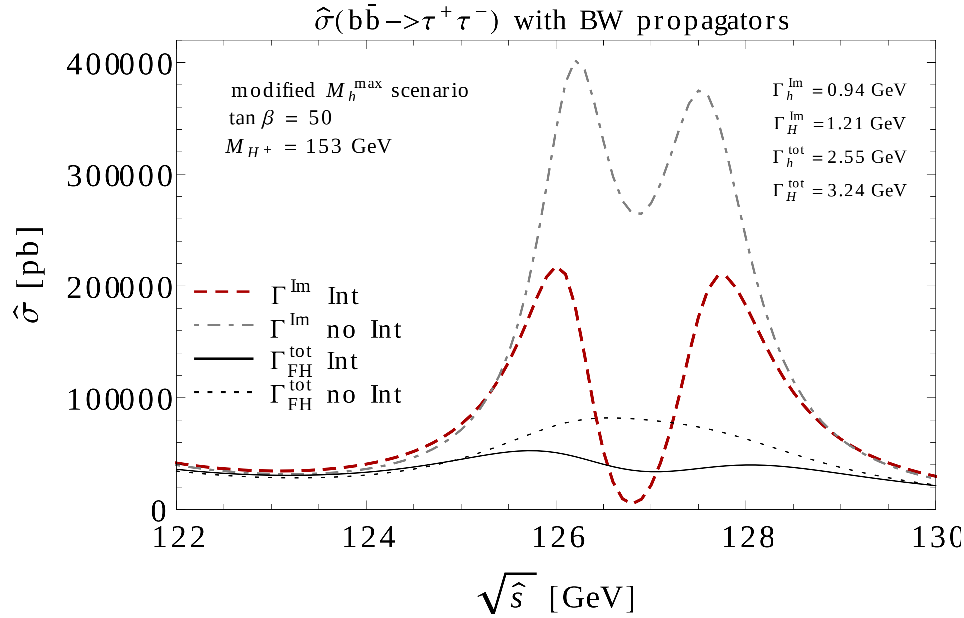

Figure 6.11.: Effect of the total width as an input for Breit-Wigner propagators: The partonic cross section $\hat{\sigma}(b\bar{b} \to \tau^+\tau^-)$ in the same modified $M_h^{\max}$-scenario as in Fig. 6.10 with $\tan\beta = 50$ and $M_{H^+} = 153\,\text{GeV}$. Breit-Wigner propagators with the total widths from the imaginary part of the complex pole including (red, dashed) and excluding (grey, dash-dotted) the interference term. Breit-Wigner propagators with the total widths from `FeynHiggs` including (black, solid) and excluding (black, dotted) the interference term.

6.6. Summary: Higgs masses and mixings in the MSSM with complex parameters

Before moving to a detailed study of interference effects in another example process, we want to briefly summarise aspects of the Higgs mass determination as well as the key features and limitations of approximating the full propagators in terms of the Breit-Wigner propagators and $\hat{\mathbf{Z}}$-factors.

We have studied the structure of the full propagators. In the case of 3×3 mixing between all three neural Higgs bosons h, H, A and the mass eigenstates h_1, h_2, h_3, each propagator has three complex poles, which are the zeros of the determinant of the inverse propagator matrix. We determined the masses in an iterative procedure and found good agreement with the eigenvalues from the diagonalisation method of `FeynHiggs`. However, the relation between the interaction and mass eigenstates is not unambiguous. The different choices are physically equivalent, but not always numerically equally stable. In this context, we propose an ordering that allows for a smooth transition between the unmixed and the mixed case.

The $\hat{\mathbf{Z}}$-factors are introduced to ensure correct on-shell properties of the S-matrix, taking also mixing of the neutral Higgs bosons into account. We have derived process independently how the full propagators can be expanded around all of their complex poles.

This approximation results in the sum of Breit-Wigner propagators of the corresponding resonances, weighted by $\hat{\mathbf{Z}}$-factors which encompass the transformation between the interaction and the mass eigenstates and transitions among the Higgs bosons, evaluated at the complex poles. We find very good agreement between the approximation in Eq. (6.16) and the full propagators. The formalism of Breit-Wigner propagators and on-shell $\hat{\mathbf{Z}}$-factors has several appealing advantages in describing the Higgs propagator mixing: Firstly, it avoids the momentum dependent evaluation of self-energies, which is a good approximation away from thresholds, and thereby simplifies and accelerates the calculation. Secondly, it enables the separation of the individual h_a contributions and the extraction of the pure interference term, which will be relevant for chapters 7-10. Thirdly, the Breit-Wigner propagator turns into a δ-distribution in the limit of a vanishing width, thus facilitating the separate calculation of the production and decay of an intermediate Higgs particle by means of the narrow-width approximation (NWA), see Sect. 7.2. On the other hand, the use of $\hat{\mathbf{Z}}$-factors is not entirely restricted to external Higgs bosons as they would appear in the NWA, but they also provide a good approximation of the mixing properties of intermediate Higgs bosons represented by a Breit-Wigner propagator in the on-shell and off-shell region. Fourthly, the Breit-Wigner formulation allows for the implementation of a more precise total width by incorporating important higher-order effects from the partial widths that are not included in the imaginary part of the complex pole with self-energies of the same order. Hence, in the following chapters, we will predominantly use the combination of $\hat{\mathbf{Z}}$-factors and Breit-Wigner propagators (or external, on-shell Higgs bosons) instead of the fully momentum dependent mixing propagators of the interaction eigenstates.

Chapter 7.

A generalised narrow-width approximation for interference effects

7.1. Factorisation vs. mass degeneracies in BSM

In sections 6.4 and 6.5, we have already noticed that interference effects between two unstable states with similar masses can be important in processes where these different quasi-degenerate states appear as intermediate particles between a given initial and final state. Calculating the full process with stable incoming and outgoing particles and taking into account all possible fields in the intermediate steps allows for the inclusion of the interference term. However, for processes involving many external legs or loop corrections, it is often not feasible to perform the full calculation. Instead, treating the on-shell production of an unstable particle and its subsequent decay separately is often more convenient if the intermediate particle can kinematically become resonant. The decay may be further decomposed into the respective steps. This approach has the advantage to simplify a complicated process by splitting it into several subprocesses that are computable with less effort so that higher-order corrections can be incorporated more easily.

This method is called the “narrow-width approximation” (NWA) because treating the resonant exchange of an unstable particle as a stable outgoing (in the production part) or incoming (in the decay) state corresponds to assuming a vanishing total width or – as an approximation – a total width that is much smaller than the mass. The application of the NWA is useful since the sub-processes can often be calculated at a higher loop order than it would be the case for the full process, and it is also beneficial in terms of computational speed. Indeed, many Monte-Carlo generators make use of the NWA. An important condition of this approximation, however, is the requirement that there should be no interference of the contribution of the intermediate particle for which the NWA is applied with any other close-by resonance, see e.g. Refs. [45, 170–172]. Hence, the applicability of the NWA in its standard version is restricted to cases without a relevant interference term. While within the SM this condition is usually valid for processes occuring at high-energy colliders such as the LHC or a future Linear Collider, many models of physics beyond the SM have mass spectra where two or more states can be nearly mass-degenerate. If the mass gap between two intermediate particles is smaller than the sum of their total widths, the interference term between the contributions from the two nearly mass-degenerate particles may become large.

For instance, mass degeneracies can be encountered in the MSSM which may, in particular, contain approximately mass-degenerate first and second generation squarks and sleptons. In the decoupling limit [173], the MSSM predicts a SM-like light Higgs boson, which is compatible with the signal discovered by ATLAS [5] and CMS [6] at a mass of about $M_h \simeq 125\,\text{GeV}$, and two further neutral Higgs bosons and a charged Higgs boson $H^{\pm}$, which are significantly heavier and nearly mass-degenerate. While in the $\mathcal{CP}$-conserving case the heavy neutral Higgs bosons H and A are $\mathcal{CP}$-eigenstates and therefore do not mix with each other (see Sect. 5.1), $\mathcal{CP}$-violating loop contributions can induce sizable interference effects [1, 2, 45, 85]. The compatibility of degenerate NMSSM Higgs masses with the observed Higgs decay rate into two photons was recently pointed out e.g. in Ref. [174]. Another example are degenerate Higgs bosons in (non-supersymmetric) two-Higgs doublet models, see for example Refs. [175,176]. Furthermore, degeneracies can also occur in models of (universal) extra dimensions where the masses at one Kaluza-Klein level are degenerate up to their SM masses and loop corrections, see for example Refs. [177–179]. Small mass differences of sequential Z' and W' bosons are analysed in an extension of the SM as an effective field theory in Ref. [180].

On the other hand, models with new particles on various mass levels often exhibit long cascade decays, so that there is a particular need in these cases for an approximation which enables the simplification of the complicated full process into smaller pieces that can be treated more easily and more precisely. However, several cases have been identified in the literature in which the NWA is insufficient due to sizeable interference effects, e.g. in the context of the MSSM in Refs. [170, 172, 181–183] and in the context of two- and multiple-Higgs models and in Higgsless models in Ref. [184].

In this chapter, we develop a generalised NWA (gNWA), which extends the standard NWA (sNWA) by providing a factorisation into on-shell production and decay while taking into account interference effects. In Ref. [45] such a method was introduced at the tree level and applied to interference effects in the MSSM Higgs sector. We extended this method further in Ref. [85], in particular by incorporating partial loop contributions into an interference weight factor. A similar coupling-based estimation of an interference between new heavy quarks at lowest order was suggested in Ref. [185]. The interference of nearly degenerate, new vector bosons was considered in Ref. [180] in an approach of the product of involved couplings and on-shell parton luminosities. Based on our work in Refs. [1, 2], we formulate in this thesis a gNWA constructed from an on-shell evaluation of the interference contributions which is applicable at the loop level, incorporating factorisable virtual and real corrections. Furthermore, we investigate different levels of approximations by further simplifying the on-shell matrix elements in the interference term by interference weight factors. We also discuss additional improvements by the incorporation of corrections that are formally of higher orders. The application to an example process follows in Sect. 9.

7.2. Concept and restrictions of the standard narrow-width approximation

Before addressing the extension of the NWA with the purpose of including an interference term, we first review the well-known and widely used standard NWA, also pointing out the underlying conditions which limit the applicability of the NWA in its original version and mentioning already existing extensions of it which address the limitations apart from interferences.

7.2.1. Basic idea of the narrow-width approximation

According to the basic idea of the NWA to factorise a complicated process into the on-shell production and the subsequent decay of a resonant particle, the following picture in Fig. 7.1 visualises the splitting of an arbitrary process. For the generic example case $ab \to cef$ involving an intermediate, resonant particle d with mass M and off-shell momentum q^2, this approach results in the production part $ab \to cd$ and decay $d \to ef$, where d appears on an external line with $q^2 = M^2$.

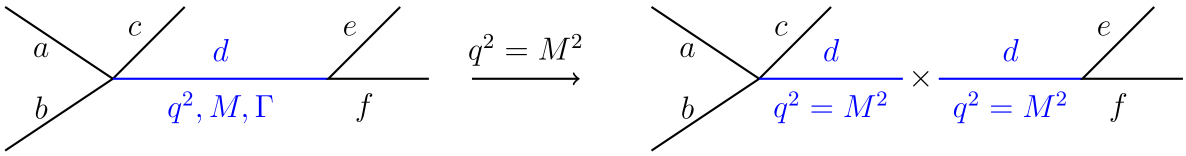

Figure 7.1.: The resonant process $ab \to cef$ via the exchange of d (with mass M, total width Γ and momentum q^2) is split into the production $ab \to cd$ and decay $d \to ef$ with particle d on-shell.

The total width Γ plays a crucial role in resonant production and decay. The NWA is based on the observation that the on-shell contribution in Eq. (6.2) is strongly enhanced if the total width is much smaller than the mass of the particle, $\Gamma \ll M$. Within its range of validity (see the discussion in the following section), the NWA provides an approximation of the cross section for the full process in terms of the product of the production cross section – or the previous step in a decay cascade – times the respective branching ratio:

$$\sigma_{ab\to cef} \simeq \sigma_{ab\to cd} \times \mathrm{BR}_{d\to ef}. \tag{7.1}$$

Although unstable particle fields do not correspond to asymptotic states, the usage of Eq. (7.1) implies the treatment of the unstable particle d as an external particle on its mass shell.

In the following, we focus on scalar propagators. Nonetheless, although the production and decay are calculated independently, the spin of an intermediate particle can be taken into account by means of spin correlations [186, 187] giving rise to spin–density matrices. While we do not consider the non-zero spin case explicitly, the formalism of spin–density matrices should be applicable to the gNWA discussed below in the same way as for the sNWA.

7.2.2. Conditions for the narrow-width approximation

The NWA can only be expected to hold reliably if the following prerequisites are fulfilled (see e.g. Refs. [170, 188]):

- A **narrow** mass peak is required in order to justify the on-shell approximation. Otherwise off-shell effects may become large, cf. e.g. [181, 189, 190].
- Furthermore, the propagator needs to be separable from the matrix element. However, loop contributions involving a particle exchange between the initial and the final state give rise to non-factorisable corrections. Hence, the application of the NWA beyond lowest order relies on the assumption that the **non-factorisable** and non-resonant contributions are sufficiently suppressed compared to the dominant contribution where the unstable particle is on resonance. Concerning the incorporation of non-factorisable but resonant contributions from photon exchange, see e.g. Ref. [191].
- Both sub-processes have to be **kinematically allowed**. For the production of the intermediate particle, this means that the centre of mass energy $\sqrt{s}$ must be well above the production threshold of the intermediate particle with mass M and the other particles in the final state of the production process, i.e. $\sqrt{s} \gg M + m_c$ for the process shown in Fig. 7.1. Otherwise, threshold effects must be considered [192].
- On the other hand, the decay channel must be kinematically open and sufficiently far above the decay **threshold**, i.e. $M \gg \sum m_f$, where m_f are the masses of the particles in the final state of the decay process, here $m_e + m_f$. Off-shell effects can be enhanced if intermediate thresholds are present. This is the case for instance for the decay of a Higgs boson with a mass of about 125 GeV into four leptons. Since for an on-shell Higgs boson of this mass this process is far below the threshold for on-shell WW and ZZ production, it suffers from a significant phase-space suppression. Off-shell Higgs contributions above the threshold for on-shell WW and ZZ production are therefore numerically more important than one would expect just from a consideration of Γ/M [193].
- As another crucial condition, **interferences** with other resonant or non-resonant diagrams have to be small because the mixed term would be neglected in the NWA. Interference effects between a narrow signal and a broad background continuum have been recently discussed in the context of the Higgs signal and constraining its total width, see for example Refs. [193–215]. But these kind of interference effects are not the focus of our work. In contrast, the major part of the following chapters is dedicated to a generalisation of the NWA for the inclusion of interference effects between nearly mass degenerate resonances [1, 45].

7.2.3. Factorisation of the phase space and cross section

In order to fix the notation used for the formulation of the gNWA in Sect. 7.3, we review some kinematic relations, using Refs. [23, 216] as resources. More details on basic kinematics used in this thesis can be found in Appendix C.

The phase space The phase space Φ is a Lorentz-invariant quantity. Its differential is denoted by $dlips$ (differential Lorentz-invariant phase space) or $d\Phi_n$. It is characterised by the number n of particles in the final state [23]

$$d\Phi_n \equiv dlips\,(P; p_1, ..., p_n) = (2\pi)^4 \delta^{(4)}(P - \sum_{f=1}^{n} p_f) \prod_{f=1}^{n} \frac{d^3 p_f}{(2\pi)^3 2E_f}, \tag{7.2}$$

where p_f and E_f for $f = 1, ..., n$ are the four-momenta and energies, respectively, of the outgoing particles, and P is the sum of the four-momenta in the initial state.

Factorisation Eq. (7.1) is based on the property of the phase space and the matrix element to be factorisable into sub-processes. The phase space element $d\Phi_n$ with n particles in the final state as in Eq. (7.2) will now be expressed as a product of the k-particle phase space Φ_k with $k < n$ and the remaining Φ_{n-k+1} [23, 216],

$$d\Phi_n = d\Phi_k \frac{dq^2}{2\pi} d\Phi_{n-k+1}, \tag{7.3}$$

where q denotes the momentum of the intermediate particle that appears in the final state of a process with $dlips(P; p_1, ..., p_{k-1}, q)$ and in the initial state of $dlips(q; p_k, ..., p_n)$. Now $\Phi_k(q)$ can be interpreted as the *production* phase space $P \to \{p_1, ..., p_{k-1}, q\}$ and $\Phi_{n-k+1}(q)$ as the *decay* phase space $q \to \{p_k, ..., p_n\}$. The factorisation of $d\Phi_n$ is exact, no approximation has been made so far because the dependence on q^2 is maintained instead of setting it on the mass shell. Next, we rewrite the amplitude with a scalar propagator as a product of the production (P) and decay (D) part such that the Breit-Wigner propagator $\Delta^{\mathrm{BW}}(q^2)$ as defined in Eq. 6.2 connects the production and decay matrix elements $\mathcal{M}_P$ and $\mathcal{M}_P$:

$$\mathcal{M} = \mathcal{M}_P \frac{1}{q^2 - M^2 + iM\Gamma} \mathcal{M}_D \quad \Rightarrow |\mathcal{M}|^2 = |\mathcal{M}_P|^2 \frac{1}{(q^2 - M^2)^2 + (M\Gamma)^2} |\mathcal{M}_D|^2. \tag{7.4}$$

Beyond the tree level, this factorisation is only possible if non-factorisable loop-contributions are absent or negligible. Regarding the application, one can classify the kinematic cases in two categories. On the one hand, for a scattering process $a, b \to X$ to any final state X (in particular $a, b \to c, e, f$ for the example in Fig. 7.1), the flux factor is given by

$$F_{\text{scatter}} = 2\lambda^{1/2}(s, m_a^2, m_b^2) \tag{7.5}$$

with the kinematic function [216]

$$\lambda(x, y, z) := x^2 + y^2 + z^2 - 2(xy + yz + zx). \tag{7.6}$$

On the other hand, for a decay process $a \to X$ (for example $a \to c, e, f$), the flux factor is determined by the mass of the decaying particle,

$$F_{\mathrm{decay}} = 2m_a. \tag{7.7}$$

Then the full cross section (or partical decay width) is given as

$$\sigma = \frac{1}{F} \int d\Phi |\mathcal{M}|^2. \tag{7.8}$$

If appropriate, the sum or average over spins is implicitly understood here. For the decomposition into production and decay, we do not only factorise the matrix elements as in Eq. (7.4). Based on Eq. (7.3), also the phase space of the full process is factorised into the production phase space Φ_P and the decay phase space Φ_D (here defined for the example process in Fig. 7.1, but they can be generalised to other external momenta), which depend on the momentum of the resonant particle:

$$\begin{aligned} d\Phi &= dlips(\sqrt{s}; p_c, p_e, p_f) \\ d\Phi_P &= dlips(\sqrt{s}; p_c, q) \\ d\Phi_D &= dlips(q; p_e, p_f). \end{aligned} \tag{7.9}$$

Under the assumption of negligible non-factorisable loop contributions, one can then express the cross section in (7.8) as

$$\sigma = \frac{1}{F} \int \frac{dq^2}{2\pi} \left(\int d\Phi_P |\mathcal{M}_P|^2 \right) \frac{1}{(q^2 - M^2)^2 + (M\Gamma)^2} \left(\int d\Phi_D |\mathcal{M}_D|^2 \right). \tag{7.10}$$

In this analytical formula of the cross section, the production and decay matrix elements and the sub-phase spaces are separated from the Breit-Wigner propagator. However, the full q^2-dependence of the matrix elements and the phase space is retained. The off-shell production cross section of a scattering process with particles a, b in the initial state and the production flux factor F reads

$$\sigma_P(q^2) = \frac{1}{F} \int d\Phi_P |\mathcal{M}_P(q^2)|^2. \tag{7.11}$$

The decay rate of the unstable particle, $d \to ef$, with energy $\sqrt{q^2}$ is obtained from the integrated squared decay matrix element divided by the decay flux factor $F_D = 2\sqrt{q^2}$,

$$\Gamma_D(q^2) = \frac{1}{F_D} \int d\Phi_D |\mathcal{M}_D(q^2)|^2. \tag{7.12}$$

Hence one can rewrite the full cross section from Eq. (7.10) as

$$\sigma = \int \frac{dq^2}{2\pi} \sigma_P(q^2) \frac{2\sqrt{q^2}}{(q^2 - M^2)^2 + (M\Gamma)^2} \Gamma_D(q^2). \tag{7.13}$$

In the limit where $(\Gamma M) \to 0$ the Dirac δ-distribution emerges from the Cauchy distribution,

$$\lim_{(M\Gamma)\to 0} \frac{1}{(q^2 - M^2)^2 + (M\Gamma)^2} = \delta(q^2 - M^2) \frac{\pi}{M\Gamma}. \tag{7.14}$$

For the integration of the δ-distribution, the integral boundaries are shifted from q^2_{max}, q^2_{min}, i.e. the upper and lower bound on q^2, respectively, to $\pm\infty$ because the contributions outside the narrow resonance region are expected to be small. So this extension of the integral should not considerably alter the result. The zero-width limit implies that the production cross section, decay width and the factor $\sqrt{q^2}$ are evaluated on-shell at $q^2 = M^2$. This applies both to the matrix elements and the phase space elements. The described approximation leads to the well-known factorisation into the production cross section times the decay branching ratio,

$$\sigma \overset{(M\Gamma)\to 0}{\to} \int_{-\infty}^{+\infty} \frac{dq^2}{2\pi} \sigma_P(q^2)\, 2\sqrt{q^2}\, \delta(q^2 - M^2) \frac{\pi}{M\Gamma} \Gamma_D(q^2) \;=\; \sigma_P(M^2) \cdot \frac{\Gamma_D(M^2)}{\Gamma} \equiv \sigma_P \cdot \text{BR}, \tag{7.15}$$

with the branching ratio $\text{BR} = \Gamma_D/\Gamma$, where Γ_D denotes the partial decay width into the particles in the final state of the considered process, and Γ is the total decay width of the unstable particle. While Eq. (7.15) has been obtained in the limit $(M\Gamma) \to 0$, it is expected to approximate the result for non-zero Γ up to terms of $\mathcal{O}(\frac{\Gamma}{M})$.

Going beyond the approximation of Eq. (7.15) for the treatment of finite width effects, the on-shell approximation can be applied just to the matrix elements for production and decay if both subprocesses are kinematically allowed while keeping a finite width in the integration over the Breit-Wigner propagator in the form of Eq. (7.13). This is gauge invariant and motivated by the consideration that the Breit-Wigner function is rapidly falling causing that only matrix elements close to the mass shell $q^2 = M^2$ contribute significantly. It results in a modified NWA improved for off-shell effects, see e.g. Ref. [193, 194],

$$\sigma^{(ofs)} = \sigma_P(M^2) \left[\int \frac{dq^2}{2\pi} \frac{2M}{(q^2 - M^2)^2 + (M\Gamma)^2} \right] \Gamma_D(M^2). \tag{7.16}$$

7.3. Formulation of the generalised narrow-width approximation at lowest order

If all conditions in Sect. 7.2.2 are fulfilled, the NWA is expected to work reliably up to terms of $\mathcal{O}(\frac{\Gamma}{M})$. This section addresses how to generalise the NWA [1, 45, 85] such that interference effects of nearly mass-degenerate resonances can be included at leading order. The formulation of the gNWA will be extended to the one-loop level in Sect. 7.4

7.3.1. Cross section with interference term

Interference effects can be large if there are several resonant diagrams whose intermediate particles (here labelled by 1 and 2) are close in mass compared to their total decay widths:

$$|M_1 - M_2| \lesssim \Gamma_1 + \Gamma_2. \tag{7.17}$$

In these nearly mass-degenerate cases, the Breit-Wigner functions $\Delta_1^{\text{BW}}(q^2)$, $\Delta_2^{\text{BW}}(q^2)$ overlap significantly, and an integral of the form

$$\int_{q^2_{\text{min}}}^{q^2_{\text{max}}} dq^2 \Delta_1^{\text{BW}}(q^2)\Delta_2^{*\text{BW}}(q^2) \cdot f(\mathcal{M}, p_i, ...) \tag{7.18}$$

is not negligible. The boundaries $q^2_{\text{min}}, q^2_{\text{max}}$ are the lower and upper limits of the kinematically allowed region of q^2, and the function f summarises a possible dependence on matrix elements $\mathcal{M}$ and momenta p_i in the phase space. Such interference effects might especially be relevant in models of new physics where an enlarged particle spectrum leads to mass degeneracies in some parts of the parameter space.

Let h_1, h_2 be two resonant intermediate particles, for example two Higgs bosons, with similar masses occurring in a process $ab \to cef$, i.e. $ab \to ch_i, h_i \to ef$ (cf. Fig. 7.1 with $d = h_1, h_2$). If non-factorisable loop corrections can be neglected, the full matrix element is given by

$$\mathcal{M} = \mathcal{M}_{ab\to ch_1}\frac{1}{q^2 - M_1^2 + iM_1\Gamma_1}\mathcal{M}_{h_1\to ef} + \mathcal{M}_{ab\to ch_2}\frac{1}{q^2 - M_2^2 + iM_2\Gamma_2}\mathcal{M}_{h_2\to ef}. \tag{7.19}$$

Here we dropped the q^2-dependence of the matrix elements for an ease of notation, but the full momentum dependence is implicitly implied. Furthermore, as mentioned above in Sect. 7.2, we explicitly treat the case of scalar resonant particles. Spin correlations of intermediate particles with non-zero spin can be taken into account using spin–density matrices. The squared matrix element contains the two separate contributions of h_1, h_2

and in the second line of Eq. (7.20) the interference term,

$$|\mathcal{M}|^2 = \frac{|\mathcal{M}_{ab\to ch_1}|^2 |\mathcal{M}_{h_1\to ef}|^2}{(q^2 - M_1^2)^2 + M_1^2\Gamma_1^2} + \frac{|\mathcal{M}_{ab\to ch_2}|^2 |\mathcal{M}_{h_2\to ef}|^2}{(q^2 - M_2^2)^2 + M_2^2\Gamma_2^2} + 2\mathrm{Re}\left\{ \frac{\mathcal{M}_{ab\to ch_1}\mathcal{M}^*_{ab\to ch_2}\mathcal{M}_{h_1\to ef}\mathcal{M}^*_{h_2\to ef}}{(q^2 - M_1^2 + iM_1\Gamma_1)(q^2 - M_2^2 - iM_2\Gamma_2)} \right\}. \tag{7.20}$$

Thus, the full cross section from Eq. (7.13) with the matrix element from Eq. (7.20) can be written as

$$\sigma_{ab\to cef} = \int \frac{dq^2}{2\pi}\left[\frac{\sigma_{ab\to ch_1}(q^2)\; 2\sqrt{q^2}\;\Gamma_{h_1\to ef}(q^2)}{(q^2 - M_{h_1}^2)^2 + (M_{h_1}\Gamma_{h_1})^2} + \frac{\sigma_{ab\to ch_2}(q^2)\; 2\sqrt{q^2}\;\Gamma_{h_2\to ef}(q^2)}{(q^2 - M_{h_2}^2)^2 + (M_{h_2}\Gamma_{h_2})^2}\right] + \int \frac{dlips(s;p_c,q)dq^2 dlips(q;p_e,p_f)}{2\pi\cdot 2\lambda^{1/2}(s,m_a^2,m_b^2)} 2\mathrm{Re}\left\{ \frac{\mathcal{M}_{ab\to ch_1}\mathcal{M}^*_{ab\to ch_2}\mathcal{M}_{h_1\to ef}\mathcal{M}^*_{h_2\to ef}}{(q^2 - M_1^2 + iM_1\Gamma_1)(q^2 - M_2^2 - iM_2\Gamma_2)} \right\}. \tag{7.21}$$

We will use Eq. (7.21) as a starting point for approximations of the full cross section. The first two terms can again be approximated by the NWA improved for off-shell effects by considering a finite width in the propagator according to Eq. (7.16), or by the usual narrow-width approximation in the limit of a vanishing width from Eq. (7.15) as $\sigma \times \mathrm{BR}$. The interference term still consists of an integral over the q^2-dependent matrix elements, the product of Breit-Wigner propagators and the phase space.

7.3.2. On-shell matrix elements

While the interference term in Eq. (7.21) depends on the momentum q^2 via the Breit-Wigner propagators and the matrix elements of the production and decay part, we now propose an approximation that simplifies the evaluation of the matrix elements of the sub-processes, but encompasses the momentum dependence of $\Delta^{\mathrm{BW}}(q^2)$. Our approach is to evaluate the production ($\mathcal{P}$) and decay ($\mathcal{D}$) matrix elements

$$\mathcal{P}_i(q^2) \equiv \mathcal{M}_{ab\to ch_i}(q^2), \quad \mathcal{D}_i(q^2) \equiv \mathcal{M}_{h_i\to ef}(q^2) \tag{7.22}$$

on the mass shell of the intermediate particle h_i [1,85]. This is motivated by the assumption of a narrow resonance region $[M_{h_i} - \Gamma_{h_i}, M_{h_i} + \Gamma_{h_i}]$ so that off-shell contributions of the matrix elements in the integral are suppressed by the non-resonant tail of the Breit-Wigner propagator if $\mathcal{P}$ and $\mathcal{D}$ vary only mildly[1] with q^2. Then the interference

[1] We refer here to partonic cross sections. For hadronic cross sections, the folding with parton density functions (pdfs), which have a pronounced q^2-dependence, needs to be taken into account.

term from the last line of Eq. (7.21) is approximated by

$$\sigma_{\rm int} = \int \frac{d\Phi_P dq^2 d\Phi_D}{2\pi F} 2\mathrm{Re} \frac{\mathcal{P}_1(q^2)\mathcal{P}_2^*(q^2)\mathcal{D}_1(q^2)\mathcal{D}_2^*(q^2)}{(q^2 - M_1^2 + iM_1\Gamma_1)(q^2 - M_2^2 - iM_2\Gamma_2)} \tag{7.23}$$

$$\begin{aligned} &= \frac{2}{F}\mathrm{Re}\int \frac{dq^2}{2\pi}\Delta_1^{\rm BW}(q^2)\Delta_2^{*\rm BW}(q^2)\left[\int d\Phi_P(q^2)\mathcal{P}_1(q^2)\mathcal{P}_2^*(q^2)\right]\left[\int d\Phi_D(q^2)\mathcal{D}_1(q^2)\mathcal{D}_2^*(q^2)\right] \\ &\simeq \frac{2}{F}\mathrm{Re}\int \frac{dq^2}{2\pi}\Delta_1^{\rm BW}(q^2)\Delta_2^{*\rm BW}(q^2)\left[\int d\Phi_P(q^2)\mathcal{P}_1(M_1^2)\mathcal{P}_2^*(M_2^2)\right] \\ &\qquad \cdot \left[\int d\Phi_D(q^2)\mathcal{D}_1(M_1^2)\mathcal{D}_2^*(M_2^2)\right]. \end{aligned} \tag{7.24}$$

Eq. (7.24) represents our master formula for the interference contribution. At this stage, we have only evaluated the matrix elements on the mass shell of the particular Higgs boson by setting $q^2 = M_{h_i}^2$ (this is also important for ensuring the gauge invariance of the considered contributions). So the on-shell matrix elements can be taken out of the q^2-integral. But the dependence of the matrix elements on further invariants and momenta is kept. For 2-body decays, it is possible to carry out the phase space integration without referring to the specific form of the matrix elements. In general, however, the matrix elements are functions of the phase space integration variables.

The approximation in Eq. (7.24) is a simplification of the full expression in Eq. (7.23) since the integrand of the q^2-integral is simplified. We will use Eq. (7.24) in the numerical calculation of an example process in Sect. 9.

We will furthermore investigate additional approximations of the integral structure in Eq. (7.24), which would simplify the application of the gNWA. This issue is discussed at the tree level in the following section.

7.3.3. On-shell phase space and interference weight factors at lowest order

The following discussion, which focuses on the tree-level case, concerns an optional technical simplification of the master formula in Eq. (7.24). It will be numerically applied in Fig. 9.4 below and extended to the 1-loop level in Sect. 9.3.

As a possible further simplification on top of the on-shell approximation for matrix elements, one can also evaluate the production and decay phase spaces on-shell. This is based on the same argument as for the on-shell evaluation of the matrix elements because off-shell phase space elements are multiplied with the non-resonant tail of Breit-Wigner functions. Now the q^2-independent matrix elements and phase space integrals can be taken out of the q^2-integral,

$$\sigma_{\rm int} \simeq \frac{2}{F}\mathrm{Re}\left\{\left[\int d\Phi_P \mathcal{P}_1(M_1^2)\mathcal{P}_2^*(M_2^2)\right]\left[\int d\Phi_D \mathcal{D}_1(M_1^2)\mathcal{D}_2^*(M_2^2)\right]\int \frac{dq^2}{2\pi}\Delta_1^{\rm BW}(q^2)\Delta_2^{*\rm BW}(q^2)\right\}. \tag{7.25}$$

The choice at which mass, M_1 or M_2, to evaluate the production and decay phase space regions is not unique. We thus introduce a weighting factor between the two possible options, as an ansatz based on the individual contributions to the production cross sections and branching ratios:

$$w_i := \frac{\sigma_{P_i}\,\mathrm{BR}_i}{\sigma_{P_1}\,\mathrm{BR}_1 + \sigma_{P_2}\,\mathrm{BR}_2}. \tag{7.26}$$

Then we define the on-shell phase space regions as the weighted sum of both phase space factors, for the production and decay subprocesses each,

$$d\Phi_{P/D} := w_1\, d\Phi_{P/D}(q^2 = M_1^2) + w_2\, d\Phi_{P/D}(q^2 = M_2^2). \tag{7.27}$$

In Eq. (7.25), a universal integral over the Breit-Wigner propagators emerges,

$$I := \int_{q^2_{\mathrm{min}}}^{q^2_{\mathrm{max}}} \frac{dq^2}{2\pi} \Delta_1^{\mathrm{BW}}(q^2)\, \Delta_2^{*\mathrm{BW}}(q^2), \tag{7.28}$$

which depends on the masses and widths of the interfering particles. Process-dependent information affects the integration boundaries $q^2_{\mathrm{min}}, q^2_{\mathrm{max}}$, but as in the sNWA, only a mild dependence on the exact boundaries is expected because the dominant contribution stems from the resonance region where both Breit-Wigner functions have large values. The integral is analytically solvable,

$$I = \left[\frac{\arctan\left[\frac{\Gamma_1 M_1}{M_1^2 - q^2}\right] + \arctan\left[\frac{\Gamma_2 M_2}{M_2^2 - q^2}\right] + \frac{i}{2}\left(\ln\left[\Gamma_1^2 M_1^2 + (M_1^2 - q^2)^2\right] - \ln\left[\Gamma_2^2 M_2^2 + (M_2^2 - q^2)^2\right]\right)}{2\pi i\left(M_1^2 - M_2^2 - i(M_1\Gamma_1 + M_2\Gamma_2)\right)}\right]_{q^2_{\mathrm{min}}}^{q^2_{\mathrm{max}}}. \tag{7.29}$$

In the limit of equal masses and widths, $M = M_1 = M_2$ and $\Gamma = \Gamma_1 = \Gamma_2$, the product of Breit-Wigner propagators becomes the absolute square, and the integral is reduced to

$$I(M,\Gamma) = \int_{q^2_{\mathrm{min}}}^{q^2_{\mathrm{max}}} dq^2 \frac{1}{(q^2 - M^2)^2 + (M\Gamma)^2} = \left[-\frac{1}{M\Gamma}\arctan\left[\frac{M^2 - q^2}{M\Gamma}\right]\right]_{q^2_{\mathrm{min}}}^{q^2_{\mathrm{max}}}. \tag{7.30}$$

This absolute square of a single Breit-Wigner function is also present in the usual NWA in Eq. (7.14), and for vanishing Γ it can be approximated by a δ-distribution. Here, however, we consider the more general case and allow for different masses and widths from the two resonant propagators. We evaluate only the matrix elements and differential phase space on-shell, but we do not perform a zero-width approximation. This approach is analogous to the finite-narrow-width approximation without the interference term in Eq. (7.16).

Under the additional assumption of equal masses, the interference part can be approximated in terms of cross sections, branching ratios and couplings in order to avoid the explicit calculation of the product of unsquared amplitudes and their conjugates. This will also avoid the phase space integrals in the interference term as in Eq. (7.25).

For this purpose, each matrix element is written as the coupling of the particular production or decay process, C_{P_i} or C_{D_i}, times the helicity part $p(M_i^2)$ or $d(M_i^2)$, respectively,

$$\mathcal{P}_i(M_i^2) = C_{P_i}\, p(M_i^2), \qquad \mathcal{D}_i(M_i^2) = C_{D_i}\, d(M_i^2). \tag{7.31}$$

The on-shell calculation of helicity matrix elements (without making use of sum rules for squared matrix elements) is demonstrated in Sect. 9.1.2 where also left- and right-handed couplings are distinguished. Here we use the schematic notation of Eq. (7.31), but it could directly be replaced by the L/R-sum as in Eq. (9.14) below.

If we then make the additional assumption $M_1 \simeq M_2$, the helicity matrix elements coincide, $p(M_1^2) \simeq p(M_2^2)$, $d(M_1^2) \simeq d(M_2^2)$. As a consequence, the matrix elements differ just by fractions of their couplings,

$$\mathcal{P}_2(M_2^2) \simeq \frac{C_{P_2}}{C_{P_1}}\mathcal{P}_1(M_1^2), \qquad \mathcal{D}_2(M_2^2) \simeq \frac{C_{D_2}}{C_{D_1}}\mathcal{D}_1(M_1^2). \tag{7.32}$$

This enables us to replace the products of an amplitude involving the resonant particle 1 with a conjugate amplitude of resonant particle 2 by absolute squares of amplitudes as follows, where $i, j \in \{1, 2\}$, $i \neq j$, and no summation over indices is implied:

$$\sigma_{\text{int}} \overset{7.25}{\simeq} 2\text{Re}\left\{\left[\frac{1}{F}\int d\Phi_P \mathcal{P}_1\mathcal{P}_2^*\right]\left[\frac{1}{2M_i}\int d\Phi_D \mathcal{D}_1\mathcal{D}_2^*\right] 2M_i \int \frac{dq^2}{2\pi}\Delta_1^{\text{BW}}(q^2)\Delta_2^{*\text{BW}}(q^2)\right\} \tag{7.33}$$

$$\overset{7.31}{\simeq} 2\text{Re}\left\{\left[\frac{1}{F}\int d\Phi_P |\mathcal{P}_i|^2\frac{C_{P_j}^*}{C_{P_i}^*}\right]\left[\frac{1}{2M_i}\int d\Phi_D |\mathcal{D}_i|^2\frac{C_{D_j}^*}{C_{D_i}^*}\right] 2M_i \int \frac{dq^2}{2\pi}\Delta_1^{\text{BW}}(q^2)\Delta_2^{*\text{BW}}(q^2)\right\} \tag{7.34}$$

$$\overset{7.11,7.12}{=} \sigma_{P_i}\,\Gamma_{D_i}\cdot 2M_i\cdot 2\text{Re}\left\{\frac{C_{P_j}^* C_{D_j}^*}{C_{P_i}^* C_{D_i}^*}\int \frac{dq^2}{2\pi}\Delta_1^{\text{BW}}(q^2)\Delta_2^{*\text{BW}}(q^2)\right\} \tag{7.35}$$

$$= \quad \sigma_{P_i}\,\text{BR}_i\cdot 2M_i\Gamma_i\cdot 2\text{Re}\left\{x_i\cdot I\right\}. \tag{7.36}$$

In the last step, we divided and multiplied by the total width Γ_i in order to obtain the branching ratio $\text{BR}_i = \frac{\Gamma_{D_i}}{\Gamma_i}$. The universal integral I over the overlapping Breit-Wigner propagators is given in Eq. (7.28). Furthermore, we defined a scaling factor as the ratio of couplings [45, 85, 185],

$$x_i := \frac{C_{P_j}^* C_{D_j}^*}{C_{P_i}^* C_{D_i}^*} = \frac{C_{P_i}C_{P_j}^* C_{D_i}C_{D_j}^*}{|C_{P_i}|^2|C_{D_i}|^2}. \tag{7.37}$$

Using Eq. (7.36) and the scaling factor x_i with $i = 1,\ j = 2$ or vice versa allows us to express σ_{int} alternatively in terms of the cross section, branching ratio, mass and width of either of the resonant particle 1 or 2. Since no summation over i or j is implied in Eq. (7.36), both contributions are accounted for by the weighting factor $w_i \in [0, 1]$ from Eq. (7.26).

In the next step, we summarise the components of σ_{int} apart from σ_{P_i} and BR_i, which also occur in the usual NWA, by defining an interference weight factor

$$R_i := 2M_i\Gamma_i w_i \cdot 2\text{Re}\{x_i I\}. \tag{7.38}$$

Hence, in this approximation of on-shell matrix elements and production and decay phase spaces with the additional condition of equal masses, the interference contribution can be written as the weighted sum

$$\sigma_{\text{int}} \simeq \sigma_{P_1}\,\text{BR}_1 \cdot R_1 + \sigma_{P_2}\,\text{BR}_2 \cdot R_2, \tag{7.39}$$

or in terms of only one of the resonant particles,

$$\sigma_{\text{int}} \simeq \sigma_{P_i}\,\text{BR}_i \cdot 2\tilde{R}_i, \tag{7.40}$$

$$\tilde{R}_i := 2M_i\Gamma_i \cdot \text{Re}\{x_i I\} \equiv \frac{R_i}{2w_i}. \tag{7.41}$$

Finally, we are able to express the cross section of the complete process in this R-factor approximation, comprising the exchange of the resonant particles 1 and 2 as well as their interference, in the following compact form

$$\sigma \simeq \sigma_{P_1}\,\text{BR}_1 \cdot (1 + R_1) + \sigma_{P_2}\,\text{BR}_2 \cdot (1 + R_2) \tag{7.42}$$

$$\simeq \sigma_{P_i}\,\text{BR}_i \cdot \,(1 + 2\tilde{R}_i) + \sigma_{P_j}\,\text{BR}_j \tag{7.43}$$

Furthermore, it is possible to replace the term $\sigma_i\,\text{BR}_i$ in the two separate processes without the interference term by the finite-width integral from Eq. (7.16).

7.3.4. Discussion of the steps of approximations

Starting from the master formula in Eq. (7.24), we presented in the previous sections two levels of approximations for the interference term with two resonant particles. The first approximation in Sect. 7.3.2 represents our main result. It relies only on the on-shell evaluation of the matrix elements, justified by a narrow resonance region, but no further assumptions (beyond those already used in the sNWA) are implied. Different masses and finite widths are taken into account. This version requires the explicit calculation of unsquared on-shell amplitudes, preventing the use of e.g. convenient spinor trace rules. Furthermore, the phase space integration depends on q^2 so that the universal, process-independent Breit-Wigner integral I from Eq. (7.28) does not appear here.

The second approximation in Sect. 7.3.3 has been formulated only at tree level so far. It is based on the additional approximation, motivated by the same argument as for the matrix elements, of setting the differential Lorentz- invariant phase spaces on-shell at either mass, scaled by a weighting factor. This simplifies the q^2-integration because only the universal integral I is left. Furthermore, it avoids the unusual calculation of on-shell amplitudes in an explicit representation (see Sect. 9.1.2) by expressing the interference part as an interference weight factor R in terms of cross sections, branching ratios, masses and widths, which are already needed in the simple NWA, in combination with the universal integral I and a scaling factor x which consists of the process-specific couplings. Yet, this approximation holds only for equal masses. As discussed in the context of Eq. (7.18), the interference term is largest if the Breit-Wigner shapes overlap significantly due to the relation $\Delta M \lesssim \Gamma_1 + \Gamma_2$. Nevertheless, the masses are not necessarily equal in the interference region. Instead, the overlap criterion in Eq. (7.17) can as well be satisfied if one of the widths is relatively large. In this respect, the equal-mass condition is more restrictive than the overlap criterion. However, the equal-mass constraint is just applied on the matrix elements and phase space, whereas different masses and widths are distinguished in the Breit-Wigner integral. The R-factor method is technically easier to handle because the constituents of R can be obtained by standard routines in program packages such as `FormCalc` [94, 119–122] and `FeynHiggs` [67, 146, 149, 150] that we use in the numerical computation. For one example process, this is done in Sect. 9. An extension of the generalised narrow-width approximation to the 1-loop level follows in the next section.

7.4. Formulation of the generalised narrow-width approximation at higher order

In our formulation of the gNWA at higher order, we will start with the method of on-shell matrix elements in Sect. 7.4.1 and turn to the R-factor approximation in Sect. 7.4.2. At the 1-loop level we write the product of the production cross-section times partial decay width in the standard NWA as

$$\sigma_P \cdot \mathrm{BR} \longmapsto \frac{\sigma_P^1 \Gamma_D^0 + \sigma_P^0 \Gamma_D^1}{\Gamma^{\mathrm{tot}}}, \tag{7.44}$$

where the total width is obtained from `FeynHiggs` [67, 146, 149, 150] incorporating corrections up to the 2-loop level as in the evaluation of the branching ratio and in the Breit-Wigner propagator. While restricting the numerator of Eq. (7.44) formally to one-loop order to enable a consistent comparison with the full process, at the end (in Sect. 9.4.3) all constituents of the NWA will be used at the highest available precision, i.e. $\sigma_P^{\mathrm{best}} \cdot \mathrm{BR}^{\mathrm{best}}$ for the most advanced prediction with the branching ratio obtained from `FeynHiggs`.

7.4.1. On-shell matrix elements at 1-loop order

In analogy to the procedure in Sect. 7.3.2 at the tree level, on-shell matrix elements are used here in the 1-loop expansion. Special attention must be paid to the cancellation of infrared (IR) divergences from virtual photons (or gluons) in 1-loop matrix elements and real photon (gluon) emission off charged external legs. In preparation for the example process $\tilde{\chi}_4^0 \to \tilde{\chi}_1^0\, h/H \to \tilde{\chi}_1^0\, \tau^+\tau^-$ (see Sect. 9.1), we focus on IR-divergences from photons in loops of the decay part and soft final state photon radiation.

The aim is to approximate only the 1-loop contribution, but to keep the full momentum dependent expression at the Born level with $\mathcal{M}_i^0 = \mathcal{M}_i^0(q^2)$,

$$|\mathcal{M}^0|^2 = |\mathcal{M}_h^0|^2 + |\mathcal{M}_H^0|^2 + 2\mathrm{Re}\left[\mathcal{M}_h^0 \mathcal{M}_H^{0*}\right]. \tag{7.45}$$

In contrast, the 1-loop matrix elements are factorised into the on-shell production and decay parts times the momentum dependent Breit-Wigner propagator $\Delta_i^{\mathrm{BW}} \equiv \Delta_i^{\mathrm{BW}}(q^2)$. The squared matrix elements are expanded up to the 1-loop order. Since the emission of soft real photons is proportional to the Born contribution, the virtual contribution is supplemented by the absolute value squared of the tree-level matrix element, multiplied by the QED-factor δ_{SB} of soft bremsstrahlung [21, 217],

$$\begin{aligned}
2\mathrm{Re}\left[\mathcal{M}^0\mathcal{M}^{1*}\right] + \delta_{\mathrm{SB}}|\mathcal{M}^0|^2 \simeq\, & 2\mathrm{Re}\left[\left(\mathcal{P}_h^1\mathcal{D}_h^0 + \mathcal{P}_h^0\mathcal{D}_h^1 + \delta_{\mathrm{SB}}\mathcal{P}_h^0\mathcal{D}_h^0\right)\mathcal{P}_h^{0*}\mathcal{D}_h^{0*}\cdot|\Delta_h^{BW}|^2\right]\\
&+ 2\mathrm{Re}\left[\left(\mathcal{P}_H^1\mathcal{D}_H^0 + \mathcal{P}_H^0\mathcal{D}_H^1 + \delta_{\mathrm{SB}}\mathcal{P}_H^0\mathcal{D}_H^0\right)\mathcal{P}_H^{0*}\mathcal{D}_H^{0*}\cdot|\Delta_H^{\mathrm{BW}}|^2\right]\\
&+ 2\mathrm{Re}\Big[\Big\{\left(\mathcal{P}_h^1\mathcal{D}_h^0 + \mathcal{P}_h^0\mathcal{D}_h^1\right)\mathcal{P}_H^{0*}\mathcal{D}_H^{0*}\\
&\qquad + \mathcal{P}_h^0\mathcal{D}_h^0\left(\mathcal{P}_H^{1*}\mathcal{D}_H^{0*} + \mathcal{P}_H^{0*}\mathcal{D}_H^{1*}\right)\\
&\qquad + \delta_{\mathrm{SB}}\,\mathcal{P}_h^0\mathcal{D}_h^0\mathcal{P}_H^{0*}\mathcal{D}_H^{0*}\Big\}\cdot\Delta_h^{\mathrm{BW}}\Delta_H^{\mathrm{BW}*}\Big].
\end{aligned} \tag{7.46}$$

The first line of Eq. (7.46) represents the pure contribution from h, factorised into production and decay, the second line accordingly for H. The third and fourth lines constitute the 1-loop and bremsstrahlung interference term as the product of h- and H-matrix elements and Breit-Wigner propagators. For a consistent comparison with the full 1-loop result, each term is restricted to 1-loop corrections in only one of the matrix elements.

The 1-loop prediction of the full process in the approximation of on-shell matrix elements consists — besides the Born cross section without an approximation[2] — of the squared contribution of h and H and the interference term $\sigma_{\mathcal{M}}^{\mathrm{int1}}$ at the strict 1-loop level[3],

$$\sigma_{\mathcal{M}}^1 = \sigma_{\mathrm{full}}^0 + \frac{\sigma_{P_h}^1\Gamma_{D_h}^0 + \sigma_{P_h}^0\Gamma_{D_h}^1}{\Gamma_h^{\mathrm{tot}}} + \frac{\sigma_{P_H}^1\Gamma_{D_H}^0 + \sigma_{P_H}^0\Gamma_{D_H}^1}{\Gamma_H^{\mathrm{tot}}} + \sigma_{\mathcal{M}}^{\mathrm{int1}}, \tag{7.47}$$

$$\begin{aligned}
\sigma_{\mathcal{M}}^{\mathrm{int1}} = \frac{2}{F}\mathrm{Re}\Bigg\{\int\frac{dq^2}{2\pi}\Delta_h^{\mathrm{BW}}(q^2)\Delta_H^{*\mathrm{BW}}(q^2)\\
\Bigg(\left[\int d\Phi_P(q^2)(\mathcal{P}_h^1\mathcal{P}_H^{0*} + \mathcal{P}_h^0\mathcal{P}_H^{1*})\right]\left[\int d\Phi_D(q^2)\mathcal{D}_h^0\mathcal{D}_H^{0*}\right]\\
+\left[\int d\Phi_P(q^2)\mathcal{P}_h^0\mathcal{P}_H^{0*}\right]\left[\int d\Phi_D(q^2)(\mathcal{D}_h^1\mathcal{D}_H^{0*} + \mathcal{D}_h^0\mathcal{D}_H^{1*} + \delta_{\mathrm{SB}}\mathcal{D}_h^0\mathcal{D}_H^{0*})\right]\Bigg)\Bigg\}.
\end{aligned} \tag{7.48}$$

[2]If the full Born cross section cannot be calculated, this term can be replaced by the gNWA at the Born level.

[3]With *strict 1-loop* we refer to the expansion of the products of matrix elements whereas 2-loop Higgs masses, total widths and wave function renormalisation factors are employed.

For the prediction with the most precise constituents, we use 2-loop branching ratios, $\mathrm{BR}_\mathrm{i}^\mathrm{best}$. We include also the products of 1-loop matrix elements. Their contribution to the interference term is denoted by $\sigma_\mathcal{M}^{\mathrm{int+}}$,

$$\sigma_\mathcal{M}^{\mathrm{int+}} = \frac{2}{F}\mathrm{Re}\left\{\int\frac{dq^2}{2\pi}\Delta_h^{\mathrm{BW}}(q^2)\Delta_H^{*\mathrm{BW}}(q^2)\right.$$
$$\left.\cdot\left[\int d\Phi_P(q^2)(\mathcal{P}_h^1\mathcal{P}_H^{0*}+\mathcal{P}_h^0\mathcal{P}_H^{1*})\right]\left[\int d\Phi_D(q^2)(\mathcal{D}_h^1\mathcal{D}_H^{0*}+\mathcal{D}_h^0\mathcal{D}_H^{1*}+\delta_\mathrm{SB}\mathcal{D}_h^0\mathcal{D}_H^{0*})\right]\right\}. \tag{7.49}$$

The approximation of the whole process based on on-shell matrix elements and incorporating higher-order corrections wherever possible is denoted by $\sigma_\mathcal{M}^{\mathrm{best}}$, which reads then

$$\sigma_\mathcal{M}^{\mathrm{best}} = \sigma_{\mathrm{full}}^0 + \sum_{i=h,H}\left(\sigma_{P_i}^{\mathrm{best}}\mathrm{BR}_i^{\mathrm{best}} - \sigma_{P_i}^0\mathrm{BR}_i^0\right) + \sigma_\mathcal{M}^{\mathrm{int1}} + \sigma_\mathcal{M}^{\mathrm{int+}}. \tag{7.50}$$

The *best* production cross section $\sigma_{P_i}^{\mathrm{best}}$ and branching ratios $\mathrm{BR}_i^{\mathrm{best}}$ mean the sum of the tree level, strict 1-loop and all available higher-order contribution to the respective quantity. Therefore, the products of tree level production cross sections and branching ratios are subtracted because their unfactorised counterparts are already contained in the full tree level term σ_{full}^0. If a more precise result of the production cross sections is available, it can be used instead of the explicit 1-loop calculation that was performed in our example process.

7.4.1.1. IR-finiteness of the factorised matrix elements

On-shell evaluation The UV-divergences of the virtual corrections are cancelled by the same counterterms as in the full process at 1-loop order. Although it would be technically possible in most processes to compute the full bremsstrahlung term without the NWA, i.e. $\delta_\mathrm{SB}\,|\mathcal{M}_{\mathrm{full}}^0|^2$, the IR-divergences from the on-shell decays need to be exactly cancelled by those from the real photon emission. But the IR-singularities in the sum of the factorised (on-shell) virtual corrections and the momentum-dependent real ones would not match each other. Consequently, the tree level matrix elements are also factorised, and the IR-divergent parts of the 1-loop decay matrix elements $\mathcal{D}_h^1(M_h^2,\overline{M}^2), \mathcal{D}_H^1(M_H^2,\overline{M}^2)$ and the soft QED-factor $\delta_\mathrm{SB}(\overline{M}^2)$ have to be calculated at the same mass $\overline{M}=M_h$ or M_H. The LO matrix elements are evaluated at their mass-shell, i.e. $\mathcal{D}_i^0(M_{h_i}^2)$. The NLO matrix elements are split into the part containing loop integrals on the one hand and the helicity matrix elements on the other hand. While the individual Higgs masses can be inserted into the finite helicity matrix elements (see Sect. 9.1.2), the loop integrals have to be evaluated at the same mass $\overline{M}^2$ as in δ_SB to preserve the IR-cancellations. Hence, a choice must be made whether to define $\overline{M}=M_h$ or M_H. We evaluate the numerical difference in Sect. 9.4.2.

The production matrix elements are completely evaluated on their respective mass-shells, $\mathcal{P}_i^0(M_{h_i}^2)$ and $\mathcal{P}_i^1(M_{h_i}^2)$. This is possible because the initial state in this example contains only neutral particles. But the calculation can be directly generalised to charged initial states according to the procedure described for the decay matrix elements. The IR-singularities in the product of initial and final state radiation are then cancelled by those from a virtual photon connecting charged legs of the initial and final state. Such non-factorisable contributions can be treated in a pole approximation in analogy to the double-pole approximation (DPA) that has been used for instance for the process $e^+e^- \to W^+W^- \to 4\,$leptons, see Ref. [218]. An alternative approach for the treatment of IR-singularities is formulated in Refs. [164, 191]. There, the singular parts from the real photon contribution are extracted, and the DPA is only applied for those terms which exactly match the singularities from the virtual photons. In our calculation, we do not split up the real corrections in this way, but employ instead the procedure described above. We discuss a possibility of splitting the diagrams with virtual photons into an IR-singular and a finite subgroup in Sect. 7.4.1.2.

Cancellation of IR-divergences According to the Kinoshita-Lee-Nauenberg (KLN) theorem [95, 96], the IR-divergence from a virtual photon is cancelled by the emission of a real photon off a charged particle from the initial or final state, i.e., in our example process as soft bremsstrahlung in the final state of a Higgs decay. We will derive the IR-finiteness of the on-shell matrix elements in analogy to the cancellation of the IR divergencies for the full 3-body decay. Writing the momentum-dependent 3-body matrix elements with the resonant particle either $h_i = h$ or H as the sum of the tree level ($\mathcal{M}^0_{h_i}$) and virtual ($\mathcal{M}^v_{h_i}$) contributions,

$$\mathcal{M}_{h_i}(q^2) = \mathcal{M}^0_{h_i}(q^2) + \mathcal{M}^v_{h_i}(q^2), \tag{7.51}$$

and adding to the squared matrix element the corresponding contribution from real soft photon ($\mathcal{M}^{\rm Br}_{h_i}$) radiation, we find

$$\begin{aligned} |\mathcal{M}_h + \mathcal{M}_H|^2 + |\mathcal{M}^{\rm Br}_h + \mathcal{M}^{\rm Br}_H|^2 = \sum_{h_i = h,H} \left(|\mathcal{M}_{h_i}|^2 + |\mathcal{M}^{\rm Br}_{h_i}|^2\right) \\ + 2{\rm Re}\left[\mathcal{M}_h \mathcal{M}^*_H + \mathcal{M}^{\rm Br}_h \mathcal{M}^{\rm Br*}_H\right]. \end{aligned} \tag{7.52}$$

Because the complete sum in Eq. (7.52) and the individual h- and H-terms are IR-finite, the interference term must be IR-finite by itself. With the proportionality of the bremsstrahlung contribution to the tree level term,

$$\mathcal{M}^{\rm Br}_h(q^2)\mathcal{M}^{\rm Br*}_H(q^2) = \delta_{\rm SB}(q^2)\mathcal{M}^0_h(q^2)\mathcal{M}^{0*}_H(q^2), \tag{7.53}$$

and keeping only the terms of $\mathcal{O}(\alpha)$ relative to the lowest order, the interference term $\mathrm{Int}^{\alpha}(q^2)$ results in

$$\mathrm{Int}^{\alpha}(q^2) = 2{\rm Re}\left[\mathcal{M}_h(q^2)\mathcal{M}^*_H(q^2)\big|_{\alpha} + \mathcal{M}^{Br}_h(q^2)\mathcal{M}^{Br*}_H(q^2)\right] \tag{7.54}$$

$$= 2{\rm Re}\left[\mathcal{M}^v_h(q^2)\mathcal{M}^{0*}_H(q^2) + \mathcal{M}^0_h(q^2)\mathcal{M}^{v*}_H(q^2) + \delta_{\rm SB}(q^2)\mathcal{M}^0_h(q^2)\mathcal{M}^{0*}_H(q^2)\right]. \tag{7.55}$$

As described above, the on-shell evaluation is performed at the individual mass M_{h_i} in all production and tree level matrix elements and the helicity elements, whereas the soft photon factor δ_{SB} and the 1-loop form factors of the decay are evaluated at the same mass $\overline{M}$ in the on-shell interference term $\mathrm{Int}^{\alpha}_{\mathrm{os}}$ of $\mathcal{O}(\alpha)$ relative to the lowest order,

$$\begin{aligned}\mathrm{Int}^{\alpha}_{\mathrm{os}} &= 2\mathrm{Re}\Big[\mathcal{M}^v_h(M_h^2,\overline{M}^2)\mathcal{M}^{0*}_H(M_H^2)+\mathcal{M}^0_h(M_h^2)\mathcal{M}^{v*}_H(M_H^2,\overline{M}^2)\\ &\qquad +\delta_{\mathrm{SB}}(\overline{M}^2)\mathcal{M}^0_h(M_h^2)\mathcal{M}^{0*}_H(M_H^2)\Big] \qquad (7.56)\\ &= 2\mathrm{Re}\Big[\Big\{\Big(\mathcal{P}^v_h(M_h^2)\mathcal{D}^0_h(M_h^2)+\mathcal{P}^0_h(M_h^2)\mathcal{D}^v_h(M_h^2,\overline{M}^2)\Big)\cdot\mathcal{P}^{0*}_H(M_H^2)\mathcal{D}^{0*}_H(M_H^2)\\ &\qquad +\mathcal{P}^0_h(M_h^2)\mathcal{D}^0_h(M_h^2)\cdot\Big(\mathcal{P}^{v*}_H(M_H^2)\mathcal{D}^{0*}_H(M_H^2)+\mathcal{P}^{0*}_H(M_H^2)\mathcal{D}^{v*}_H(M_H^2,\overline{M}^2)\Big)\\ &\qquad +\delta_{\mathrm{SB}}(\overline{M}^2)\,\mathcal{P}^0_h(M_h^2)\mathcal{D}^0_h(M_h^2)\,\mathcal{P}^{0*}_H(M_H^2)\mathcal{D}^{0*}_H(M_H^2)\Big\}\,\Delta_h(q^2)\Delta^*_H(q^2)\Big]\,. \qquad (7.57)\end{aligned}$$

Since the virtual production matrix elements are IR-finite in our example process, we can drop the first term in each of the brackets in the first and second line of Eq. (7.57) for the discussion of IR-singularities, which are contained in $\mathrm{Int}^{\alpha}_{\mathrm{os}}|_{\mathrm{IR}}$,

$$\begin{aligned}\mathrm{Int}^{\alpha}_{\mathrm{os}}|_{\mathrm{IR}} = 2\mathrm{Re}\Bigg[&\mathcal{P}^0_{\mathrm{h}}(\mathrm{M}_{\mathrm{h}}^2)\mathcal{P}^{0*}_{\mathrm{H}}(\mathrm{M}_{\mathrm{H}}^2)\cdot\Delta_{\mathrm{h}}(\mathrm{q}^2)\Delta^*_{\mathrm{H}}(\mathrm{q}^2)\cdot\\ &\Big(\mathcal{D}^v_h(M_h^2,\overline{M}^2)\mathcal{D}^{0*}_H(M_H^2)+\mathcal{D}^0_h(M_h^2)\mathcal{D}^{v*}_H(M_H^2,\overline{M}^2)+\delta_{\mathrm{SB}}(\overline{M}^2)\mathcal{D}^0_h(M_h^2)\mathcal{D}^{0*}_H(M_H^2)\Big)\Bigg].\end{aligned} \qquad (7.58)$$

Moreover, the $M^2_{h_i}$-dependent helicity matrix elements $d_{h_i}(M^2_{h_i})$ from Sect. (9.1.2) can be factored out by $\mathcal{D}_{h_i} = C_{h_i} d_{h_i}$ so that the IR-singularities from $\mathrm{Int}^{\alpha}_{\mathrm{os}}|_{\mathrm{IR}}$ can be further extracted:

$$\begin{aligned}\mathrm{Int}^{\alpha}_{\mathrm{os}}|_{\mathrm{IR}} = 2\mathrm{Re}\,\big[&\mathcal{P}^0_h(M_h^2)\mathcal{P}^{0*}_H(M_H^2)\cdot\Delta_h(q^2)\Delta^*_H(q^2)\cdot d_h(M_h^2)\,d^*_H(M_H^2)\\ &\Big(C^v_h(\overline{M}^2)C^{0*}_H+C^0_hC^{v*}_H(\overline{M}^2)+\delta_{\mathrm{SB}}(\overline{M}^2)C^0_hC^{0*}_H\Big)\Big]\,.\end{aligned} \qquad (7.59)$$

Compared to Eq. (7.55) which can also be factorised into q^2-dependent form factors and helicity matrix elements, the structure of the IR-singularities is the same. In Eq. (7.59), all of those contributions are just evaluated at $\overline{M}^2$ instead of q^2. Hence the cancellation works analogously so that Eq. (7.56) is an IR-finite formulation of the factorised interference term. Because the $\hat{\mathbf{Z}}$-factors can be factored out in the same way for the on-shell approximation as for the full matrix elements, their inclusion preserves the cancellations of IR-divergences.

7.4.1.2. Separate calculation of photon diagrams

As an alternative to the method described above, it is possible to reduce the number of diagrams whose loop integrals need to be evaluated at the common mass $\overline{M}$ instead of their on-shell mass M_i by splitting the 1-loop decay matrix elements into an IR-finite and an IR-divergent part,

$$\mathcal{D}_i^1 = \mathcal{D}_i^{1,\text{no}\gamma} + \mathcal{D}_i^{1,\gamma}. \tag{7.60}$$

Both subgroups of diagrams are rendered UV-finite by the corresponding counterterms. Since the diagrams without any photon are already IR-finite, their loop integrals can safely be calculated on-shell, $\mathcal{D}_i^{1,\text{no}\gamma}(M_{h_i}^2)$. Hence, only the loop-integrals of the photon contribution need to be evaluated at a fixed mass $\overline{M}$, resulting in $\mathcal{D}_i^{1,\gamma}(M_{h_i}^2, \overline{M}^2)$ and $\delta_{\text{SB}}(\overline{M}^2)$.

If the fixed Higgs mass were inserted into both the loop integrals and the helicity matrix elements, the IR-cancellation would work in the same way as for the unfactorised process, just with the special choice of $q^2 = \overline{M}^2$. In our approach, the helicity matrix elements are determined at the specific masses M_{h_i} as it is demonstrated in Eqs. (9.26) and (9.36). Furthermore, those mass values are equal in the matrix elements at lowest and higher orders as loop-corrected masses are used also at the improved Born level. Because the M_{h_i}-dependent helicity matrix elements can be factored out, the IR-singularities cancel in the decay contribution to the interference term of $\mathcal{O}(\alpha)$ relative to the lowest order, with $\mathcal{D}_i^0$ at $M_{h_i}^2$,

$$(\mathcal{D}_h \mathcal{D}_H^*)^\alpha = \mathcal{D}_h^{1,\gamma}(M_h^2, \overline{M}^2)\mathcal{D}_H^{0*} + \mathcal{D}_h^0 \mathcal{D}_H^{1,\gamma*}(M_H^2, \overline{M}^2) + \delta_{\text{SB}}(\overline{M}^2)\mathcal{D}_h^0 \mathcal{D}_H^{0*}. \tag{7.61}$$

On the one hand, this approach requires the separate calculation of purely photonic and non-photonic contributions. On the other hand, it enables the on-shell evaluation of IR-finite integrals and is thus closer to the full result. However, in case of a virtual photino contribution one needs to be careful not to break supersymmetry by treating the photon differently than its superpartner. Thus, the possibility of such a separate treatment of the photon diagrams, whose numerical impact is small in the studied example process, should be considered in view of the investigated model and its particle content.

7.4.2. Interference weight factors at higher order

In the previous section, we derived how to include virtual and real contributions in the product of factorised matrix elements in a UV- and IR-finite way. However, special attention is needed to ensure the correct treatment of the on-shell matrix elements of the interference contribution.

7.4.2.1. Consistent interference weight factors at 1-loop order

We now discuss additional approximations with which the R-factor method introduced in Sect. 7.3.3 can be extended beyond the tree level. We develop a method that facilitates an approximation of the interference term based on higher-order cross sections and decay widths, but only tree level couplings. This technically simpler treatment comes at the price of the further assumption, as in the tree level version of the interference weight factor, that both Higgs masses be equal. Thus, the method presented in this section is an optional, additional approximation with respect to Eq. (7.46).

Under the assumption of equal masses, the product of unsquared matrix elements for the production and decay of h and H can be re-expressed at the tree level in terms of either h or H with the help of Eq. (7.37). Hence, one can choose to keep the 1-loop matrix elements and to replace only the tree level ones so that only lowest-order couplings will be present in the x-factor. We will now apply this prescription to the third term in Eq. (7.46) containing the 1-loop virtual corrections to the interference term Int^v:

$$\begin{aligned}
\mathrm{Int}^v &= 2\mathrm{Re}\left[\left\{\left(\mathcal{P}_h^1\mathcal{D}_h^0+\mathcal{P}_h^0\mathcal{D}_h^1\right)\mathcal{P}_H^{0*}\mathcal{D}_H^{0*}+\mathcal{P}_h^0\mathcal{D}_h^0\left(\mathcal{P}_H^{1*}\mathcal{D}_H^{0*}+\mathcal{P}_H^{0*}\mathcal{D}_H^{1*}\right)\right\}\Delta_h^{\mathrm{BW}}\Delta_H^{\mathrm{BW}*}\right]\\
&\simeq 2\mathrm{Re}\left[\left(\mathcal{P}_h^1\mathcal{D}_h^0+\mathcal{P}_h^0\mathcal{D}_h^1\right)\mathcal{P}_h^{0*}\mathcal{D}_h^{0*}\cdot\frac{C_{P_H}^{0*}}{C_{P_h}^{0*}}\frac{C_{D_H}^{0*}}{C_{D_h}^{0*}}\cdot\Delta_h^{\mathrm{BW}}\Delta_H^{\mathrm{BW}*}\right]\\
&\quad+2\mathrm{Re}\left[\left\{\mathcal{P}_H^0\mathcal{D}_H^0\cdot\frac{C_{P_h}^0}{C_{P_H}^0}\frac{C_{D_h}^0}{Cc_{D_H}^0}\left(\mathcal{P}_H^{1*}\mathcal{D}_H^{0*}+\mathcal{P}_H^{0*}\mathcal{D}_H^{1*}\right)\Delta_h^{\mathrm{BW}}\Delta_H^{\mathrm{BW}*}\right\}^*\right]\\
&= 2\mathrm{Re}\left[\left(\mathcal{P}_h^1\mathcal{P}_h^{0*}|\mathcal{D}_h^0|^2+|\mathcal{P}_h^0|^2\mathcal{D}_h^1\mathcal{D}_h^{0*}\right)x_h^0\cdot\Delta_h^{\mathrm{BW}}\Delta_H^{\mathrm{BW}*}\right]\\
&\quad+2\mathrm{Re}\left[\left(\mathcal{P}_H^1\mathcal{P}_H^{0*}|\mathcal{D}_H^0|^2+|\mathcal{P}_H^0|^2\mathcal{D}_H^1\mathcal{D}_H^{0*}\right)x_H^0\cdot\Delta_H^{\mathrm{BW}}\Delta_h^{\mathrm{BW}*}\right].
\end{aligned}\tag{7.62}$$

Hence we exploited the choice of expressing the product of h- and H-matrix elements either in a weighted sum of both or in terms of one of them. The latter choice, as selected in Eq. (7.62), has the advantage that the matrix elements containing loop contributions of h and only tree level contributions of H are transformed in terms of h and vice versa. Including the flux factor and the phase space integrals as in Eq. (7.35), adding soft bremsstrahlung according to the last line of Eq. (7.46) and keeping in mind that

$$\frac{1}{F}\int d\Phi_P 2\mathrm{Re}\left[\mathcal{P}_i^1\mathcal{P}_i^{0*}\right]=\sigma_{P_i}^1,\qquad \frac{1}{2M_i}\int d\Phi_D\left(2\mathrm{Re}\left[\mathcal{D}_i^1\mathcal{D}_i^{0*}\right]+\delta_{\mathrm{SB}}|\mathcal{D}_i^0|^2\right)=\Gamma_{D_i}^1,\tag{7.63}$$

the expressions from Eq. (7.62) lead to

$$\sigma_{\mathrm{int}}^{1,R}=\frac{\sigma_{P_h}^1\Gamma_{D_h}^0+\sigma_{P_h}^0\Gamma_{D_h}^1}{\Gamma_h^{\mathrm{tot}}}\tilde{R}_h+\frac{\sigma_{P_H}^1\Gamma_{D_H}^0+\sigma_{P_H}^0\Gamma_{D_H}^1}{\Gamma_H^{\mathrm{tot}}}\tilde{R}_H,\tag{7.64}$$

where $\tilde{R}_i$ has been defined in Eq. (7.41).

7.4.2.2. Interference weight factors beyond the 1-loop level

Eq. (7.64) is meant for the consistent comparison with the full result in the strict one-loop expansion. Using the most precise predictions of all components and the unfactorised tree level result leads to the final prediction:

$$\sigma_R^{\mathrm{best}}=\sigma_{\mathrm{full}}^0+\sum_{i=h,H}\left(\sigma_{P_i}^{\mathrm{best}}\mathrm{BR}_i^{\mathrm{best}}-\sigma_{P_i}^0\mathrm{BR}_i^0\right)+\sigma_R^{\mathrm{int1}}+\sigma_R^{\mathrm{int+}},\tag{7.65}$$

$$\sigma_R^{\mathrm{int1}}=\left(\sigma_{P_h}^1\mathrm{BR}_h^0+\sigma_{P_h}^0\mathrm{BR}_h^1\right)\tilde{R}_h+\left(\sigma_{P_H}^1\mathrm{BR}_H^0+\sigma_{P_H}^0\mathrm{BR}_H^1\right)\tilde{R}_H,\tag{7.66}$$

$$\sigma_R^{\mathrm{int+}}=\frac{1}{2}\sigma_{P_h}^1\left(\mathrm{BR}_h^1\tilde{R}_h+\mathrm{BR}_H^1\tilde{R}_{hH}\right)+\frac{1}{2}\sigma_{P_H}^1\left(\mathrm{BR}_H^1\tilde{R}_H+\mathrm{BR}_h^1\tilde{R}_{Hh}\right),\tag{7.67}$$

where σ_R^{int1} denotes the contribution to the interference term for which the product of production cross sections and partial decay widths is restricted to the 1-loop level, but the branching ratios are at all levels normalised to the 2-loop total width from `FeynHiggs` [67, 146, 149, 150]. In addition, $\sigma_R^{\text{int+}}$ contains terms beyond the 1-loop level. In Eq. (7.67), we introduced the generalised interference weight factors $\tilde{R}_{ij}$,

$$\tilde{R}_{ij} = 2M_j\Gamma_j \text{Re}\left\{x_{ij}I\right\}, \tag{7.68}$$

involving the scaling factors x_{ij},

$$x_{ij} = \frac{C_{P_h}C^*_{P_H}C_{D_h}C^*_{D_H}}{|C_{P_i}|^2|C_{D_j}|^2}, \tag{7.69}$$

to account for the product of 1-loop production and decay matrix elements in Eq. (7.49). For the most precise prediction, the 1-loop branching ratios in Eqs. (7.66, 7.67) can additionally be replaced by $\text{BR}_i^{\text{best}} - \text{BR}_i^0$ which is beyond the $\mathcal{M}$-method in Eq. (7.49). As in Eq. (7.50) for the $\mathcal{M}$-method, the products of tree level production cross section and branching ratios have to be subtracted because their contribution is already accounted for by σ^0_{full}. The most precise branching ratios can be obtained from `FeynHiggs` [67, 146, 149, 150] including full 1-loop and leading 2-loop corrections.

Chapter 8.

Neutralino 3-body decay with interfering Higgs bosons

Within the MSSM, we study a simple example process which features for certain parameter choices a sizeable interference term between the contributions of two neutral Higgs bosons. In this and the next chapter, we restrict the discussion to the MSSM with real parameters so that only the $\mathcal{CP}$-even Higgs bosons can mix and interfere among each other. Afterwards, $\mathcal{CP}$-violating mixing and interference will be the topic of Chap. 10.

8.1. Full example process $\tilde{\chi}_4^0 \to \tilde{\chi}_1^0 \tau^+\tau^-$ via h, H at leading order

In the following, we will consider Higgs production from the decay of the heaviest neutralino and its subsequent decay into a pair of τ-leptons, $\tilde{\chi}_4^0 \to \tilde{\chi}_1^0 \tau^+\tau^-$ via the exchange of the Higgs bosons h and H, see Fig. 8.1. The focus of the chosen example process lies on providing a test case for the method rather than on the phenomenology of the process itself. For a comparison with the gNWA in Chap. 9, we have chosen a process which can be calculated also at the 1-loop level without the on-shell approximation. Furthermore, it is a useful example process because of its simple kinematics, where the full process is a 3-body decay, which can be decomposed into two simple 2-body decays, see Fig. 9.1.

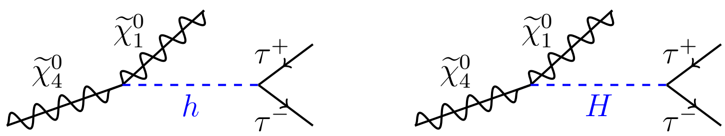

Figure 8.1.: $\tilde{\chi}_4^0 \to \tilde{\chi}_1^0\tau^+\tau^-$ with h or H as intermediate particle in the two interfering diagrams. The decay process is treated as a 3-body decay here and will be decomposed into two 2-body decays in Chap. 9.

Moreover, the intermediate particles are scalars. Thus, for this process the treatment of interference effects can be trivially disentangled from any spin correlations between production and decay. Due to the neutralinos in the initial state and in the first decay step, soft bremsstrahlung only appears in the final state, and there is no photon exchange between the initial and final state. Restricting this test case to the MSSM with real parameters, only the two $\mathcal{CP}$-even states h, H mix due to $\mathcal{CP}$-conservation, instead of the 3×3 mixing of h, H, A in the complex case. We neglect non-resonant diagrams from sleptons, which is a good approximation for the case of heavy sleptons. Slepton contributions to neutralino 3-body decays have been analysed in Ref. [107]. As a first step, we also neglect the exchange of an intermediate pseudoscalar A, Goldstone boson G and Z-boson for the purpose of a pure comparison of the factorised and the full Higgs contribution. For the most accurate prediction within the gNWA, which will be discussed in Sect. 9.4.3, we will add the tree-level A, G- and Z-exchange, but they do not interfere with h and H in the $\mathcal{CP}$-conserving case of real parameters.

The decay width will be calculated using `FeynArts-3.7` [114–118], `FormCalc-7.4` [94, 119–122] and `LoopTools-2.8` [94, 219], both as a 3-body decay with the full matrix element and in the narrow-width approximation as a combination of two 2-body decays - with and without the interference term. Precise quantities of the Higgs sector such as masses, widths and $\hat{\mathbf{Z}}$-factors are obtained from `FeynHiggs-2.9.3`. In this and the following section, the gNWA will be applied at the tree level. The application at the loop level has been introduced conceptually in Sect. 8.2 and will be presented numerically in Sect. 9.4.

8.1.1. 3-body decays: leading order matrix element

In order to compare the gNWA to the unfactorised LO result, we calculate the amplitude $\mathcal{M}^2_{h_k}$ of the 3-body decay via $h_k = h, H$. From the matrix element of the form

$$\mathcal{M}_{h_k} = iC_{h_k\tilde{\chi}^0_i\tilde{\chi}^0_j} C_{h_k\tau\tau} \bar{u}(p_4, s_4) v(p_3, s_3) \frac{1}{q^2 - M^2_{h_k} + iM_{h_k}\Gamma_{h_k}} \bar{u}(p_2, s_2) u(p_1, s_1) \tag{8.1}$$

we obtain the spin-averaged, squared amplitude consisting of the separate h, H contributions and the interference contribution,

$$\begin{aligned}\overline{|\mathcal{M}|^2} = 8(p_1 \cdot p_2 + m_{\tilde{\chi}^0_1} m_{\tilde{\chi}^0_4})(p_3 \cdot p_4 - m^2_\tau) \Bigg(&\frac{|C_{h\tilde{\chi}^0_1\tilde{\chi}^0_4}|^2 |C_{h\tau\tau}|^2}{(q^2 - m^2_h)^2 + m^2_h \Gamma^2_h} + \frac{|C_{H\tilde{\chi}^0_1\tilde{\chi}^0_4}|^2 |C_{H\tau\tau}|^2}{(q^2 - m^2_H)^2 + m^2_H \Gamma^2_H} \\ &+ 2\mathrm{Re}\left[C_{h\tilde{\chi}^0_1\tilde{\chi}^0_4} C^*_{H\tilde{\chi}^0_1\tilde{\chi}^0_4} C_{h\tau\tau} C^*_{H\tau\tau} \cdot \Delta^{\mathrm{BW}}_h(q^2) \Delta^{*\mathrm{BW}}_H(q^2) \right] \Bigg),\end{aligned} \tag{8.2}$$

where the momenta and masses are labelled as $p_1 \to p_2, p_3, p_4$ with $m_1 \equiv m_{\tilde{\chi}^0_4}, m_2 \equiv m_{\tilde{\chi}^0_1}, m_3 = m_4 \equiv m_\tau$. In order to calculate the decay width in one of the Gottfried-Jackson frames [186], the products of momenta are rewritten in terms of two combined invariant masses, here e.g. m_{23}, m_{24}:

$$\begin{aligned} p_1 \cdot p_2 &= \frac{1}{2}(m^2_{23} + m^2_{24}) - m^2_\tau, \qquad p_3 \cdot p_4 = \frac{1}{2}\left(m^2_1 + m^2_2 - m^2_{23} - m^2_{24}\right), \\ q^2 &= (p_1 - p_2)^2 = m^2_1 + m^2_2 - m^2_{23} - m^2_{24}. \end{aligned} \tag{8.3}$$

This yields the partial decay width for the 3-body decay [23],

$$\Gamma = \frac{1}{(2\pi)^3} \frac{1}{32 m_{\tilde{\chi}_4^0}^3} \int |\mathcal{M}|^2 dm_{23}^2 dm_{24}^2, \tag{8.4}$$

which we will use for a comparison with the gNWA.

8.2. Full 3-body decay at the one-loop level

The numerical validation of the gNWA at the next-to-leading order requires the calculation of the example process $\tilde{\chi}_4^0 \to \tilde{\chi}_1^0 \tau^+ \tau^-$ with intermediate h and H as the full 3-body decay including virtual and real corrections.

8.2.1. Treatment of the Higgs propagators

In principle, we could employ the full mixing Higgs propagators including the momentum dependent self-energies to describe the Higgs exchange in our example process. However, the purpose of this unfactorised calculation is – in addition to the phenomenological one-loop analysis of this 3-body decay – the consistent comparison with the gNWA at NLO where the Higgs bosons appear as external particles. Accordingly, in the NWA, the Higgs states are normalised by $\hat{\mathbf{Z}}$-factors. Thus it is desirable to treat the Higgs bosons in the 3-body decay in the same way in order to disentangle the uncertainty introduced by the factorisation from the expansion of the full mixing propagators around the complex poles. As we showed process independently in Chapter 6, the sum of Breit-Wigner propagators combined with $\hat{\mathbf{Z}}$-factors provides indeed a good approximation of the full mixing propagators. Therefore we apply the Breit-Wigner propagators parametrised by the loop corrected masses and total widths in the 3-body decay. Even though we use Eq. (6.16) instead of the fully momentum dependent propagators Δ_{ij}, we refer to the calculation of the 3-body decay as the "full" result as opposed to the factorised one. In addition, in the three-body decay at one-loop order, the Higgs propagator with momentum-dependent self-energies would only occur at the strict one-loop level, while the $\hat{\mathbf{Z}}$-factors incorporate important higher-order contributions. The $\hat{\mathbf{Z}}$-factors are already used for the improved Born level. The Breit-Wigner approach has the further advantage that it allows us to implement the total Higgs widths as sums of the partial decay width at the highest avaible order from `FeynHiggs`, both in the Breit-Wigner propagators of the unfactorised process and in the branching ratio of the decay.

Technical realisation In conclusion, the use of $\hat{\mathbf{Z}}$-factors on the internal Higgs lines (but outside loops[1]) is consistent and physically meaningful. However, applying $\hat{\mathbf{Z}}$-factors for Higgs boson propagators appearing inside loops would destroy the cancellation of

[1] In the terminology of `FeynArts` [114–118], a propagator can have three possible attributes: "External" refers to an external line, "Internal" denotes an internal propagator which is not part of any loop, and "Loop" is inside a loop [220]. (Furthermore, an external propagator can be incoming, outgoing or undirected, but we do not need this distinction in our discussion.)

UV-divergences between loop diagrams and counterterms needed for the renormalisation. In order to avoid this trouble and to allow at the same time for $\hat{\mathbf{Z}}$-factors in lowest-order Higgs boson propagators, we modified the `Hmix.mod` model file from `FeynArts` [114–118]. In the distributed add-on model file, the two new scalar classes S[0] and S[10] replace the interaction eigenstates h=S[1], H=S[2], A=S[3]. The couplings C of S[0] and S[10] are constructed as a linear combination of the couplings of S[1], S[2] and S[3] to any other particles X [123, 160]:

$$C_{S[0,\{a\}]X} = \sum_{i=1}^{3} \mathbf{U}_{ai} C_{S[i]X}, \tag{8.5}$$

$$C_{S[10,\{a\}]X} = \sum_{i=1}^{3} \hat{\mathbf{Z}}_{ai} C_{S[i]X}. \tag{8.6}$$

Thereby, inserting S[0] corresponds to using effective couplings, see Sect. 5.6. The original `Hmix.mod` model file allows the scalar S[0] with $\mathbf{U}$ on all kinds of propagators whereas the use of S[10] is restricted to external lines so that in this implementation, $\hat{\mathbf{Z}}$-factors are only applied to Higgs bosons in the initial or final state. However, as we derived in Eqs. (6.16) and (6.21), $\hat{\mathbf{Z}}$-factors encode the mixing properties of the full Higgs propagators close to the complex poles and achieve in combination with the Breit-Wigner propagators a good approximation of the full mixing. Fig. 6.9 highlights the importance of including relevant imaginary parts, which are disregarded by the $\mathbf{U}$-matrix. As a consequence, on internal lines (outside loops) the scalars S[10] containing $\hat{\mathbf{Z}}$-factors should be preferred over S[0] comprising $\mathbf{U}$-factors. Hence, we redefined the insertion of a neutral Higgs boson in the following way:

- Inside loops, only the lowest order Higgs states h, H, A are inserted with their tree level masses and unmixed couplings[2].
- On internal lines ("intermediate", out of loops) and on external lines, the mixed states $h_a = S[10, \{a\}]$, with $a = 1, 2, 3$, are inserted.

This method results in Eq. (5.72) for external Higgs bosons and in Eq. (6.22), as intended. We also apply scalars S[10] with $\hat{\mathbf{Z}}$-factors at the lowest order so that "tree" level always means the improved Born level in our calculations.

8.2.2. Contributing diagrams

In addition to the Born level diagrams depicted in Fig. 9.1, we now need to compute the vertex, self-energy, box and real corrections to our example process in the unfactorised version. Ref. [107] provides a 1-loop calculation of the decay of the next-to-lightest neutralino $\tilde{\chi}_2^0$ into $\tilde{\chi}_1^0$ and a pair of leptons, thus a similar process, but with a dominant contribution from an on-shell slepton, while the Higgs propagators are treated as non-

[2] Technically, we achieved this by allowing S[0] in loops with the class description `Mass[Loop]`$\to$ `MHiggstree` and setting $\mathbf{U} = \mathbb{1}$. This procedure is possible because we do not use $\mathbf{U}$ anywhere else in the calculation. Otherwise we could have defined a new class of scalars in the add-on modelfile or modified the use of the original scalars S[1|2|3].

resonant. In the following, we focus on the diagrams contributing to resonant intermediate Higgs bosons, as well as box-diagrams with and without Higgs bosons. The 1-loop integrals are computed with `LoopTools` [94, 219].

8.2.2.1. Virtual corrections at the neutralino-Higgs vertex

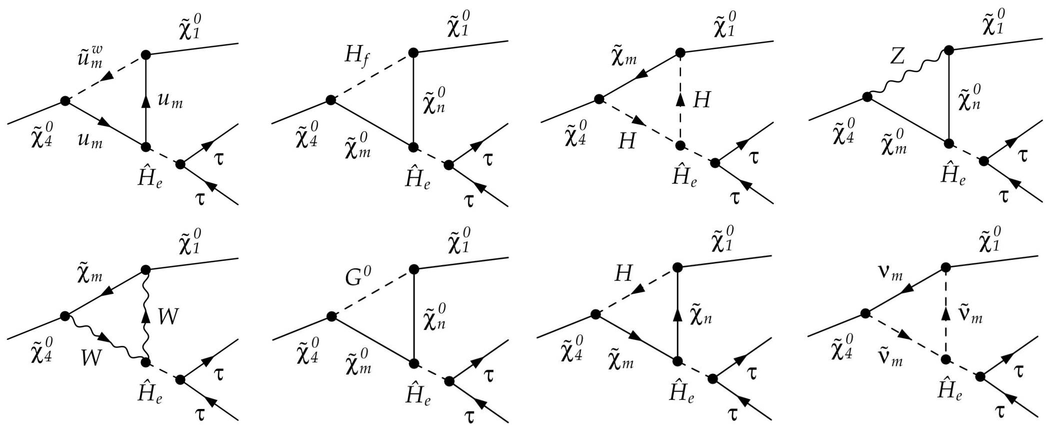

Figure 8.2.: Example triangle diagrams of the 3-body decay $\tilde{\chi}_4^0 \to \tilde{\chi}_1^0 \tau^+\tau^-$ with 1-loop corrections at the $\tilde{\chi}_4^0\tilde{\chi}_1^0\hat{H}_e$-vertex, where $\hat{H}_e$ denotes a Higgs boson mixed by $\hat{\mathbf{Z}}$-factors, H_f an internal Higgs boson (see text) and $H \equiv H^\pm$. u and $\tilde{u}$ represent the up-type (s)quarks, $\tilde{\chi}^0$ are the neutralinos and $\tilde{\chi}$ the charginos.

Virtual SM and MSSM particles contribute to the correction of the $\tilde{\chi}_i^0\tilde{\chi}_j^0 h_k$-vertex. A selection of diagrams is displayed in Fig. 8.2. We treat here the intermediate Higgs bosons $\hat{H}_e$ appearing outside of the vertex loop contribution with $\hat{\mathbf{Z}}$-factors at the connecting vertices, while H_f denotes an internal Higgs boson within the loop without any $\hat{\mathbf{Z}}$- or $\mathbf{U}$-factors ($e, f = 1, 2, 3$), as discussed above. Furthermore, $H \equiv H^\pm$ denotes the charged Higgs bosons. The neutralinos are labelled by $\tilde{\chi}_n^0$, $n = 1, 2, 3, 4$ and the charginos by $\tilde{\chi}_m$, $m = 1, 2$. The first example diagram contains up-type quarks u_m and a squark $\tilde{u}_m^w$ of generation $m = 1, 2, 3$ and type $w = 1, 2$.

The triangle corrections appearing at the $\tilde{\chi}_i^0\tilde{\chi}_j^0 h_k$-vertex are renormalised by the counterterm

$$
\begin{aligned}
\delta C_{ijk}^{R/L} &= \frac{e}{2c_W s_W}\delta c_{ijk}^{(*)} + \left(\delta Z_e - \frac{\delta s_W}{s_W} - \frac{\delta c_W}{c_W}\right) C_{ijk}^{R/L} \\
&\quad + \frac{1}{2}\sum_{l=1}^{4}(\delta Z_{li}^{R/L}\, C_{ljk}^{R/L} + \delta \bar{Z}_{jl}^{L/R}\, C_{ilk}^{R/L} + \delta Z_{h_k h_l} C_{ijk}^{R/L})
\end{aligned}
\tag{8.7}
$$

in the on-shell scheme, see Ref. [109] and references therein. In Eq. (8.7), $h_l = \{h, H, A, G\}$ for $l = 1, 2, 3, 4$, denote the neutral Higgs and Goldstone bosons. The parameters M_1, M_2, μ are related to the choice of the three electroweakinos which are renormalised on-shell and thus define the choice for the on-shell renormalisation scheme for the neutralino-chargino sector, as explained in Sect. 3.3.3. In our scenario used for the numerical analysis, we identify $\widetilde{\chi}_1^0$ as the most bino-like, $\widetilde{\chi}_3^0$ as the most higgsino-like and $\widetilde{\chi}_4^0$ as the most wino-like state and hence renormalise these three neutralinos on-shell. By this choice of an NNN scheme, we avoid large mass corrections to the remaining neutralino and the charginos. Alternatively, $\widetilde{\chi}_2^0$ instead of $\widetilde{\chi}_4^0$ could be identified as the most wino-like state because the two corresponding elements in the matrix N, which diagonalises the neutralino mass matrix (see Sect. 3.3.3), have nearly the same magnitude. Thus, this alternative choice would lead to a comparable sensitivity to the three parameters of this sector and thereby also to a stable renormalisation scheme. But since $\widetilde{\chi}_4^0$ is involved in our process as an external particle, we prefer to set it on-shell. The 1-loop effect on the 2-body decay widths $\Gamma(\widetilde{\chi}_4^0 \to \widetilde{\chi}_1^0 h/H)$ is shown in Fig. 9.6.

8.2.2.2. Virtual corrections at the Higgs- $\tau^+\tau^-$ vertex and real photon emission

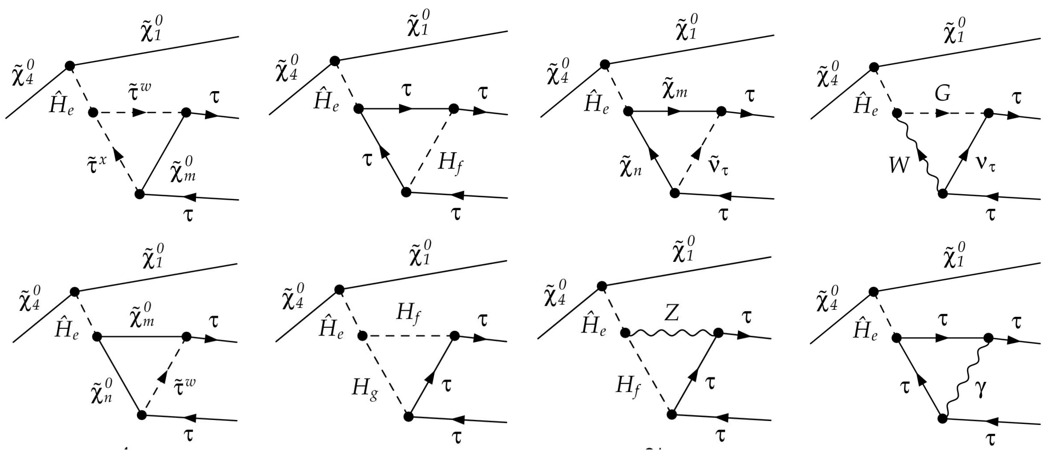

Figure 8.3.: Example triangle diagrams of the 3-body decay $\widetilde{\chi}_4^0 \to \widetilde{\chi}_1^0\tau^+\tau^-$ with 1-loop corrections at the $\hat{H}_e\tau^+\tau^-$-vertex, where the particles are labelled as is Fig. 8.2.

Furthermore, the $h_k\tau^+\tau^-$-vertex diagrams shown in Fig. 8.3 are UV-divergent, and the last diagram is also IR-divergent due to the virtual photon. The UV-divergences are cancelled by the counterterm, analogous to the SM, $\delta C_{h_k\tau^+\tau^-} = \delta C^L_{h_k\tau\tau}\omega_L + \delta C^R_{h_k\tau\tau}\omega_R$, with [21, 98]

$$\delta C^{L/R}_{h_k\tau^+\tau^-} = C^{\text{tree}}_{h_k\tau^+\tau^-} \cdot \Bigg(\delta Z_e + \frac{1}{2}\delta Z_{h_k h_k} + \frac{1}{2}\delta Z_{hH}\frac{C^{\text{tree}}_{h_l\tau\tau}}{C^{\text{tree}}_{h_k\tau\tau}} - \frac{\delta M_W^2}{2M_W^2} - \frac{\delta s_W}{s_W} + s_\beta^2\delta t_\beta$$
$$+\frac{\delta m_\tau}{m_\tau} + \frac{1}{2}\left\{\delta Z_\tau^{L/R} + \delta Z_\tau^{R/L\dagger}\right\}\Bigg), \tag{8.8}$$

where $k, l = h, H$ and $\delta Z_\tau^{L/R}$ are the left-/right-handed field renormalisation constants of the τ-lepton. The tree-level couplings $C^{\text{tree}}_{h_k\tau^+\tau^-}$ are given in Eq. (3.49). The IR-divergent terms vanish for squared matrix elements in the combination of virtual corrections containing a photon in the loop with real photons emitted as soft bremsstrahlung (SB) off one of the τ-leptons. Soft photons are defined by the energy cut-off $E_{\text{soft}}^{\text{max}}$. As a prescription for the energy cut-off we use here a fraction of the mass of the decaying particle, namely $E_\gamma \leq E_{\text{soft}}^{\text{max}} = 0.1 m_{\tilde{\chi}_4^0}$. All photons below this energy are considered as soft so that they are described by the soft photon factor δ_{SB} multiplying the tree level result,

$$\Gamma_{\text{SB}} = \delta_{\text{SB}}\, \Gamma^{\text{tree}}. \tag{8.9}$$

We use the result for δ_{SB} of Ref. [21] implemented in `FormCalc` [94, 119–122]. More details on the separation of soft and hard, collinear and non-collinear QED corrections for this process can be found in Ref. [107].

8.2.2.3. Self-energies involving mixing of neutral bosons

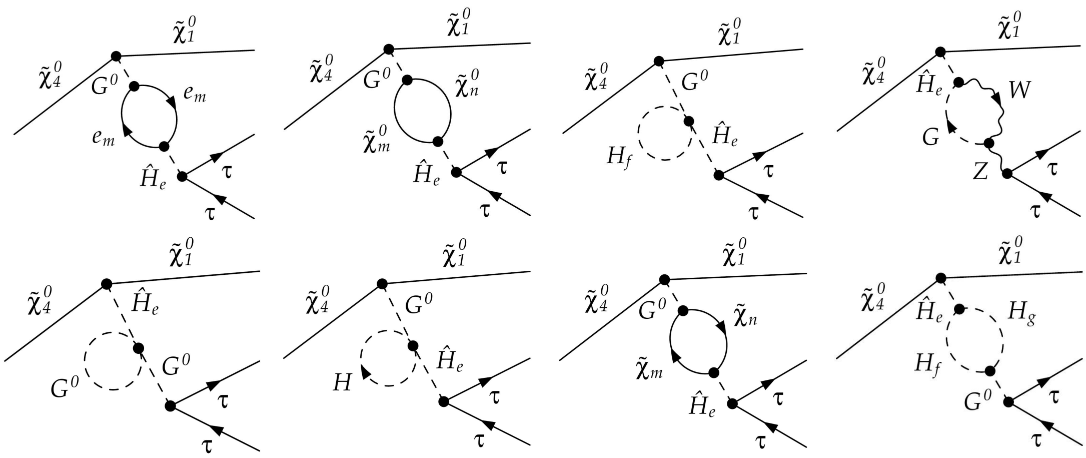

Figure 8.4.: Example self-energy diagrams contributing to the 3-body decay $\tilde{\chi}_4^0 \to \tilde{\chi}_1^0 \tau^+ \tau^-$ with 1-loop corrections to the Higgs propagator which mixes with the neutral Goldstone boson G^0 and the Z-boson. As in Fig. 8.2, $\hat{H}_e$ denotes a $\hat{\mathbf{Z}}$-mixed neutral Higgs boson and H_f an internal Higgs boson (see text).

The diagrams with self-energy corrections of the intermediate Higgs boson $\hat{H}_e$ are classified in two categories. On the one hand, there are the mixing contributions between the three neutral Higgs bosons (reduced to 2×2 mixing in case of real MSSM parameters). They are approximated by the $\hat{\mathbf{Z}}$-factors, which were checked to accurately reproduce the full Higgs propagator mixing close to the complex pole (see Chap. 6 and Refs. [3, 45]). Consequently, no explicit propagator corrections with Higgs self-energies are included. With the $\hat{\mathbf{Z}}$-factors, the strict one-loop order is extended to take more precise mixing effects in the Higgs sector into account. On the other hand, the $\hat{\mathbf{Z}}$-factors do not contain mixing with other neutral particles. Hence, the propagator corrections of a Higgs with the neutral Goldstone boson G and the Z-boson are calculated explicitly. Some example diagrams are shown in Fig. 8.4. However, in case of $\mathcal{CP}$-conservation, the mixing between h/H and G/Z vanishes.

8.2.2.4. Box diagrams

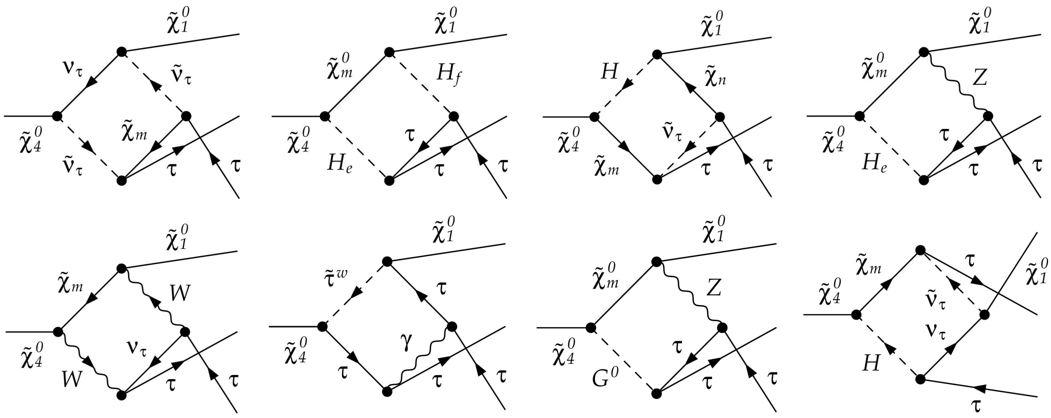

Figure 8.5.: Example box diagrams of the 3-body decay $\tilde{\chi}_4^0 \to \tilde{\chi}_1^0 \tau^+\tau^-$ (with and without Higgs bosons), where the particles are labelled as is Fig. 8.2. Only internal Higgs bosons H_f appear in the loop.

Finally, the $\tilde{\chi}_4^0$ cannot only decay into $\tilde{\chi}_1^0\tau^+\tau^-$ via a resonant Higgs boson[3], but also through box diagrams. Fig. 8.5 depicts some example diagrams with and without Higgs bosons. No counterterms are necessary because the boxes are UV-finite by themselves. The box diagrams are explicitly calculated including the full MSSM spectrum in the loops, but, as expected, those non-resonant contributions are found to be numerically suppressed. This is important for the comparison with the gNWA at the 1-loop level in Sect. 9.4.1 since the boxes cannot be factorised.

8.2.3. Modified $M_h^{\max}$ scenario

In order to evaluate the full process numerically, we specify a scenario. In this study, we restrict the MSSM parameters to be real so that there is no new source of $\mathcal{CP}$-violation compared to the SM and only the two $\mathcal{CP}$-even neutral Higgs bosons, h and H, mix and interfere with each other. The aim here is not to determine the parameters which are currently preferred by recent limits from experiments, but to provide a setting in which interference effects between h and H become large in order to investigate the performance of the generalised narrow-width approximation for this simple example process.

The $M_h^{\max}$ scenario [168, 169] is defined such that the loop corrections to the mass M_h reach their maximum for fixed $\tan\beta$, M_A and M_{SUSY}. This requires a large stop mixing, i.e. a large off-diagonal element X_t of the stop mixing matrix in Eq. (3.14). A small mass difference $\Delta M \equiv M_H - M_h$ requires a rather low value of M_A, or equivalently $M_{H^\pm}$, and a high value of $\tan\beta$. On the other hand, $\tan\beta$ must not be chosen too large because otherwise the bottom Yukawa coupling would be enhanced to a non-perturbative

[3]or a resonant slepton, but we focus on resonant Higgs bosons - for the inclusion of all particles see Sect. 9.4.3.

value. We modify[4] the $M_h^{\max}$ scenario such that M_h is not maximised, but the mass difference ΔM is reduced by raising X_t. As one of the Higgs sector input parameters, we choose $M_H^{\pm}$ for a later extension to $\mathcal{CP}$-violating mixings instead of M_A, which is more commonly used in the MSSM with real parameters. The charged Higgs mass is scanned over the range $M_{H^\pm} \in$[151 GeV, 155 GeV]. The other parameters are defined in Tab. 8.1, and we assume universal trilinear couplings $A_f = A_t$.

M_1	M_2	M_3	M_{SUSY}	X_t	μ	t_β	$M_{H^\pm}$
100 GeV	200 GeV	800 GeV	1 TeV	2.5 TeV	200 GeV	50	(153 GeV)

Table 8.1.: Parameter settings of the modified $M_h^{\max}$ scenario in our numerical analysis. A value in brackets indicates that the parameter is varied around this central value.

8.2.4. Comparison of the tree level and 1-loop result

Fig. 8.6 shows the resulting decay width of $\tilde{\chi}_4^0$ into $\tilde{\chi}_1^0$ and a $\tau^+\tau^-$-pair as the full 3-body decay. As mentioned above, the Z-, A-, G- and slepton-exchange is not included in this section, but the interference between the contributions of h and H to the 3-body decay is taken into account. The tree-level and 1-loop results are based on the product of $\hat{\mathbf{Z}}$-factors and Breit-Wigner propagators with higher-order Higgs masses and total widths. As discussed above, this is referred to as the full result that will consistently serve as a reference for the validation of the gNWA at the 1-loop level.

The full 1-loop decay width includes the vertex corrections at the production and the decay vertex and box contributions as well as self-energy corrections to the propagator and bremsstrahlung off the τ-leptons in the final state. The NLO decay width (solid) is enhanced relative to the LO result (dashed) in most of the analysed parameter interval, up to 11%, as the plot of the ratio $r = (\Gamma^{\mathrm{loop}} - \Gamma^{\mathrm{tree}})/\Gamma^{\mathrm{tree}}$ shows. However, around $M_{H^\pm} \simeq 152\,\mathrm{GeV}$, the 1-loop corrections vanish.

In the next chapter, we will calculate the same process using the NWA at lowest and next-to-leading order.

[4]Our modification of the $M_h^{\max}$ should not be confused with the “updated” $M_h^{\max}$ scenario defined in Ref. [167].

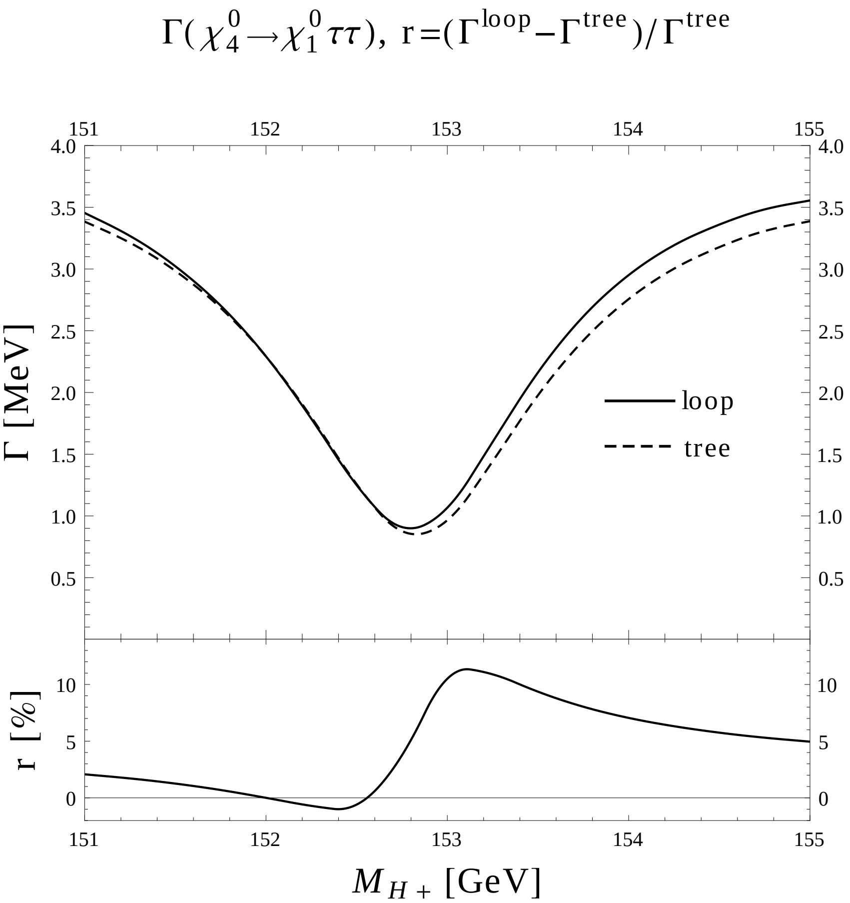

Figure 8.6.: The 1→3 decay width $\Gamma(\tilde{\chi}^0_4 \to \tilde{\chi}^0_1 \tau^+\tau^-)$. **Upper panel:** Tree-level mediated by resonant h, H including their interference (dashed) and full 1-loop result with vertex, soft photon and propagator corrections to the resonant h, H-exchange and, in addition, non-resonant box contributions (solid), both supplemented by higher-order Higgs masses, total widths and $\hat{\mathbf{Z}}$-factors. **Lower panel:** Relative loop contribution $r = (\Gamma^{\text{loop}} - \Gamma^{\text{tree}})/\Gamma^{\text{tree}}$ in percent.

Chapter 9.

Application of the generalised NWA

We validate the method for the example process from Chap. 8 by confronting the one-loop result within the gNWA with the result of the full process at the tree and the one-loop level. In the considered example process we study interference effects between the two neutral $\mathcal{CP}$-even MSSM Higgs bosons h and H and how they can be approximated by the gNWA introduced in Chap. 7. Besides the validation against the full NLO result for this process, we also incorporate contributions beyond the one-loop level into the gNWA. The discussed cases are meant to illustrate that the proposed method is applicable to a wide range of possible processes in different models.

9.1. Example process at lowest order in the gNWA

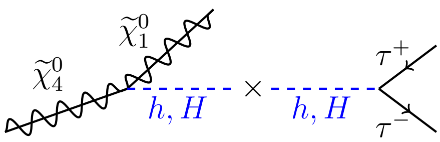

Figure 9.1.: The 3-body decay $\tilde{\chi}_4^0 \to \tilde{\chi}_1^0 \tau^+\tau^-$ with h or H as intermediate particle in the two interfering diagrams from Fig. 8.1 is decomposed into two 2-body decays $\tilde{\chi}_4^0 \to \tilde{\chi}_1^0 h/H$ and $h/H \to \tau^+\tau^-$.

The example process of the 3-body decay $\tilde{\chi}_4^0 \to \tilde{\chi}_1^0 \tau^+\tau^-$ with the intermediate, resonant Higgs bosons h and H is now decomposed by means of the NWA into two subsequent 2-body decays for the production ($\tilde{\chi}_4^0 \to \tilde{\chi}_1^0 h/H$) and the decay ($h/H \to \tau^+\tau^-$) of either of the two Higgs bosons, see Fig. 9.1 in comparison to Fig. 8.1. Both subprocesses and the interference term will first be computed at the tree level. In Sects. 8.2 and 9.4, the application of the gNWA at the loop level will follow.

9.1.1. Decomposition of the full process into 2-body decays

In this section, we calculate the 2-body decay widths of the subprocesses needed in the NWA. The matrix element for the production of $h_k = h, H$ is

$$\mathcal{M}_{\tilde{\chi}_4^0\tilde{\chi}_1^0 h_k} = i\bar{u}_2 C_{h_k\tilde{\chi}_4^0\tilde{\chi}_1^0} u_1, \tag{9.1}$$

$$|\mathcal{M}_{\tilde{\chi}_4^0\tilde{\chi}_1^0 h_k}|^2 = |C_{h_k\tilde{\chi}_4^0\tilde{\chi}_1^0}|^2 2(p_1 p_2 + m_{\tilde{\chi}_4^0} m_{\tilde{\chi}_1^0})\,. \tag{9.2}$$

In the rest frame of $\widetilde{\chi}_4^0$ we have $p_1 p_2 = m_1 E_2$ with

$$E_2 = \frac{m_1^2 + m_2^2 - M_{h_k}^2}{2m_1}\,. \tag{9.3}$$

Then the decay width of $\widetilde{\chi}_4^0 \to \widetilde{\chi}_1^0 h_k$ for the production of $h_k = \{h, H\}$ equals

$$\Gamma(\widetilde{\chi}_4^0 \to \widetilde{\chi}_1^0 h_k) = \frac{|C_{h_k \widetilde{\chi}_4^0 \widetilde{\chi}_1^0}|^2}{16\pi m_{\widetilde{\chi}_4^0}^3} \left((m_{\widetilde{\chi}_4^0} + m_{\widetilde{\chi}_1^0})^2 - M_{h_k}^2\right) \sqrt{(m_{\widetilde{\chi}_4^0}^2 - m_{\widetilde{\chi}_1^0}^2 - M_{h_k}^2)^2 - 4 m_{\widetilde{\chi}_1^0}^2 M_{h_k}^2}\,. \tag{9.4}$$

Summing over spins in the final states, the partial decay widths of h and H into a pair of τ-leptons and the branching ratios read at tree level, improved by 2-loop Higgs masses and total widths from `FeynHiggs` [67, 146, 149, 150],

$$\Gamma(h_k \to \tau\tau) = \frac{1}{\pi} |C_{h_k \tau\tau}|^2 \frac{\left[\frac{M_{h_k}^2}{4} - m_\tau^2\right]^{3/2}}{M_{h_k}^2}, \qquad \mathrm{BR}_k = \frac{\Gamma(h_k \to \tau^+\tau^-)}{\Gamma_{h_k}^{\mathrm{tot}}}, \tag{9.5}$$

where $\Gamma_{h_k}^{\mathrm{tot}}$ is the total width. Loop-corrections to the partial decay widths of these subprocesses are calculated with `FormCalc` [94, 119–122] in Sect. 9.3.1.

9.1.2. Formalism of unsquared matrix elements in all helicity configurations

For the calculation of the interference term according to Eq. (7.24), we need the on-shell matrix elements of the production and decay part. Instead of evaluating absolute values of squared, spin-averaged matrix elements by applying spinor traces, we now aim at expressing the unsquared matrix elements explicitly in order to evaluate them on the appropriate mass shell. Therefore, we need to represent spin wave functions in terms of energy and mass. Following Ref. [221], a Dirac spinor with an arbitrary helicity can be written as

$$u(p) = \begin{pmatrix} \sqrt{E+m}\;\chi \\ \sqrt{E-m}\;\vec{\sigma}\cdot\hat{p}\;\chi \end{pmatrix}, \tag{9.6}$$

where χ is a two-component spinor. The eigenstates χ of the helicity operator $\vec{\sigma}\cdot\hat{p}$ with eigenvalues $\lambda = \pm\frac{1}{2}$ satisfy

$$\left[\frac{1}{2}\vec{\sigma}\cdot\hat{p}\right]\chi_\lambda = \lambda\chi_\lambda. \tag{9.7}$$

For the unit vector $\hat{p}$ in the direction parametrised by the polar angle θ and azimuthal angle ϕ relative to the z-axis, the two-component spinors are expressed as

$$\chi_{+1/2}(\hat{p}) = \begin{pmatrix} \cos\frac{\theta}{2} \\ e^{i\phi}\sin\frac{\theta}{2} \end{pmatrix}, \qquad \chi_{-1/2}(\hat{p}) = \begin{pmatrix} -e^{-i\phi}\sin\frac{\theta}{2} \\ \cos\frac{\theta}{2} \end{pmatrix}. \tag{9.8}$$

For the specific choice of $\vec{p} \propto e_z$ we have $\theta = 0$ and ϕ is arbitrary so that it can be set to 0. Thus, the 2-spinors take the simpler form

$$\chi_{1/2}(\hat{p} = e_z) = e_1 \equiv \begin{pmatrix} 1 \\ 0 \end{pmatrix}, \qquad \chi_{-1/2}(\hat{p} = e_z) = e_2 \equiv \begin{pmatrix} 0 \\ 1 \end{pmatrix}. \tag{9.9}$$

We label the unit vectors in space as $\{e_x, e_y, e_z\}$ whereas the basis of the 2-spinors is denoted by $\{e_1, e_2\}$. The two-component spinors in the opposite momentum direction $\hat{p} = -\hat{e}_z$ are constructed using

$$\chi_{-\lambda}(-\hat{p}) = \xi_\lambda \chi_\lambda(\hat{p}) \tag{9.10}$$

from Ref. [221] with $\xi_\lambda = 1$ in the Jacob-Wick convention for a second particle spinor [222], resulting in

$$\chi_{+1/2}(-e_z) = e_2, \qquad \chi_{-1/2}(-e_z) = e_1. \tag{9.11}$$

Defining $\epsilon_+ := \sqrt{E+m}$ and $\epsilon_- := \sqrt{E-m}$ for a simpler notation, we can rewrite the particle and antiparticle four-component spinors as

$$u_\lambda(p) = \begin{pmatrix} \epsilon_+\chi_\lambda(\hat{p}) \\ 2\lambda\,\epsilon_-\chi_\lambda(\hat{p}) \end{pmatrix} = \begin{pmatrix} \rho^\lambda \\ \psi^\lambda \end{pmatrix}, \qquad v_\lambda(p) = \begin{pmatrix} \epsilon_-\chi_{-\lambda}(\hat{p}) \\ -2\lambda\,\epsilon_+\chi_{-\lambda}(\hat{p}) \end{pmatrix} = \begin{pmatrix} \sigma^\lambda \\ \varphi^\lambda \end{pmatrix}. \tag{9.12}$$

Here we introduced the nomenclature ρ/ψ for the upper/lower 2-spinor within a particle 4-spinor u and likewise σ/φ for an antiparticle v. For later use, we now list the combinations of $\lambda = \pm\frac{1}{2}$ and $\hat{p} = \pm e_z$ explicitly:

$$\begin{aligned} u_+(e_z) &= \begin{pmatrix} \epsilon_+e_1 \\ \epsilon_-e_1 \end{pmatrix}, \quad u_-(e_z) = \begin{pmatrix} \epsilon_+e_2 \\ -\epsilon_-e_2 \end{pmatrix}, \quad u_+(-e_z) = \begin{pmatrix} \epsilon_+e_2 \\ \epsilon_-e_2 \end{pmatrix}, \quad u_-(-e_z) = \begin{pmatrix} \epsilon_+e_1 \\ -\epsilon_-e_1 \end{pmatrix}, \\ v_+(e_z) &= \begin{pmatrix} \epsilon_-e_2 \\ -\epsilon_+e_2 \end{pmatrix}, \quad v_-(e_z) = \begin{pmatrix} \epsilon_-e_1 \\ \epsilon_+e_1 \end{pmatrix}, \quad v_+(-e_z) = \begin{pmatrix} \epsilon_-e_1 \\ -\epsilon_+e_1 \end{pmatrix}, \quad v_-(-e_z) = \begin{pmatrix} \epsilon_-e_2 \\ \epsilon_+e_2 \end{pmatrix}. \end{aligned} \tag{9.13}$$

In the following, we will apply this formalism to Higgs production and decay within our example process.

9.1.2.1. Higgs production

As illustrated in Fig. 9.1, the incoming spinor u_1 (in the example case $\widetilde{\chi}_4^0$) decays into u_2 ($\widetilde{\chi}_1^0$) and a scalar (h/H). The matrix element $\mathcal{P}$ of this production process is decomposed into a right- and left-handed part,

$$\mathcal{P} = \bar{u}_2 C_R \omega_R u_1 + \bar{u}_2 C_L \omega_L u_1, \tag{9.14}$$

where $C_{R/L}$ are form factors. Using γ^0, γ^5 in the Dirac representation, and the 2-spinor notation introduced in Eq. (9.12), we calculate the spinor chains with arbitrary helicity of $\lambda_1, \lambda_2 = \pm\frac{1}{2}$,

$$p_R := \bar{u}_2 \omega_R u_1 = \frac{1}{2}(\rho_2^* - \psi_2^*)(\rho_1 + \psi_1), \tag{9.15}$$

$$p_L := \bar{u}_2 \omega_L u_1 = \frac{1}{2}(\rho_2^* + \psi_2^*)(\rho_1 - \psi_1). \tag{9.16}$$

Given the 2-body decay in the rest frame of particle 1, it follows that $E_1 = m_1$ and consequently $\epsilon_- = 0$, $\psi_1 = 0$. In order to obtain the helicity matrix elements $p_{R/L}^{\lambda_2\lambda_1}$, we insert the explicit spinors from Eq. (9.13) into the generic Eq. (9.16):

$$\begin{aligned}
p_R^{++} &= \bar{u}_{2+}\omega_R u_{1+} = \frac{1}{2}(\epsilon_{2+} - \epsilon_{2-})\epsilon_{1+}\; e_1 \cdot e_1 \\
&= \frac{1}{2}\left(\sqrt{E_2 + m_2} - \sqrt{E_2 - m_2}\right)\sqrt{2m_1}, \\
p_L^{++} &= \frac{1}{2}\left(\sqrt{E_2 + m_2} + \sqrt{E_2 - m_2}\right)\sqrt{2m_1}, \\
p_R^{--} &= p_L^{++}, \quad p_L^{--} = p_R^{++}, \\
p_{R/L}^{+-} &= p_{R/L}^{-+} \propto e_1 \cdot e_2 \equiv 0.
\end{aligned} \tag{9.17}$$

Since the helicity matrix elements are real, their complex conjugates $p_{R/L}^* = \bar{u}_1 \omega_{L/R} u_2$ are equal to the results in Eq. (9.17). The products of matrix elements are summed over all helicity combinations (but no averaging is done yet), with $i, j \in \{R, L\}$, leading to[1]

$$A_{ij} := \sum_{\lambda_1,\lambda_2=\pm 1/2} p_i \cdot p_j^*, \tag{9.18}$$

$$\begin{aligned}
A_{RR} &= A_{RR}^{++} + A_{RR}^{--} = 2m_1 E_2 = m_1^2 + m_2^2 - M^2, \\
A_{LL} &= A_{LL}^{++} + A_{LL}^{--} = A_{RR}, \\
A_{RL} &= A_{RL}^{++} + A_{RL}^{--} = 2m_1 m_2, \\
A_{LR} &= A_{LR}^{++} + A_{LR}^{--} = A_{RL},
\end{aligned} \tag{9.19}$$

[1] These helicity matrix elements correspond to the `FormCalc-HelicityMEs` via $A_{ij} = 4 \cdot \mathrm{MatF}(i,j)$. The factor of 4 arises because the `FormCalc` expressions are multiplied later on by 2 for each external fermion.

where the energy relation of a 2-body decay with $m_1 \to \{m_2, M\}$ was applied:

$$E_2 = \frac{m_1^2 + m_2^2 - M^2}{2m_1}. \tag{9.20}$$

Finally, the squared production matrix element is constructed as

$$\begin{aligned} \mathcal{P}\mathcal{P}^* &= \sum_{i,j=R,L} C_i C_j^* A_{ij} \\ &= (|C_R|^2 + |C_L|^2)(m_1^2 + m_2^2 - M^2) + (C_R C_L^* + C_L C_R^*)\, 2m_1 m_2. \end{aligned} \tag{9.21}$$

If the left- and right-handed form factors coincide ($C_L = C_R \equiv C$), Eq. (9.21) is reduced to

$$(\mathcal{P}\mathcal{P}^*)_C = 2|C|^2 \left((m_1 + m_2)^2 - M^2\right). \tag{9.22}$$

However, in the interference term we need the product $\mathcal{P}_h\mathcal{P}_H^*$ with different Higgs masses in E_2 from Eq. (9.20). This distinction leads to

$$A_{ij} = \sum_{\lambda_1,\lambda_2=\pm 1/2} p_i^h \cdot p_j^{H*}, \tag{9.23}$$

$$A_{RR} = A_{LL} = m_1 \left(\epsilon_{2+}^h \epsilon_{2+}^H + \epsilon_{2-}^h \epsilon_{2-}^H\right), \tag{9.24}$$

$$A_{RL} = A_{LR} = m_1 \left(\epsilon_{2+}^h \epsilon_{2+}^H - \epsilon_{2-}^h \epsilon_{2-}^H\right). \tag{9.25}$$

As before, we give the resulting product of matrix elements for the independent $C_{R/L}$ and for simpler use in the special case of $C_{R/L} \equiv C$,

$$\begin{aligned} \mathcal{P}_h\mathcal{P}_H^* =& (C_R^h C_R^{H*} + C_L^h C_L^{H*}) m_1 \left(\epsilon_{2+}^h \epsilon_{2+}^H + \epsilon_{2-}^h \epsilon_{2-}^H\right) \\ &+ (C_R^h C_L^{H*} + C_L^h C_R^{H*}) m_1 \left(\epsilon_{2+}^h \epsilon_{2+}^H - \epsilon_{2-}^h \epsilon_{2-}^H\right) \end{aligned} \tag{9.26}$$

$$\xrightarrow{C} 4C^h C^{H*} m_1 \epsilon_{2+}^h \epsilon_{2+}^H = 2C^h C^{H*} \sqrt{(m_1+m_2)^2 - M_h^2}\,\sqrt{(m_1+m_2)^2 - M_H^2}. \tag{9.27}$$

Eq. (9.26) shows that the method of on-shell matrix elements enables us to distinguish between different masses of the intermediate particles, in this example M_h and M_H.

9.1.2.2. Higgs decay

In the decay of a Higgs boson into a pair of fermions, the representation of antiparticle spinors from Eq. (9.13) is also needed. Furthermore, the fermions are generated back to back in the rest frame of the decaying Higgs boson. So if we align the momentum direction of the particle spinor u_4 with the z-axis, $\hat{p}_4 = e_z$, the momentum of the antiparticle spinor v_3 points into the direction of $\hat{p}_3 = -e_z$.

Analogously to Eq. (9.14), the decay matrix element is in general composed of a left- and right-handed part,

$$\mathcal{D} = \bar{u}_4 C_R \omega_R v_3 + \bar{u}_4 C_L \omega_L v_3, \tag{9.28}$$

$$d_R := \bar{u}_4(e_z)\omega_R v_3(-e_z) = \frac{1}{2}(\rho_4^* - \psi_4^*)(\sigma_3 + \varphi_3), \tag{9.29}$$

$$d_L := \bar{u}_4(e_z)\omega_R v_3(-e_z) = \frac{1}{2}(\rho_4^* + \psi_4^*)(\sigma_3 - \varphi_3). \tag{9.30}$$

With the mass M of the decaying Higgs boson, the fermion masses $m_3 = m_4 \equiv m$ and the resulting energies $E_3 = E_4 \equiv \frac{M}{2}$, the spinor chains d_R, d_L are now calculated for all helicity configurations of $\lambda_3, \lambda_4 = \pm\frac{1}{2}$,

$$\begin{aligned} d_R^{++} &= d_L^{--} = \sqrt{E^2 - m^2} - E, \\ d_L^{++} &= d_R^{--} = \sqrt{E^2 - m^2} + E, \qquad d_{R/L}^{+-} = d_{R/L}^{-+} = 0. \end{aligned} \tag{9.31}$$

Summing over all helicity combinations, we obtain

$$A_{RR} = A_{LL} = M^2 - 2m^2, \qquad A_{RL} = A_{LR} = -2m^2. \tag{9.32}$$

So the product of on-shell decay matrix elements results in

$$\mathcal{D}\mathcal{D}^* = \left(|C_R|^2 + |C_L|^2\right)\left(M^2 - 2m^2\right) - \left(C_R C_L^* + C_L C_R^*\right) 2m^2. \tag{9.33}$$

In case of identical left- and right-handed couplings C of the decay vertex, Eq. (9.33) simplifies to

$$\mathcal{D}\mathcal{D}^* = 2|C|^2(M^2 - 4m^2). \tag{9.34}$$

As in the production case, we are interested in the contribution to the on-shell interference term, so we distinguish between $E_h = \frac{M_h}{2}$ and $E_H = \frac{M_H}{2}$,

$$\begin{aligned} A_{RR} = A_{LL} &= 2\left(\sqrt{(E_h^2 - m^2)(E_H^2 - m^2)} + E_h E_H\right), \\ A_{RL} = A_{LR} &= 2\left(\sqrt{(E_h^2 - m^2)(E_H^2 - m^2)} - E_h E_H\right). \end{aligned} \tag{9.35}$$

Finally, the product of decay matrix elements with different masses reads

$$\begin{aligned} \mathcal{D}_h \mathcal{D}_H^* = {} & 2\left(C_R^h C_R^{H*} + C_L^h C_L^{H*}\right)\left(\sqrt{(E_h^2 - m^2)(E_H^2 - m^2)} + E_h E_H\right) \\ & + 2\left(C_R^h C_L^{H*} + C_L^h C_R^{H*}\right)\left(\sqrt{(E_h^2 - m^2)(E_H^2 - m^2)} - E_h E_H\right) \end{aligned} \tag{9.36}$$

$$\xrightarrow{C} 8 C^h C^{H*} \sqrt{\left(\frac{M_h^2}{4} - m^2\right)\left(\frac{M_H^2}{4} - m^2\right)}, \tag{9.37}$$

where the last line applies for identical L/R form factors.

The outcome of the explicit spinor representations in the context of factorising a longer process into production and decay is the possibility to express the interference term with on-shell matrix elements depending on the mass of the intermediate particle. The method was here introduced in a generic way and then applied to the example of Higgs production and decay with two external fermions in each subprocess in the rest frames of the decaying particles.

9.2. Numerical evaluation at lowest order

9.2.1. Higgs masses and widths in the modified $M_h^{\max}$ scenario

For the numerical application of the gNWA to the example process of $\tilde{\chi}_4^0 \to \tilde{\chi}_1^0\, h/H \to \tilde{\chi}_1^0\, \tau^+\tau^-$ and the validation against the full calculation, we choose again the modified $M_h^{\max}$ scenario defined in Sect. 8.2.3. The resulting Higgs masses and widths are of crucial interest regarding the applicability of the standard NWA and for the significance of the interference term. Under variation of the input Higgs mass $M_{H^\pm}$, the resulting masses and widths of the interfering neutral Higgs bosons h, H change as shown in Fig. 9.2 with results from `FeynHiggs` [67, 146, 149, 150] including dominant 2-loop corrections. Fig. 9.2(a) displays the dependence of the masses of h (blue, dotted) and H (green, dashed) on $M_{H^\pm}$. Within the analysed parameter range of $M_{H^\pm} = 151...155\,\text{GeV}$, their mass difference ΔM (red) in Fig. 9.2(b) is around its minimum at $M_{H^\pm} \simeq 153\,\text{GeV}$ smaller than both total widths Γ_h (blue, dotted) and Γ_H (green, dashed). While Γ_h decreases, Γ_H increases with increasing $M_{H^\pm}$. This is caused by a change of the predominantly diagonal or off-diagonal structure of the $\hat{\mathbf{Z}}$-matrix which has a cross-over around $M_{H^\pm} \simeq 153\,\text{GeV}$ in this scenario. Since both widths contribute to the overlap of the two resonances, the ratio $R_{M\Gamma} = \Delta M/(\Gamma_h + \Gamma_H)$ gives a good indication of the parameter region of most significant interference. This is visualised (in orange) in Fig. 9.2(c) and compared to the ratios $\Delta M/\Gamma_h$ (blue, dotted) and $\Delta M/\Gamma_H$ (green, dashed), which only take one of the widths into account and are therefore a less suitable criterion for the importance of the interference term. Fig. 9.2(d) presents the ratio Γ_i/M_i for $i = h$ (blue, dotted) and H (green, dashed) as a criterion for a *narrow* width. Both ratios lie in the range of about 0.5% to 3.5%, and this represents the expected order of the NWA uncertainty.

9.2.2. Results for tree level process $\tilde{\chi}_4^0 \to \tilde{\chi}_1^0\, h/H \to \tilde{\chi}_1^0\, \tau^+\tau^-$

In order to understand the possible impact of interference terms, we confront the prediction of the standard NWA (sNWA) with the 3-body decay width of our example process $\tilde{\chi}_4^0 \to \tilde{\chi}_1^0 \tau^+\tau^-$ at the tree level (improved by 2-loop predictions for the masses, widths and $\hat{\mathbf{Z}}$-factors) in the modified $M_h^{\max}$ scenario.

First of all, we verify that the other conditions from Sect. 7.2.2 for the NWA are met. The widths of the involved Higgs bosons do not exceed 3.5% of their masses, hence they can be considered *narrow* (see Fig. 9.2(d)). At tree level, there are no unfactorisable contributions so that the scalar propagator is separable from the matrix elements. Besides,

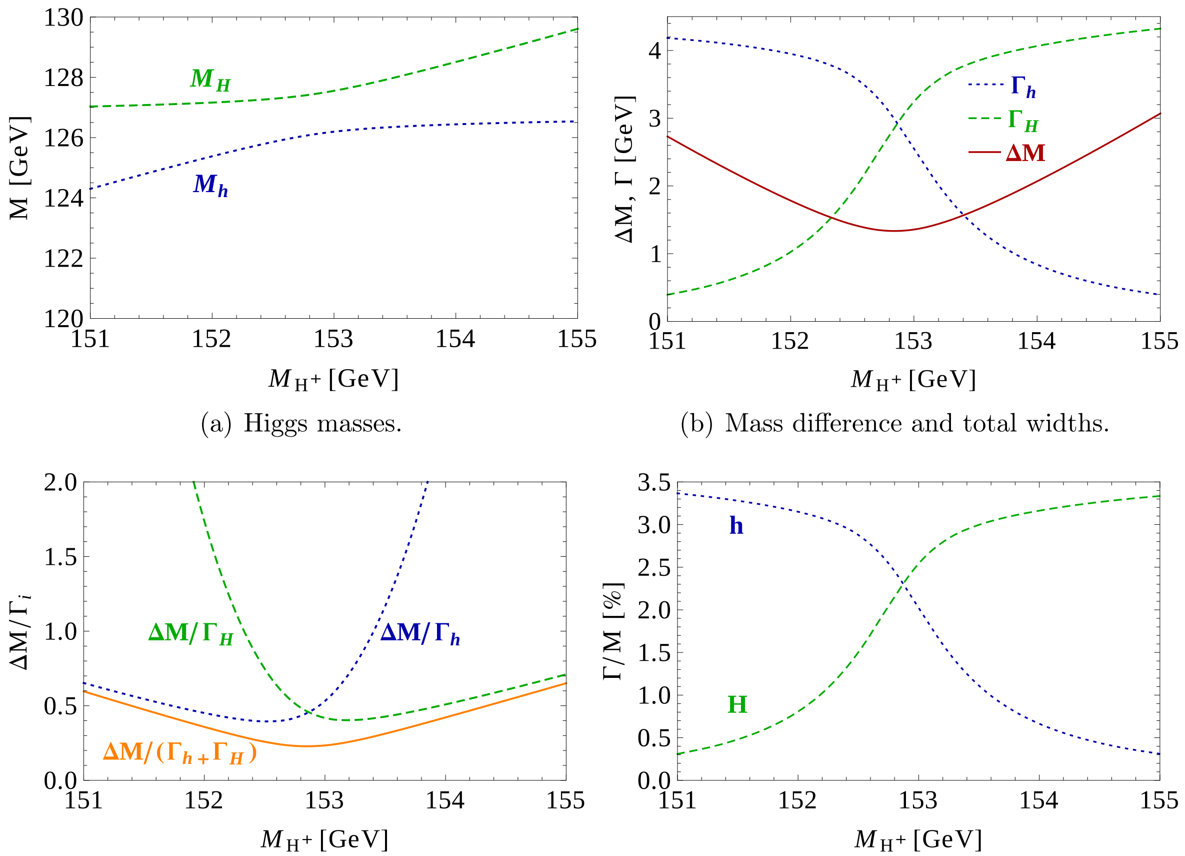

(a) Higgs masses.

(b) Mass difference and total widths.

(c) Ratio of mass difference and total widths.

(d) Ratio of total widths and masses.

Figure 9.2.: Higgs masses and widths from `FeynHiggs` [67, 146, 149, 150] including dominant 2-loop corrections in the modified $M_h^{\max}$ scenario. **(a):** Higgs masses M_h (blue, dotted) and M_H (green, dashed). **(b):** Mass difference $\Delta M \equiv M_H - M_h$ (red) compared to total widths Γ_h (blue, dotted) and Γ_H (green, dashed). **(c):** Mass difference ΔM divided by total width of h (blue, dotted), H (green, dashed) and sum of both widths (orange). **(d):** Ratio Γ_i/M_i for h (blue, dotted) and H (green, dashed).

our scenario is far away from the production and decay thresholds since $M_{h_k} \gg 2m_\tau$ holds independently of the parameters, and with neutralino masses of $m_{\tilde{\chi}_4^0} \simeq 264.9\,\text{GeV}$ and $m_{\tilde{\chi}_1^0} \simeq 92.6\,\text{GeV}$, also $m_{\tilde{\chi}_4^0} - (m_{\tilde{\chi}_1^0} + M_{h_k}) > 32\,\text{GeV}$ does not violate the threshold condition. The neutralino masses are independent of $M_{H^\pm}$. Thus, the NWA is applicable for the individual contributions of h and H, so the factorised versions

$$\Gamma^i_{\text{NWA}} := \Gamma_{P_i}(\tilde{\chi}_4^0 \to \tilde{\chi}_1^0 h_i)\,\text{BR}_i(h_i \to \tau^+\tau^-) \tag{9.38}$$

should agree with the separate terms of the 3-body decays via the exchange of only one of the Higgs bosons, h_i,

$$\Gamma^i_{1\to3} := \Gamma(\tilde{\chi}_4^0 \xrightarrow{h_i} \tilde{\chi}_1^0 \tau^+\tau^-) \tag{9.39}$$

within the uncertainty of $\mathcal{O}\left(\frac{\Gamma_{h_i}}{M_{h_i}}\right)$. This is tested in Fig. 9.3. The blue lines compare $\Gamma^h_{1\to 3}$ (solid) with the factorised process $\Gamma^h_{\rm NWA}$ (dotted), the green lines represent the corresponding expressions for H. The standard narrow-width approximation (sNWA) is composed of the *incoherent* sum of both factorised processes, i.e.,

$$\Gamma_{\rm sNWA} = \Gamma_{P_h}\,{\rm BR}_h + \Gamma_{P_H}\,{\rm BR}_H. \tag{9.40}$$

This is confronted with the incoherent sum of the 3-body decays which are only h-mediated or H-mediated. For a direct comparison with the sNWA, the interference term is not included,

$$\Gamma^{\rm incoh}_{1\to 3} = \Gamma^h_{1\to 3} + \Gamma^H_{1\to 3}. \tag{9.41}$$

The sNWA (dotted) and the incoherent sum of the 3-body decay widths are both shown in grey. Their relative deviation of $0.8-3.3\%$ is of the order of the ratio Γ/M from Fig. 9.2(d). Consequently, the NWA is applicable to the terms of the separate h/H-exchange within the expected uncertainty.

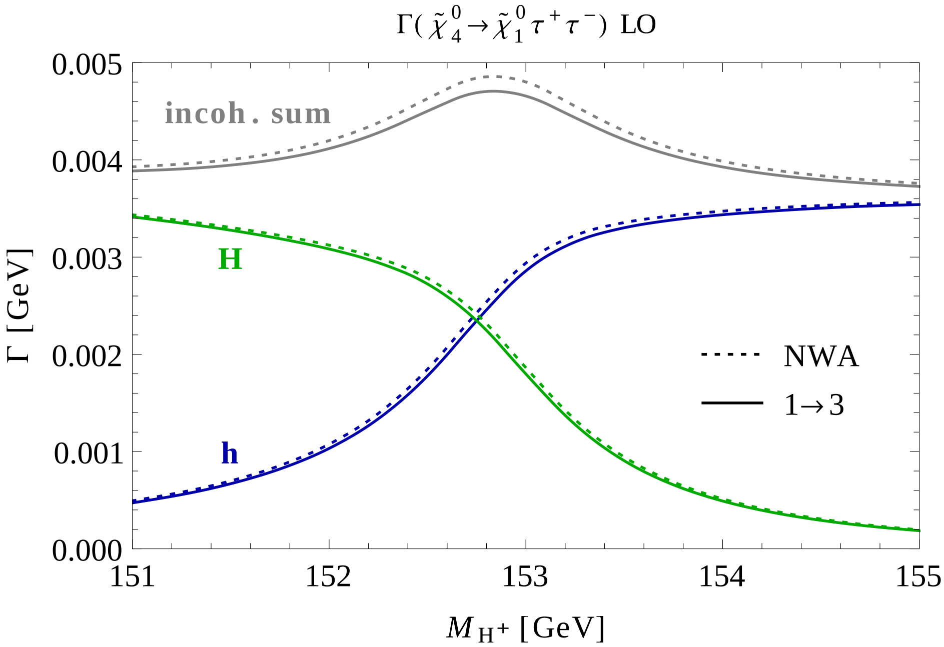

Figure 9.3.: The 1→3 decay width (solid) of $\tilde{\chi}^0_4 \to \tilde{\chi}^0_1\tau^+\tau^-$ at tree level with separate contributions from h (blue), H (green) and their incoherent sum (grey) confronted with the sNWA (dotted).

However, the fifth condition in Sect. 7.2.2 concerns the absence of a large interference with other diagrams. But with $\Delta M < \Gamma_h + \Gamma_H$ throughout the analysed parameter range (see Fig. 9.2(c)), we expect a sizeable interference effect in this scenario owing to a considerable overlap of the Breit-Wigner propagators and a sizeable mixing between h and H. Since the masses and widths of the interfering Higgs bosons depend on $M_{H^\pm}$, the size of the interference term varies with the input charged Higgs mass. Based on the minimum of the ratio $R_{\Gamma M} = \Delta M/(\Gamma_h + \Gamma_H)$ and a significant mixing between h and H, we expect the most significant interference contribution near $M_{H^\pm} = 153\,\text{GeV}$.

Fig. 9.4 presents the partial decay width $\Gamma(\tilde{\chi}_4^0 \to \tilde{\chi}_1^0\tau^+\tau^-)$ in dependence of the input Higgs mass $M_{H^\pm}$. In the sNWA (grey), the interference term is absent. In contrast, the full 3-body decay[2] (black) takes the h and H propagators and their interference into account. Comparing the prediction of the sNWA with the full 3-body decay width

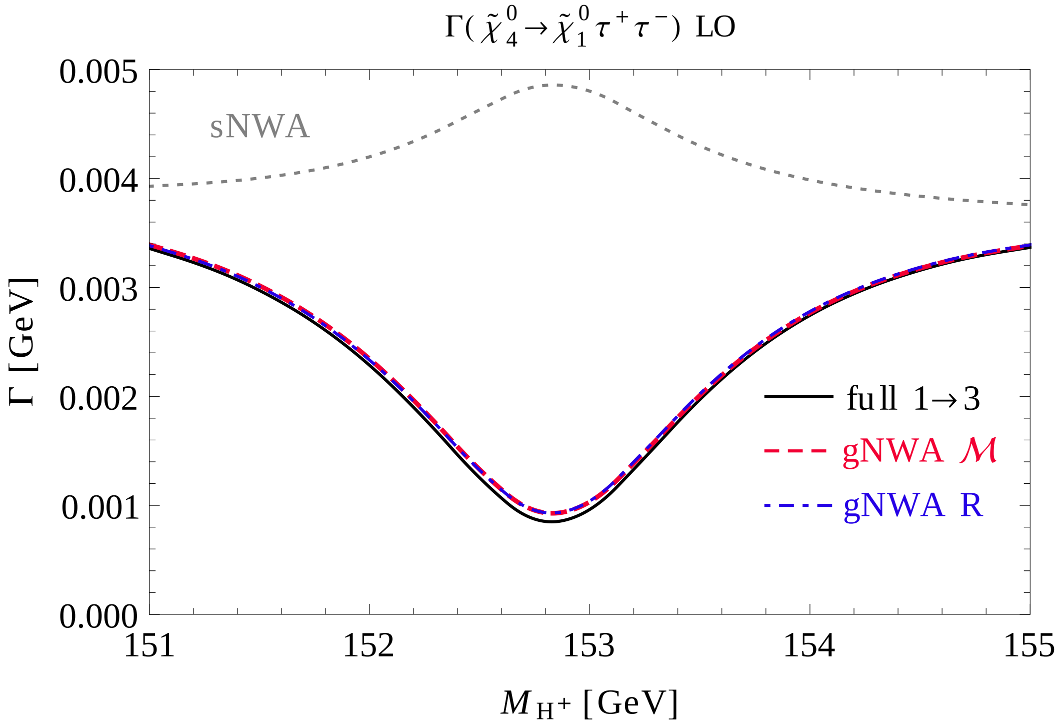

Figure 9.4.: The 1→3 decay width of $\tilde{\chi}_4^0 \to \tilde{\chi}_1^0\tau^+\tau^-$ at tree level with contributions from h, H including their interference (black) confronted with the NWA: sNWA without the interference term (grey, dotted), gNWA including the interference term based on on-shell matrix elements denoted by $\mathcal{M}^2$ (red, dashed) and on the R-factor approximation denoted by R (blue, dash-dotted).

reveals an enormous discrepancy between both results, especially in the region of the smallest ratio $R_{\Gamma M}$ around $M_{H^\pm} \simeq 153\,\text{GeV}$, due to a large negative interference term. Consequently, the NWA in its standard version is insufficient in this parameter scenario.

In the generalised narrow-width approximation, on the other hand, the sNWA is extended by incorporating the on-shell interference term. The red line indicates the prediction of the complete process in the gNWA using the on-shell evaluation of unsquared matrix elements in the interference term as derived conceptually in Eq. (7.24) and explicitly in Sect. 9.1.2. Furthermore, the blue line demonstrates the result of the

[2] In this section, the *full* tree level refers to the sum of h- and H-mediated 3-body decays including the interference term (but without A- and Z-boson exchange or non-resonant propagators) at the improved Born level, i.e. including Higgs masses, total widths and $\hat{\mathbf{Z}}$-factors at the leading 2-loop level from `FeynHiggs` [67, 146, 149, 150].

gNWA using the additional approximation of interference weight factors R defined in Eq. (7.38). While the sNWA overestimates the full result by a factor of up to 5.5 on account of the neglected destructive interference, both variants of the gNWA result in a good approximation of the full 3-body decay width.

The slight relative deviation between either form of the gNWA and the full result amounts to $(\Gamma_{\text{gNWA}} - \Gamma_{1\to3})/\Gamma_{\text{sNWA}} \simeq 0.4\% - 1.7\%$ if normalised to the sNWA and to $(\Gamma_{\text{gNWA}} - \Gamma_{1\to3})/\Gamma_{1\to3} \simeq 0.5\% - 9.2\%$ if normalised to the 3-body decay width. The largest relative deviation between Γ_{gNWA} and $\Gamma_{1\to3}$ arises in the region where the reference value $\Gamma_{1\to3}$ itself is very small so that a small deviation has a pronounced relative effect. This uncertainty, however, is not intrinsically introduced by the approximated interference term, but it stems from the factorised constituents Γ^h_{NWA}, Γ^H_{NWA} already present in the sNWA, see Fig. 9.3.

9.3. Example process at 1-loop order in the gNWA

Motivated by the good performance of the gNWA at the tree level, in this section we investigate the application of the generalised narrow-width approximation at the loop level by incorporating 1-loop corrections of the production and decay part into the predictions.

In this example, the calculation of the full process at the 1-loop level is still manageable (see Sect. 8.2), where *full* here means the 3-body decays with Breit-Wigner propagators and $\hat{\mathbf{Z}}$-factors, though without the Z-, A- and G-boson exchange. But we aim at validating the generalised narrow-width approximation at the 1-loop level so that it can be applied on kinematically more complicated processes for which the factorisation into production and decay is essential to enable the computation of higher order corrections.

Our strategy is to combine the NLO corrections for the production and decay subprocesses in such a way that the gNWA prediction can be consistently compared to the full 1-loop calculation. Only the box diagrams are left out in the gNWA compared to the 3-body decays.

9.3.1. 2-body decays in the production and decay parts

The gNWA at NLO requires the 1-loop contributions to the 2-body decays as subprocesses. For the production, we calculate the full 1-loop corrections to $\Gamma(\tilde{\chi}^0_4 \to \tilde{\chi}^0_1 h/H)$ in the NNN on-shell renormalisation scheme, see Refs. [109–111], with the same choice of on-shell states as in the 3-body-decay described in Sect. 8.2.2.1. Higgs mixing is taken into account by $\hat{\mathbf{Z}}$-factors, but mixing with G-/Z-bosons is generated explicitly, which, however, vanishes in this $\mathcal{CP}$-conserving scenario. Some example diagrams for vertex corrections are shown in Fig. 9.5(a). Fig. 9.6(a) presents the resulting 2-body decay widths for the production of h (blue) and H (green) at the tree level (dashed) and the 1-loop level (solid). While the 1-loop corrections increase $\Gamma(\tilde{\chi}^0_4 \to \tilde{\chi}^0_1 h)$, they decrease the production of H from the decay of $\tilde{\chi}^0_4$. The substantial relative effect can be seen in Fig. 9.6(b).

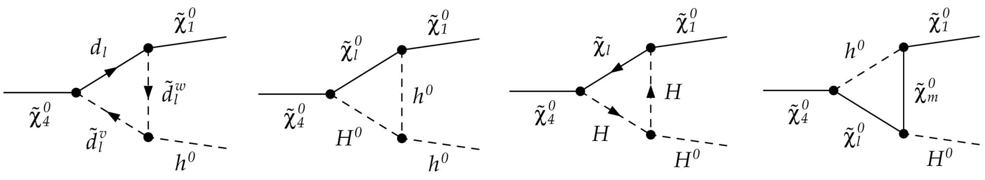

(a) Higgs production

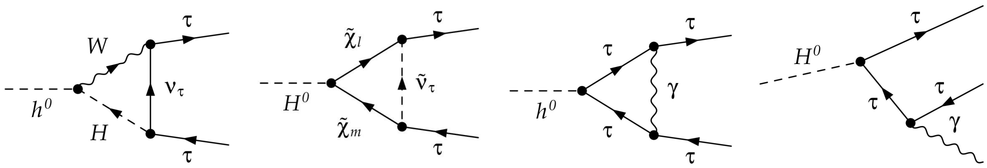

(b) Higgs decay.

Figure 9.5.: Example diagrams of the 2-body decays for **(a)** Higgs production in $\tilde{\chi}_4^0 \to \tilde{\chi}_1^0 h/H$ with vertex corrections and **(b)** Higgs decay in $h/H \to \tau^+\tau^-$ with vertex and real corrections.

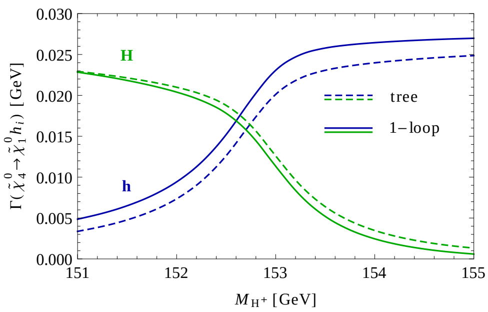

(a) Higgs production in $\tilde{\chi}_4^0 \to \tilde{\chi}_1^0 h/H$.

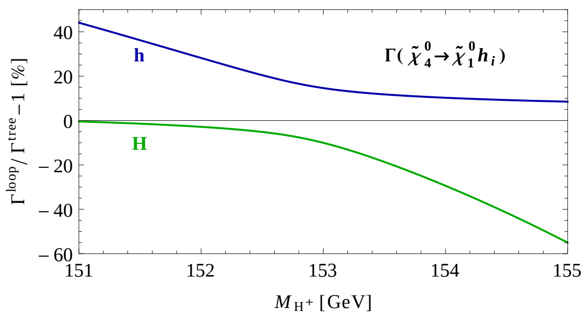

(b) Relative loop contribution in $\tilde{\chi}_4^0 \to \tilde{\chi}_1^0 h/H$.

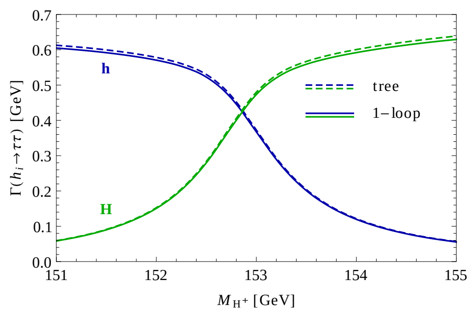

(c) Higgs decay $h/H \to \tau^+\tau^-$.

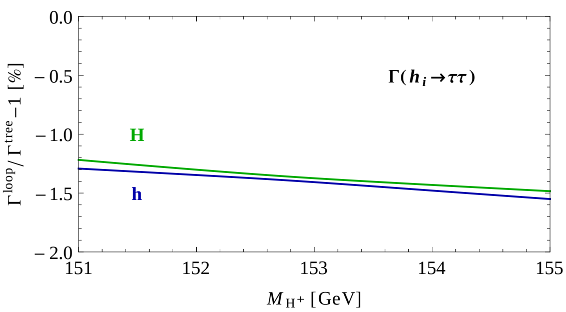

(d) Relative loop contribution in $h/H \to \tau^+\tau^-$.

Figure 9.6.: 2-body decay widths of **(a)** $\tilde{\chi}_4^0 \to \tilde{\chi}_1^0 h_i$ and **(c)** $h_i \to \tau^+\tau^-$ with $h_i = h$ (blue) and H (green) at the tree level (dashed) or at the 1-loop level (solid), and the relative effect of the loop contributions **(b)**, **(d)**.

For the decay, the full vertex corrections to $h_i \to \tau^+\tau^-$ are included. Furthermore, real soft photon emission off the τ-leptons in the final state is included. In order to allow for a meaningful comparison between the gNWA and the full calculation, the energy cut-off is defined by the same value $E_{\mathrm{soft}}^{\mathrm{max}} = 0.1 m_{\tilde{\chi}_4^0}$ as in the 3-body decay. Example diagrams are displayed in Fig. 9.5(b), where the last two cases are IR-divergent. The emission of a real photon is not directly calculated as a 3-body decay, but still with the 2-body phase space in the soft-photon approximation. The numerical influence of the corrections of $\mathcal{O}(\alpha)$ on $\Gamma(h_i \to \tau^+\tau^-)$ is shown in Fig. 9.6(c). The 1-loop and real corrections slightly decrease both decay rates (for $h_i = h, H$) by 1.2% to 1.5% as displayed in Fig. 9.6(d).

9.4. Numerical validation of the gNWA at higher order

The on-shell factorisation of the interference term has already been applied at the leading order in Sect. 9.2.2. In this section, we will investigate this approximation at the next-to-leading order. Since a wide range of processes even with many external particles can be computed at lowest order without applying the NWA, we use the full leading order result of the three-body decay (i.e., without NWA) and add the 1-loop contribution for which we use the gNWA. With this procedure, we apply the on-shell approximation only when necessary without introducing an avoidable uncertainty at the tree level. As a further step, one could split the real photon contribution into IR-singular and finite terms and apply the NWA only on the singular ones according to Refs. [164, 191].

9.4.1. On-shell matrix elements and R-factor approximation

In Fig. 9.7, we compare the numerical results of the method of on-shell matrix elements using Eqs. (7.47) and (7.48), denoted by $\mathcal{M}^2$, and of the interference weight factor approximation from Eq. (7.64), denoted by $\tilde{R}$, with the full 1-loop result as calculated in Sect. 9.4. The upper panel shows the prediction of the partial width $\Gamma(\tilde{\chi}_4^0 \to \tilde{\chi}_1^0 \tau^+\tau^-)$. The lines of the gNWA based on matrix elements (red, dashed) and the full 1-loop calculation (black, solid) lie nearly on top of one another. Also the additional $\tilde{R}$-factor approximation (blue, dash-dotted) yields a good qualitative agreement with the full result, but less accurate than achieved by the on-shell matrix elements. The lower panel visualises the relative deviation of the decay width predicted by the two versions of the gNWA from the full result. As expected, the R-factor method reproduces the full result best where the difference between M_h and M_H is smallest, i.e., in the centre of the analysed parameter interval. But the assumption of equal masses becomes worse away from the centre of the analysed interval, leading to a deviation from the full 1-loop result of up to 4.5%. Thus, for those parameters the matrix element method performs clearly better within an accuracy of better than 1%.

In order to further investigate how well the gNWA predicts the interference term at the 1-loop level, we take a closer look in Fig. 9.8 at the pure loop contribution $\Gamma^{\mathrm{loop,pure}} = \Gamma^{\mathrm{loop}} - \Gamma^{\mathrm{tree}}$ of the full three-body decay (black, solid), the gNWA using on-shell matrix elements (red, dashed, denoted by $\mathcal{M}^2$) and the $\tilde{R}$-factor approximation (blue, dash-dotted, denoted by $\tilde{R}$). While at the tree level we found that both versions of

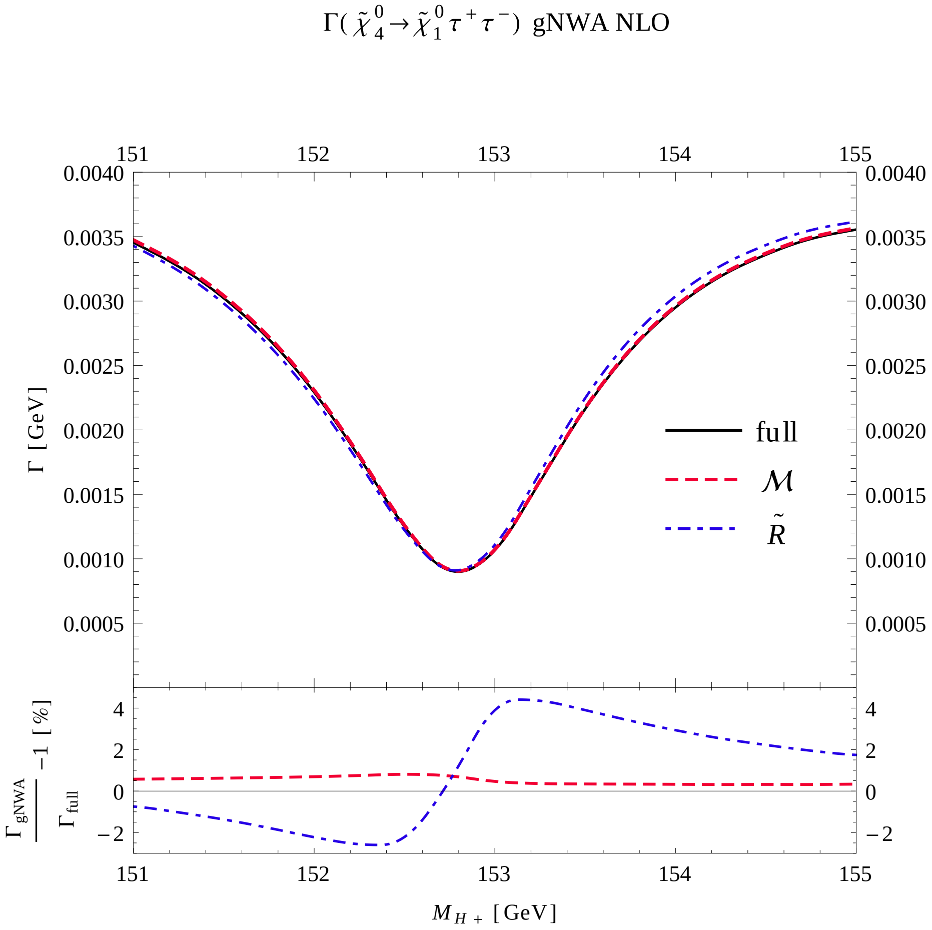

Figure 9.7.: Upper panel: The decay width $\tilde{\chi}_4^0 \to \tilde{\chi}_1^0 \tau^+\tau^-$ at the 1-loop level with resonant h, H-exchange and, for the full 3-body decay (black, solid), with box contributions. The gNWA with on-shell matrix elements is denoted by $\mathcal{M}^2$ (red, dashed), and the gNWA with interference weight factors is denoted by $\tilde{R}$ (blue, dash-dotted). **Lower panel:** The relative deviation of the gNWA (matrix element and R-factor approximation) from the full 1-loop result in percent.

the gNWA work comparably well (see Fig. 9.4), the $\mathcal{M}^2$-method provides a significantly better prediction of the interference term at the 1-loop level.

When the gNWA is used to approximate one-loop effects, we need to compare the accuracy of the approximation with the overall size of the loop correction. Fig. 9.9 provides a comparison between the precision of the gNWA with respect to the full calculation (for on-shell matrix elements denoted by $\mathcal{M}^2$ in red and the R-factor approximation denoted by $\tilde{R}$ in blue) and the relative size of the 1-loop correction to the 3-body decay width in black. While the loop correction ranges from -1% to 11% in this example case, the deviation of the matrix element method from the full result remains below 1%. The uncertainty of this approximation is therefore significantly smaller than the typical size of the loop correction in this case. The deviation of the R-factor approximation from the

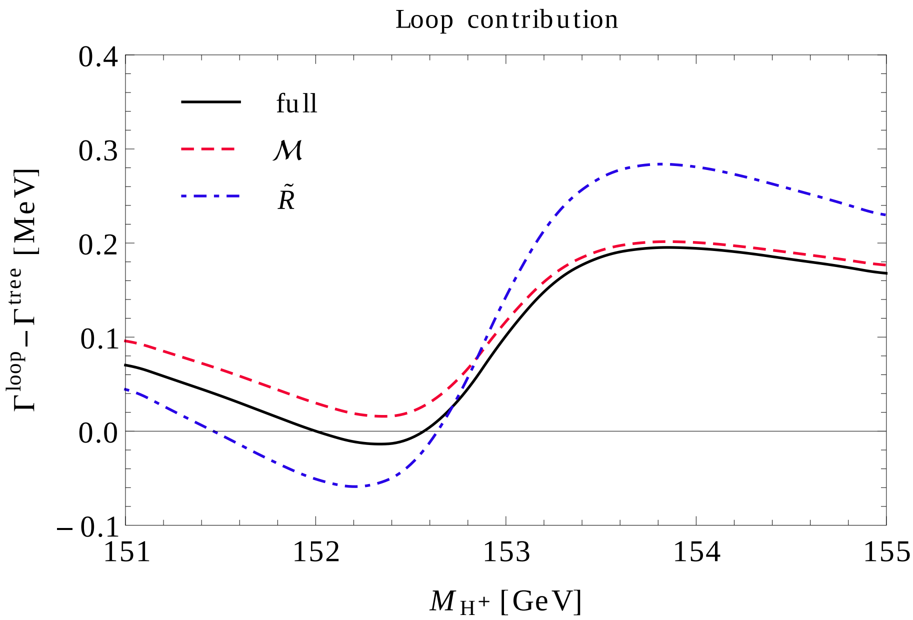

Figure 9.8.: Pure loop contributions in the full calculation (black, solid) and approximated by the gNWA using the matrix element method denoted by $\mathcal{M}^2$ (red, dashed) and using the R-factor approximation denoted by $\tilde{R}$ (blue, dash-dotted).

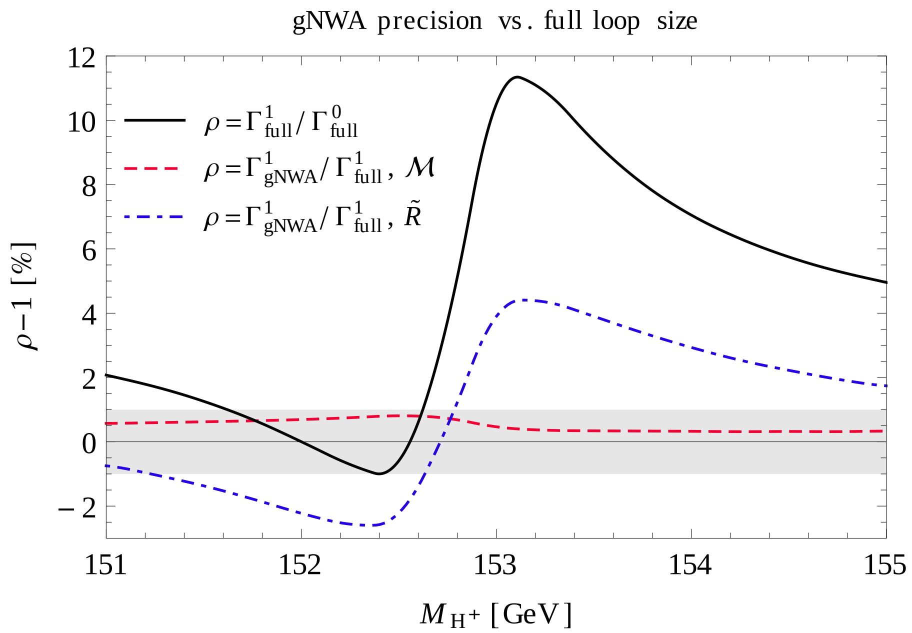

Figure 9.9.: Precision of the gNWA at the 1-loop level using the matrix element method denoted by $\mathcal{M}^2$ (red, dashed) and using the R-factor approximation denoted by $\tilde{R}$ (blue, dash-dotted) compared to the relative size of the loop contribution in the full calculation (black). The $\pm 1\%$ region is indicated in grey.

full result is found to be larger, within -3% to 4.5% in this case, but it is still about a factor of two smaller than the size of the loop correction in the region where the latter is sizable.

The plot shows that the overall performance of the gNWA with the $\mathcal{M}$-method is good except for the region around $M_{H^\pm} \simeq 152\,\text{GeV}-152.5\,\text{GeV}$ where the $\mathcal{M}$-method uncertainty exceeds the relative size of the full loop correction slightly. But here the full loop correction is in fact very small. Keeping in mind that the full calculation is subject to uncertainties itself (e.g. from missing higher-order corrections) which might reach the level of 1% (for illustration, the $\pm 1\%$ range is indicated in the plot), the $\mathcal{M}$-method can be regarded as adequate to approximate loop corrections to the interference term within the expected uncertainty of the full result (as long as non-factorisable corrections remain numerically suppressed). On the other hand, the R-factor method gives rise to larger deviations and should therefore be regarded as a simple estimate of the higher-order result including interference effects.

9.4.2. Separate treatment of photon contributions

As discussed in Sect. 7.4.1.2, the factor δ_{SB}, which multiplies the squared tree level matrix element to account for the contribution of soft bremsstrahlung, and the IR-divergent loop integrals must be evaluated at the same mass to enable the cancellation of IR-singularities between real and virtual photon contributions. In order to reduce the ambiguity whether to choose the common mass $\overline{M} = M_h$ or M_H, the IR-finite diagrams can be evaluated at their correct mass shell. Fig. 9.10 compares the dependence of the gNWA result on the ambiguous mass choice, i.e., the relative deviation between $\Gamma_{\text{gNWA}}(\overline{M} = M_h)$ and $\Gamma_{\text{gNWA}}(\overline{M} = M_H)$, for the matrix element method. The dashed green line represents the universal treatment where the loop integrals in all decay one-loop matrix elements are evaluated at $\overline{M}^2$ whereas the solid red line shows the separate calculation of the photonic contribution as described in Sect. 7.4.1.2. The impact of the dependence of the gNWA on the choice of the mass $\overline{M}$ is found to be rather small, giving rise to a maximum deviation of 0.23% for the universal treatment of all one-loop matrix elements for the decay. Restricting this approximation just to the photonic contribution is seen to have an insignificant effect in this example, reducing the deviation to 0.2%.

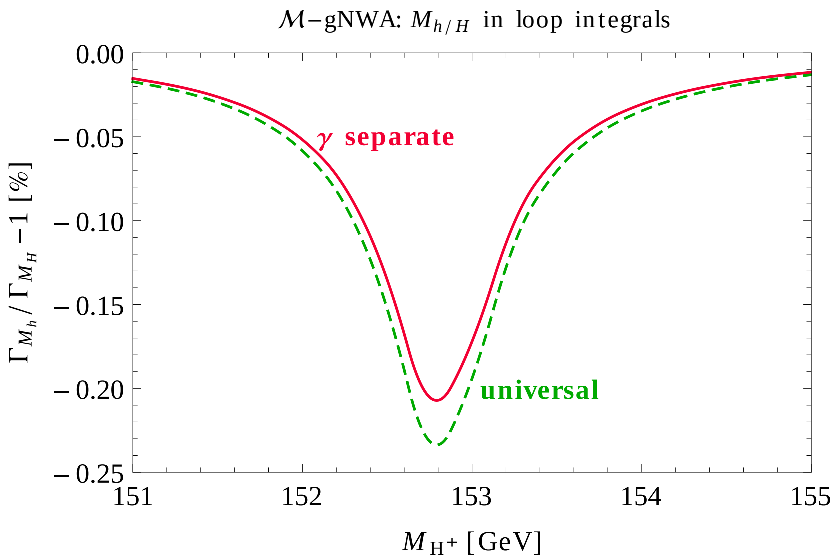

Figure 9.10.: Impact of the dependence of the gNWA on the choice of the mass $\overline{M}$ (see text). The relative deviation between Γ_{M_h} and Γ_{M_H}, where $\Gamma_{M_i} \equiv \Gamma^{\mathcal{M}^2}_{\text{gNWA}}(\overline{M}^2 = M_i^2)$, is shown for the universal treatment of all one-loop matrix elements for the decay and for the case where the photonic contribution is treated separately.

9.4.3. gNWA prediction with most precise input values

As a first step, we defined the gNWA at the 1-loop order for a consistent comparison between the gNWA and the full 1-loop calculation. As an exception, the Higgs masses, total widths and wave function normalisation factors $\hat{\mathbf{Z}}$ have been obtained from `FeynHiggs` [67, 146, 149, 150] at the 2-loop order and used both in the gNWA and the full calculation. In this section we want to exploit the factorisation and include all components at the highest available precision. This means for the gNWA with the on-shell matrix element method and the R-factor approximation that we use the calculated 1-loop production part and the `FeynHiggs` branching ratios in $\Gamma_P(\tilde{\chi}_4^0 \to \tilde{\chi}_1^0 h_i)\cdot\text{BR}_D(h_i \to \tau^+\tau^-)$. Furthermore, the product of on-shell matrix elements from Eq. (7.46) is expanded up to the product of 1-loop matrix elements in Eq. (7.50). The higher-order extension of the R-factor approximation is defined in Eq. (7.65).

So far we have neglected additional contributions that do not play a role in the discussion of the interference effects between contributions with h and H exchange in the decay of $\tilde{\chi}_4^0 \to \tilde{\chi}_1^0\tau^+\tau^-$ for the considered $\mathcal{CP}$-conserving scenario. In order to obtain a more phenomenological prediction of $\Gamma(\tilde{\chi}_4^0 \to \tilde{\chi}_1^0\tau^+\tau^-)$ we now take into account also the resonant exchange of the $\mathcal{CP}$-odd Higgs boson A, the neutral Goldstone boson G and the Z-boson, as well as the non-resonant 3-body decay via a $\tilde{\tau}$. We include the contributions from A, G, Z and $\tilde{\tau}$-exchange at the tree-level, while at the loop level we incorporate the most precise gNWA result (where those additional contributions are neglected). Fig. 9.11(a) shows the prediction of the higher-order improved gNWA, supplemented by the full tree-level contribution including A, G, Z and $\tilde{\tau}$-exchange diagrams, as solid lines using on-shell matrix elements (red) and the R-factor approximation (blue). The corresponding results where the A, G, Z and $\tilde{\tau}$-exchange contributions have been neglected are indicated by the dashed lines. The contributions from A, G, Z and $\tilde{\tau}$ are found to yield a non-negligible upward shift in this example.

Fig. 9.11(b) shows the impact of including the most precise branching ratios and the product of 1-loop matrix elements in the gNWA, denoted by $\Gamma^{\mathrm{best}}_{\mathrm{gNWA}}$. For the matrix element method (in red, denoted by $\mathcal{M}^2$), this amounts to up to 1.2% relative to the 1-loop formulation used above for the comparison with the result for the 3-body decay. For the R-factor approximation (in blue, denoted by $\tilde{R}$), the effect of up to 0.4% is smaller because the effect on the interference term beyond the 1-loop order turns out to be negative. With reference to the gNWA including only h and H, the relative impact of the higher-order corrections is slightly higher (1.6% for the matrix element method and 0.6% for the R-factor approximation).

The numerical size of the contributions beyond the 1-loop order depends on the process and scenario, but the gNWA allows for their inclusion also in the interference term.

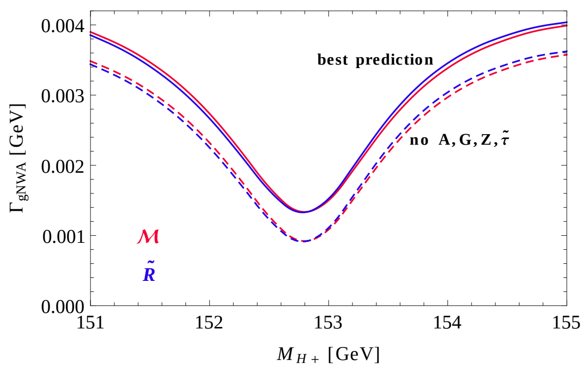

(a) Including A, Z, G, $\tilde{\tau}$-exchange.

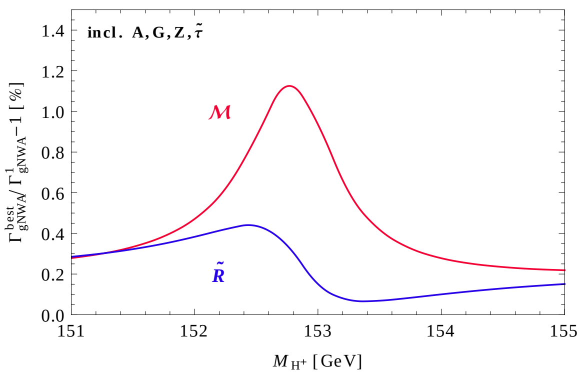

(b) Relative effect on gNWA.

Figure 9.11.: **(a)** The gNWA using the most accurate predictions for all parts of the process, supplemented with a tree-level result with (solid) and without (dashed) the additional A, G, Z and $\tilde{\tau}$-exchange contributions, for the $\mathcal{M}^2$-method (red) and the $\tilde{R}$-approximation (blue). **(b)** The relative effect of the most precise branching ratios and the product of 1-loop terms on the prediction of the gNWA with on-shell matrix elements (red, denoted by $\mathcal{M}^2$) and the R-factor approximation (blue, denoted by $\tilde{R}$).

9.5. Summary: Concept and application of the gNWA

In Chapters 7-9, we have formulated and tested a generalisation of the standard narrow-width approximation that extends the applicability of this important tool to scenarios where interference effects between nearly mass-degenerate particles are important. This can be the case in many extensions of the SM where the spectrum of the new particles is such that the mass difference between two or more particles is smaller than the sum of their total decay widths. In such a case, their resonances overlap so that the interference cannot be neglected if the two states mix. In order to still enable the convenient factorisation of a more complicated process into production and decay of an intermediate particle, we have demonstrated how to factorise also the interference term. This is achieved by evaluating the production and decay matrix elements on the mass-shells of the resonant particles in analogy to the terms present in the standard NWA. If one additionally assumes equal masses of the intermediate particles, it is possible to further approximate the interference contribution by an interference weight factor, R, in terms of production cross sections, decay branching fractions, ratios of couplings and a universal, process independent integral over Breit-Wigner propagators.

We have developed this generalised narrow-width approximation both at the tree-level and at one-loop order. Following the analytic derivations, we have discussed the application to a simple example process in the context of the MSSM with real parameters. We have considered the three-body decay of the heaviest neutralino via a resonant neutral, $\mathcal{CP}$-even Higgs boson, h or H, into the lightest neutralino and a pair of τ-leptons. This process is well-suited for a test of the gNWA since it is sufficiently simple so that the full process can be calculated at the loop level and compared with the predictions of the gNWA. Within the gNWA this process can be decomposed into basic kinematic building blocks, namely two subsequent 2-body decays, and the interference contributions involve only scalar particles. The discussion of interference effects can therefore be disentangled from spin-correlation issues. Furthermore, the process involves charged external particles, so that the issue of the cancellation of IR divergencies between virtual loop corrections and bremsstrahlung contributions is relevant, while the fact that only the final state particles are charged reduces the complexity of the IR-divergent contributions and makes their treatment transparent.

We have validated the gNWA at the Born level (supplemented by higher-order Higgs masses, widths and $\hat{\mathbf{Z}}$-factors for the mixing) and at the 1-loop level including corrections of $\mathcal{O}(\alpha)$ with respect to the lowest order. Within the considered parameter region, the chosen modified $M_h^{\max}$-scenario leads to a small difference between the loop-corrected masses of M_h and M_H smaller than their total widths. This configuration results in a large negative interference term so that in the standard NWA, where the interference contribution is not taken into account, the 3-body decay width is overestimated by a factor of up to five in this example. Hence, the standard NWA is clearly insufficient in this scenario. The inclusion of the factorised interference term, however, leads to an agreement with the unfactorised decay width within few percent. At the tree level, the method of on-shell matrix elements and the R-factor approximation lead to very similar results.

However, at the Born level the methods for calculating multi-leg processes without further approximations are very advanced. Accordingly, a particular interest in the NWA concerns its application to the loop level, where the difficulty in computing processes involving a variety of different mass scales grows very significantly with the number of external legs of the process. In many cases the factorisation into different sub-processes provided by the NWA is essential to enable the computation of higher-order contributions. In cases where a full tree level calculation is feasible, the NWA can therefore be applied just at the loop level in order to facilitate the computation of the higher-order corrections, while the lowest order contributions are evaluated without further approximations in order to avoid an unnecessary theoretical uncertainty.

For a validation of the gNWA beyond the LO we have performed the 1-loop calculation of $\Gamma(\tilde{\chi}_4^0 \to \tilde{\chi}_1^0 \tau^+ \tau^-)$ including all vertex corrections, self-energies involving Higgs-Goldstone/Z mixing, Higgs-Higgs mixing contributions via finite wave function normalisation factors, box diagrams, as well as soft photon radiation. All higher order corrections except for the box diagrams factorise, which makes a separate calculation of the 1-loop production and decay part possible as long as the non-factorisable contributions remain sufficiently small. We have shown that within the gNWA the factorised interference term at the next-to-leading order is both UV- and IR-finite. In order to preserve the cancellations of IR-singularities between virtual and real photon contributions also in the on-shell matrix elements, all IR-divergent integrals in matrix elements and the soft-photon factor were evaluated at the same mass value. This prescription could be further improved by extracting the singular parts from the real photon contribution and applying the NWA only to those terms which match the singularities from the virtual photons. Furthermore, we have extended the interference weight factor to the 1-loop level. In the numerical comparison to the 3-body decay width, the gNWA based on 1-loop on-shell matrix elements agrees with the full 1-loop result within an accuracy of better than 1%, which is much below the typical size of the loop corrections in this case. The gNWA with interference weight factors, on the other hand, deviates from the full result by up to 4%, which is still about a factor of two smaller than the size of the loop correction in the region where the latter is sizable. Therefore the method of on-shell matrix elements appears to be a well-suited approach for predicting the interference term at 1-loop order within roughly the remaining theoretical uncertainty of the full result, while the additional R-factor approximation may be of interest as a technically simpler rough estimate of the higher-order result including interference effects.

In our discussion we have first focussed on the strict $\mathcal{O}(\alpha)$ contribution relative to the lowest order within the gNWA (except for masses, total widths and wave function normalisation factors, for which we have incorporated dominant 2-loop contributions throughout this work) for the purpose of a consistent comparison with the 3-body decay width. In the most accurate final result the factorisation into subprocesses for production and decay has the virtue that higher-order corrections can naturally be implemented into each of the subprocesses, which formally corresponds to a higher-order effect for the full process. This applies also to the interference term, where we have discussed the incorporation of higher-order contributions for the two considered versions of the gNWA.

While much of our discussion has been directed to the specific example process that we have investigated, we have provided a generic formulation of the gNWA and we have commented on various features that are relevant for more complicated processes. The method presented here should therefore be transferable to processes with more external legs, with a more complicated structure of IR divergencies, and to cases where the interference arises between particles of non-zero spin.

Chapter 10.

Interference and complex phase effects in Higgs searches at the LHC

After the methodological studies in the previous chapters about the approximation of interference terms, we will now investigate phenomenological implications of interference effects on the interpretation of searches at the LHC for additional neutral MSSM Higgs bosons. In particular, we focus on interference effects between the heavy Higgs bosons h_2 and h_3. They are nearly mass-degenerate in large parts of the parameter space. In the context of $\mathcal{CP}$-violating mixing, their interference term is expected to become significant so that one needs to re-evaluate the limits that have been obtained by assuming real MSSM parameters and neglecting interference effects between all neutral Higgs bosons.

In this chapter, we briefly quote the properties of the discovered Higgs boson and summarise the search strategies for additional Higgs bosons at the LHC. Beyond the assumptions employed so far in the collider searches, we examine the overall effect of a complex phase on the cross section $\sigma(b\bar{b} \to \tau^+\tau^-)$ with s-channel Higgs exchange. Furthermore, we distinguish the overall phase effect from the genuine interference effect.

10.1. Status of Higgs searches interpreted in MSSM scenarios

A Higgs boson has been discovered by ATLAS [5] and CMS [6]. The combined analyses of both experiments result in a mass of $M_h^{\text{exp}} = 125.09 \pm 0.24\,\text{GeV}$ [223]. Investigations of the spin J and tensor coupling structure reveal that this particle has spin 0 [224, 225]. All measurements are up to now consistent with the SM hypothesis of a $\mathcal{CP}$-even scalar with $J^{\mathcal{PC}} = 0^{++}$ [226, 227], but a substantial admixture of a $\mathcal{CP}$-odd component cannot be ruled out at the present level of sensitivity. The Higgs boson is searched for in several bosonic ($\gamma\gamma$, ZZ, $Z\gamma$, WW) and fermionic ($\tau^+\tau^-$, $\mu^+\mu^-$, $b\bar{b}$) decay channels in combination with various production modes (gluon fusion, weak vector boson fusion, Higgs strahlung and in association with $t\bar{t}$) [228, 229]. So far, the $\gamma\gamma, ZZ, WW$ decay modes have been established and there is evidence for the decay into $\tau^+\tau^-$ [230, 231]. Among the production modes, the $t\bar{t}$-associated production has the largest uncertainty, but the best-fit results for the signal strengths, branching fractions and couplings to fermions and vector bosons determined from those analyses are in general compatible with the expectations for a SM Higgs boson of the measured mass, see Refs. [228, 229] and references therein.

Although the discovered scalar has quite SM Higgs-like properties, significant deviations from the SM are possible in individual Higgs couplings, cross sections and branching ratios. Moreover, the SM might be the low-energy limit of a more fundamental theory with more than one Higgs boson. Any viable BSM model must accomodate a SM-like Higgs boson with the measured mass. Both at LEP [232] and at the Tevatron [233–236], searches for several Higgs bosons in a two-Higgs-doublet model and the MSSM have been performed.

At the LHC, neutral MSSM Higgs bosons are for low and medium values of $\tan\beta$ predominantly produced in gluon fusion, $gg \to h_a$ $(a = 1, 2, 3)$. At high $\tan\beta$, the production in association with a pair of bottom quarks dominates due to the enhanced bottom Yukawa coupling involved in $b\bar{b} \to h_a$ (in the five-flavour scheme where the bottom quark is regarded as a parton in the proton) and in $gg \to b\bar{b}h_a$ (in the four-flavour scheme whithout a bottom parton density distribution in the proton). Searches for neutral MSSM Higgs bosons during Run I of the LHC have been carried out in the $\tau^+\tau^-$ [237–240], in the $\mu^+\mu^-$ [241–243] and in the $b\bar{b}$ [244] decay channels, but no evidence for additional Higgs bosons has been found yet. The decay modes to down-type fermions are enhanced at large $\tan\beta$ whereas the branching ratios of the heavy Higgs bosons into vector bosons vanish in the decoupling limit (see Sect. 3.3.4.4). The non-observation up to now can be translated into limits of the underlying parameters of the hypothesized model, here the MSSM, where the $\tau^+\tau^-$-channel provides much stronger constraints than the $\mu^+\mu^-$ final state.

The results of the searches are on the one hand reported as nearly model-independent limits on the product of the on-shell production cross section (separately in the gg and $b\bar{b}$ production mechanism) and the branching ratio (into $\tau^+\tau^-$, $\mu^+\mu^-$ or $b\bar{b}$) of a scalar resonance as a function of its mass, assuming a narrow width. On the other hand, these limits are interpreted in example scenarios within the MSSM parameter space. The analyses with $\tau^+\tau^-$ final states by CMS [239] and ATLAS [240] are presented in several MSSM benchmark scenarios such as the (updated) $M_h^{\rm max}$ and the $M_h^{\rm mod\pm}$ scenarios defined in Refs. [167, 169]. Furthermore, the CMS search [239] is also interpreted in the other benchmark scenarios of Ref. [167]. In the $M_h^{\rm max}$ scenario, the radiative corrections to the lightest Higgs boson mass are maximised. In the decoupling region and for $\tan\beta \gtrsim 10$, the prediction for M_{h_1} overshoots the measured mass of the SM-like Higgs boson in this scenario. Hence, if the observed state should be identified with the lightest MSSM Higgs boson, the allowed parameter space in the $M_h^{\rm max}$ scenario is severely restricted. However, reducing the stop mixing parameter yields a value of M_{h_1} that is in agreement with the measured Higgs mass within the theory-dominated (conservative) uncertainty of $\Delta M_{h_1} = 3\,\text{GeV}$ in the major part of the parameter space. This is realised in the $M_h^{\rm mod\pm}$ scenario, where the $\pm$ refers to the sign of X_t in the particular version of the scenario. The standard value of the higgsino mass parameter is $\mu = 200\,\text{GeV}$ in the $M_h^{\rm mod\pm}$ scenario. However, leading threshold corrections Δ_b to the relation between the bottom quark mass and the bottom Yukawa coupling are generated by $\tilde{b}\tilde{g}$ and $\tilde{t}\tilde{\chi}^\pm$ one-loop diagrams which depend on μ and $\tan\beta$ and modify the bottom Yukawa coupling.

For large values of $\tan\beta$, these terms can become very important. At the two-loop level, the Δ_b corrections also enter the Higgs mass prediction. As a consequence, the exclusion bounds from searches for heavy MSSM Higgs bosons are affected by Δ_b and therefore by the absolute values and signs of $\mu m_{\tilde{g}}$ and μA_t. In order to account for this dependence, the variation of $\mu = \pm 200, \pm 500, \pm 1000$ GeV within the benchmark scenarios was proposed in Refs. [167, 245, 246].

In Fig. 10.1, we show the exclusion bounds obtained with `HiggsBounds-4.2.0` [247–250] linked to `FeynHiggs-2.10.2` in the $M_h^{\mathrm{mod}+}$ scenario for the default value of $\mu = 200$ GeV (green) and for $\mu = 1000$ GeV (orange) as one of the suggested modifications. `HiggsBounds` confronts predictions of cross sections, branching ratios, masses and total widths of neutral and charged Higgs bosons with cross section limits from LEP, the Tevatron and the LHC. Based on the expected limit of a model prediction, the analysis with the highest sensitivity is determined for each Higgs boson of the model. If the model prediction for this particular analysis is larger than the observed limit, the model point is excluded at the 95% confidence level (CL).

Fig. 10.1 shows the $M_{H^\pm} - \tan\beta$ plane of the $M_h^{\mathrm{mod}+}$ scenario where the horizontal band at low $\tan\beta$ is excluded by LEP results whereas the upper left part of the plane is excluded by searches at the LHC. The scenario with $\mu = 1000$ GeV provides stronger limits because in this case the decay channel of a heavy Higgs boson into higgsino-like neutralinos and charginos is kinematically closed. Consequently, the branching ratios of the visible channels into $\tau^+\tau^-$ and $\mu^+\mu^-$ are increased so that the searches become more sensitive.

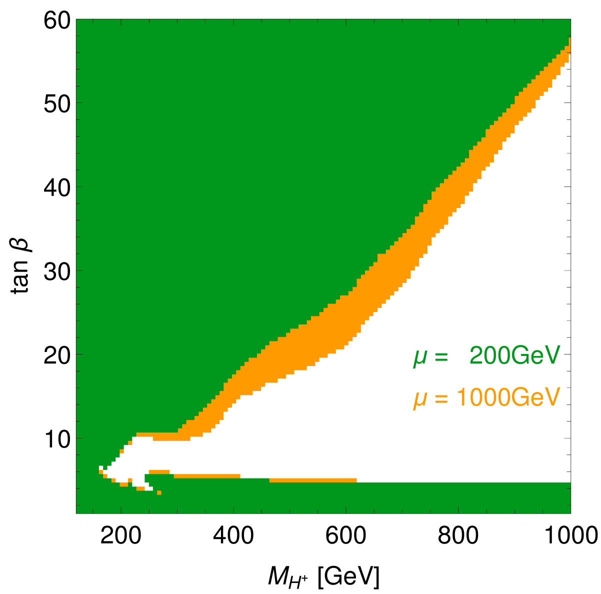

Figure 10.1.: Excluded parameter regions in the $M_h^{\mathrm{mod}+}$ scenario obtained with `HiggsBounds` for $\mu = 200$ GeV (green) and $\mu = 1000$ GeV (orange).

The unexcluded parameter region is mostly compatible with the measured mass of about 125 GeV within the theoretical uncertainty of about ± 3 GeV [167]. Thus the scenario is phenomenologically interesting. Instead of requiring the lightest neutral Higgs boson h_1 to have a mass close to the observed one, the role of the observed state could in principle also be played by the second lightest neutral MSSM Higgs boson [167, 251, 252]. Here, however we focus on scenarios where the additional Higgs bosons are heavier than $M_h^{\rm exp}$.

One such benchmark scenario is the light $\tilde{\tau}$ scenario [167] characterised by $\mu = 500\,\text{GeV}$, $A_{\tilde{\tau}} = 0$ and $M_{\tilde{l}_3} = 245\,\text{GeV}$ (the other parameters can be found in Tab. A.1). The phenomenology of this scenario features an enhanced diphoton rate of Higgs decays, but in the context of $\mathcal{CP}$-violation we are mostly interested in the consequences of the enhanced μ-parameter. In Sect. 10.2.1, we will study this scenario in addition to the $M_h^{\rm mod+}$ scenario with $\mu = 200\,\text{GeV},\ 500\,\text{GeV},\ 1000\,\text{GeV}$.

10.2. Relative impact of ϕ_{A_t} on cross sections

Factorising the search results into the production and decay part, as employed in `HiggsBounds` and experimental analyses, limits the applicability by the same conditions as those of the sNWA, see Sect. 7.2.2, for example assuming small widths of all Higgs bosons compared to their masses and vanishing interference terms. Furthermore, no complex MSSM parameters have been considered up to now in the presentation of LHC limits in benchmark scenarios. We therefore propose to take interference effects between several Higgs resonances into account (which may already arise in the case of real parameters, though restricted to low values of M_A and large $\tan\beta$) and to allow for complex parameters in a modification of the already existing benchmark scenarios. In particular, we consider the phase ϕ_{A_t} of the trilinear coupling of $\tilde{t}$ squarks, which is least restricted by current experimental bounds (see Sect. 3.4) and has an important effect on Higgs observables owing to the numerical relevance of stop loops. By setting

$$A_b = A_\tau = A_t, \tag{10.1}$$

all trilinear couplings of sfermions from the third generation obtain the same phase. We evaluate the effect of ϕ_{A_t} on the cross section $\sigma(b\bar{b} \to \tau^+\tau^-)$ mediated by Higgs bosons while neglecting non-Higgs contributions. On the one hand, we perform the full propagator calculation including momentum dependent mixing self-energies as described in Eq. (6.17). On the other hand, we apply the approximation of Breit-Wigner propagators combined with the on-shell $\hat{\mathbf{Z}}$-factors according to Eq. (6.21). The couplings of the Higgs bosons to a pair of bottom quarks or tau leptons are given in Eq. (3.49). We compute the relative effect of the complex phase ϕ_{A_t} on the cross section with respect to the cross section in the case of real parameters. Furthermore we evaluate the relative contribution of the interference term compared to the incoherent sum of the individual resonances. Our approach is to calculate the higher-order propagator corrections, but to treat the vertices only at the tree level since the impact of vertex corrections factorises in this context. Vertex corrections to the production and decay subprocesses are already contained in e.g. `FeynHiggs` [67, 146, 149, 150] and other public codes that compute Higgs cross sections and branching ratios. Non-factorisable box diagrams are not covered by our approach, but they are expected to be numerically suppressed in the Higgs resonance region. In the comparison of model predictions and experimental results, we will combine the relative interference or complex phase contribution based on propagator type corrections to rescale the product of state-of-the-art production cross sections and branching ratios in order to obtain an improved prediction.

We determine which two among the three neutral MSSM Higgs bosons are closest in mass. Accordingly, we calculate the cross section at the centre-of-mass energy

$$\sqrt{s} = \overline{M} = \begin{cases} \frac{1}{2}(M_{h_2} + M_{h_1}), & \text{if } \; M_{h_2} - M_{h_1} < M_{h_3} - M_{h_2} \\ \frac{1}{2}(M_{h_2} + M_{h_3}), & \text{if } \; M_{h_2} - M_{h_1} \geq M_{h_3} - M_{h_2} \end{cases} \tag{10.2}$$

so that h_2 is always involved in the degeneracy.

10.2.1. Overall non-zero phase effects

A complex phase influences several quantities, such as the propagator-type corrections and the resulting $\hat{\mathbf{Z}}$-factors, which turn from the 2×2 case of real parameters to 3×3 matrices in the presence of a non-vanishing phase, enabling especially the $\mathcal{CP}$-violating mixing between h_2 and h_3. In turn, the mixing structure alters the couplings and total widths. Another important effect is visible in the masses, which are via loop diagrams sensitive to the full particle content and parameters from all sectors of the MSSM, particularly to A_t and its phase. As an example, Fig. 10.2 shows the dependence of M_{h_1}, obtained with `FeynHiggs`, on ϕ_{A_t} for $M_{H^\pm} = 250\,\text{GeV}$ (blue) and $M_{H^\pm} = 600\,\text{GeV}$ (red) with $\tan\beta = 10$ (dotted) and $\tan\beta = 30$ (solid) in the $M_h^{\text{mod}+}$ scenario with $\mu = 200\,\text{GeV}$. A non-zero phase reduces the mass value with respect to $M_{h_1}(\phi_{A_t} = 0)$, and M_{h_1} has a minimum around $\phi_{A_t} = \pi$, i.e. for a negative, real A_t. In scenarios that are in accordance with the measured Higgs mass, the predicion of M_{h_1} should not deviate from M_h^{exp} by more than ΔM_{h_1} as a necessary condition. The allowed mass window is indicated in grey for $\Delta M_{h_1} = 3\,\text{GeV}$. If the theory uncertainty shrank to $\Delta M_{h_1} = 2\,\text{GeV}$, the allowed masses would correspond to the range limited by the grey, dashed lines. For $\tan\beta = 10$ in this example, $M_{h_1}(\phi_{A_t} = 0)$ is close to 125 GeV, while around $\phi_{A_t} \simeq \pi$ values slightly below the uncertainty band are obtained[1]. In our investigation of non-zero phase effects in several scenarios, we will always exclude the parameter regions where the lightest Higgs mass $M_{h_1}(\phi_{A_t})$ is in conflict with the allowed range of $M_h^{\text{exp}} \pm 3\,\text{GeV}$.

In order to quantify the relative impact of ϕ_{A_t} on a cross section σ, we define the following quantity

$$\delta = \frac{\sigma(\phi_{A_t} \neq 0)}{\sigma(\phi_{A_t} = 0)} - 1, \tag{10.3}$$

and evaluate the cross section $\sigma(b\bar{b} \to \tau^+\tau^-)$ using the full mixing propagators. Fig. 10.3 provides the numerical results for δ in the $M_h^{\text{mod}+}$ scenario and the light $\tilde{\tau}$ scenario. In most of the $M_{H^\pm}$-$\tan\beta$ plane, Fig. 10.3(a) shows moderate negative effects down to $\delta \simeq -10\%$ in the $M_h^{\text{mod}+}$ scenario with the default value of $\mu = 200$, and $\phi_{A_t} = \pi/4$ in comparison

[1]This could be compensated by increasing $|A_t|$.

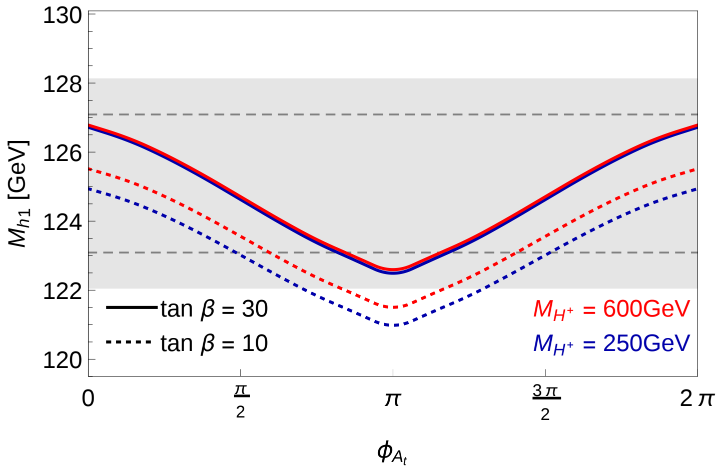

Figure 10.2.: Dependence of M_{h_1} (from `FeynHiggs`) on ϕ_{A_t} for $M_{H^\pm} = 250\,\text{GeV}$ (blue) and $M_{H^\pm} = 600\,\text{GeV}$ (red); $\tan\beta = 10$ (dotted) and $\tan\beta = 30$ (solid) in the $M_h^{\text{mod+}}$ scenario with $\mu = 200\,\text{GeV}$. The mass window of $M_h^{\text{exp}} \pm \Delta M_{h_1}$ is shaded in grey for $\Delta M_{h_1} = 3\,\text{GeV}$. The dashed, grey lines indicate $\Delta M_{h_1} = 2\,\text{GeV}$.

to the original scenario with real parameters. This means that the cross section including the non-vanishing value of ϕ_{A_t} is slightly smaller that the cross section for $\phi_{A_t} = 0$. The red dashed line indicates the $\delta = 0$ contour of a vanishing net effect. In the corner of relatively low $M_{H^\pm}$ and $\tan\beta$, the cross section $\sigma(\phi_{A_t} = \pi/4)$ is larger than $\sigma(\phi_{A_t} = 0)$. The white areas are excluded in this scenario owing to $|M_{h_1}(\phi_{A_t} = \pi/4) - M_h^{\text{exp}}| > 3\,\text{GeV}$. Further constraints from collider limits will be considered in Sect. 10.3; here we focus on describing the change of cross sections.

In Fig. 10.3(b) we notice a stronger reduction of the cross section caused by the maximal phase $\phi_{A_t} = \pi/2$, down to $\delta \simeq -30\%$, and a smaller region where the cross section is enhanced.

Fig. 10.3(c) differs from Fig. 10.3(b) by the value of μ: as recommended in Ref. [167], we consider also $\mu = 500\,\text{GeV}$ within the $M_h^{\text{mod+}}$ scenario. As pointed out in Ref. [253], $\mathcal{CP}$-violating terms in the matrix of squared Higgs masses scale with $\text{Im}\,[\mu A_t]\,/M_{\text{SUSY}}^2$. Thus, the enhanced higgsino mass parameter leads to more sizeable effects of ϕ_{A_t} on σ, where δ can be as low as 60% in a small region at relatively low $M_{H^\pm}$ and $\tan\beta$. In addition, δ is smaller than -30% in the upper left half of the analysed parameter plane.

This significant suppression of σ for $\mu = 500\,\text{GeV}$ does not exclusively occur in the $M_h^{\text{mod+}}$ scenario. It can be observed, for example, also in the light $\tilde{\tau}$ scenario whose default value of μ is 500 GeV, see Fig. 10.3(d). The contours of δ from $\phi_{A_t} = \pi/2$ resemble the pattern in the $M_h^{\text{mod+}}$ scenario with the same values of μ and ϕ_{A_t}.

Hence, our analysis of modified cross sections in presence of $\phi_{A_t} \neq 0$ is in agreement with the predicted strong dependence of $\mathcal{CP}$-violating effects on the imaginary part of the product of μA_t. The effects for $\mu = 200\,\text{GeV}$ and $\phi_{A_t} = \pi/4$ in the $M_h^{\text{mod+}}$ scenario are of the order of a few percent and therefore expected to be hardly detectable. In the same scenario, but with the maximal $\phi_{A_t} = \pi/2$, the most significant effects arise in the deeply excluded region at low $M_{H^\pm}$ and very high $\tan\beta$, but the moderate effects in the center of the analysed parameter plane might be required to be included for an accurate interpretation of Higgs searches in a complex benchmark scenario. The impact of ϕ_{A_t} is even more pronounced in combination with a larger value of μ so that effects of the order of those in Figs. 10.3(c) and 10.3(d) are expected to lead to a significant shift of exclusion bounds obtained for the corresponding scenarios with real parameters. We will recalculate exclusion limits in Sect. 10.3, where we will directly compare the theoretical prediction with and without the interference term.

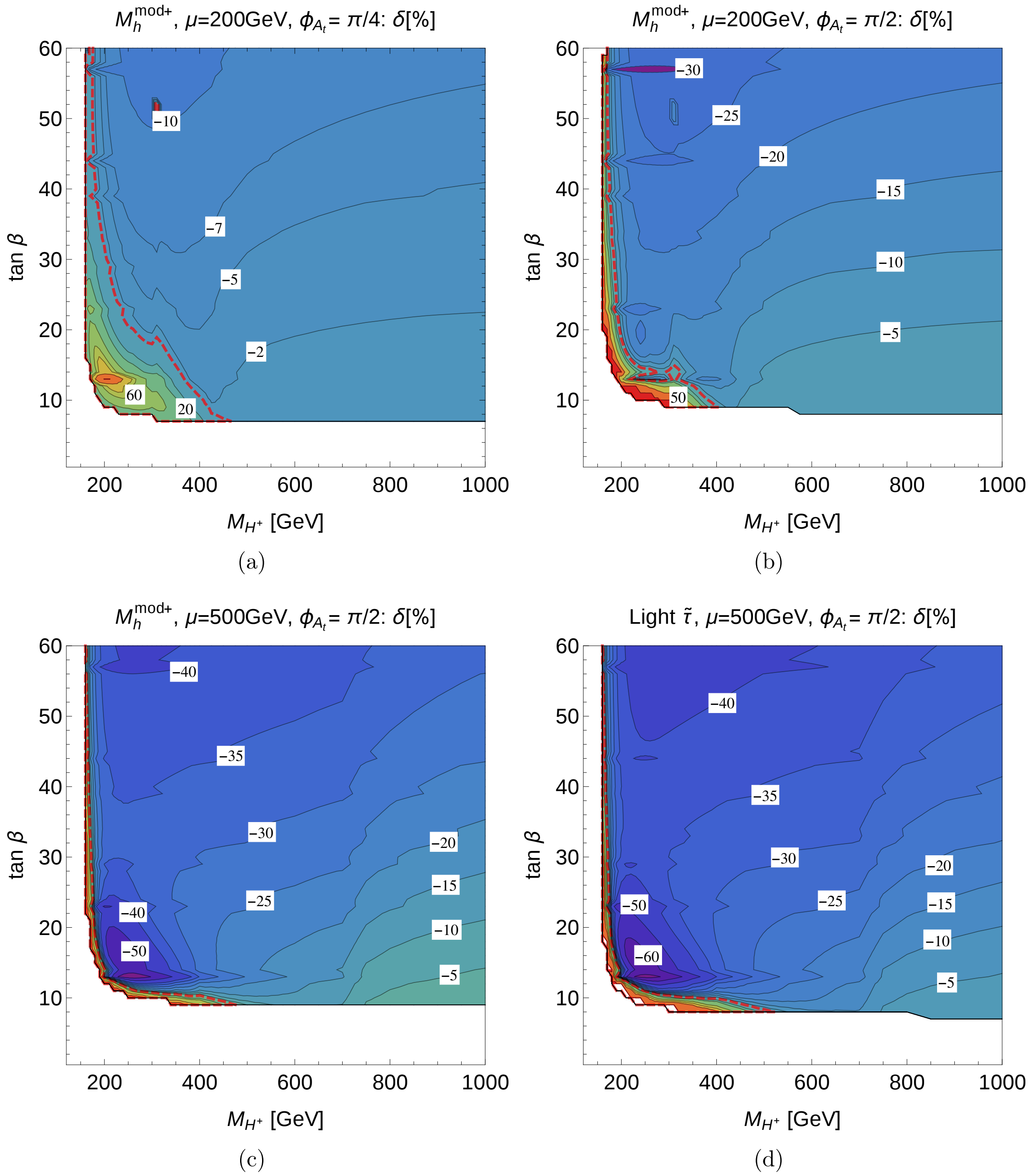

Figure 10.3.: Relative impact $\delta = (\sigma_\phi - \sigma_0)/\sigma_0$ of the phase $\phi \equiv \phi_{A_t}$ on the cross section $\sigma(b\bar{b} \to \tau^+\tau^-)$ via Higgs propagators including the full mixing. **(a-c):** $M_h^{\text{mod+}}$ scenario with $\mu = 200\,\text{GeV}$ and $\phi_{A_t} = \pi/4$ **(a)** versus $\phi_{A_t} = \pi/2$ **(b)** and $\mu = 500\,\text{GeV}$, $\phi_{A_t} = \pi/2$ **(c)**. Light $\tilde{\tau}$ scenario with $\mu = 500\,\text{GeV}$, $\phi_{A_t} = \pi/2$ **(d)**. The white areas correspond to $|M_{h_1}(\phi_{A_t}) - M_h^{\text{exp}}| > 3\,\text{GeV}$.

10.2.2. Distinction between interference and other phase effects

In the previous section, we have discussed the effect of the phase ϕ_{A_t} by comparing the cross section $\sigma(\phi_{A_t} \neq 0)$ in the case of complex parameters with $\sigma(\phi_{A_t} = 0)$, both calculated using the full mixing propagators. In this section we would like to disentangle the *overall* phase effect (influencing not only the interference term, but also masses, couplings and widths) from the *pure interference* effect. We investigate both effects in the $M_h^{\text{mod+}}$ scenario with $\mu = 1000\,\text{GeV}$. In order to avoid tension with present or future EDM constraints on ϕ_{A_t} (see Sect. 3.4), we restrict this phase to the value of $\pi/4$ in this section.

Fig. 10.4(a) shows the overall phase effect δ defined in Eq. (10.3) based on the full propagators. Similar to Figs. 10.3(c) and 10.3(d), the most significant effects arise for low $M_{H^\pm}$ and low $\tan\beta$, here down to a minimum of $\delta = -96.8\%$, whereas in the central part of the parameter plane δ ranges from -10% to -20%.

In contrast, for the determination of the pure interference, we switch to the Breit-Wigner propagators where the mixing is expressed by the $\hat{\mathbf{Z}}$-factors. The performance of this approximation confronted with the full propagators has been examined in Chapter 6 where we found very accurate agreement between both calculations, with only small deviations in scenarios of large mixing. The $M_h^{\text{mod+}}$ scenario with $\mu = 1000\,\text{GeV}$ and $\phi_{A_t} = \pi/4$ exhibits indeed substantial mixing. We therefore calculate the relative deviation ϵ between the cross section σ_{full} based on the full propagators and the cross section $\sigma_{\text{coh}}^{\text{BW}\hat{\mathbf{Z}}}$ based on the coherent sum of Breit-Wigner propagators with $\hat{\mathbf{Z}}$-factors, where the total widths are obtained from the imaginary parts of the complex poles,

$$\epsilon = \frac{\sigma_{\text{coh}}^{\text{BW}\hat{\mathbf{Z}}}(\phi_{A_t})}{\sigma_{\text{full}}(\phi_{A_t})} - 1. \tag{10.4}$$

Fig. 10.4(b) reveals that both methods agree very well, with a maximum deviation of $\pm 2\%$ around $M_{H^\pm} = 500\,\text{GeV},\ \tan\beta = 28$ and of about 0.8% along the green band. Otherwise the two calculations lead to the same results within 0.1%. Hence the use of Breit-Wigner propagators is suitable in this context. As highlighted in Sect. 6.2.4, the formulation of the Higgs propagators in the mass basis conveniently enables the separation of the individual resonances. Their incoherent sum is denoted by σ_{incoh} and the coherent sum including the interference term by σ_{coh}, both calculated with $\phi_{A_t} \neq 0$. As a measure of the relative contribution of the interference term

$$\sigma_{\text{int}} = \sigma_{\text{coh}} - \sigma_{\text{incoh}}, \tag{10.5}$$

we define

$$\eta = \frac{\sigma_{\text{coh}}(\phi_{A_t})}{\sigma_{\text{incoh}}(\phi_{A_t})} - 1 = \frac{\sigma_{\text{int}}(\phi_{A_t})}{\sigma_{\text{incoh}}(\phi_{A_t})}. \tag{10.6}$$

Fig. 10.4(c) displays η, which indicates a destructive interference, i.e. $\eta < 0$, throughout the parameter plane (apart from the red region of $0 \leq \eta < 0.4\%$ in the lower left corner and the narrow stripe at $M_{H^\pm} \leq 130\,\text{GeV}$). η reaches a minimum of -96.9%

at $M_{H^\pm} = 480\,\text{GeV}$, $\tan\beta = 29$ so that the cross section is almost completely erased by the drastic, negative interference term. Around this minimum, there is a "valley" of substantial destructive interference, covering large parts of the $M_{H^\pm}$-$\tan\beta$ plane.

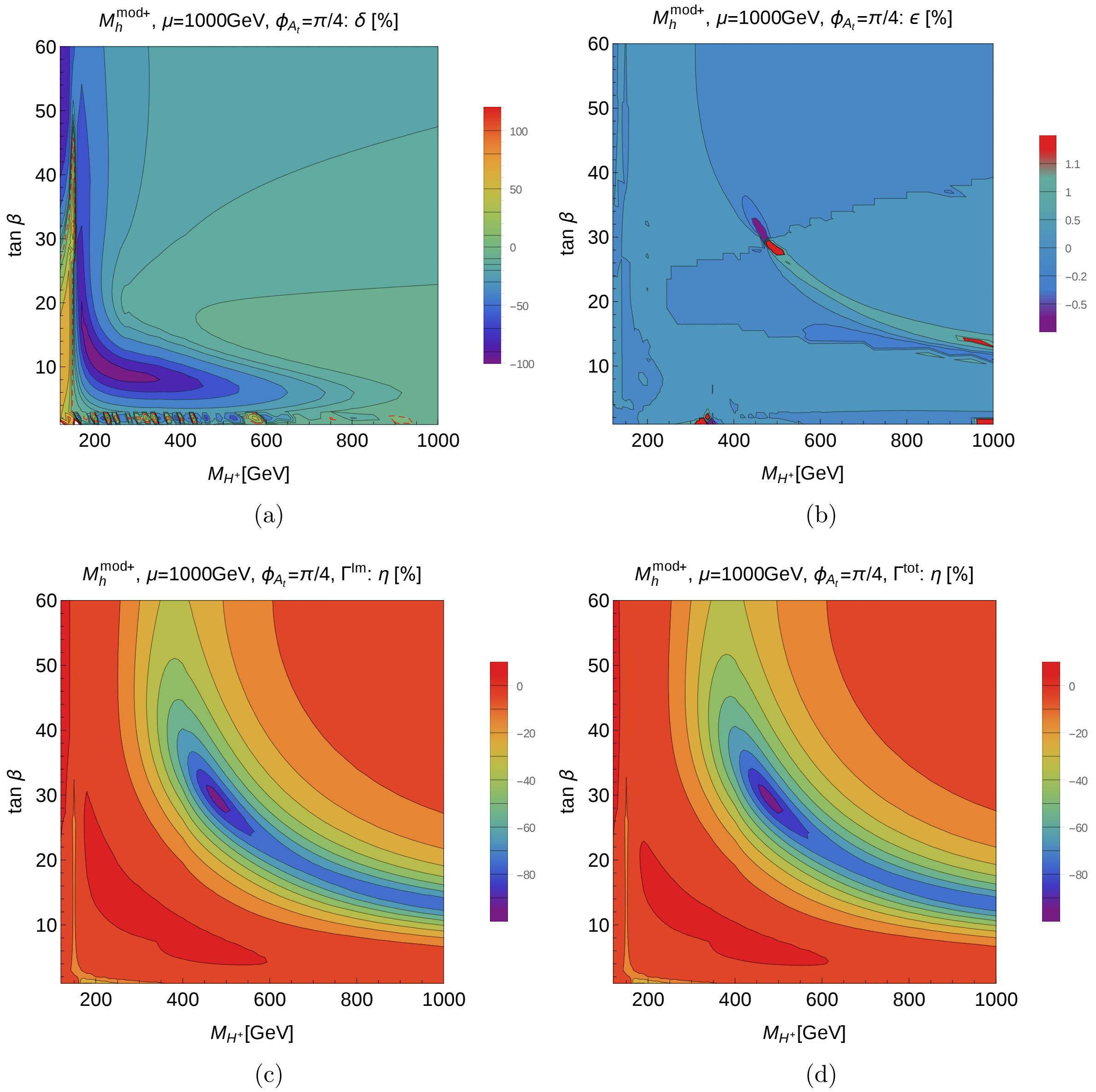

Figure 10.4.: Impact of $\phi_{A_t} = \pi/4$ in the $M_h^{\text{mod+}}$ scenario with $\mu = 1000\,\text{GeV}$ on the cross section $\sigma(b\bar{b} \to \tau^+\tau^-)$ via neutral Higgs bosons: **(a)** overall phase effect δ, **(b)** relative difference ϵ between the full propagator mixing and the Breit-Wigner approximation with $\hat{\mathbf{Z}}$-factors using the total width Γ^{Im} from the imaginary part of the complex pole, **(c)** pure interference effect η based on Breit-Wigner propagators with Γ^{Im}, and **(d)** η based on Breit-Wigner propagators with the total width Γ^{tot} from `FeynHiggs`.

In Fig. 10.4(c), the Breit-Wigner functions Δ_a^{BW} are based on the total widths $\Gamma_{h_a}^{\mathrm{Im}}$ obtained from the imaginary part of the complex pole, see Eq. (6.40). By contrast, the total widths $\Gamma_{h_a}^{\mathrm{tot}}$ as the sum of the partial widths according to Eq. (6.39) from `FeynHiggs` are inserted into the Breit-Wigner propagators in Fig. 10.4(d). Due to the $p^2 = 0$ approximation of the partial two-loop self-energies used in `FeynHiggs`, $\Gamma_{h_a}^{\mathrm{Im}}$ corresponds to a tree-level width. The total width $\Gamma_{h_a}^{\mathrm{tot}}$ reaches significantly larger values than $\Gamma_{h_a}^{\mathrm{Im}}$, particularly in the interference region due to the $\hat{\mathbf{Z}}$-factor enhancement. As a consequence, the cross section is suppressed by the larger width, as in Sect. 6.5, resulting in a substantial difference between $\sigma_{\mathrm{coh}}^{\mathrm{BW}\hat{\mathbf{Z}}}(\Gamma_{h_a}^{\mathrm{Im}})$ and $\sigma_{\mathrm{coh}}^{\mathrm{BW}\hat{\mathbf{Z}}}(\Gamma_{h_a}^{\mathrm{tot}})$. However, the pronounced dependence on Γ_{h_a} cancels out in the ratio in Eq. (10.6) so that the results of η in Fig. 10.4(d) are nearly identical to those in Fig. 10.4(c). Within the region of most significant interference, where $\eta \leq -50\%$, both implementations of the total width agree with each other at a precision of 2%. For $M_{H^\pm} \lesssim 300\,\mathrm{GeV}$ or $\tan\beta \lesssim 8$, the two methods lead to slightly different results of η because in that region the mass differences between the M_{h_a} are larger than in the decoupling regime. So the precise values of the total widths do matter in the question if or how much two close-by, but not exactly degenerate, resonances overlap. This affects mainly the interference between h_1 and h_2. In the remaining parameter plane, h_2 and h_3, which are involved in the relevant interference, are quasi degenerate while h_1 is much lighter. Therefore the $h_2 - h_3$ overlap is equally fulfilled also for a smaller width because

$$R_{32} := \frac{M_{h_3} - M_{h_2}}{\Gamma_{h_2} + \Gamma_{h_3}} \ll 1 \tag{10.7}$$

(see Fig. 10.5(a)) for any method of the total width, and the relative deviation of the two versions of η does not exceed 5%. Hence, while $\Gamma_{h_a}^{\mathrm{tot}}$ gives a more complete result, both versions of η are equally suited for determining the impact of the interference on exclusion bounds. Here we use $\Gamma_{h_a}^{\mathrm{Im}}$, which matches the method of full propagators.

In order to understand the location of the strongest interference, we examine the couplings that play a role in the interference term compared to those in the incoherent sum:

$$c_{23} = \frac{2\mathrm{Re}[g_{h_2\tau\tau}\, g_{h_2bb}\, g_{h_3\tau\tau}^{*}\, g_{h_3bb}^{*}]}{|g_{h_2\tau\tau}\, g_{h_2bb}|^2 + |g_{h_3\tau\tau}\, g_{h_3bb}|^2}, \tag{10.8}$$

where $g_{h_af\bar{f}}$ with $a = 1,2,3,\ f = \tau, b$ are the tree-level couplings $g_{if\bar{f}}$ from Eq. (3.49) for $i = h, H, A$, combined with two-loop $\hat{\mathbf{Z}}$-factors from `FeynHiggs-2.10.2` according to Eq. (5.73):

$$g_{h_af\bar{f}} = \sum_{i=h,H,A} \hat{\mathbf{Z}}_{ai} g_{if\bar{f}}. \tag{10.9}$$

Since the masses m_τ, m_b and other constants cancel out in Eq. (10.8), the ratio c_{23} is determined by the $\hat{\mathbf{Z}}$-factors and the angles $\cos\alpha$ and $\sin\beta$. Fig. 10.5(b) shows that c_{23} already indicates the interference region whereas effective couplings based on real $\mathbf{U}$-factors in Fig. 10.5(c) or the pure tree-level couplings in Fig. 10.5(d) yield a completely different pattern. The interference contribution in the squared matrix element is proportional to [45]

$$|\mathcal{M}|^2_{\text{int}} \propto c_\beta^{-4}\, 2\text{Re}\left[(c_\alpha^2 \hat{\mathbf{Z}}_{2H}\hat{\mathbf{Z}}^*_{3H} + s_\beta^2 \hat{\mathbf{Z}}_{2A}\hat{\mathbf{Z}}^*_{3A})^2 \Delta_2^{\text{BW}}(s)\Delta_3^{\text{BW}*}(s)\right]. \tag{10.10}$$

In the decoupling region of $m_A \gg M_Z$ and for $\tan\beta \gg 1$, the heavy Higgs bosons h_2 and h_3 have very similar masses $M_{h_2} \simeq M_{h_3}$ and widths $\Gamma_{h_2} \simeq \Gamma_{h_3}$ so that the product $\Delta_2^{\text{BW}}(s)\Delta_3^{\text{BW}*}(s) \simeq |\Delta_2^{\text{BW}}|^2$ becomes approximately real. In this limit, the relations $\hat{\mathbf{Z}}_{2H} \simeq \hat{\mathbf{Z}}_{3A}$ and $\hat{\mathbf{Z}}_{2A} \simeq -\hat{\mathbf{Z}}_{3H}$ and $\cos\alpha \simeq \sin\beta$ simplify Eq. (10.10) to:

$$|\mathcal{M}|^2_{\text{int}} \propto -8t_\beta^4\, (\text{Im}\hat{\mathbf{Z}}_{2H}\, \text{Re}\hat{\mathbf{Z}}_{2A} - \text{Re}\hat{\mathbf{Z}}_{2H}\, \text{Im}\hat{\mathbf{Z}}_{2A})^2\, |\Delta_2^{\text{BW}}(s)|^2. \tag{10.11}$$

Hence Eq. (10.11) reveals that in the decoupling limit the interference term of h_2 and h_3 can only contribute substantially if the two following conditions are met. Firstly, a large mixing is needed. This means that the 2-3 submatrix of $\hat{\mathbf{Z}}$ must not be purely diagonal ($\hat{\mathbf{Z}}_{2A} = \hat{\mathbf{Z}}_{3H} = 0$, $\hat{\mathbf{Z}}_{2H} = \hat{\mathbf{Z}}_{3A} = 1$) or purely off-diagonal ($\hat{\mathbf{Z}}_{2H} = \hat{\mathbf{Z}}_{3A} = 0$, $\hat{\mathbf{Z}}_{2A} = \hat{\mathbf{Z}}_{3H} = 1$), where one of the mass eigenstates would be a completely H-like scalar and the other a completely A-like pseudoscalar. Instead, all four involved $\hat{\mathbf{Z}}$-matrix elements should have non-vanishing values.

Secondly, a non-zero interference term requires imaginary parts of the $\hat{\mathbf{Z}}$-factors, which originate from the imaginary parts of the Higgs self-energies. Consequently, replacing the $\hat{\mathbf{Z}}$-factors by real $\mathbf{U}$-factors in an effective coupling approach renders the interference term zero in the decoupling limit even though the $\mathbf{U}$-matrix may contain equally large diagonal and off-diagonal elements. Even if the conditions of mixing elements and imaginary parts a fulfilled, there might still be a cancellation between the two terms within the bracket in Eq. (10.11).

Outside the decoupling limit, with unequal masses, widths and mixing properties of h_2 and h_3, the full product of angles from the couplings, $\hat{\mathbf{Z}}$-factors and complex Breit-Wigner functions has to be taken into account. Thereby, a significant interference term can also arise without the above-mentioned conditions. However, in the relevant part of the considered parameter plane, the decoupling limit is reached. Given the quasi-degeneracy of M_{h_2} and M_{h_3} shown in Fig. 10.5(a), the structure of the $\hat{\mathbf{Z}}$-matrix provides in fact a well-suited indication of the relevance of the interference term. In particular, the square of the bracket and the absolute square of the Breit-Wigner function in combination with the overall minus sign in Eq. (10.11) explain the observed *destructive* interference effect.

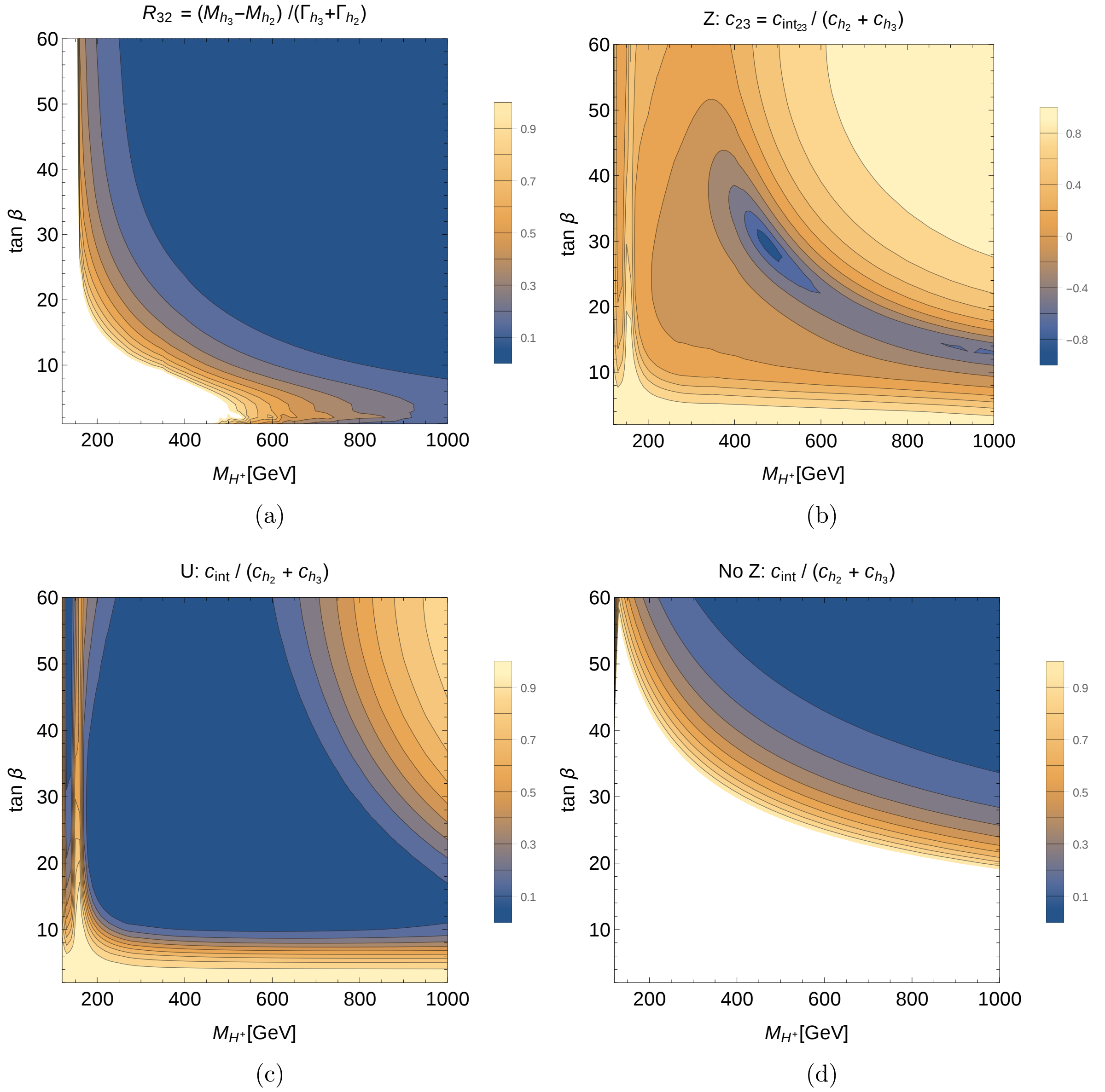

Figure 10.5.: **(a):** Ratio R_{32} of mass difference $M_{h_3} - M_{h_2}$ and sum of total widths $\Gamma_{h_2} + \Gamma_{h_3}$. **(b):** Ratio c_{23} of couplings in the interference term compared to those in the incoherent sum, including $\hat{\mathbf{Z}}$-factors; **(c):** as in (b), but including **U**-factors; **(d):** as in (b) , but for tree-level couplings with neither $\hat{\mathbf{Z}}$ nor **U**. All values are obtained from `FeynHiggs`.

10.3. Impact on exclusion limits

Given the remarkably large interference effects that we encountered in the previous section, it is necessary to reconsider the interpretation of experimental searches for additional neutral Higgs bosons if one wants to include complex phases in the MSSM. The interference terms between h_1, h_2, h_3 need to be included in the theoretical prediction in order to allow for a consistent comparison.

In order to include the interference effect in the evaluation within `HiggsBounds-4.2.0` [247–250], appropriate input data is needed in the form of modified individual contributions of h_1, h_2 and h_3. Therefore, the overall interference σ_{int} term is split into the three combinations of h_a and h_b $(a, b = 1, 2, 3)$:

$$\sigma = \sigma_{h_1} + \sigma_{h_2} + \sigma_{h_3} + \sigma_{\text{int}_{12}} + \sigma_{\text{int}_{13}} + \sigma_{\text{int}_{23}} \tag{10.12}$$

$$= \sigma_{h_1}\left(1 + \frac{\sigma_{\text{int}_{12}} + \sigma_{\text{int}_{13}}}{2\,\sigma_{h_1}}\right) + \sigma_{h_2}\left(1 + \frac{\sigma_{\text{int}_{12}} + \sigma_{\text{int}_{23}}}{2\,\sigma_{h_2}}\right) + \sigma_{h_3}\left(1 + \frac{\sigma_{\text{int}_{13}} + \sigma_{\text{int}_{23}}}{2\,\sigma_{h_3}}\right) \tag{10.13}$$

$$= \sigma_{h_1}(1 + \eta_1) + \sigma_{h_2}(1 + \eta_2) + \sigma_{h_3}(1 + \eta_3), \tag{10.14}$$

where the individual interference contributions η_a for each Higgs boson h_a and $b, c \neq a$ are defined as

$$\eta_a = \frac{\sigma_{\text{int}_{\text{ab}}} + \sigma_{\text{int}_{\text{ac}}}}{2\,\sigma_{h_a}}. \tag{10.15}$$

The η_a are applied to modify the prediction of $\sigma(b\bar{b} \to h_a)$ in the input data for `HiggsBounds` by rescaling

$$\frac{\sigma^{\text{MSSM}}(b\bar{b} \to h_a)}{\sigma^{\text{SM}}(b\bar{b} \to h_a)} \quad \longrightarrow \quad \frac{\sigma^{\text{MSSM}}(b\bar{b} \to h_a)}{\sigma^{\text{SM}}(b\bar{b} \to h_a)} \cdot (1 + \eta_a) \tag{10.16}$$

for $a = 2$ and 3 while the effect for h_1 can be neglected in the present analysis. `HiggsBounds` then compares the modified production ratio, normalised by the SM expectation, times the MSSM branching ratio of $h_a \to \tau^+\tau^-$ with the observed limit. The reduced rates on account of the destructive interference term between h_2 and h_3 lead to an interesting outcome: Some parameter points that are excluded when the interference term is not taken into account despite the non-vanishing value of $\phi_{A_t} = \pi/2$ or in the $\mathcal{CP}$-conserving case where the interference term is absent have a model expectation smaller than the observed limit if the $\mathcal{CP}$-violating interference term is included. Consequently they can no longer be excluded at the 95% CL. For the $M_h^{\text{mod}+}$ scenario with $\mu = 1000$ GeV and $\phi_{A_t} = \pi/4$, such an effect is shown in Fig. 10.6, where the blue region corresponds to the conventional use of `HiggsBounds` based on the sNWA, i.e. neglecting the interference term. In contrast, the interference term parametrised by η_2 and η_3 is taken into account in the results shown in red. We notice that a substantial, previously excluded area centered between $M_{H^\pm} \sim 450$ GeV and 700 GeV for $\tan\beta$ between roughly 18 and 32 remains now open, following the shape of the region where the interference effect is most significant in Fig. 10.4(c). Furthermore, the exclusion bounds are slightly weakened in the high-$M_{H^\pm}$ range.

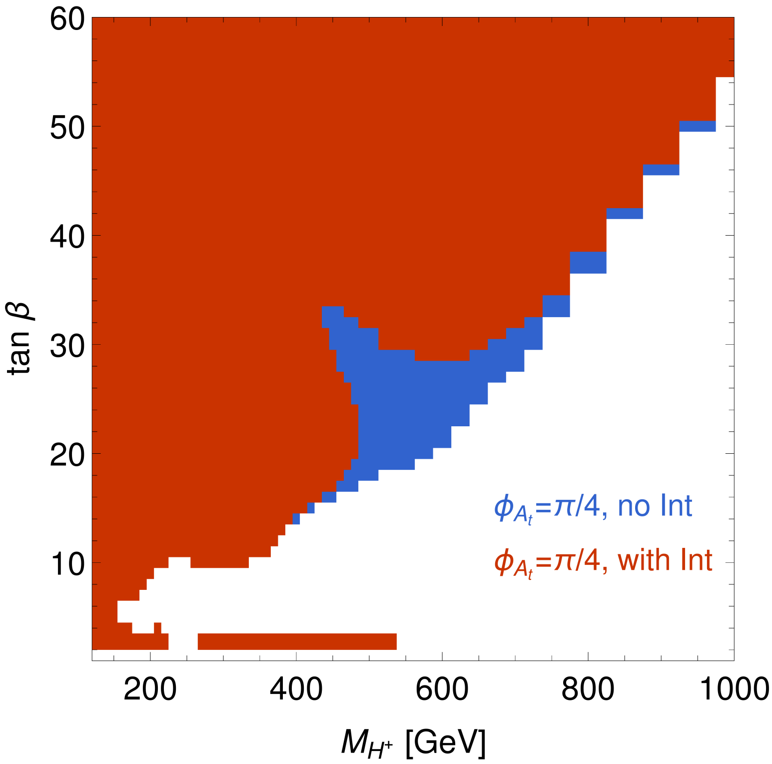

Figure 10.6.: Parameter regions excluded by `HiggsBounds` for $\mu = 1000\,\text{GeV}$, $\phi_{A_t} = \pi/4$ without the interference term (blue) and including the interference term (red) by modifying the input data for `HiggsBounds` with η (see text).

10.4. Summary and outlook: $\mathcal{CP}$-violating interference in LHC Higgs searches

In this chapter, we have investigated the impact of the phase ϕ_{A_t} on the cross section $\sigma(b\bar{b} \to \tau^+\tau^-)$ via Higgs exchange, both in the full propagator calculation and in the approach of Breit-Wigner propagators and have found very good agreement between these two methods. A complex phase does not only give rise to a $\mathcal{CP}$-violating interference term, but it also affects for example masses, widths and the mixing structure. The effect of ϕ_{A_t} is amplified by a large value of μ, which we evaluated for different combinations of μ and ϕ_{A_t}.

In a second step, we disentangled the overall phase effect from the genuine interference effect. By exploiting the formalism of the Breit-Wigner propagators in the mass basis to treat each resonance separately, we calculated the difference between the coherent and incoherent sum of the contributions of three neutral MSSM Higgs bosons. We found very large, negative interference effects in the $M_h^{\text{mod}+}$ scenario with $\mu = 1000\,\text{GeV}$ and

$\phi_{A_t} = \pi/4$, which arise from the strong propagator mixing that is also reflected by the $\hat{\mathbf{Z}}$-matrix. In particular, the imaginary parts of the Higgs self-energies are essential for a sizeable interference term between h_2 and h_3 in the decoupling limit.

Such a drastic interference effect can reduce the theoretical prediction for the MSSM Higgs production from $b\bar{b}$ and the subsequent decay into $\tau^+\tau^-$ so significantly that it becomes smaller than the actually observed limit. Consequently, a noticeable region of the parameter space that was excluded in the case where the interference term was absent cannot be excluded anymore if the interference is properly taken into account. This scenario highlights the importance of the interference term in the correct interpretation of experimental results and motivates further studies of $\mathcal{CP}$-violating benchmark scenarios.

In future investigations, we will analyse the impact of additional imaginary parts of MSSM parameters that influence the Higgs sector notably, such as the phase ϕ_{M_3} of the gluino mass parameter, ϕ_μ (albeit severely constrained) and independent phases of ϕ_{A_b} and ϕ_{A_τ}. In order to improve the sensitivity to interference effects at low and medium values of $\tan\beta$, we will also include the interference term in the process $gg \to h_a \to \tau^+\tau^-$. In conclusion, the above studies motivate the analysis of experimental results in run II of the LHC in scenarios with complex parameters, taking interference effects into account.

Chapter 11.

Conclusions

In this thesis we have investigated interference effects of new particles beyond the SM, particularly in the Higgs sector of the MSSM both for the cases of real and complex parameters. We have approached this topic from three different perspectives - from aspects of higher-order calculations over the development of a new method to the comparison with LHC data.

In Chapters 7-9, we have formulated and validated a model-independent method to facilitate the calculation of interference terms between quasi mass-degenerate particles in an on-shell approximation, incorporating also higher-order corrections. Our method thereby extends the standard narrow-width approximation, which does not take interference terms into account.

In Chapters 5 and 6, we have analysed the mixing structure of neutral Higgs bosons in the MSSM including the case of CP-violation induced by complex phases. We have derived an approximation of the full propagators in terms of Breit-Wigner propagators and on-shell mixing factors, which conveniently allows to calculate the interference term.

Finally in Chapter 10, we have studied the phenomenological implications of interferences between neutral MSSM Higgs bosons for the case of complex parameters in view of the search results at the LHC. Strongly destructive effects open up parameter regions that would be regarded as excluded if no interference terms were taken into account.

In the following, we will summarise our main results of these three directions.

Higher-order mixing and $\mathcal{CP}$-violating effects in the MSSM Higgs sector

The Higgs sector of the MSSM is via loop diagrams highly sensitive to parameters from all MSSM sectors. Particularly, if some parameters have imaginary parts, these lead to $\mathcal{CP}$-violation in the Higgs sector so that the neutral scalars h, H and the pseudoscalar A mix into the mass eigenstates h_1, h_2, h_3. Neglecting mixing with Goldstone and gauge bosons, the full propagators of the interaction eigenstates, containing momentum dependent mixing self-energies, have three complex poles. We derived analytically that the full propagators can be approximated by Breit-Wigner propagators of the corresponding mass eigenstates, multiplied by on-shell wave function normalisation factors ($\hat{\mathbf{Z}}$). We tested and confirmed that the $\hat{\mathbf{Z}}$-factors accurately reproduce the mixing properties, in particular also the imaginary parts, while the Breit-Wigner propagators contain the leading momentum dependence. A single Breit-Wigner propagator arises from the expansion of a full propagator around one of its complex poles. By taking the sum of all three Breit-Wigner propagators combined with the appropriate $\hat{\mathbf{Z}}$-factors for the transition between mass and interaction eigenstates, this approximation is valid in all resonance regions and covers especially also the case of nearby poles and overlapping resonances. The formalism of Breit-Wigner propagators and $\hat{\mathbf{Z}}$-factors benefits from the possibility to implement the most accurate value of the total width, including higher-order terms beyond those present in the full propagators. Furthermore it enables to separate the contributions of each of the mass eigenstates and to determine their interference conveniently.

Interference effects in BSM processes with a generalised NWA

We developed a generalisation of the well-known NWA in order to include also interference terms in the useful factorisation of a complicated process into the on-shell production and the subsequent decay of an unstable particle with a narrow width. Interferences in BSM models can occur if the mass difference of two states is smaller than the sum of their total widths such that their resonances overlap. We factorise the interference contribution in terms of on-shell matrix elements, which can optionally be further simplified as interference weight factors and a process-independent integral to be combined with the standard NWA. Processes with many external legs can often be calculated at tree-level without the NWA. Hence the main advantage of the generalised NWA lies in the application to processes where the factorisation into production and decay subprocesses is indispensable to make calculations at higher order feasible. Therefore we introduced the gNWA both at lowest order and for one-loop and real corrections in a UV- and IR-finite way, as we showed explicitely.

For a validation of the gNWA concept, we calculated the decay width $\Gamma(\widetilde{\chi}_4^0 \to \widetilde{\chi}_1^0 \tau^+\tau^-)$ on the one hand as a three-body decay via intermediate Higgs bosons and on the other hand factorised into two steps of the two-body decays $\widetilde{\chi}_4^0 \to \widetilde{\chi}_1^0 h/H$ and $h/H \to \tau^+\tau^-$. Both calculations were performed at the tree-level and at one-loop order with additional soft photon radiation, supplemented by two-loop $\hat{\mathbf{Z}}$-factors, which account for the $h-H$ mixing. In the modified $M_h^{\max}$ scenario with real parameters we found a substantial destructive interference effect between the two $\mathcal{CP}$-even Higgs bosons if their mass difference is smaller than the sum of their total widths and mixing is present. This caused an enormous discrepancy between the sNWA and the three-body decay by up to a factor of 5. In contrast, the gNWA reproduced the unfactorised result within an uncertainty of few percent. Calculating the full lowest-order result and factorising only the loop contribution further improved the accuracy of the gNWA prediction. Hence our gNWA is a useful tool to combine higher-order and interference effects while maintaining the beneficial factorisation into production and decay (as long as non-factorisable terms such as box diagrams are small). Moreover, higher-order corrections to each of the subprocesses can be readily combined resulting in terms beyond the achievable order of the unfactorised process. We introduced the gNWA in a model-independent way so that it can be applied to other processes and BSM models.

Impact of complex phases on Higgs searches at the LHC

Interference effects between Higgs bosons can become highly relevant in the assessment of excluded and allowed parameter configurations. While the $\mathcal{CP}$-conserving interference between h and H is restricted to a narrow parameter region with real parameters, h_2 and h_3 can be quasi mass-degenerate, mix and interfere in a large part of the MSSM parameter space in the case of $\mathcal{CP}$-violating phases. The dominant influence on the Higgs sector is caused by the phase of the trilinear stop coupling, ϕ_{A_t}, which is augmented by large values of μ. We studied different combinations of ϕ_{A_t} and μ as modifications of the $M_h^{\mathrm{mod+}}$ scenario. For the process of $b\bar{b} \to h_{1,2,3} \to \tau^+\tau^-$ with $\mu = 1000\,\mathrm{GeV}$ and $\phi_{A_t} = \pi/4$, we distinguished the overall non-zero phase effect from the genuine interference effect. We found a drastic destructive interference between h_2 and h_3 of up to -97% in the decoupling regime so that a considerable parameter region escaped the exclusion bounds.

In conclusion, interference effects between quasi mass-degenerate particles can be very important in the interpretation of experimental results from searches for new physics at the LHC and future colliders. We provided model-independently a generalised NWA for the efficient calculation of interference terms at higher order. Particularly in the MSSM Higgs sector with complex parameters, huge $\mathcal{CP}$-violating interference effects lead to a significant shift of current exclusion limits. In order to fully exploit the eagerly awaited data of the LHC Run II, such effects should be taken into account as precisely as possible.

Appendix A.

Parameter values in MSSM scenarios

Scenario	M_h^{max}	mod. M_h^{max}	$M_h^{\text{mod+}}$	$\mathbb{C}M_h^{\text{mod+}}$	light $\tilde{\tau}$
Reference	[168, 169]	our modification	[167]	our modification	[167]
M_{SUSY}	1000	1000	1000	1000	1000
$M_{\tilde{l}_3}$	1000	1000	1000	1000	245
X_t/M_{SUSY}	2	2.5	1.5	1.5	1.6
A_b	A_t	A_t	A_t	A_t	A_t
A_τ	A_t	A_t	A_t	A_t	0
$A_{f_{1,2}}$	0	0	0	0	0
ϕ_{A_t}	0	0	0	var	0
μ	± 200	200	200^*	200^*	500
M_1	GUT	100	GUT	GUT	GUT
M_3	800	800	1500	1500	1500

Table A.1.: Overview of parameter values in GeV (apart from the dimensionless ratio) for scenarios that are used or referred to in this thesis. X_t is given in the on-shell scheme. $A_t = X_t + \mu \cot\beta$ in all listed scenarios. GUT denotes the relation in Eq. (3.13) between M_1 and M_2. The asterisk denotes the variation $\mu = \pm 200, \pm 500, \pm 1000$ GeV. var implies variation, in this thesis $\phi_{A_t} = 0, \pi/4, \pi/2$. Further details can be found in the references.

Appendix B.

Details of the renormalisation of the neutralino-chargino sector

B.1. Renormalisation transformations

The counterterms of the elements of the neutralino and chargino mass matrices X, Y are given by

$$\delta Y_{11} = \delta M_1 \tag{B.1}$$

$$\delta X_{11} = \delta Y_{22} = \delta M_2 \tag{B.2}$$

$$\delta X_{22} = -\delta Y_{34} = -\delta Y_{43} = \delta\mu \tag{B.3}$$

$$\delta X_{12} = \left(\frac{\delta M_W}{M_W} + \frac{\delta s_\beta}{s_\beta}\right) \cdot X_{12} = \frac{s_\beta \delta M_W^2}{\sqrt{2} M_W} + \sqrt{2} s_\beta c_\beta^2 M_W \delta t_\beta. \tag{B.4}$$

$$\delta X_{21} = \left(\frac{\delta M_W}{M_W} + \frac{\delta c_\beta}{c_\beta}\right) \sqrt{2} M_W c_\beta = \frac{\delta M_W^2}{M_W} \frac{c_\beta}{\sqrt{2}} - \sqrt{2} M_W c_\beta s_\beta^2 \delta t_\beta \tag{B.5}$$

$$\delta Y_{14} = \delta Y_{41} = \frac{s_\beta s_W}{2M_Z} \delta M_Z^2 + M_Z s_W s_\beta c_\beta^2 \delta t_\beta + M_Z s_\beta \delta s_W, \tag{B.6}$$

$$\delta Y_{23} = \delta Y_{32} = \frac{c_\beta c_W}{2M_Z} \delta M_Z^2 + M_Z c_W c_\beta s_\beta^2 \delta t_\beta - M_Z c_\beta \delta c_W, \tag{B.7}$$

$$\delta Y_{24} = \delta Y_{42} = -\frac{s_\beta c_W}{2M_Z} \delta M_Z^2 - M_Z c_W s_\beta c_\beta^2 \delta t_\beta - M_Z s_\beta \delta c_W, \tag{B.8}$$

$$\delta Y_{13} = \delta Y_{31} = -\frac{c_\beta s_W}{2M_Z} \delta M_Z^2 + M_Z s_W c_\beta s_\beta^2 \delta t_\beta - M_Z c_\beta \delta s_W. \tag{B.9}$$

We obtain the renormalised Lagrangian

$$
\begin{aligned}
\mathcal{L}_{\chi_0} \to \frac{1}{2}\overline{\widetilde{\chi}_i^0}&\left[(1+\frac{1}{2}\delta\bar{Z}_0^L)_{ik}\omega_R + (1+\frac{1}{2}\delta\bar{Z}_0^R)_{ik}\omega_L\right] \\
&\cdot\left[\not{p}\delta_{kl} - \omega_L(N^*\{Y+\delta Y\}N^\dagger)_{kl} - \omega_R(N\{Y^\dagger+\delta Y^\dagger\}N^T)_{kl}\right] \\
&\cdot\left[(1+\frac{1}{2}\delta Z_0^L)_{lj}\omega_L + (1+\frac{1}{2}\delta Z_0^R)_{lj}\omega_R\right]\widetilde{\chi}_j^0 \\
= \mathcal{L}_{\chi_0}^{\text{Born}} &+ \frac{1}{2}\overline{\widetilde{\chi}_i^0}\not{p}[\underbrace{\frac{1}{2}(\delta\bar{Z}_0^R+\delta Z_0^R)}_{\Delta\Sigma_{ij}^R}\omega_R + \underbrace{\frac{1}{2}(\delta\bar{Z}_0^L+\delta Z_0^L)}_{\Delta\Sigma_{ij}^L}\omega_L]_{ij}\widetilde{\chi}_j^0 \\
&- \frac{1}{2}\overline{\widetilde{\chi}_i^0}\omega_R\underbrace{[N\delta Y^\dagger N^T + \frac{1}{2}(NY^\dagger N^T\delta Z_0^R + \delta\bar{Z}_0^L NY^\dagger N^T)]_{ij}}_{-\Delta\Sigma_{ij}^{SR}}\widetilde{\chi}_j^0 \\
&- \frac{1}{2}\overline{\widetilde{\chi}_i^0}\omega_L\underbrace{[N^*\delta YN^\dagger + \frac{1}{2}(N^*YN^\dagger\delta Z_0^L + \delta\bar{Z}_0^R N^*YN^\dagger)]_{ij}}_{-\Delta\Sigma_{ij}^{SL}}\widetilde{\chi}_j^0 + \mathcal{O}(\delta^2).
\end{aligned}
\tag{B.10}
$$

B.2. Parameter renormalisation in the NNN schemes

In a general scheme with $\widetilde{\chi}_i^0, \widetilde{\chi}_j^0$ and $\widetilde{\chi}_k^0$ on-shell, the solution of Eq. (4.38) implies [45]

$$
\begin{aligned}
\delta|M_1| = [&(\text{Re}\{e^{-i\phi_\mu}N_{i3}N_{i4}\}\text{Re}\{N_{j2}^2\} - \text{Re}\{e^{-i\phi_\mu}N_{j3}N_{j4}\}\text{Re}\{N_{i2}^2\})N_k \\
&+ (\text{Re}\{e^{-i\phi_\mu}N_{j3}N_{j4}\}\text{Re}\{e^{-i\phi_{M_1}}N_{k2}^2\} - \text{Re}\{e^{-i\phi_\mu}N_{k3}N_{k4}\}\text{Re}\{N_{j2}^2\})N_i \\
&+ (\text{Re}\{e^{-i\phi_\mu}N_{k3}N_{k4}\}\text{Re}\{N_{i2}^2\} - \text{Re}\{e^{-i\phi_\mu}N_{i3}N_{i4}\}\text{Re}\{N_{k2}^2\})N_j]/L
\end{aligned}
\tag{B.11}
$$

$$
\begin{aligned}
\delta|M_2| = [&(\text{Re}\{e^{-i\phi_\mu}N_{j3}N_{j4}\}\text{Re}\{e^{-i\phi_{M_1}}N_{i1}^2\} - \text{Re}\{e^{-i\phi_\mu}N_{i3}N_{i4}\}\text{Re}\{e^{-i\phi_{M_1}}N_{j1}^2\})N_k \\
&+ (\text{Re}\{e^{-i\phi_\mu}N_{k3}N_{k4}\}\text{Re}\{e^{-i\phi_{M_1}}N_{j1}^2\} - \text{Re}\{e^{-i\phi_\mu}N_{j3}N_{j4}\}\text{Re}\{e^{-i\phi_{M_1}}N_{k1}^2\})N_i \\
&+ (\text{Re}\{e^{-i\phi_\mu}N_{i3}N_{i4}\}\text{Re}\{e^{-i\phi_{M_1}}N_{k1}^2\} - \text{Re}\{e^{-i\phi_\mu}N_{k3}N_{k4}\}\text{Re}\{e^{-i\phi_{M_1}}N_{i1}^2\})N_j]/L
\end{aligned}
\tag{B.12}
$$

$$
\begin{aligned}
\delta|\mu| = -[&(\text{Re}\{N_{i2}^2\}\text{Re}\{e^{-i\phi_{M_1}}N_{j1}^2\} - \text{Re}\{e^{-i\phi_{M_1}}N_{i1}^2\}\text{Re}\{N_{j2}^2\})N_k \\
&+ (\text{Re}\{N_{j2}^2\}\text{Re}\{e^{-i\phi_{M_1}}N_{k1}^2\} - \text{Re}\{e^{-i\phi_{M_1}}N_{j1}^2\}\text{Re}\{N_{k2}^2\})N_i \\
&+ (\text{Re}\{N_{j2}^2\}\text{Re}\{e^{-i\phi_{M_1}}N_{k1}^2\} - \text{Re}\{e^{-i\phi_{M_1}}N_{k1}^2\}\text{Re}\{N_{k2}^2\})N_j]/(2L),
\end{aligned}
\tag{B.13}
$$

where we defined the following shorthand notations:

$$
\begin{aligned}
N_i :=\ & \mathrm{Re}\{m_{\widetilde{\chi}_i^0}\left[\Sigma_{ii}^{L}(m_{\widetilde{\chi}_i^0}^2) + \Sigma_{ii}^{R}(m_{\widetilde{\chi}_i^0}^2)\right] + \left[\Sigma_{ii}^{SL}(m_{\widetilde{\chi}_i^0}^2) + \Sigma_{ii}^{SR}(m_{\widetilde{\chi}_i^0}^2)\right]\} \\
& - 4\sum_{k=1}^{2}\sum_{l=3}^{4}\delta Y_{lk}\mathrm{Re}\{N_{ik}N_{il}\} \qquad \text{(B.14)} \\
L :=\ & 2(\mathrm{Re}\{e^{-i\phi_{M_1}}N_{k1}^2\}\left[\mathrm{Re}\{e^{-i\phi_\mu}N_{i3}N_{i4}\}\mathrm{Re}\{N_{j2}^2\} - \mathrm{Re}\{e^{-i\phi_\mu}N_{j3}N_{j4}\}\mathrm{Re}\{N_{i2}^2\}\right] \\
& + \mathrm{Re}\{N_{k2}^2\}\left[\mathrm{Re}\{e^{-i\phi_\mu}N_{j3}N_{j4}\}\mathrm{Re}\{e^{-i\phi_{M_1}}N_{i1}^2\} - \mathrm{Re}\{e^{-i\phi_\mu}N_{i3}N_{i4}\}\mathrm{Re}\{e^{-i\phi_{M_1}}N_{j1}^2\}\right] \\
& + \mathrm{Re}\{e^{-i\phi_\mu}N_{k3}N_{k4}\}\left[\mathrm{Re}\{N_{i2}^2\}\mathrm{Re}\{e^{-i\phi_{M_1}}N_{j1}^2\} - \mathrm{Re}\{N_{j2}^2\}\mathrm{Re}\{e^{-i\phi_{M_1}}N_{i1}^2\}\right]). \qquad \text{(B.15)}
\end{aligned}
$$

Appendix C.

Kinematic relations

We list some basic kinematic relations that are useful for the calculation of decay widths [23, 216].

2-body decay

For a decay with $p_a \to p_{b,\,c}$, the momenta and energies in the final state are determined by the following mass relations.

$$|\vec{p}| \equiv |\vec{p_b}| \equiv |\vec{p_c}| = \frac{\sqrt{(m_a^2 - (m_b + m_c)^2)\,(m_a^2 - (m_b - m_c)^2)}}{2m_a} \tag{C.1}$$

$$|\vec{p}|^2 = \frac{(m_a^2 - m_b^2 + m_c^2)^2}{4m_a^2} - m_c^2 = \frac{(m_a^2 + m_b^2 - m_c^2)^2}{4m_a^2} - m_b^2 \tag{C.2}$$

$$E_b = \frac{m_a^2 + m_b^2 - m_c^2}{2m_a} \tag{C.3}$$

$$E_c = \frac{m_a^2 - m_b^2 + m_c^2}{2m_a} \tag{C.4}$$

Special case of equal masses In the case of particles with the same mass $m_b = m_c$ in the final state, the energies are reduced to

$$E_b = E_c = \frac{m_a}{2}, \qquad\qquad |\vec{p_b}|^2 = |\vec{p_c}|^2 = \frac{m_a^2}{4} - m_b^2.$$

Width With the 2-body phase space and the flux factor $F = 2\sqrt{s} = 2m_a$, the differential width reads

$$d\Gamma = \frac{1}{F}|\mathcal{M}|^2 dlips(a;b,c) = \frac{1}{32\pi^2}|\mathcal{M}|^2 \frac{|\vec{p_b}|}{m_a^2} d\phi d\cos\theta. \tag{C.5}$$

3-body decay

The phase space is more complicated for 3 particles in the final state: $a \to b, c, d$. With $p_{ij} := p_i + p_j$ and $m_{ij}^2 = p_{ij}^2$, it is convenient to choose a frame in which a pair of particles is produced at rest. According to the three possible pairs within the three-body final state, there exist three equivalent, so-called Gottfried-Jackson frames [186]. With the choice of the bc-rest frame $\vec{p}_b + \vec{p}_c = 0$, the phase space can be parametrised in the following way [23]:

$$d\Gamma = \frac{1}{(2\pi)^3}\frac{1}{8m_a}|\mathcal{M}|^2 dE_b dE_c = \frac{1}{(2\pi)^3}\frac{1}{32m_a^3}|\mathcal{M}|^2 dm_{bc}^2 dm_{cd}^2 \tag{C.6}$$

The energies

$$E_c^* := \frac{m_{bc}^2 - m_b^2 + m_c^2}{2m_{bc}} \qquad E_d^* := \frac{-m_{bc}^2 + m_a^2 - m_d^2}{2m_{bc}} \tag{C.7}$$

are the boosted energies of c and d in the m_{bc} rest frame. The integration limits of m_{cd} are functions of m_{bc} which itself is limited by the kinematic bounds of the momentum relation $p_a - p_d = p_b + p_c$:

$$\begin{aligned} &(E_c^* + E_d^*)^2 - \left(\sqrt{E_c^{*2} - m_c^2} + \sqrt{E_d^{*2} - m_d^2}\right)^2 \leq m_{cd}^2 \\ \leq\ &(E_c^* + E_d^*)^2 - \left(\sqrt{E_c^{*2} - m_c^2} - \sqrt{E_d^{*2} - m_d^2}\right)^2, \end{aligned} \tag{C.8}$$

$$(m_b + m_c)^2 \leq m_{bc}^2 \leq (m_a - m_d)^2. \tag{C.9}$$

The upper bound is reached if particle d is produced at rest, the lower bound if b and c are at rest.

Acknowledgements

First and foremost, I would like to thank my supervisor Georg Weiglein for his support, encouragement, detailed explanations and motivating discussions during the years of my PhD and also my master's thesis.

I thank Géraldine Servant, who kindly agreed to review my dissertation, and Jan Louis, Jürgen Reuter and Christian Sander for being the referees in my examination committee.

I am very thankful to Silja Thewes for tireless numerical comparisons and countless stimulating discussions, to Oscar Stål for his good ideas and efficient HiggsBounds support that made the comparison to LHC limits possible before the thesis submission, and to Sven Heinemeyer for many useful suggestions. Furthermore I am grateful to Aoife Bharucha, Christian Veelken and Thomas Hahn for very helpful discussions.

Big thanks go to Andi Weiler for enabling me to work at CERN for several months and for very interesting discussions, to Howie Haber for the hospitality in Santa Cruz, and to both of them for their support in the postdoc applications.

I wish to express my gratitude to Sarah Andreas, Peter Drechsel, Stefan Liebler and Matthias Schlaffer, who read parts of the thesis draft and gave me valuable feedback.

Arnulf Quadt and Mrs Schrempp sparked my interest in particle physics many years ago and I am happy to thank them for their very helpful support and advice since then.

At DESY, I enjoyed excellent lectures in particular by Gudi Moortgat-Pick, Jörn Kersten, Georg Weiglein, Andi Weiler and Felix Brümmer. Moreover I wish to thank the organisers, lecturers and PhD students of the Cargèse, TASI, Göttingen and Maria Laach summer schools.

I appreciate the stimulating programme and financial support from the Studienstiftung des deutschen Volkes during my studies and the PhD. Furthermore I acknowledge the funding from DESY, the IRTG travel funds of the SFB 676 and the scholarship of the PIER Helmholtz Graduate School for the stay at CERN.

It is or was a pleasure to share the office at DESY with Sarah, Valerie, Matthias, Joules and Bijan - thank you all for the good atmosphere! To Joules, Bijan and Falk, I am also grateful for their help with computer problems. For all the physics discussions, lunch, coffee and Franzbrötchen breaks, language tandems, Doppelkopf and many other activities at and outside DESY, I would like to thank Christoph, Daniel, Falk, Felix B., Felix K., Ido, Julia, Jürgen, Laura, Paola, Paolo, Peter, Sebastian, Shruti, Stefan, Stefano, Václav and the whole theory group. In particular I thank Sarah, Aoife and Valerie for many special moments and their encouragement. At CERN I also enjoyed the hospitality of the theory department and the time with Fréderic, Christina and Ania.

The last years would not have been the same without my music friends from the Hauke-Haien-Quintett and the joyful rehearsals and concerts with the JPON, the orchestra at Hamburg's music academy, Trío Teórico, Ceilidh band, String Theory Quintet and the duos with Benedict and Mr Buchmüller. Many thanks for the acoustic and human harmony!

My heartfelt thanks go to my parents and my grandmother for always being supportive and interested in my activities and for making me relax in Hannover, to my brother for all the fun and to my cousin Leonie for our great time together in Hamburg. Last but most deeply, I thank you, Matthias, for being exactly as you are, cheering me up and for the all-round service in the last weeks and various other stressful periods!

Bibliography

[1] E. Fuchs, S. Thewes, and G. Weiglein, "Interference effects in BSM processes with a generalised narrow-width approximation," arXiv:1411.4652 [hep-ph].

[2] E. Fuchs, "Interference effects of neutral MSSM Higgs bosons with a generalised narrow-width approximation," arXiv:1411.5239 [hep-ph].

[3] A. Fowler, E. Fuchs, and G. Weiglein, "Breit-Wigner approximation of full Higgs propagator mixing in the MSSM." in preparation.

[4] E. Fuchs, S. Heinemeyer, O. Stal, and G. Weiglein, "Impact of $\mathcal{CP}$-violating phases on searches for MSSM Higgs bosons at the LHC." in preparation.

[5] G. Aad and others [ATLAS Collaboration], "Observation of a new particle in the search for the Standard Model Higgs boson with the ATLAS detector at the LHC," *Phys.Lett.* **B716** (2012) 1–29, arXiv:1207.7214 [hep-ex].

[6] S. Chatrchyan and others [CMS Collaboration], "Observation of a new boson at a mass of 125 GeV with the CMS experiment at the LHC," *Phys.Lett.* **B716** (2012) 30–61, arXiv:1207.7235 [hep-ex].

[7] P. W. Higgs, "Broken Symmetries and the Masses of Gauge Bosons," *Phys.Rev.Lett.* **13** (1964) 508–509.

[8] P. W. Higgs, "Broken symmetries, massless particles and gauge fields," *Phys.Lett.* **12** (1964) 132–133.

[9] F. Englert and R. Brout, "Broken Symmetry and the Mass of Gauge Vector Mesons," *Phys.Rev.Lett.* **13** (1964) 321–322.

[10] G. Guralnik, C. Hagen, and T. Kibble, "Global Conservation Laws and Massless Particles," *Phys.Rev.Lett.* **13** (1964) 585–587.

[11] T. Kibble, "Symmetry breaking in nonAbelian gauge theories," *Phys.Rev.* **155** (1967) 1554–1561.

[12] S. Glashow, "Partial Symmetries of Weak Interactions," *Nucl.Phys.* **22** (1961) 579–588.

[13] A. Salam, "Weak and Electromagnetic Interactions," *Conf.Proc.* **C680519** (1968) 367–377.

[14] S. Weinberg, "A Model of Leptons," *Phys.Rev.Lett.* **19** (1967) 1264–1266.

[15] S. Glashow, J. Iliopoulos, and L. Maiani, "Weak Interactions with Lepton-Hadron Symmetry," *Phys.Rev.* **D2** (1970) 1285–1292.

[16] M. Gell-Mann, "Symmetries of baryons and mesons," *Phys.Rev.* **125** (1962) 1067–1084.

[17] M. Gell-Mann, "A Schematic Model of Baryons and Mesons," *Phys.Lett.* **8** (1964) 214–215.

[18] Y. Ne'eman, "Derivation of strong interactions from a gauge invariance,"

Nucl.Phys. **26** (1961) 222–229.

[19] G. Zweig, "An SU(3) model for strong interaction symmetry and its breaking. Version 2,".

[20] M. Bohm, A. Denner, and H. Joos, *Gauge theories of the strong and electroweak interaction*. Vieweg+Teubner Verlag, 2001.

[21] A. Denner, "Techniques for calculation of electroweak radiative corrections at the one loop level and results for W physics at LEP-200," *Fortsch.Phys.* **41** (1993) 307–420, `arXiv:0709.1075 [hep-ph]`.

[22] H. E. Logan, "TASI 2013 lectures on Higgs physics within and beyond the Standard Model," `arXiv:1406.1786 [hep-ph]`.

[23] **Particle Data Group** Collaboration, K. Olive *et al.*, "Review of Particle Physics," *Chin.Phys.* **C38** (2014) 090001.

[24] M. E. Peskin and D. V. Schroeder, "An Introduction to quantum field theory,".

[25] G. 't Hooft, "Renormalization of Massless Yang-Mills Fields," *Nucl.Phys.* **B33** (1971) 173–199.

[26] G. 't Hooft and M. Veltman, "Regularization and Renormalization of Gauge Fields," *Nucl.Phys.* **B44** (1972) 189–213.

[27] J. Goldstone, A. Salam, and S. Weinberg, "Broken Symmetries," *Phys. Rev.* **127** (1962) 965–970.

[28] Y. Nambu and G. Jona-Lasinio, "Dynamical Model of Elementary Particles Based on an Analogy with Superconductivity. 1.," *Phys.Rev.* **122** (1961) 345–358.

[29] N. Cabibbo, "Unitary Symmetry and Leptonic Decays," *Phys.Rev.Lett.* **10** (1963) 531–533.

[30] M. Kobayashi and T. Maskawa, "CP Violation in the Renormalizable Theory of Weak Interaction," *Prog. Theor. Phys.* **49** (1973) 652–657.

[31] U. Amaldi, W. de Boer, and H. Furstenau, "Comparison of grand unified theories with electroweak and strong coupling constants measured at LEP," *Phys.Lett.* **B260** (1991) 447–455.

[32] **Super-Kamiokande** Collaboration, Y. Fukuda *et al.*, "Evidence for oscillation of atmospheric neutrinos," *Phys.Rev.Lett.* **81** (1998) 1562–1567, `arXiv:hep-ex/9807003 [hep-ex]`.

[33] B. Cleveland, T. Daily, J. Davis, Raymond, J. R. Distel, K. Lande, *et al.*, "Measurement of the solar electron neutrino flux with the Homestake chlorine detector," *Astrophys.J.* **496** (1998) 505–526.

[34] **Planck** Collaboration, P. Ade *et al.*, "Planck 2013 results. XVI. Cosmological parameters," *Astron.Astrophys.* **571** (2014) A16, `arXiv:1303.5076 [astro-ph.CO]`.

[35] A. Sakharov, "Violation of CP Invariance, c Asymmetry, and Baryon Asymmetry of the Universe," *Pisma Zh.Eksp.Teor.Fiz.* **5** (1967) 32–35.

[36] R. Haag, J. T. Lopuszanski, and M. Sohnius, "All Possible Generators of Supersymmetries of the s Matrix," *Nucl. Phys.* **B88** (1975) 257.

[37] C. Csaki, "TASI lectures on extra dimensions and branes," `arXiv:hep-ph/0404096 [hep-ph]`.

[38] R. Contino, "The Higgs as a Composite Nambu-Goldstone Boson," arXiv:1005.4269 [hep-ph].

[39] H. Georgi and S. Glashow, "Unity of All Elementary Particle Forces," *Phys.Rev.Lett.* **32** (1974) 438–441.

[40] S. P. Martin, "A Supersymmetry Primer," arXiv:hep-ph/9709356.

[41] I. J. R. Aitchison, "Supersymmetry and the MSSM: An Elementary introduction," arXiv:hep-ph/0505105.

[42] J. F. Gunion, H. E. Haber, G. L. Kane, and S. Dawson, "The Higgs Hunter's Guide," *Front.Phys.* **80** (2000) 1–448.

[43] J. Kersten and G. Weiglein, "Lecture on phenomenology of physics beyond the SM." DESY, 2011.

[44] G. Weiglein, "Lecture on Higgs physics." DESY, 2013/14.

[45] A. Fowler, "Higher order and CP-violating effects in the neutralino and Higgs boson sectors of the MSSM." PhD Thesis, Durham, 2010.

[46] S. R. Coleman and J. Mandula, "All Possible Symmetries of the S Matrix," *Phys. Rev.* **159** (1967) 1251–1256.

[47] H. P. Nilles, "Supersymmetry, Supergravity and Particle Physics," *Phys.Rept.* **110** (1984) 1–162.

[48] H. E. Haber and G. L. Kane, "The Search for Supersymmetry: Probing Physics Beyond the Standard Model," *Phys.Rept.* **117** (1985) 75–263.

[49] R. Barbieri, "Looking Beyond the Standard Model: The Supersymmetric Option," *Riv.Nuovo Cim.* **11N4** (1988) 1–45.

[50] G. R. Farrar and P. Fayet, "Phenomenology of the Production, Decay, and Detection of New Hadronic States Associated with Supersymmetry," *Phys.Lett.* **B76** (1978) 575–579.

[51] H. Goldberg, "Constraint on the Photino Mass from Cosmology," *Phys.Rev.Lett.* **50** (1983) 1419.

[52] J. R. Ellis, J. Hagelin, D. V. Nanopoulos, K. A. Olive, and M. Srednicki, "Supersymmetric Relics from the Big Bang," *Nucl.Phys.* **B238** (1984) 453–476.

[53] G. D'Ambrosio, G. Giudice, G. Isidori, and A. Strumia, "Minimal flavor violation: An Effective field theory approach," *Nucl.Phys.* **B645** (2002) 155–187, arXiv:hep-ph/0207036 [hep-ph].

[54] A. J. Buras, "Minimal flavor violation," *Acta Phys.Polon.* **B34** (2003) 5615–5668, arXiv:hep-ph/0310208 [hep-ph].

[55] R. Barbieri, G. Isidori, J. Jones-Perez, P. Lodone, and D. M. Straub, "U(2) and Minimal Flavour Violation in Supersymmetry," *Eur.Phys.J.* **C71** (2011) 1725, arXiv:1105.2296 [hep-ph].

[56] T. Hahn, "Routines for the diagonalization of complex matrices," arXiv:0607103v2 [pysics.comp-ph].

[57] T. Takagi, "On an algebraic problem related to an analytic theorem of Carathéodory and Fejér and on an allied theorem of Landau.," *Japanese J. Math.* **1** (1927) 83.

[58] R. Peccei and H. R. Quinn, "CP Conservation in the Presence of Instantons,"

Phys.Rev.Lett. **38** (1977) 1440–1443.

[59] R. Peccei and H. R. Quinn, "Constraints Imposed by CP Conservation in the Presence of Instantons," *Phys.Rev.* **D16** (1977) 1791–1797.

[60] U. Ellwanger, C. Hugonie, and A. M. Teixeira, "The Next-to-Minimal Supersymmetric Standard Model," *Phys.Rept.* **496** (2010) 1–77, `arXiv:0910.1785 [hep-ph]`.

[61] Barate, R. and others, LEP Working Group for Higgs boson searches, ALEPH Collaboration, DELPHI Collaboration, L3 Collaboration, OPAL Collaboration, "Search for the standard model Higgs boson at LEP," *Phys.Lett.* **B565** (2003) 61–75, `arXiv:hep-ex/0306033 [hep-ex]`.

[62] H. E. Haber and R. Hempfling, "Can the mass of the lightest Higgs boson of the minimal supersymmetric model be larger than m(Z)?," *Phys.Rev.Lett.* **66** (1991) 1815–1818.

[63] J. R. Ellis, G. Ridolfi, and F. Zwirner, "Radiative corrections to the masses of supersymmetric Higgs bosons," *Phys.Lett.* **B257** (1991) 83–91.

[64] R. Barbieri and M. Frigeni, "The Supersymmetric Higgs searches at LEP after radiative corrections," *Phys.Lett.* **B258** (1991) 395–398.

[65] J. R. Ellis, G. Ridolfi, and F. Zwirner, "On radiative corrections to supersymmetric Higgs boson masses and their implications for LEP searches," *Phys.Lett.* **B262** (1991) 477–484.

[66] J. Espinosa and M. Quiros, "Two loop radiative corrections to the mass of the lightest Higgs boson in supersymmetric standard models," *Phys.Lett.* **B266** (1991) 389–396.

[67] S. Heinemeyer, W. Hollik, and G. Weiglein, "The Masses of the neutral CP - even Higgs bosons in the MSSM: Accurate analysis at the two loop level," *Eur. Phys. J.* **C9** (1999) 343–366, `arXiv:hep-ph/9812472`.

[68] J. Gunion, H. Haber, and J. Wudka, "Sum rules for Higgs bosons," *Phys.Rev.* **D43** (1991) 904–912.

[69] J. Gunion, B. Grzadkowski, H. Haber, and J. Kalinowski, "LEP limits on CP violating nonminimal Higgs sectors," *Phys.Rev.Lett.* **79** (1997) 982–985, `arXiv:hep-ph/9704410 [hep-ph]`.

[70] J. F. Gunion and H. E. Haber, "The CP conserving two Higgs doublet model: The Approach to the decoupling limit," *Phys.Rev.* **D67** (2003) 075019, `arXiv:hep-ph/0207010 [hep-ph]`.

[71] C. Baker, D. Doyle, P. Geltenbort, K. Green, M. van der Grinten, *et al.*, "An Improved experimental limit on the electric dipole moment of the neutron," *Phys.Rev.Lett.* **97** (2006) 131801, `arXiv:hep-ex/0602020 [hep-ex]`.

[72] B. Regan, E. Commins, C. Schmidt, and D. DeMille, "New limit on the electron electric dipole moment," *Phys.Rev.Lett.* **88** (2002) 071805.

[73] W. Griffith, M. Swallows, T. Loftus, M. Romalis, B. Heckel, *et al.*, "Improved Limit on the Permanent Electric Dipole Moment of Hg-199," *Phys.Rev.Lett.* **102** (2009) 101601.

[74] W. Hollik, J. I. Illana, S. Rigolin, and D. Stockinger, "One loop MSSM

contribution to the weak magnetic dipole moments of heavy fermions," *Phys.Lett.* **B416** (1998) 345–352, arXiv:hep-ph/9707437 [hep-ph].

[75] W. Hollik, J. I. Illana, S. Rigolin, and D. Stockinger, "Weak electric dipole moments of heavy fermions in the MSSM," *Phys.Lett.* **B425** (1998) 322–328, arXiv:hep-ph/9711322 [hep-ph].

[76] F. del Aguila, M. Gavela, J. Grifols, and A. Mendez, "Specifically Supersymmetric Contribution to Electric Dipole Moments," *Phys.Lett.* **B126** (1983) 71.

[77] A. Pilaftsis, "Higgs boson two loop contributions to electric dipole moments in the MSSM," *Phys.Lett.* **B471** (1999) 174–181, arXiv:hep-ph/9909485 [hep-ph].

[78] O. Lebedev, K. A. Olive, M. Pospelov, and A. Ritz, "Probing CP violation with the deuteron electric dipole moment," *Phys.Rev.* **D70** (2004) 016003, arXiv:hep-ph/0402023 [hep-ph].

[79] J. Ellis, F. Moortgat, G. Moortgat-Pick, J. Smillie, and J. Tattersall, "Measurement of CP Violation in Stop Cascade Decays at the LHC," *Eur.Phys.J.* **C60** (2009) 633–651, arXiv:0809.1607 [hep-ph].

[80] M. Brhlik, G. J. Good, and G. L. Kane, "Electric dipole moments do not require the CP violating phases of supersymmetry to be small," *Phys.Rev.* **D59** (1999) 115004, arXiv:hep-ph/9810457 [hep-ph].

[81] V. D. Barger, T. Falk, T. Han, J. Jiang, T. Li, *et al.*, "CP violating phases in SUSY, electric dipole moments, and linear colliders," *Phys.Rev.* **D64** (2001) 056007, arXiv:hep-ph/0101106 [hep-ph].

[82] Y. Li, S. Profumo, and M. Ramsey-Musolf, "A Comprehensive Analysis of Electric Dipole Moment Constraints on CP-violating Phases in the MSSM," *JHEP* **1008** (2010) 062, arXiv:1006.1440 [hep-ph].

[83] J. Engel, M. J. Ramsey-Musolf, and U. van Kolck, "Electric Dipole Moments of Nucleons, Nuclei, and Atoms: The Standard Model and Beyond," *Prog.Part.Nucl.Phys.* **71** (2013) 21–74, arXiv:1303.2371 [nucl-th].

[84] M. Frank, T. Hahn, S. Heinemeyer, W. Hollik, H. Rzehak, and G. Weiglein, "The Higgs boson masses and mixings of the complex MSSM in the Feynman-diagrammatic approach," *JHEP* **02** (2007) 047, arXiv:hep-ph/0611326.

[85] E. Fuchs, "Interference Effects in the MSSM in a Generalised Narrow-Width Approximation." Master's Thesis, Göttingen/ DESY, II.Physik-UniGö-MSc-2012/03, 2012.

[86] G. Passarino and M. Veltman, "One Loop Corrections for e+ e- Annihilation Into mu+ mu- in the Weinberg Model," *Nucl.Phys.* **B160** (1979) 151.

[87] D. Capper, D. Jones, and P. van Nieuwenhuizen, "Regularization by Dimensional Reduction of Supersymmetric and Nonsupersymmetric Gauge Theories," *Nucl.Phys.* **B167** (1980) 479.

[88] W. Siegel, "Supersymmetric Dimensional Regularization via Dimensional Reduction," *Phys.Lett.* **B84** (1979) 193.

[89] W. Hollik, E. Kraus, M. Roth, C. Rupp, K. Sibold, and D. Stöckinger, "Renormalization of the minimal supersymmetric standard model," *Nucl.Phys.* **B639** (2002) 3–65, arXiv:hep-ph/0204350 [hep-ph].

[90] A. Signer and D. Stockinger, "Factorization and regularization by dimensional reduction," *Phys.Lett.* **B626** (2005) 127–138, arXiv:hep-ph/0508203 [hep-ph].

[91] D. Stockinger, "Regularization by dimensional reduction: consistency, quantum action principle, and supersymmetry," *JHEP* **0503** (2005) 076, arXiv:hep-ph/0503129 [hep-ph].

[92] W. Hollik and H. J. Timme, "Renormalization scheme dependence of electroweak radiative corrections," *Z. Phys.* **C33** (1986) 125.

[93] F. del Aguila, A. Culatti, R. Munoz Tapia, and M. Perez-Victoria, "Techniques for one loop calculations in constrained differential renormalization," *Nucl.Phys.* **B537** (1999) 561–585, arXiv:hep-ph/9806451 [hep-ph].

[94] T. Hahn and M. Perez-Victoria, "Automatized one-loop calculations in four and D dimensions," *Comput. Phys. Commun.* **118** (1999) 153–165, arXiv:hep-ph/9807565.

[95] T. Kinoshita, "Mass singularities of Feynman amplitudes," *J.Math.Phys.* **3** (1962) 650–677.

[96] T. Lee and M. Nauenberg, "Degenerate Systems and Mass Singularities," *Phys.Rev.* **133** (1964) B1549–B1562.

[97] F. Bloch and A. Nordsieck, "Note on the Radiation Field of the electron," *Phys.Rev.* **52** (1937) 54–59.

[98] K. Williams, *The Higgs Sector of the Complex Minimal Supersymmetric Standard Model*. PhD thesis, Durham, 2008.

[99] M. Steinhauser, "Leptonic contribution to the effective electromagnetic coupling constant up to three loops," *Phys.Lett.* **B429** (1998) 158–161, arXiv:hep-ph/9803313 [hep-ph].

[100] H. Burkhardt and B. Pietrzyk, "Low energy hadronic contribution to the QED vacuum polarization," *Phys.Rev.* **D72** (2005) 057501, arXiv:hep-ph/0506323 [hep-ph].

[101] A. Lahanas, K. Tamvakis, and N. Tracas, "One loop corrections to the neutralino sector and radiative electroweak breaking in the MSSM," *Phys.Lett.* **B324** (1994) 387–396, arXiv:hep-ph/9312251 [hep-ph].

[102] D. Pierce and A. Papadopoulos, "Radiative corrections to neutralino and chargino masses in the minimal supersymmetric model," *Phys.Rev.* **D50** (1994) 565–570, arXiv:hep-ph/9312248 [hep-ph].

[103] D. Pierce and A. Papadopoulos, "The Complete radiative corrections to the gaugino and Higgsino masses in the minimal supersymmetric model," *Nucl.Phys.* **B430** (1994) 278–294, arXiv:hep-ph/9403240 [hep-ph].

[104] H. Eberl, M. Kincel, W. Majerotto, and Y. Yamada, "One loop corrections to the chargino and neutralino mass matrices in the on-shell scheme," *Phys.Rev.* **D64** (2001) 115013, arXiv:hep-ph/0104109 [hep-ph].

[105] T. Fritzsche and W. Hollik, "Complete one loop corrections to the mass spectrum of charginos and neutralinos in the MSSM," *Eur.Phys.J.* **C24** (2002) 619–629, arXiv:hep-ph/0203159 [hep-ph].

[106] W. Oller, H. Eberl, W. Majerotto, and C. Weber, "Analysis of the chargino and

neutralino mass parameters at one loop level," *Eur.Phys.J.* **C29** (2003) 563–572, arXiv:hep-ph/0304006 [hep-ph].

[107] M. Drees, W. Hollik, and Q. Xu, "One-loop calculations of the decay of the next-to-lightest neutralino in the MSSM," *JHEP* **0702** (2007) 032, arXiv:hep-ph/0610267 [hep-ph].

[108] A. Chatterjee, M. Drees, S. Kulkarni, and Q. Xu, "On the On-Shell Renormalization of the Chargino and Neutralino Masses in the MSSM," *Phys.Rev.* **D85** (2012) 075013, arXiv:1107.5218 [hep-ph].

[109] A. Fowler and G. Weiglein, "Precise Predictions for Higgs Production in Neutralino Decays in the Complex MSSM," *JHEP* **1001** (2010) 108, arXiv:0909.5165 [hep-ph].

[110] A. Bharucha, A. Fowler, G. Moortgat-Pick, and G. Weiglein, "Consistent on shell renormalisation of electroweakinos in the complex MSSM: LHC and LC predictions," *JHEP* **1305** (2013) 053, arXiv:1211.3134 [hep-ph].

[111] A. Bharucha, S. Heinemeyer, F. von der Pahlen, and C. Schappacher, "Neutralino Decays in the Complex MSSM at One-Loop: a Comparison of On-Shell Renormalization Schemes," *Phys.Rev.* **D86** (2012) 075023, arXiv:1208.4106 [hep-ph].

[112] D. M. Pierce, J. A. Bagger, K. T. Matchev, and R.-J. Zhang, "Precision corrections in the minimal supersymmetric standard model," *Nucl.Phys.* **B491** (1997) 3–67, arXiv:hep-ph/9606211 [hep-ph].

[113] A. Bharucha, "Chargino Production at a future LC in the MSSM with complex Parameters: NLO Corrections," arXiv:1202.6284 [hep-ph].

[114] J. Kublbeck, M. Bohm, and A. Denner, "FeynArts: Computer algebraic generation of Feynman graphs and amplitudes," *Comput.Phys.Commun.* **60** (1990) 165–180.

[115] A. Denner, H. Eck, O. Hahn, and J. Kublbeck, "Feynman rules for fermion number violating interactions," *Nucl.Phys.* **B387** (1992) 467–484.

[116] J. Kublbeck, H. Eck, and R. Mertig, "Computeralgebraic generation and calculation of Feynman graphs using FeynArts and FeynCalc," *Nucl.Phys.Proc.Suppl.* **29A** (1992) 204–208.

[117] T. Hahn, "Generating Feynman diagrams and amplitudes with FeynArts 3," *Comput. Phys. Commun.* **140** (2001) 418–431, arXiv:hep-ph/0012260.

[118] T. Hahn and C. Schappacher, "The implementation of the minimal supersymmetric standard model in FeynArts and FormCalc," *Comput. Phys. Commun.* **143** (2002) 54–68, arXiv:hep-ph/0105349.

[119] T. Hahn, "Generating and calculating one loop Feynman diagrams with FeynArts, FormCalc, and LoopTools," arXiv:hep-ph/9905354 [hep-ph].

[120] T. Hahn, "Automatic loop calculations with FeynArts, FormCalc, and LoopTools," *Nucl.Phys.Proc.Suppl.* **89** (2000) 231–236, arXiv:hep-ph/0005029.

[121] T. Hahn and M. Rauch, "News from FormCalc and LoopTools," *Nucl. Phys. Proc. Suppl.* **157** (2006) 236–240, arXiv:hep-ph/0601248.

[122] T. Hahn, "A Mathematica interface for FormCalc-generated code," *Comput. Phys. Commun.* **178** (2008) 217–221, arXiv:hep-ph/0611273.

[123] T. Fritzsche, T. Hahn, S. Heinemeyer, F. von der Pahlen, H. Rzehak, *et al.*, "The Implementation of the Renormalized Complex MSSM in FeynArts and FormCalc," *Comput.Phys.Commun.* **185** (2014) 1529–1545, arXiv:1309.1692 [hep-ph].

[124] T. Hahn, S. Heinemeyer, F. von der Pahlen, H. Rzehak, and C. Schappacher, "Fully Automated Calculations in the complex MSSM," *PoS* **LL2014** (2014) 080, arXiv:1407.0231 [hep-ph].

[125] R. Hempfling and A. H. Hoang, "Two loop radiative corrections to the upper limit of the lightest Higgs boson mass in the minimal supersymmetric model," *Phys.Lett.* **B331** (1994) 99–106, arXiv:hep-ph/9401219 [hep-ph].

[126] A. Dabelstein, "The One loop renormalization of the MSSM Higgs sector and its application to the neutral scalar Higgs masses," *Z.Phys.* **C67** (1995) 495–512, arXiv:hep-ph/9409375 [hep-ph].

[127] J. Casas, J. Espinosa, M. Quiros, and A. Riotto, "The Lightest Higgs boson mass in the minimal supersymmetric standard model," *Nucl.Phys.* **B436** (1995) 3–29, arXiv:hep-ph/9407389 [hep-ph].

[128] M. Carena, J. Espinosa, M. Quiros, and C. Wagner, "Analytical expressions for radiatively corrected Higgs masses and couplings in the MSSM," *Phys.Lett.* **B355** (1995) 209–221, arXiv:hep-ph/9504316 [hep-ph].

[129] S. Heinemeyer, W. Hollik, and G. Weiglein, "The Mass of the lightest MSSM Higgs boson: A Compact analytical expression at the two loop level," *Phys.Lett.* **B455** (1999) 179–191, arXiv:hep-ph/9903404 [hep-ph].

[130] M. Carena, H. Haber, S. Heinemeyer, W. Hollik, C. Wagner, *et al.*, "Reconciling the two loop diagrammatic and effective field theory computations of the mass of the lightest CP - even Higgs boson in the MSSM," *Nucl.Phys.* **B580** (2000) 29–57, arXiv:hep-ph/0001002 [hep-ph].

[131] S. Heinemeyer, W. Hollik, H. Rzehak, and G. Weiglein, "High-precision predictions for the MSSM Higgs sector at O(alpha(b) alpha(s))," *Eur.Phys.J.* **C39** (2005) 465–481, arXiv:hep-ph/0411114 [hep-ph].

[132] R. Harlander, P. Kant, L. Mihaila, and M. Steinhauser, "Higgs boson mass in supersymmetry to three loops," *Phys.Rev.Lett.* **100** (2008) 191602, arXiv:0803.0672 [hep-ph].

[133] P. Kant, R. Harlander, L. Mihaila, and M. Steinhauser, "Light MSSM Higgs boson mass to three-loop accuracy," *JHEP* **1008** (2010) 104, arXiv:1005.5709 [hep-ph].

[134] R.-J. Zhang, "Two loop effective potential calculation of the lightest CP even Higgs boson mass in the MSSM," *Phys.Lett.* **B447** (1999) 89–97, arXiv:hep-ph/9808299 [hep-ph].

[135] J. R. Espinosa and R.-J. Zhang, "Complete two loop dominant corrections to the mass of the lightest CP even Higgs boson in the minimal supersymmetric standard model," *Nucl.Phys.* **B586** (2000) 3–38, arXiv:hep-ph/0003246 [hep-ph].

[136] G. Degrassi, P. Slavich, and F. Zwirner, "On the neutral Higgs boson masses in the MSSM for arbitrary stop mixing," *Nucl.Phys.* **B611** (2001) 403–422, arXiv:hep-ph/0105096 [hep-ph].

[137] A. Brignole, G. Degrassi, P. Slavich, and F. Zwirner, "On the O(alpha(t)**2) two loop corrections to the neutral Higgs boson masses in the MSSM," *Nucl.Phys.* **B631** (2002) 195–218, arXiv:hep-ph/0112177 [hep-ph].

[138] A. Brignole, G. Degrassi, P. Slavich, and F. Zwirner, "On the two loop sbottom corrections to the neutral Higgs boson masses in the MSSM," *Nucl.Phys.* **B643** (2002) 79–92, arXiv:hep-ph/0206101 [hep-ph].

[139] S. P. Martin, "Complete two loop effective potential approximation to the lightest Higgs scalar boson mass in supersymmetry," *Phys.Rev.* **D67** (2003) 095012, arXiv:hep-ph/0211366 [hep-ph].

[140] S. Heinemeyer, W. Hollik, and G. Weiglein, "Electroweak precision observables in the minimal supersymmetric standard model," *Phys.Rept.* **425** (2006) 265–368, arXiv:hep-ph/0412214 [hep-ph].

[141] B. Allanach, A. Djouadi, J. Kneur, W. Porod, and P. Slavich, "Precise determination of the neutral Higgs boson masses in the MSSM," *JHEP* **0409** (2004) 044, arXiv:hep-ph/0406166 [hep-ph].

[142] S. Borowka, T. Hahn, S. Heinemeyer, G. Heinrich, and W. Hollik, "Momentum-dependent two-loop QCD corrections to the neutral Higgs-boson masses in the MSSM," *Eur.Phys.J.* **C74** no. 8, (2014) 2994, arXiv:1404.7074 [hep-ph].

[143] D. A. Demir, "Effects of the supersymmetric phases on the neutral Higgs sector," *Phys.Rev.* **D60** (1999) 055006, arXiv:hep-ph/9901389 [hep-ph].

[144] A. Pilaftsis and C. E. Wagner, "Higgs bosons in the minimal supersymmetric standard model with explicit CP violation," *Nucl.Phys.* **B553** (1999) 3–42, arXiv:hep-ph/9902371 [hep-ph].

[145] M. Carena, J. R. Ellis, A. Pilaftsis, and C. Wagner, "Renormalization group improved effective potential for the MSSM Higgs sector with explicit CP violation," *Nucl.Phys.* **B586** (2000) 92–140, arXiv:hep-ph/0003180 [hep-ph].

[146] S. Heinemeyer, W. Hollik, H. Rzehak, and G. Weiglein, "The Higgs sector of the complex MSSM at two-loop order: QCD contributions," *Phys.Lett.* **B652** (2007) 300–309, arXiv:0705.0746 [hep-ph].

[147] K. E. Williams, H. Rzehak, and G. Weiglein, "Higher order corrections to Higgs boson decays in the MSSM with complex parameters," *Eur.Phys.J.* **C71** (2011) 1669, arXiv:1103.1335 [hep-ph].

[148] W. Hollik and S. Paßehr, "Higgs boson masses and mixings in the complex MSSM with two-loop top-Yukawa-coupling corrections," *JHEP* **1410** (2014) 171, arXiv:1409.1687 [hep-ph].

[149] S. Heinemeyer, W. Hollik, and G. Weiglein, "FeynHiggs: a program for the calculation of the masses of the neutral CP-even Higgs bosons in the MSSM," *Comput. Phys. Commun.* **124** (2000) 76–89, arXiv:hep-ph/9812320.

[150] G. Degrassi, S. Heinemeyer, W. Hollik, P. Slavich, and G. Weiglein, "Towards high-precision predictions for the MSSM Higgs sector," *Eur. Phys. J.* **C28** (2003) 133–143, arXiv:hep-ph/0212020.

[151] T. Hahn, S. Heinemeyer, W. Hollik, H. Rzehak, and G. Weiglein, "High-precision

predictions for the light CP-even Higgs Boson Mass of the MSSM," *Phys.Rev.Lett.* **112** (2014) 141801, arXiv:1312.4937 [hep-ph].

[152] H. Lehmann, K. Symanzik, and W. Zimmermann, "On the formulation of quantized field theories," *Nuovo Cim.* **1** (1955) 205–225.

[153] A. Dabelstein, "Fermionic decays of neutral MSSM Higgs bosons at the one loop level," *Nucl.Phys.* **B456** (1995) 25–56, arXiv:hep-ph/9503443 [hep-ph].

[154] S. Heinemeyer, W. Hollik, J. Rosiek, and G. Weiglein, "Neutral MSSM Higgs boson production at e+ e- colliders in the Feynman diagrammatic approach," *Eur.Phys.J.* **C19** (2001) 535–546, arXiv:hep-ph/0102081 [hep-ph].

[155] P. H. Chankowski, S. Pokorski, and J. Rosiek, "Complete on-shell renormalization scheme for the minimal supersymmetric Higgs sector," *Nucl.Phys.* **B423** (1994) 437–496, arXiv:hep-ph/9303309 [hep-ph].

[156] K. Williams and G. Weiglein, "Precise predictions for $h_a \to h_b h_c$ decays in the complex MSSM," *Phys.Lett.* **B660** (2008) 217–227, arXiv:0710.5320 [hep-ph].

[157] T. Hahn, S. Heinemeyer, W. Hollik, H. Rzehak, G. Weiglein, *et al.*, "Higher-Order Corrected Higgs Bosons in FeynHiggs 2.5," *Pramana* **69** (2007) 861–870, arXiv:hep-ph/0611373 [hep-ph].

[158] S. Heinemeyer, W. Hollik, and G. Weiglein, "Decay widths of the neutral CP even MSSM Higgs bosons in the Feynman diagrammatic approach," *Eur.Phys.J.* **C16** (2000) 139–153, arXiv:hep-ph/0003022 [hep-ph].

[159] T. Hahn, S. Heinemeyer, and G. Weiglein, "MSSM Higgs boson production at the linear collider: Dominant corrections to the WW fusion channel," *Nucl.Phys.* **B652** (2003) 229–258, arXiv:hep-ph/0211204 [hep-ph].

[160] T. Hahn, S. Heinemeyer, W. Hollik, H. Rzehak, and G. Weiglein, "Higgs Masses and More in the Complex MSSM with FeynHiggs," arXiv:0710.4891 [hep-ph].

[161] T. Hahn, "Routines for the diagonalization of complex matrices," arXiv:physics/0607103 [physics].

[162] D. Wackeroth and W. Hollik, "Electroweak radiative corrections to resonant charged gauge boson production," *Phys.Rev.* **D55** (1997) 6788–6818, arXiv:hep-ph/9606398 [hep-ph].

[163] A. Freitas, W. Hollik, W. Walter, and G. Weiglein, "Electroweak two loop corrections to the M(W) - M(Z) mass correlation in the standard model," *Nucl.Phys.* **B632** (2002) 189–218, arXiv:hep-ph/0202131 [hep-ph].

[164] M. W. Grunewald, G. Passarino, E. Accomando, A. Ballestrero, P. Bambade, *et al.*, "Reports of the Working Groups on Precision Calculations for LEP2 Physics: Proceedings. Four fermion production in electron positron collisions," arXiv:hep-ph/0005309 [hep-ph].

[165] E. N. Argyres, W. Beenakker, G. J. van Oldenborgh, A. Denner, S. Dittmaier, *et al.*, "Stable calculations for unstable particles: Restoring gauge invariance," *Phys.Lett.* **B358** (1995) 339–346, arXiv:hep-ph/9507216 [hep-ph].

[166] W. Beenakker, G. J. van Oldenborgh, A. Denner, S. Dittmaier, J. Hoogland, *et al.*, "The Fermion loop scheme for finite width effects in e^+e^- annihilation into four fermions," *Nucl.Phys.* **B500** (1997) 255–298, arXiv:hep-ph/9612260 [hep-ph].

[167] M. Carena, S. Heinemeyer, O. Stål, C. Wagner, and G. Weiglein, "MSSM Higgs Boson Searches at the LHC: Benchmark Scenarios after the Discovery of a Higgs-like Particle," *Eur.Phys.J.* **C73** no. 9, (2013) 2552, arXiv:1302.7033 [hep-ph].

[168] M. S. Carena, S. Heinemeyer, C. E. M. Wagner, and G. Weiglein, "Suggestions for improved benchmark scenarios for Higgs- boson searches at LEP2," arXiv:hep-ph/9912223.

[169] M. S. Carena, S. Heinemeyer, C. Wagner, and G. Weiglein, "Suggestions for benchmark scenarios for MSSM Higgs boson searches at hadron colliders," *Eur.Phys.J.* **C26** (2003) 601–607, arXiv:hep-ph/0202167 [hep-ph].

[170] D. Berdine, N. Kauer, and D. Rainwater, "Breakdown of the Narrow Width Approximation for New Physics," *Phys. Rev. Lett.* **99** (2007) 111601, arXiv:hep-ph/0703058.

[171] K. Hagiwara, W. Kilian, F. Krauss, T. Ohl, T. Plehn, D. Rainwater, J. Reuter, and S. Schumann, "Supersymmetry simulations with off-shell effects for CERN LHC and ILC," *Phys. Rev.* **D73** (2006) 055005, arXiv:hep-ph/0512260 [hep-ph].

[172] J. Reuter, "Off-Shell and Interference Effects for SUSY Particle Production," *eConf* **C0705302** (2007) SUS14, arXiv:0709.0068 [hep-ph].

[173] H. E. Haber and Y. Nir, "Multiscalar Models With a High-energy Scale," *Nucl.Phys.* **B335** (1990) 363.

[174] J. F. Gunion, Y. Jiang, and S. Kraml, "Could two NMSSM Higgs bosons be present near 125 GeV?," *Phys.Rev.* **D86** (2012) 071702, arXiv:1207.1545 [hep-ph].

[175] P. Ferreira, R. Santos, H. E. Haber, and J. P. Silva, "Mass-degenerate Higgs bosons at 125 GeV in the two-Higgs-doublet model," *Phys.Rev.* **D87** no. 5, (2013) 055009, arXiv:1211.3131 [hep-ph].

[176] A. Drozd, B. Grzadkowski, J. F. Gunion, and Y. Jiang, "Two-Higgs-Doublet Models and Enhanced Rates for a 125 GeV Higgs," *JHEP* **1305** (2013) 072, arXiv:1211.3580 [hep-ph].

[177] T. Appelquist, H.-C. Cheng, and B. A. Dobrescu, "Bounds on universal extra dimensions," *Phys.Rev.* **D64** (2001) 035002, arXiv:hep-ph/0012100 [hep-ph].

[178] H.-C. Cheng, K. T. Matchev, and M. Schmaltz, "Bosonic supersymmetry? Getting fooled at the CERN LHC," *Phys.Rev.* **D66** (2002) 056006, arXiv:hep-ph/0205314 [hep-ph].

[179] D. Hooper and S. Profumo, "Dark matter and collider phenomenology of universal extra dimensions," *Phys.Rept.* **453** (2007) 29–115, arXiv:hep-ph/0701197 [hep-ph].

[180] J. de Blas, J. Lizana, and M. Perez-Victoria, "Combining searches of Z' and W' bosons," *JHEP* **1301** (2013) 166, arXiv:1211.2229 [hep-ph].

[181] M. Gigg and P. Richardson, "Simulation of Finite Width Effects in Physics Beyond the Standard Model," arXiv:0805.3037 [hep-ph].

[182] J. Kalinowski, W. Kilian, J. Reuter, T. Robens, and K. Rolbiecki, "Pinning down the Invisible Sneutrino," *JHEP* **10** (2008) 090, arXiv:0809.3997 [hep-ph].

[183] C. F. Uhlemann, "Narrow-Width Approximation in the Minimal Supersymmetric

Standard Model." Diploma Thesis, Würzburg, 2007.

[184] G. Cacciapaglia, A. Deandrea, and S. De Curtis, "Nearby resonances beyond the Breit-Wigner approximation," *Phys. Lett.* **B682** (2009) 43–49, arXiv:0906.3417 [hep-ph].

[185] D. Barducci, A. Belyaev, J. Blamey, S. Moretti, L. Panizzi, *et al.*, "Towards model-independent approach to the analysis of interference effects in pair production of new heavy quarks," *JHEP* **1407** (2014) 142, arXiv:1311.3977 [hep-ph].

[186] K. Gottfried and J. D. Jackson, "On the Connection between production mechanism and decay of resonances at high-energies," *Nuovo Cim.* **33** (1964) 309–330.

[187] D. A. Dicus, E. Sudarshan, and X. Tata, "Factorization theorem for decaying spinning particles," *Phys.Lett.* **B154** (1985) 79.

[188] N. Kauer, "Narrow-width approximation limitations," *Phys. Lett.* **B649** (2007) 413–416, arXiv:hep-ph/0703077.

[189] C. F. Uhlemann and N. Kauer, "Narrow-width approximation accuracy," *Nucl. Phys.* **B814** (2009) 195–211, arXiv:0807.4112 [hep-ph].

[190] E. Accomando, D. Becciolini, A. Belyaev, S. Moretti, and C. Shepherd-Themistocleous, "Z' at the LHC: Interference and Finite Width Effects in Drell-Yan," *JHEP* **1310** (2013) 153, arXiv:1304.6700 [hep-ph].

[191] A. Denner, S. Dittmaier, M. Roth, and D. Wackeroth, "Electroweak radiative corrections to e+ e- – W W – 4 fermions in double pole approximation: The RACOONWW approach," *Nucl.Phys.* **B587** (2000) 67–117, arXiv:hep-ph/0006307 [hep-ph].

[192] N. Kauer, "A threshold-improved narrow-width approximation for BSM physics," *JHEP* **04** (2008) 055, arXiv:0708.1161 [hep-ph].

[193] N. Kauer and G. Passarino, "Inadequacy of zero-width approximation for a light Higgs boson signal," *JHEP* **1208** (2012) 116, arXiv:1206.4803 [hep-ph].

[194] N. Kauer, "Inadequacy of zero-width approximation for a light Higgs boson signal," *Mod.Phys.Lett.* **A28** (2013) 1330015, arXiv:1305.2092 [hep-ph].

[195] S. Goria, G. Passarino, and D. Rosco, "The Higgs Boson Lineshape," *Nucl.Phys.* **B864** (2012) 530–579, arXiv:1112.5517 [hep-ph].

[196] L. J. Dixon and Y. Li, "Bounding the Higgs Boson Width Through Interferometry," *Phys.Rev.Lett.* **111** (2013) 111802, arXiv:1305.3854 [hep-ph].

[197] F. Caola and K. Melnikov, "Constraining the Higgs boson width with ZZ production at the LHC," *Phys.Rev.* **D88** (2013) 054024, arXiv:1307.4935 [hep-ph].

[198] J. M. Campbell, R. K. Ellis, and C. Williams, "Bounding the Higgs width at the LHC using full analytic results for $gg- > e^-e^+\mu^-\mu^+$," *JHEP* **1404** (2014) 060, arXiv:1311.3589 [hep-ph].

[199] J. M. Campbell, R. K. Ellis, and C. Williams, "Bounding the Higgs width at the LHC: Complementary results from $H \to WW$," *Phys.Rev.* **D89** no. 5, (2014) 053011, arXiv:1312.1628 [hep-ph].

[200] J. M. Campbell, R. K. Ellis, and C. Williams, "Gluon-Gluon Contributions to W+ W- Production and Higgs Interference Effects," *JHEP* **1110** (2011) 005, arXiv:1107.5569 [hep-ph].

[201] N. Kauer, "Interference effects for $H \to WW/ZZ \to \ell\bar{\nu}_\ell\bar{\ell}\nu_\ell$ searches in gluon fusion at the LHC," arXiv:1310.7011 [hep-ph].

[202] M. Bonvini, F. Caola, S. Forte, K. Melnikov, and G. Ridolfi, "Signal-background interference effects for $gg \to H \to W^+W^-$ beyond leading order," *Phys.Rev.* **D88** (2013) 034032, arXiv:1304.3053 [hep-ph].

[203] L. J. Dixon and M. S. Siu, "Resonance continuum interference in the diphoton Higgs signal at the LHC," *Phys.Rev.Lett.* **90** (2003) 252001, arXiv:hep-ph/0302233 [hep-ph].

[204] D. de Florian, N. Fidanza, R. Hernández-Pinto, J. Mazzitelli, Y. Rotstein Habarnau, *et al.*, "A complete $O(\alpha_S^2)$ calculation of the signal-background interference for the Higgs diphoton decay channel," *Eur.Phys.J.* **C73** (2013) 2387, arXiv:1303.1397 [hep-ph].

[205] S. P. Martin, "Interference of Higgs diphoton signal and background in production with a jet at the LHC," *Phys.Rev.* **D88** (2013) 013004, arXiv:1303.3342 [hep-ph].

[206] M. J. Dolan, C. Englert, N. Greiner, and M. Spannowsky, "Further on up the road: $hhjj$ production at the LHC," arXiv:1310.1084 [hep-ph].

[207] F. Cascioli, S. Hoeche, F. Krauss, P. Maierhofer, S. Pozzorini, *et al.*, "Precise Higgs-background predictions: merging NLO QCD and squared quark-loop corrections to four-lepton + 0,1 jet production," arXiv:1309.0500 [hep-ph].

[208] M. Chen, T. Cheng, J. S. Gainer, A. Korytov, K. T. Matchev, *et al.*, "The role of interference in unraveling the ZZ-couplings of the newly discovered boson at the LHC," arXiv:1310.1397 [hep-ph].

[209] Y. Chen and R. Vega-Morales, "Extracting Effective Higgs Couplings in the Golden Channel," arXiv:1310.2893 [hep-ph].

[210] S. Liebler, G. Moortgat-Pick, and G. Weiglein, "Off-shell effects in Higgs processes at a linear collider and implications for the LHC," arXiv:1502.07970 [hep-ph].

[211] S. Liebler, "Off-shell effects in Higgs decays to heavy gauge bosons and signal-background interference in Higgs decays to photons at a linear collider," arXiv:1503.07830 [hep-ph].

[212] N. Kauer, "Off-shell Higgs signal and total width determination at the LHC," arXiv:1502.02581 [hep-ph].

[213] J. M. Campbell, R. K. Ellis, E. Furlan, and R. Röntsch, "Interference effects for Higgs boson mediated Z-pair plus jet production," *Phys.Rev.* **D90** no. 9, (2014) 093008, arXiv:1409.1897 [hep-ph].

[214] **CMS** Collaboration, V. Khachatryan *et al.*, "Constraints on the Higgs boson width from off-shell production and decay to Z-boson pairs," *Phys.Lett.* **B736** (2014) 64, arXiv:1405.3455 [hep-ex].

[215] **ATLAS** Collaboration, G. Aad *et al.*, "Determination of the off-shell Higgs boson signal strength in the high-mass ZZ and WW final states with the ATLAS

detector," arXiv:1503.01060 [hep-ex].
[216] E. Byckling and K. Kajantie, *Particle Kinematics*. WILEY, 1972.
[217] T. Hahn, "FormCalc 7 User's Guide," 2012.
[218] A. Denner, S. Dittmaier, and M. Roth, "Nonfactorizable photonic corrections to e+ e- – W W – four fermions," *Nucl.Phys.* **B519** (1998) 39–84, arXiv:hep-ph/9710521 [hep-ph].
[219] T. Hahn, "Feynman Diagram Calculations with FeynArts, FormCalc, and LoopTools," *PoS* (2010) 078, arXiv:1006.2231 [hep-ph].
[220] T. Hahn, "FeynArts 3.8 User's Guide," 2014.
[221] H. E. Haber, "Spin formalism and applications to new physics searches," arXiv:hep-ph/9405376 [hep-ph].
[222] M. Jacob and G. Wick, "On the general theory of collisions for particles with spin," *Annals Phys.* **7** (1959) 404–428.
[223] **ATLAS, CMS** Collaboration, G. Aad *et al.*, "Combined Measurement of the Higgs Boson Mass in pp Collisions at $\sqrt{s} = 7$ and 8 TeV with the ATLAS and CMS Experiments," arXiv:1503.07589 [hep-ex].
[224] **ATLAS** Collaboration, G. Aad *et al.*, "Evidence for the spin-0 nature of the Higgs boson using ATLAS data," *Phys.Lett.* **B726** (2013) 120–144, arXiv:1307.1432 [hep-ex].
[225] **CMS** Collaboration, S. Chatrchyan *et al.*, "Study of the Mass and Spin-Parity of the Higgs Boson Candidate Via Its Decays to Z Boson Pairs," *Phys.Rev.Lett.* **110** no. 8, (2013) 081803, arXiv:1212.6639 [hep-ex].
[226] **ATLAS** Collaboration, "Study of the spin and parity of the Higgs boson in HVV decays with the ATLAS detector." ATLAS-CONF-2015-008, ATLAS-COM-CONF-2015-006, 2015.
[227] **CMS** Collaboration, V. Khachatryan *et al.*, "Constraints on the spin-parity and anomalous HVV couplings of the Higgs boson in proton collisions at 7 and 8 TeV," arXiv:1411.3441 [hep-ex].
[228] **CMS** Collaboration, V. Khachatryan *et al.*, "Precise determination of the mass of the Higgs boson and tests of compatibility of its couplings with the standard model predictions using proton collisions at 7 and 8 TeV," arXiv:1412.8662 [hep-ex].
[229] "Measurements of the Higgs boson production and decay rates and coupling strengths using pp collision data at 7 and 8 TeV in the ATLAS experiment," Tech. Rep. ATLAS-CONF-2015-007, CERN, Geneva, Mar, 2015. http://cds.cern.ch/record/2002212.
[230] **CMS** Collaboration, S. Chatrchyan *et al.*, "Evidence for the 125 GeV Higgs boson decaying to a pair of τ leptons," *JHEP* **1405** (2014) 104, arXiv:1401.5041 [hep-ex].
[231] **ATLAS** Collaboration, G. Aad *et al.*, "Evidence for the Higgs-boson Yukawa coupling to tau leptons with the ATLAS detector," *JHEP* **1504** (2015) 117, arXiv:1501.04943 [hep-ex].
[232] **ALEPH, DELPHI, L3, OPAL, LEP Working Group for Higgs Boson Searches** Collaboration, S. Schael *et al.*, "Search for neutral MSSM Higgs bosons

at LEP," *Eur.Phys.J.* **C47** (2006) 547–587, arXiv:hep-ex/0602042 [hep-ex].

[233] **CDF** Collaboration, T. Aaltonen *et al.*, "Search for Higgs bosons predicted in two-Higgs-doublet models via decays to tau lepton pairs in 1.96-TeV p anti-p collisions," *Phys.Rev.Lett.* **103** (2009) 201801, arXiv:0906.1014 [hep-ex].

[234] **D0** Collaboration, V. M. Abazov *et al.*, "Search for neutral Higgs bosons in the multi-b-jet topology in 5.2fb^{-1} of $p\bar{p}$ collisions at $\sqrt{s} = 1.96$ TeV," *Phys.Lett.* **B698** .

[235] **D0** Collaboration, V. M. Abazov *et al.*, "Search for Higgs bosons decaying to $\tau\tau$ pairs in $p\bar{p}$ collisions at $\sqrt{s} = 1.96$ TeV," *Phys.Lett.* **B707** (2012) 323–329, arXiv:1106.4555 [hep-ex].

[236] **CDF** Collaboration, T. Aaltonen *et al.*, "Search for Higgs Bosons Produced in Association with b-quarks," *Phys.Rev.* **D85** (2012) 032005, arXiv:1106.4782 [hep-ex].

[237] **CMS** Collaboration, S. Chatrchyan *et al.*, "Search for Neutral MSSM Higgs Bosons Decaying to Tau Pairs in pp Collisions at $\sqrt{s} = 7$ TeV," *Phys.Rev.Lett.* **106** (2011) 231801, arXiv:1104.1619 [hep-ex].

[238] S. Chatrchyan and others [CMS Collaboration], "Search for neutral Higgs bosons decaying to τ pairs in pp collisions at $\sqrt{s} = 7$ TeV," *Phys.Lett.* **B713** (2012) 68–90, arXiv:1202.4083 [hep-ex].

[239] **CMS** Collaboration, V. Khachatryan *et al.*, "Search for neutral MSSM Higgs bosons decaying to a pair of tau leptons in pp collisions," *JHEP* **1410** (2014) 160, arXiv:1408.3316 [hep-ex].

[240] **ATLAS** Collaboration, G. Aad *et al.*, "Search for neutral Higgs bosons of the minimal supersymmetric standard model in pp collisions at $\sqrt{s} = 8$ TeV with the ATLAS detector," *JHEP* **1411** (2014) 056, arXiv:1409.6064 [hep-ex].

[241] **CMS** Collaboration, "Search for Neutral MSSM Higgs Bosons in the $\mu\mu$ final state with the CMS experiment in pp Collisions at sqrt s =7 TeV." CMS-PAS-HIG-12-011, 2012.

[242] **CMS** Collaboration, A. Perieanu, "Search for Neutral MSSM Higgs Bosons in the $\mu\mu$ final state with the CMS experiment in pp Collisions at sqrtS = 7 TeV," *PoS* **ICHEP2012** (2013) 089.

[243] **ATLAS** Collaboration, S. Thoma, "Search for the neutral MSSM Higgs bosons in the $H \to \tau^+\tau^-$ and $H \to \mu^+\mu^-$ decay modes with the ATLAS detector at the LHC," *PoS* **ICHEP2012** (2013) 069.

[244] **CMS** Collaboration, S. Chatrchyan *et al.*, "Search for a Higgs boson decaying into a b-quark pair and produced in association with b quarks in proton-proton collisions at 7 TeV," *Phys.Lett.* **B722** (2013) 207–232, arXiv:1302.2892 [hep-ex].

[245] M. Carena, S. Heinemeyer, C. Wagner, and G. Weiglein, "MSSM Higgs boson searches at the Tevatron and the LHC: Impact of different benchmark scenarios," *Eur.Phys.J.* **C45** (2006) 797–814, arXiv:hep-ph/0511023 [hep-ph].

[246] S. Gennai, S. Heinemeyer, A. Kalinowski, R. Kinnunen, S. Lehti, *et al.*, "Search for heavy neutral MSSM Higgs bosons with CMS: Reach and Higgs-mass precision,"

Eur.Phys.J. **C52** (2007) 383–395, arXiv:0704.0619 [hep-ph].
[247] P. Bechtle, O. Brein, S. Heinemeyer, G. Weiglein, and K. E. Williams, "HiggsBounds: Confronting Arbitrary Higgs Sectors with Exclusion Bounds from LEP and the Tevatron," *Comput.Phys.Commun.* **181** (2010) 138–167, arXiv:0811.4169 [hep-ph].
[248] P. Bechtle, O. Brein, S. Heinemeyer, G. Weiglein, and K. E. Williams, "HiggsBounds 2.0.0: Confronting Neutral and Charged Higgs Sector Predictions with Exclusion Bounds from LEP and the Tevatron," *Comput.Phys.Commun.* **182** (2011) 2605–2631, arXiv:1102.1898 [hep-ph].
[249] P. Bechtle, O. Brein, S. Heinemeyer, O. Stal, T. Stefaniak, *et al.*, "Recent Developments in HiggsBounds and a Preview of HiggsSignals," *PoS CHARGED2012* (2012) 024, arXiv:1301.2345 [hep-ph].
[250] P. Bechtle, O. Brein, S. Heinemeyer, O. Stål, T. Stefaniak, *et al.*, "HiggsBounds – 4: Improved Tests of Extended Higgs Sectors against Exclusion Bounds from LEP, the Tevatron and the LHC," *Eur.Phys.J.* **C74** no. 3, (2014) 2693, arXiv:1311.0055 [hep-ph].
[251] S. Heinemeyer, O. Stal, and G. Weiglein, "Interpreting the LHC Higgs Search Results in the MSSM," *Phys.Lett.* **B710** (2012) 201–206, arXiv:1112.3026 [hep-ph].
[252] P. Bechtle, S. Heinemeyer, O. Stal, T. Stefaniak, G. Weiglein, *et al.*, "MSSM Interpretations of the LHC Discovery: Light or Heavy Higgs?," *Eur.Phys.J.* **C73** no. 4, (2013) 2354, arXiv:1211.1955 [hep-ph].
[253] M. Carena, J. R. Ellis, A. Pilaftsis, and C. Wagner, "CP violating MSSM Higgs bosons in the light of LEP-2," *Phys.Lett.* **B495** (2000) 155–163, arXiv:hep-ph/0009212 [hep-ph].

List of figures

List of tables